Loughborough University
Institutional Repository

Model-based fault detection and control design - applied to a pneumatic Stewart-Gough platform

This item was submitted to Loughborough University's Institutional Repository by the/an author.

Additional Information:

- A Doctoral Thesis. Submitted in partial fulfillment of the requirements for the award of Doctor of Philosophy of Loughborough University.

Metadata Record: https://dspace.lboro.ac.uk/2134/6243

Publisher: © Karmjit Singh Grewal

Please cite the published version.

Thesis Access Form

Copy No…………...…………………**Location**……………………………………………………….

Author: Karmjit Singh Grewal…...……………………………………………………………………

Title: Model-based fault detection and control design – Applied to a pneumatic Stewart-Gough platform…..

Status of access: OPEN

Moratorium Period:…………………………………years, ending…………../…………200………………

Conditions of access approved by (CAPITALS): Roger Dixon

Supervisor (Signature)……………...……………………………...

Department of Electronic and Electrical Engineering…………………………...………………………

Author's Declaration: *I agree the following conditions:*
Open access work shall be made available (in the University and externally) and reproduced as necessary at the discretion of the University Librarian or Head of Department. It may also be digitised by the British Library and made freely available on the Internet to registered users of the EThOS service subject to the EThOS supply agreements.
*The statement itself shall apply to **ALL** copies including electronic copies:*

This copy has been supplied on the understanding that it is copyright material and that no quotation from the thesis may be published without proper acknowledgement.

Restricted/confidential work: All access and any photocopying shall be strictly subject to written permission from the University Head of Department and any external sponsor, if any.

Author's signature…*Karmjit Singh Grewal*……..Date…24th May 2010……

users declaration: for signature during any Moratorium period (Not Open work): *I undertake to uphold the above conditions:*			
Date	Name (CAPITALS)	Signature	Address

Model-based fault detection and control design – Applied to a pneumatic Stewart-Gough platform

by

(Karmjit Singh Grewal)

A doctoral thesis submitted in partial fulfilment of the requirements

for the award of Doctor of Philosophy of

Loughborough University

February, 2010

CERTIFICATE OF ORIGINALITY

This is to certify that I am responsible for the work submitted in the thesis, that the original work is my own except as specified in acknowledgments or in footnotes, and that neither the thesis nor the original work contained therein has been submitted to this or any other institution for a degree.

Karmjit Singh Grewal................................. (Signed)

24th May 2010……………………..…………………………(Date)

Abstract* (Page ii)

Abstract

The safety and functionality of engineering systems can be affected adversely by faults or wear in system components. Therefore, methods for detecting such faults/wear and ameliorating their effects to avoid system failure are important. Designing schemes for the detection and diagnosis of faults is becoming increasingly important in engineering due to the complexity of modern industrial systems and growing demands for quality, cost efficiency, reliability, and the safety issue. In safety/mission critical applications, fault detection can be combined with accommodation/reconfiguration (after a fault) to achieve fault tolerance allowing the system to complete or abort its function in a way that is sub-optimal but does achieve the design objective.

This thesis discusses research carried-out on the development and validation of a model-based fault detection and isolation (FDI) system for a pneumatically actuated Stewart platform. The Stewart-Gough platform provides six degrees of freedom consisting of three translational and three rotational degrees of freedom (x, y, z, pitch, roll, & yaw). As these platforms can be fast acting (rapid motion) and can handle reasonable loads, they can become dangerous, especially when fault(s) in the platform mechanism, drivetrain or control system occur. Therefore, as a safety critical application it is imperative that fault tolerant schemes are applied in order to provide a safe working environment.

The design concept of the FDI scheme for the full Stewart-Gough platform is first designed using a single cylinder set-up. This modular concept is adopted so that a robust fault tolerant control scheme can be designed basically off-line (i.e. not attached to the Stewart–Gough platform). This approach is adopted as requirements are easier to understand using a single cylinder set-up. The modular design approach subdivides the whole system into smaller sections (modules) that can be independently created and then used in the complete Stewart-Gough platform.

The main contributions of the work are that a pneumatically actuated Stewart-Gough platform has been designed, built, and commissioned. A mathematical model has been

developed and has been validated against experimental results. Two control approaches have been designed and compared. A fundamental comparative study of parity equations and Kalman filter observer banks for fault detection in pneumatic actuators has been conducted. The parity equations and Kalman filter approaches have been extended to provide a combined fault detection scheme. The FDI and control schemes have been combined in a modular Fault Tolerant Control (FTC) scheme for a pneumatic cylinder.

The resulting FTC scheme has been validated by experimentation and demonstrated on the single cylinder test rig. The FTC scheme has been extended to all 6 cylinders (and including fault management at top level) of Stewart-Gough platform. The FTC scheme has been validated by experimentation and demonstrated on the Stewart-Gough platform test rig. The designed FDI scheme performance has been assessed by experimentation.

Key words: Fault detection; residual generation; Kalman filter; parity equations; accommodation; control; modelling; Stewart-Gough platform; pneumatic.

Acknowledgements* (Page iv)

Acknowledgements

First and foremost, I would like to pay the greatest respect to the Lord Almighty and the divine spiritual throne of Lopon (Punjab, India). Including, my parents and my elders.

A special thank you to my wife Sandeep, my children Jaswinder, Pritpal and Simranpal for being so understanding, supportive and thoughtful during this project, their support during this project was immeasurable.

An exceptionally special thank you to my PhD supervisor Dr Roger Dixon, for his continuous support, understanding, guidance and encouragement, without any of these special attributes this project would not have been possible, his door was always open.

A special thank you to Professor Roger Goodall and my industrial supervisor Dr John Pearson (SEIC) for all their support and encouragement.

I would like to take this opportunity to thank the university teaching staff and the technical support staff (workshop and IT services) for their help, support and for giving me the benefit of their vast engineering experience.

Finally, last but not least, I would like to thank all my colleagues past and present from the Control Systems Group within the Electrical and Electronic Engineering department at Loughborough University, for all their support, understanding and encouragement, and in particular putting up with me throughout the duration of the project.

Karmjit Singh Grewal

Loughborough University (2010)

List of Figures

List of Tables

Contents

Chapter 1

Introduction

1.1   Background

This thesis addresses the design and development of a fault tolerant control scheme for a pneumatic Stewart-Gough platform.

In systems, every component has been designed to provide certain function(s) and the overall system works satisfactorily only if all the components provide the service they are designed for. However, a fault in any one of these components usually changes the performance of the overall system.

In order to avoid deterioration or damage to systems and human operators, faults have to be found as quickly as possible and decisions have to be made to kerb the propagation of their effects and corrective action may be taken. The human operator can correct system errors, by simply closing down the part of the process which is faulty or failed or by re-scheduling the feedback control or set point parameters (Patton, 1997). On the other hand, automatic system reconfiguration or control system reconfiguration may be acceptable. However, this approach may have limited authority.

In the field of safety-critical control the need for meaningful and reliable practical fault diagnosis and the need to provide the human operator with fault diagnosis information are imperative. Safety critical applications refer to those operations where failure would endanger human safety and/or environmental conditions, including system damage. Examples of such situations would include avionic and nuclear applications. The costs associated with accidents in either of these areas are immense, and as such a great deal of effort has gone into advancing the theory and practice of fault-tolerant systems within these industries (Patton, 1997).

The degree to which a system will be developed to accommodate faults will depend on the application. A fault tolerant system may only accommodate a single fault or may be made multi-fault tolerant. However, it is important to note that no system can be made that will manage or tolerant every fault: there will always be some combination of events and failures that will lead to the disruption of the system. This is demonstrated in the history of manned space flight programs. These programs take fault tolerance to its farthest extremes, yet they have suffered failures that resulted in injury and death. A general definition of a

fault tolerant scheme is that it is a process that (i) detects a fault; (ii) isolates the detected fault and, (iii) initialises an action(s) to resolve the fault. The actions could be either to accommodate the fault or take the necessary action to make the system safe.

1.2 General approaches to fault tolerant systems

Depending on how the redundancy is being utilized, most methods of fault tolerant schemes can be described as either passive or active approaches.

1.2.1 Passive Fault-Tolerant approach

A passive fault-tolerant system is one that takes no action to detect faults or reconfigure its system to accommodate them. As this method's passivity suggests, the achievable levels of fault tolerance are very limited: the fixed controller, based on a nominal model of the plant, is the only form of fault compensation. Thus, the term passive fault-tolerance is actually referring to the robust control techniques. A well-designed, robust feedback controller will reduce the plant's output sensitivity to measurement errors and disturbance inputs (Siljak, 1980), and in this sense, the system is error-tolerant. If the system's behaviour under known fault conditions is also considered during the design of the robust controller, then some fault-tolerance may also be achieved.

However, the design will only be able to accommodate a small number of faults. Nonetheless, this may be suitable for restricted cases, perhaps where a fault has a small effect on the system. If the effects of faults are similar to the effects of errors and disturbances on the system, then robustness to these faults may be achieved through passive methods (Shieh *et al*, 1988). In a passive approach, the conceivable system component failures are assumed to be known a priori, and the control system takes into account all of these failure modes in the design stage. Once the control system is designed, it will remain fixed during the entire system operation. Even in the event of component failures, the control system should still be able to maintain the designed performance. In other words, in passive fault tolerant control the system control designer has to ensure that

the control system works under all possible system operating scenarios that includes potential component failures.

Generally, passive approaches have the following characteristics

- Robustness to certain known faults
- Using a hardware redundancy (multiple actuator and sensors)

1.2.2 Active Fault-Tolerant approach

In contrast to passive approaches, active fault-tolerance takes actions to detect and isolate faults within the system and perform some action to accommodate those faults.

An active fault-tolerant scheme is typically composed of the plant itself, including its sensors and actuators, a Fault Detection and Isolation (FDI) unit, some form of controller and a fault management system. The FDI unit is responsible for monitoring the system in order to identify faults when they occur and determine their location. The FDI unit then sends this information to the management system which makes decisions on what action(s) to take.

FDI has an imperative role in the active approach to attaining fault-tolerance. When using direct redundancy, extra hardware or components provide additional signals. These can be used to generate residual signals by direct comparison. Voting techniques can be used to indicate and possibly isolate a faulty component. When analytical redundancy is used analytical relationships are used to produce additional (or back-up) signals, as well as the residual signals. When the system is fault-free, all of the residuals should be close to zero (zero mean). After a fault occurs, the system that is used for residual generation and decision-making is responsible for identifying and isolating the location of the fault. The system can then be reconfigured, if possible. This depends on the type of system and type of fault. Sometimes the only means of accommodation/reconfiguration is to bring the system back to a safe position.

Essentially, in a model-based fault detection-isolation scheme the mathematical models are utilised to quantify the expected behaviours of the system. The quantities which are often used are the system states, system parameters, and the system input(s) and output(s). The reasoning behind using an active fault-tolerant approach is that, in contrast to a passive fault-tolerant control system, instead of relying on a fixed controller for all

conceivable situations, an active fault-tolerant system reacts to the detected faults by taking the appropriate actions, so that the system stability can be maintained and performance is still acceptable or to ensure the system is made safe. The different approaches to model-based FDI are further discussed in chapter 2.

1.3   Problem statement

Studies have shown that an internal fluid (fuel) can alter the natural frequencies and vibration modes of an aircraft structure. Part of the ongoing research by the project sponsors BAE Systems is to improve model representation of aircraft reliability, safety and control. This involves taking into account the influence of internal liquids (fuels) in the models, also referred to as fluid slosh. Where, slosh refers to the movement of liquid inside another object (fuel tank) which is, typically, also under motion. In aircraft, interaction of the slosh dynamics with the control system may have a direct impact on vehicle stability and performance (Nichkawde *et al* 2004). Working to the guidelines set by the project sponsors BAE Systems, the aim of this Ph.D thesis research is to find a way to (i) physically represent methods of providing an actual experimental test rig to simulate the fluid dynamics within a fuel tank under motion. (ii) Develop an approach to designing fault detection and accommodation schemes that could be demonstrated and later applied to other systems.

The proposed test rig is a Stewart-Gough platform; this provides six degrees of freedom consisting of three translational and three rotational degrees of freedom (x, y, z, pitch, roll, & yaw). The platform design provides a large amount of rigidity/stiffness, for a given structural mass, and thus provides significant positional accuracy. The design of the Stewart-Gough platform (shown in Figure 1.1) is a parallel mechanism consisting of a rigid body mobile plate, connected to a fixed base plate and is defined by at least three stationary points on the fixed (grounded) base connected to six independent kinematic legs. Six legs are connected to both the base and top plate by rotational joints in parallel located at both ends of the six legs. The legs are designed with an upper body and lower body that can be adjusted. This allows for the length of each leg to be varied. The linear extension and retraction of the six actuators gives the platform six degrees of freedom positioning capabilities.

As these platforms can be fast acting (rapid motion) and can handle reasonable loads, they can become dangerous, especially when fault(s) in the platform mechanism, drivetrain or control system occur. Therefore, as a safety critical application it is imperative that fault tolerant schemes are applied in order to provide a safe working environment.
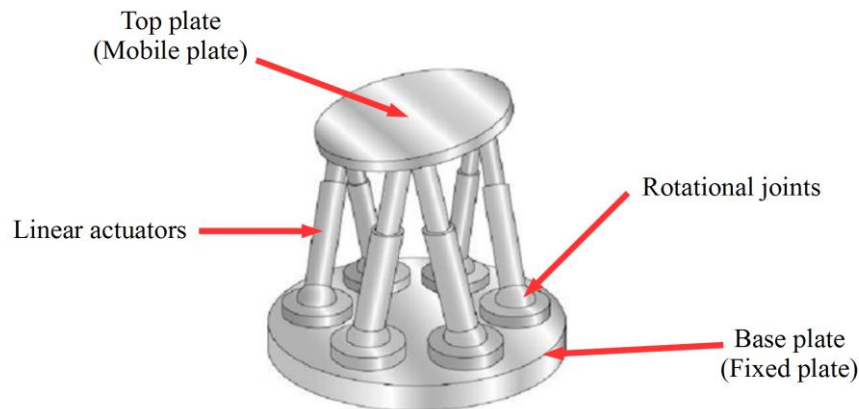
Figure 1.1: Diagram of Stewart-Gough platform

Since control and monitoring methods rely on the information received from the sensors, it makes sense to make full use of all the measured parameters available from the system in both control and monitoring. For this thesis the design approaches for both are based on models; it also seems appropriate to undertake a (model-based) co-design of both control and monitoring tasks.

Working with the guidelines set by the project sponsors BAE Systems the approach is based on an active fault-tolerant strategy and focused on a model-based fault tolerant scheme for a pneumatically actuated Stewart-Gough platform.

Currently, electromechanical, hydraulic and pneumatic drives are most widely used as actuation systems. However, all these actuation systems have serious drawbacks, limiting their inherent performance characteristics. The types of linear actuation systems are discussed below.

Electrically driven actuators are normally used where movement is required for a number of intermediate positioning, particularly when these positions need to be changed easily. They can also control speed and acceleration rate to a high accuracy independently of the load (Krivts and Krejnin, 2006). This allows smooth motion to be performed in

situations where this is a critical performance factor. In addition, electromechanical actuators can be used where increased complex motions profiles are needed, such as registration (component location) and contouring. The use of electrical motors without torque-magnifying reducers is limited to direct-drive systems. These employ large DC torque motors that are heavy and inefficient. To increase the torque output to useful levels, gear reducers are almost universally used. However, employing gear reducers, there is an increase torque-to-weight and power-to-weight ratio. This must be traded off against the large increase in reflected inertia (load inertia / gearing ratio^2).

Using conventional rotating electrical motors to achieve linear motion requires transformational (conversion) elements such as ball screws or timing belts. The main advantage of electrical motors with transformational elements is that they will allow using a low-cost motor that delivers high torque but runs at low speeds.

Electrical linear motors are used in applications requiring high speeds, acceleration, and accuracy. The design, benefits by having the motor and load directly and rigidly connected. This improves simplicity, efficiency, and positioning accuracy. The primary limitation of electromechanical drives is their relatively low power-to-weight, power-volume ratio, and payload-to-weight ratio. A comparative study (shown in Table 1.1) by Krivts and Krejnin (2006) describes the characteristics for electrical, hydraulic, and pneumatic motors. From this table it can be seen that the electrical motor has the poorest ratios, and this limits its applications.

Table 1.1: Characteristics of motors

	Pneumatic motor	Hydraulic motor	Electrical motor
Power-to-weight ratio (kW/kg)	0.3-0.4	0.5-1	0.03-0.1
Power-to-volume ratio (kW /m^3)	1×10^{-3}-1.2×10^{-3}	~ 2×10^{-3}	0.05×10^{-3}-0.2×10^{-3}
Payload-to-weight ratio (N/kg)	11	20	3.5

Generally, the linear motion systems with electrical motors and transformational elements have positioning accuracy of approximately 5-10μm (best case) and velocity up to 500-600 mm/s. For the electrical linear motors the position accuracy is up to 0.1μm, and velocity is up to 1.5m/s.

Hydraulic actuators (direct drive type), which have the highest torque and power characteristics (Table 1.1) of any of the actuation methods, are capable of performing tasks that involve the application of thousands of Newton-meters of torque and many kilowatts of power output. Other aspects that make a hydraulic actuator useful are the low compressibility of hydraulic fluids and high stiffness which leads to a high natural frequency and rapid response. This means that processes employing hydraulic actuators can execute very quick movements with great force. Hydraulic actuators have low noise levels and relative safety during operation.

One of the main concerns with hydraulic systems is the containment of the fluid within the actuation system. Not only can the fluid cause contamination of the surrounding environment, but leakage can contaminate the oil and possibly lead to damage of interior surfaces (i.e. cylinder bores, valves). In addition, the hydraulic fluid is flammable and pressurised, so leaks could pose a hazard to equipment, personnel and environment. This also adds to undesirable additional maintenance to maintain a clean, sealed system. Other drawbacks include lags in the control of the system due to the transmission lines and oil viscosity changes due to temperature change. Extreme temperature changes in the hydraulic fluid can be drastic enough to form vapour bubbles when combined with the changes in fluid pressure, this phenomenon is called cavitation[1].

Hydraulic actuation systems can develop controlled stroke speeds up to 1 m/s, and positioning accuracy of approximately 1-5μm. Nearly 70% of today's positioning applications move loads of between 1 and 10kg with accuracy between ±0.02 and ±0.2mm (Krivts and Krejnin (2006).

Pneumatic actuators are still among the most widely used in automation processes. As a rule, these actuators are direct-drive systems. Pneumatic actuators have been used in devices when lightweight, small-size systems with relatively high payload-to-weight ratio are needed. They are a preferred medium because they are relatively inexpensive (pneumatic technology costs approximately 15 to 20% of an electrical system and is up to

---

[1] Cavitation is the formation of vapour bubbles of a flowing liquid in a region where the pressure of the liquid falls below its vapour pressure. During operation, as temperature and pressure fluctuate, these bubbles alternately form and collapse. At times, when a vapour bubble is collapsing, the fluid will strike interior surfaces that have vapour-filled pores and high surge pressures and will be exhibited at the bottom of these pores. The cavitation can dislodge metal particles in the pore area and leave a metallic material within the fluid. The degradation of the interior surfaces and contamination of the fluid can result in a loss of performance of the system.

4-5 times less costly than the equivalent hydraulic system), simple to install and maintain, offer robust design and operation, and are available in a wide range of standard sizes and design alternatives. They offer high cycle rates and are cleaner and non-flammable when compared to hydraulics, making pneumatics more desirable in certain environments. Furthermore, pneumatic devices are less sensitive to temperature changes and contamination.

Pneumatic actuators are ideally suited to fixed travel applications and the control of force, where precise control of speed is not a prime requirement. New technologies today integrate the power of air with electronic closed-loop control; this combination of technologies can provide much higher acceleration and deceleration capabilities. This position, velocity, and force-control system is typically lower in cost compared with electrical motion systems. These servo pneumatic systems retain the advantages of standard pneumatics and add the opportunity for closed-loop, controlled accurate positioning to within fractions of a millimetre in systems in which position can be approached rapidly and without overshoot..

Generally, servo pneumatic actuators are similar to hydraulic servo actuators and use proportional or servo pneumatic valves, relying on the integration of electronics closed-loop control. Pneumatic actuators have the following main disadvantages: poor damping, high air compressibility, nonlinearites, and mechanical friction. With advances in pneumatic control theory, and the combination of fast acting valves, including advances in electronics and software, servo pneumatic systems are capable of positioning accuracy within a range of 0.05mm (Lee *et al*, 2001). This level of precision is sufficient for an estimated 80% of typical industrial applications. The linear motion systems with pneumatic actuators and hard mechanical stops have positioning accuracy of about 10μm (best case) and velocity of up to 2.5m/s. For systems with servo or proportional valves the position accuracy is up to 50μm, and velocity up to 2.5m/s (Krivts and Krejnin 2006).

For this work linear motion to the Stewart-Gough platform legs is to be provided by pneumatic actuation. The reason for the choice of pneumatics is (i) there are very few applications using pneumatic actuation for a Stewart-Gough platform, and (ii) as far as the author is aware a model-based fault tolerant scheme for a pneumatically actuated Stewart-Gough platform has not been explored.

1.4   Objectives

The first phase of the work focussed on the modelling and control of a single pneumatic cylinder. The second involved design of the model-based fault tolerant scheme on the single pneumatic cylinder set-up. The final step was to apply this modular design (of control and monitoring) across all six legs of the Stewart-Gough platform. The main research objectives were:

1. To develop a pneumatically actuated Stewart-Gough platform.
2. To design and apply a suitable controller.
3. To develop fault detection algorithms for the main system (pneumatic) faults.
4. To develop a fault management system ensuring appropriate (safe) action is taken in the event faults occur.
5. The embodiment of objectives 2, 3 and 4 in a Fault Tolerant Control system.
6. Validation of the above design process (objectives 2-5) and resulting design by experiments on the Stewart-Gough platform.

1.5   Contributions

In pursuing this research, certain contributions have been made in designing and implementing a fault tolerant scheme for a pneumatically actuated Stewart-Gough platform, which includes the ability to inject a range of faults (representative of the key real world fault scenarios). The main contributions were

- A pneumatically actuated Stewart-Gough platform has been designed, built, and commissioned.
- A mathematical model has been developed and has been validated against experimental results.
- Two control approaches have been designed and compared.
- A fundamental comparative study of parity equations and Kalman filter observer banks for fault detection in pneumatic actuators has been conducted.

- Extension of the parity equations and Kalman filter approach to provide a combined Fault detection scheme.

- Combination of the FDI and control in a modular Fault Tolerant Control scheme for a pneumatic actuator – validation by experiment.

- Extension of application of Fault Tolerant Control to all 6 actuators (and including fault management at top level) of Stewart-Gough platform - validation by experiment.

1.6   Publications

In the research work, leading to this thesis, the author has published the following conference and journal papers:

- Grewal, K.S., Dixon, R., and Pearson, J. (2008). Development of a fault tolerant actuation system- modelling and validation. *Actuator 08, 11th international conference on new actuators,* Bremen, Germany, 9 – 11 June 2008, pp, 469-472.

- Grewal, K.S., Dixon, R., and Pearson, J. (2008). Application of fault detection and isolation to a pneumatic actuation system. IN: Burnham, K.J. & Linden, J.G (eds.). *Proceedings of the 23rd IAR Workshop on Advanced Control and Diagnosis*, 27-28 November 2008, Control Theory and Applications Centre, Coventry University, UK, pp. 350-355.

- Grewal, K.S., Dixon, R., and Pearson, J. (2009). Comparison of two model based residual generation schemes for the purpose of fault detection and isolation applied to a pneumatic actuation system. IN: *Proceedings of 7th IFAC Symposium on Fault Detection, Supervision and Safety of Technical Processes. SafeProcess 2009*, Barcelona, Spain, 30 June - 3 July 2009, pp.1420-1425.

- Grewal, K.S., Dixon, R., and Pearson, J. (2010). Model-based fault detection and control design − Applied to a pneumatic Stewart-Gough platform. Accepted for presentation at *Actuator 10, 12ᵗʰ international conference on new actuators,* Bremen, Germany, 14 − 16 June 2010.

- A conference paper submitted and waiting review (IFAC Mechatronic systems, Boston, 2010).

- Two journal papers are in preparation.

1.7 *Thesis overview*

This chapter has given a general overview of the aims of this thesis; including, a broad description of fault tolerant systems. The objectives and contributions of the research are also outlined. The remainder of this thesis has the following organisation. Chapter two provides a literature review of current methods of techniques that may be useful for the project. The review discusses a wide range of FDI techniques in the field of fault tolerant systems, including reviewing types of Stewart-Gough platform applications. Chapter three describes the experimental set-up, for the single pneumatic cylinder rig and the full pneumatic Stewart-Gough platform. These two systems are the target for the fault tolerant scheme. Their designs are discussed in detail. Chapter four details the pneumatic system modelling and model validation for the single actuator test-rig. Chapter five describes the control strategies to control both test rigs. Chapter six describes the input (kinematics) equations for the Stewart-Gough Platform. Chapter seven discusses the model based fault detection strategies and details the fault detection/isolation scheme. Chapter eight is dedicated to the results and analysis for the single cylinder test rig. Chapter nine presents the results for the Stewart-Gough platform test rig. Chapter ten concludes the thesis, it gives an overview of the main results and summarises the generic design process taken to develop the model-based fault tolerant scheme. Finally, directions for further research will be suggested.

Chapter 2

Literature review

2.1   Introduction

As previously stated in chapter 1 active fault-tolerance is to be used for the pneumatically actuated Stewart-Gough platform. One of the main components within an active fault tolerant scheme is the FDI unit. This literature review will focus on a variety of different approaches to FDI within a fault tolerant scheme. However, the main concern for this work is using analytical redundancy with model-based methods. The review also briefly describes types of Stewart-Gough platforms available and will focus on the methods of providing movement to the platforms.

2.2   Fault tolerant systems

Fault tolerant systems is a research area that is becoming increasingly important due to the growing complexity of modern industrial systems and growing demands for quality, cost efficiency, reliability, and more importantly the safety issue (Al-Najjar, 1996). So that operators and manufacturers maintain a competitive edge, their machines and processes are set at optimal operating conditions (Chen and Patton, 1999). Fault tolerant systems support this objective by predicting failures and, if a failure occurs, by identifying the reasons following the failure (Blanke *et al*, 2003). Early detection of possible faults allows maintenance work to take place before a system malfunctions in a way that may cause damage and obstructions to the overall operation. This can improve the level of plant safety, and increase up time and productivity. Many systems depend on automatic control for satisfactory operation. In order to achieve and maintain system stability and assure satisfactory and safe operation, there is an increasing demand for systems to continue acceptable operation following faults or failures. Therefore, fault/failure detection, fault identification and accommodation have always been an important aspect of a fault tolerant system design (Theilliol *et al*, 1998).

Feedback control systems may be vulnerable to faults within the control loop (Blanke *et al*, 1995; Isermann, 1997). Feedback actions may cause abrupt responses, which may

include system damage when a fault does occur. These faults can be detected using model-based methods for FDI.

When developing a fault tolerant system, the basic *a priori* information needed is a set of faults and the relationship between the observations (symptoms) and the fault (Chen and Patton, 1999). There is a variety of literature concerning FDI systems. See for example (Willsky, 1976; Patton *et al*, 1989; Patton *et al*, 1995; Patton, 1997; Frank and Ding, 1997; Patton *et al,* 2000; Blanke *et al*, 1995). A systematic and comparative study by Venkatasubramaniam *et al* (2003a, b, and c) describes various diagnostic methods from different points of view showing that system fault detection and diagnosis methods can be categorized into three main groups. Namely, quantitative model-based methods, qualitative model-based methods, and process history based models. The classification of the diagnostic systems is shown in Figure 2.1 (Venkatasubramaniam *et al,* 2003a, b, c).
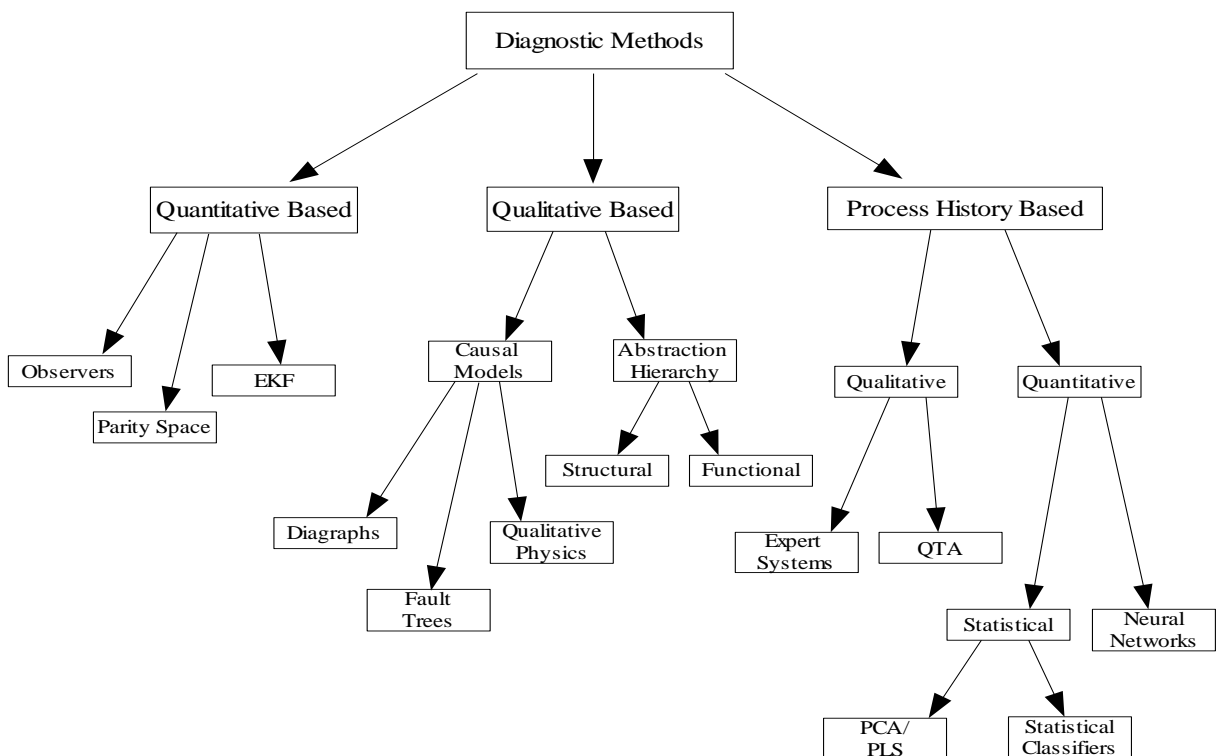
Figure 2.1: Classification of the diagnostic systems

2.3. *Quantitative model-based*

Quantitative model-based methods correspond to modelling the physical process by using some mathematical functional relationships of the inputs and outputs of the system. Consider the feedback control system with an input **u**, and output **y**, shown in Figure 2.2. The system consists of the actuators, components and the sensors. Frank (1990) suggests that for a realistic representation with respect to a FDI task, it is important to model all effects that can lead to alarms or false alarms. These include, (i) Faults in the actuators. That is, in the components or in the sensors of the plant. (ii) Modelling errors between the actual system and the mathematical representation. (iii) System noise including noise measurement.
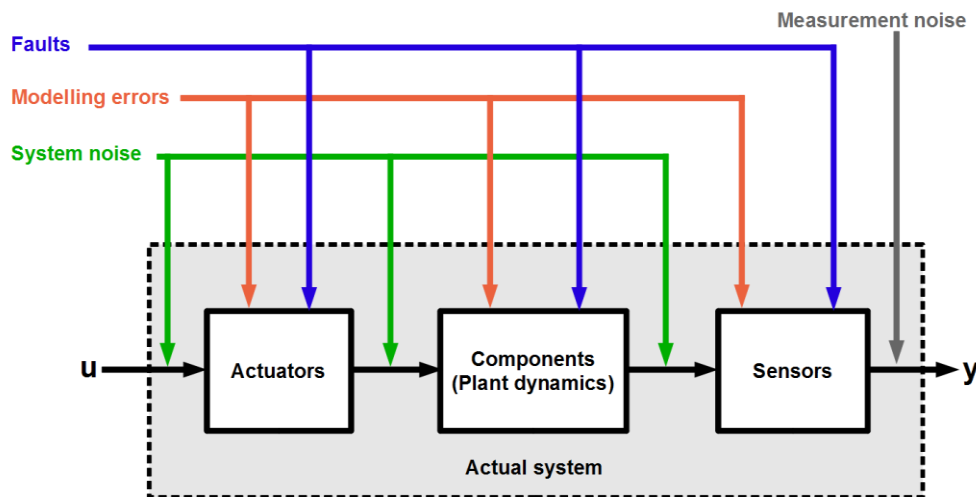
Figure 2.2: Feedback control system.

2.3.1. *Basic concepts of model-based FDI schemes*

A traditional approach to fault tolerance is based on hardware or physical redundancy methods to use multiple sensors, actuators, components to measure a particular variable. Typically, using these concepts voting techniques are applied to the hardware redundant system to decide if a fault has occurred or not and then to identify its location among the

entire set of redundant system components. One of the major problems inherited with hardware redundancy is the extra equipment and maintenance costs.

Model-based Fault Detection and Isolation (FDI) uses the principles of analytical redundancy to first detect deviations from normal behaviour in a system, and then to isolate the particular component that has a fault. Typically, model-based analytical estimates are compared with measured variables to generate residuals. The residuals will be zero mean when the system is operating normally and will exceed a threshold when a fault arises. There are a number of approaches to model-based residual generation. For example, observer-based approaches including Kalman filters (Frank, 1987a), parity relations approaches (Gertler and Singer, 1990) and parameter estimation (Patton *et al* 2000; Isermann, 1997). Useful surveys of these and other FDI methods can be found in Patton (1997), Blanke *et al* (1997), Isermann (1984), and Willsky (1976).

The general procedure of model-based Fault detection and isolation (FDI) is the evaluation of the redundancy given by the mathematical model of the system (Frank, 1990; Patton, 1997; Frank *et al*, 2000; Isermann, 2006). The procedure can be divided into the two following stages.

i. *Generation of residuals* – Outputs and inputs of the system are processed by an appropriate algorithm (processor) to generate residual signals. The residual must be non-zero when a fault occurs and zero mean when no fault occurs.

ii. *Decision and isolation of the faults* – (Residual evaluation) the residuals are examined for the likelihood of faults which include for example (time, location). Once this is established, a decision rule is applied to determine if any faults have occurred.

For the application of model-based fault detection methods, the process configurations shown in Figure 2.3 have to be distinguished. The overall fault detection improves greatly from case (1) to case (2) to case (3) or case (4); this is due to the availability of more measurements. For SISO processes (Figure 2.3.1) only one residual can be generated. With this distinguishing between different faults is very difficult. However, for SISO processes with intermediate measurements (Figure 2.3.2) more freedom in the design using parity equations can be obtained. The same can be said about the SIMO and MIMO processes.
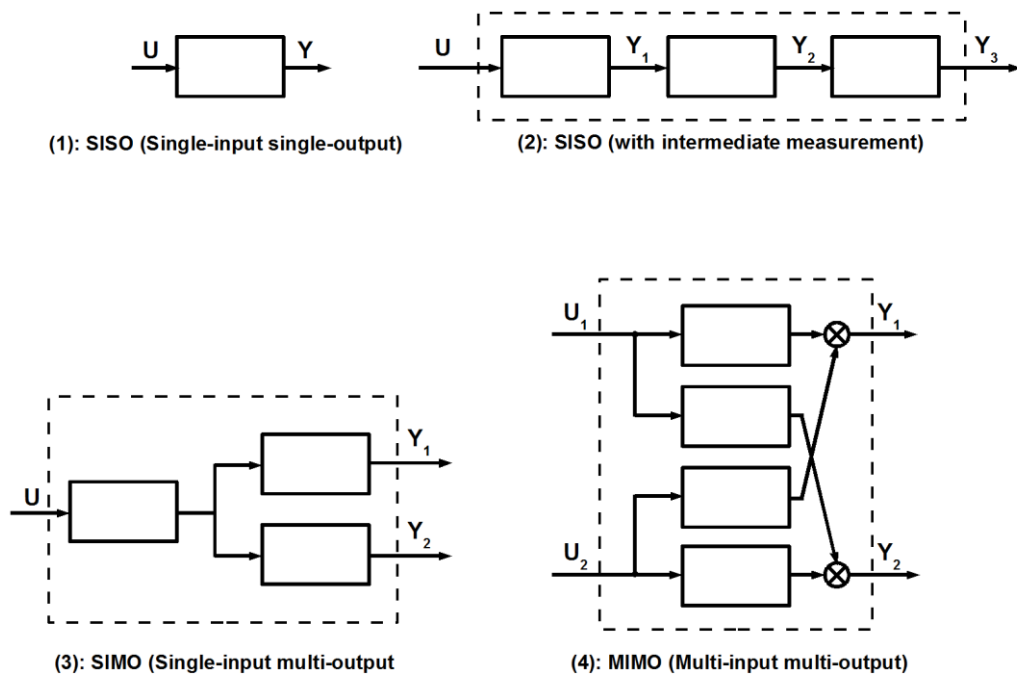
Figure 2.3: Process configurations for model-based fault detection

Figure 2.4 depicts the schematic structure of a FDI procedure using analytical redundancy. The analytical approach requires that a residual generator perform a validation of the nominal relationships of the system, using the actual input, **u**, and the measured output, **y** (Frank, 1987b; Frank, 1990; Frank, 1996; Isermann, 1984).
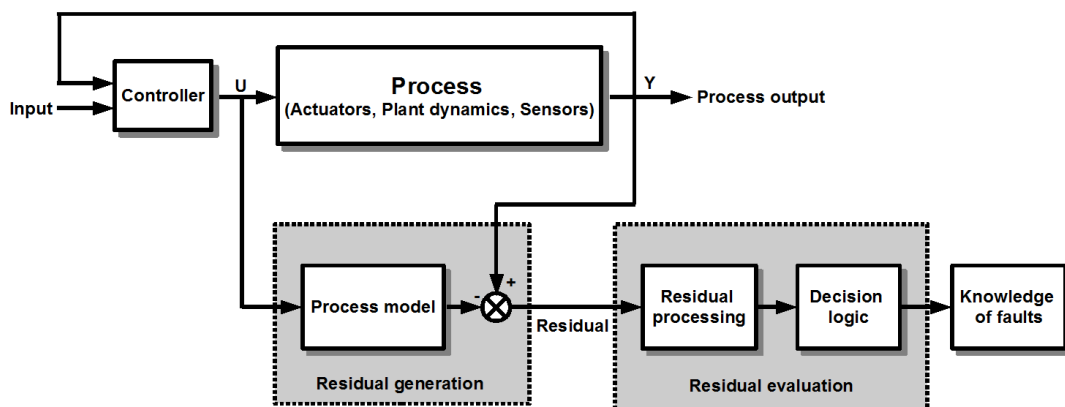
Figure 2.4: Schematic structure of a FDI procedure using analytical redundancy.

With a great deal of literature regarding the residual generation, see for example, (Patton *et al*, 1995; Patton, 1997) there is a variety of different approaches to the problem of FDI using analytical redundancy. These include:

- *The parity space approach* - This approach is to check the consistency of the mathematical equations of the system (analytical redundancy relations) by using the actual measurements. A fault is declared once predetermined error boundaries are exceeded. The analytical redundancy relations include (i) direct redundancy, which is a relationship among instantaneous redundant sensor outputs (output error). (ii) Temporal redundancy, (differential or difference equations) the dynamic relationships between sensor and actuator inputs (polynomial or equation errors) (Potter and Suman, 1977; Desai and Ray, 1981; Gertler, 1998). Figure 2.5 shows the output error arrangement.
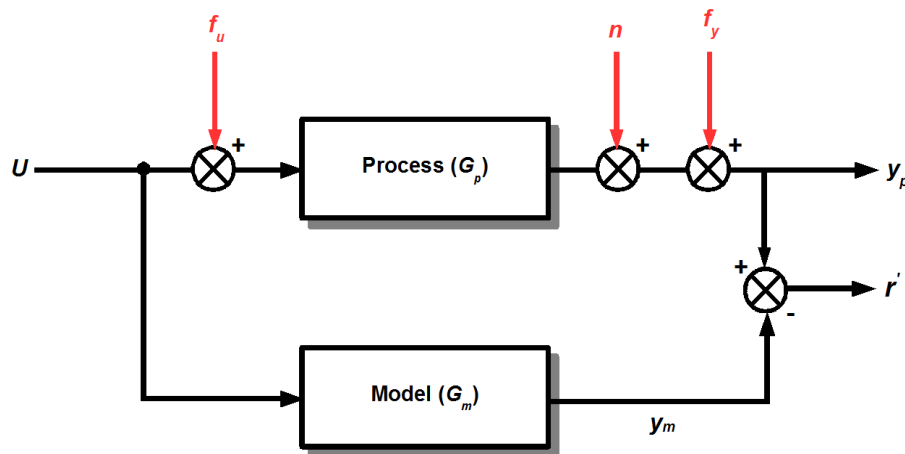
Figure 2.5: Residual generation with parity equations using output error

In order to describe this technique (Figure 2.5), a single output system is considered (Isermann, 1984). A system can be described by the transfer function

$$G_p(s) = \frac{y_p(s)}{u(s)} = \frac{B_p(s)}{A_p(s)} \tag{1}$$

The model of the process is given by

$$G_m(s) = \frac{y_m(s)}{u(s)} = \frac{B_m(s)}{A_m(s)} \tag{2}$$

The model is assumed to be known where the model parameters are also known and fixed. Therefore the process is described by

$$G_p(s) = G_m(s) + \Delta G_m(s) \tag{3}$$

Where $\Delta G_m(s)$ describes the modelling errors. The residuals for the output error method can be formulated as

$$
\begin{aligned}
r'(s) = y_p(s) - y_m(s) &= y_p(s) - G_m(s)u(s) \\
&= G_p(s)[u(s) + f_u(s)] + n(s) + f_y(s) - G_m(s)u(s) \\
&= \Delta G_m(s)u(s) + G_p(s)f_u(s) + n(s) + f_y(s) \tag{4}
\end{aligned}
$$

The residual is zero mean if model and process are matching, if there are no additive faults f_u and f_y and no noise (n). However, due to modelling errors(ΔG_m), noise (n) and input signal (u) some deviations are shown. With the additive faults the residual changes are identical with the output fault f_y and filtered by the process G_p for the input faults f_u.

- *The observer approach* - The basic idea of the observer approach is to reconstruct the outputs of the system from the measurements or subsets of the measurements with the aid of observers or Kalman filters (Kalman 1960) using the estimation error as a residual for the detection and isolation of the faults (Clark *et al*, 1975; Willsky, 1976; Frank and Keller, 1980). Isermann (1997) describes the full order observer which consists of a parallel model of the process with a feedback of the estimation error. The fundamental concept of an analytical observer-based residual generator is illustrated in Figure 2.6. This shows a linear full order observer, where *f* is the vector of faults to be detected, represented by (unknown) time functions, *d* denotes the vector of unknown inputs and *K* is the observer feedback matrix (Kalman gain). This includes disturbances, noise and modelling errors. The fault

detection scheme should be insensitive to these unknown inputs. The principle of a residual generator (Frank and Ding, 1997) is to generate a vector *r(t)* such that *r(t)* = 0 as *f(t)*= 0 including

- *r(t)* ≠ 0 **as** *f(t)* ≠ 0 for fault detection.
- $\lim_{t \to \infty}[f(t) - r(t)] = 0$ for fault identification.

Where f_i represents the different faults to be isolated, r_i is the subsequent subsets of residuals.
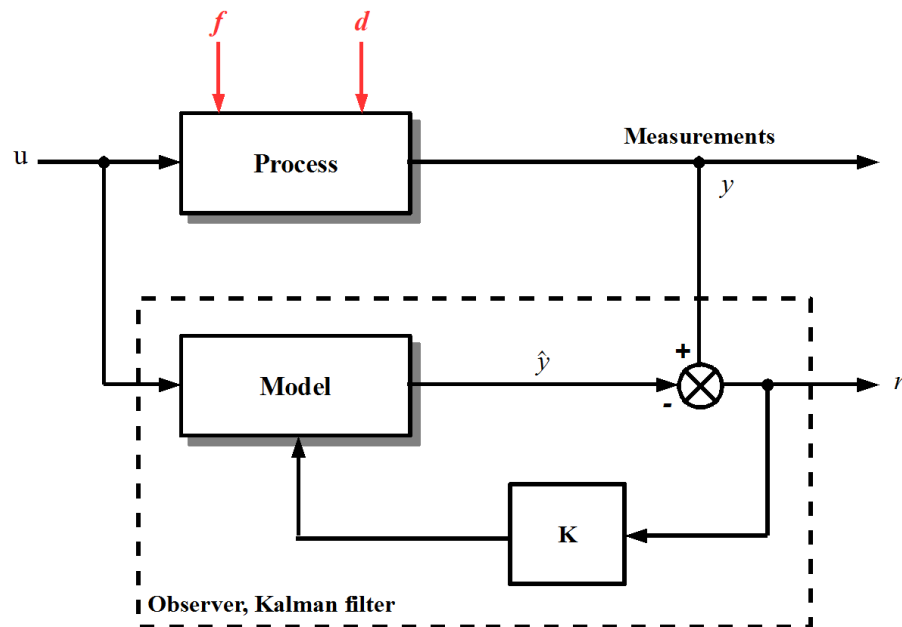
Figure 2.6: Full order observer for residual generation

Among various estimator schemes (Albertos and Goodwin, 2002; Onken and Stuckenburg, 1979; Derkert *et al*, 1977; and Willsky, 1976), the dedicated observer scheme (DOS) proposed by Clarke (1978) is one of the most well known approaches for FDI. In the DOS, each sensor is dedicated to one observer or measurement estimator. It is assumed that the system is observable from each measured variable of the system/process. Each dedicated observer estimates the state variables based on the individual

measurements and the corresponding input (u). The structure of the dedicated observer scheme is illustrated in Figure 2.7. One of the major advantages of the observer-based fault detection schemes is that robustness with respect to model uncertainties can readily be accomplished.
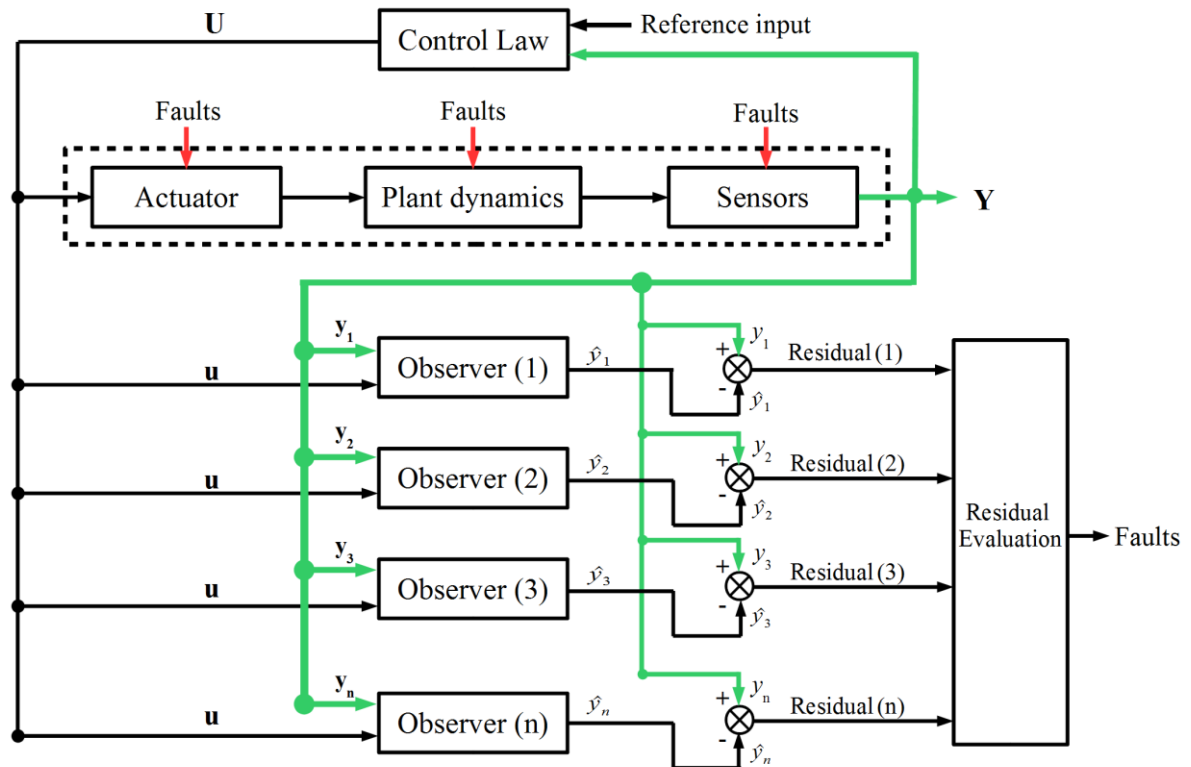
Figure 2.7: Dedicated observer scheme

- *The parameter identification approach* - This approach uses the effects of faults on the physical parameters of a system. The parameters include, friction, mass, viscosity, resistance among others. The basic idea behind the application of parameter estimation to FDI is the on-line estimation with their nominal values. The resulting deviations are the residuals used for FDI. (See for example, Frank *et al,* 2000; Isermann, 1993; and Isermann, 1984).

2.4. *Qualitative models*

Qualitative models are expressed in the terms of qualitative functions around different units in a system. Qualitative models can be developed as qualitative causal models or abstraction hierarchies (Venkatasubramaniam *et al* (2003b). Figure 2.8 depicts the qualitative model forms. The development of knowledge- based systems is based on the transfer of existing knowledge of engineers, process operators, and maintenance personnel.
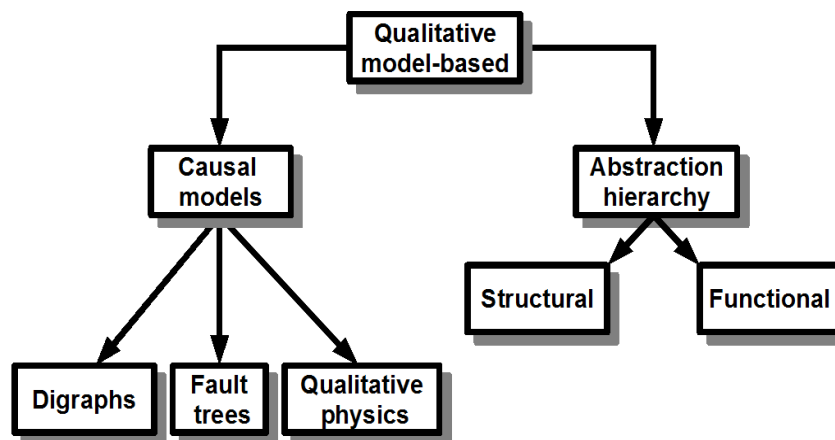
Figure 2.8: Forms of qualitative knowledge

When complete information about a system is not available, the qualitative based techniques for FDI can be used. These make use of the available incomplete information by building a qualitative model, so that the analysis and reasoning can be carried out. The qualitative model is based on qualitative differential equations. These equations have the same structure as the corresponding ordinary differential equation, which model the dynamics of a system in continuous time. However, the parameter data is only of semi-quantitative nature that is partially or frequently known (Frank *et al,* 2000). From this a constrained model is obtained, which consists of qualitative variables representing the physical parameters of the system and a group of constraints of how these parameters are related to each other (Zhuang and Frank, 1997; Frank *et al,* 2000; Zhao and Xu, 2004; and Venkatasubramaniam *et al,* 2003b). Venkatasubramaniam *et al* (2003b) goes on to mention various forms of Qualitative knowledge systems.

2.5. *Process history based schemes*

In quantitative or qualitative model based approaches priori knowledge about the system is required. However, in process history based methods, large amounts of historical process data are needed. The method used to utilise this data is known as feature extraction (Venkatasubramaniam *et al,* 2003c). The methods in which knowledge can be extracted from the process history are depicted in Figure 2.9.
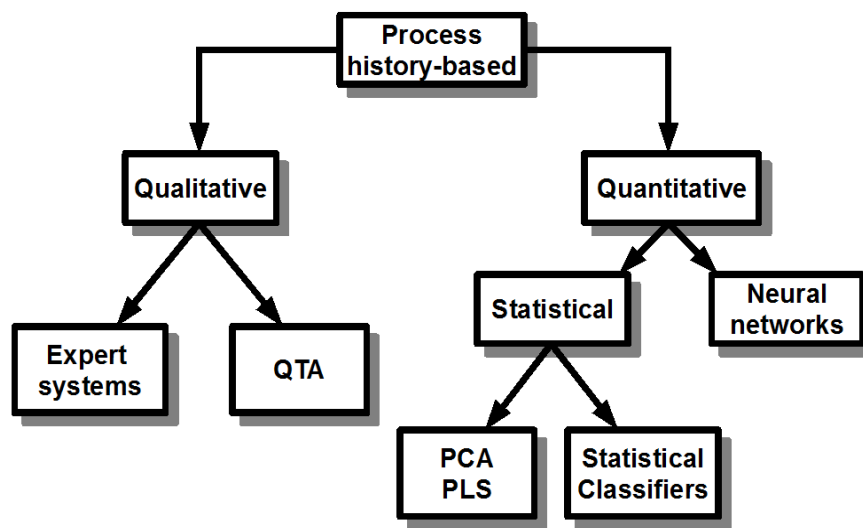
Figure 2.9: Categorization of process history-based schemes

Qualitative feature extraction is based on the expert system approach. Expert systems are specialized systems that solve problems in a narrow field of expertise. Components involved in an expert system include, choice of knowledge representation, knowledge acquisition, the coding of knowledge in a knowledge base, the development of inference procedures for diagnostic reasoning and the development of input and output interfaces (Venkatasubramaniam *et al,* 2003c; and Henley, 1984). Other methods dealing with Qualitative feature extraction is the extraction of trend information (Qualitative trend analysis – QTA). Trend modelling can be adapted to elucidate the various important events occurring in a process. This is more associated with chemical process systems (Cheng and Stephanopoulos, 1990). Quantitative feature extraction essentially involves pattern recognition as a method of problem solving. The aim of the pattern recognition is the

classification of data points to pre-determined classes. Statistical methods use knowledge of a priori class distributions to achieve classification. Methods involved with quantitative feature extraction include, principal component analysis (PCA) or partial least squares (PLS) methods extract (Geladi and Kowalski, 1986) in information about major trends in the data using a small number of related factors. Statistical methods use knowledge of a priori class distributions to perform categorization. Neural networks use a functional method for the decision rule this classifies the parameters. Neural networks used for fault diagnosis may be classed in two dimensions (i) the architecture of the network, such as sigmoidal, radial basis and (ii) the learning strategy which includes, supervised and unsupervised learning.

2.6   *Stewart-Gough platform types*

The Stewart platform originated from the mechanism designed by Stewart (1965) for flight simulation. The Platform is a parallel manipulator consisting of two rigid bodies: a moving platform, and a base (Figure 1.1). The position and orientation (pose) of the base are fixed. The base and platform are connected with six extensible legs via spherical or revolute joints. For a set of given values for the lengths of the six legs, the position and orientation of the platform could generally be determined. The Stewart platform has in the past twenty years been applied to various fields such as robotics, numerically controlled machine, machine tool applications, nano-technology and surgical medical procedures (Figure 2.10). Compared to serial mechanisms, the main advantages of the Stewart platform are its inherent stiffness and high load/weight ratio. For an in depth survey, see for example Dasgupta and Mruthyunjaya (2000).

Many variants of the Stewart platform were introduced for different purposes. Most of these variants are special forms of the Stewart-Gough platform illustrated in Figure 1.1, and depend on the application they are intended for. Faugere and Lazard (1995) gave a classification of all special forms of the Stewart platform. Baron and Angles (2000) studied the possibilities of using three possible joints, the revolute joint, the spherical joint and the prismatic joint, to connect the legs and the platforms.

Various methods have been used in order to extend and retract the platform legs so that orientation and movement can be achieved. The most common approach has been

hydraulics, in particular where increased load carrying capacities and force handling capabilities are required. Another common approach is to use electro-mechanical actuators; these provide good control and positional accuracies. One technology which is uncommon as a means to provide movement of the legs is pneumatics, for this technology the most common approach is using pneumatic flexible muscles or fluid muscles (Verrelst *et al*, 2000). The use of linear actuators is limited, as far as the author is aware only limited applications in literature have applied this technology (Boian *et al,* 2005; Girone *et al*, 2001). Where, in both cases the designs are used for mobility purposes to aid patient rehabilitation. Due to the limited use of the pneumatic linear actuator within a Stewart-Gough platform design, for this thesis six pneumatic linear actuators are used. The design and control of the pneumatically actuated Stewart-Gough platform is described in Chapter 3 and Chapter 5, respectively.
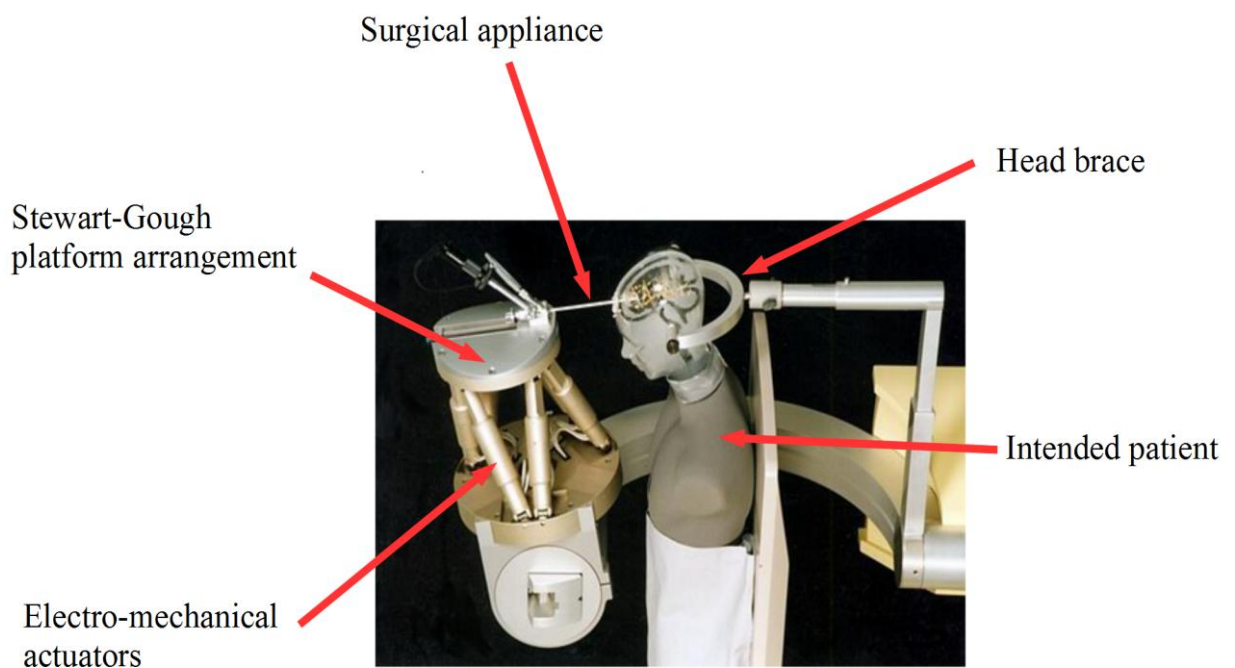
Figure 2.10: Stewart-Gough platform (Hexapod) Surgical Robot with Endoscope.

2.7   Conclusion

This literature review has presented various methods of fault detection and isolation.

The choice of methods for the purpose of FDI is often not as straightforward as it may seem. The main factor to be considered is the availability of the system (process) information. Information from normal system operation (no faults, normal system behaviour) must be received, in order to act as a benchmark for a base for comparison. This is usually achieved by expressing the normal system operation in terms of system models. This modelling procedure is necessary to have relationships between physical and model parameters. System models can be represented in different formats (quantitative or qualitative). Patton *et al* (1995) suggests that the first decisive factor in choosing model-based methods is the availability of the model, and secondly, is the choice of fault diagnosis methods. This depends largely on the problem being solved. The choice in which type of model should be used for fault diagnosis schemes largely depends on the control designer's preferences. For this work the Kalman filter and parity equations methods are used. These are formulated and discussed in chapter 7. The advantage for choosing these methods is, as a validated model has be formulated and is available (chapter 4), it seems appropriate to apply a model-based scheme. As no knowledge of the system is known (i.e. the system is built from scratch) knowledge based techniques are not applied.

It is clear from the examples given in literature that there have been no model-based fault-tolerant industrial applications within the field of pneumatic actuation systems. Most of the literature for fault detection in pneumatics deals with process history-based FDI approaches (see for example, Lipnickas *et al,* 2004; and Uppal and Patton, 2006). This work aims to demonstrate a model-based FDI for an individual pneumatic actuator and ultimately extend and demonstrate it on a Stewart-Gough platform system.

Chapter 3

Experimental set-up

The overall aim is to design and implement a fault tolerant scheme for a Stewart-Gough platform. However, the first stage of this was to develop and demonstrate the methods on a single cylinder pneumatic set-up. Once successful these methods would be extended and applied to the Stewart-Gough platform. These two experiments have been designed and built from scratch as part of the research. The control objectives of the pneumatic system are:

- Settling time is less than 0.2 sec.
- Maximum 2% overshoot.
- Maximum 2% steady state error.
- Gain margin 8dB.
- Phase margin 60 degrees.

In this chapter, section 3.1 gives details of the individual elements of the single actuator test rig and section 3.2 describes the 6-degrees of freedom Stewart-Gough platform that has been built.
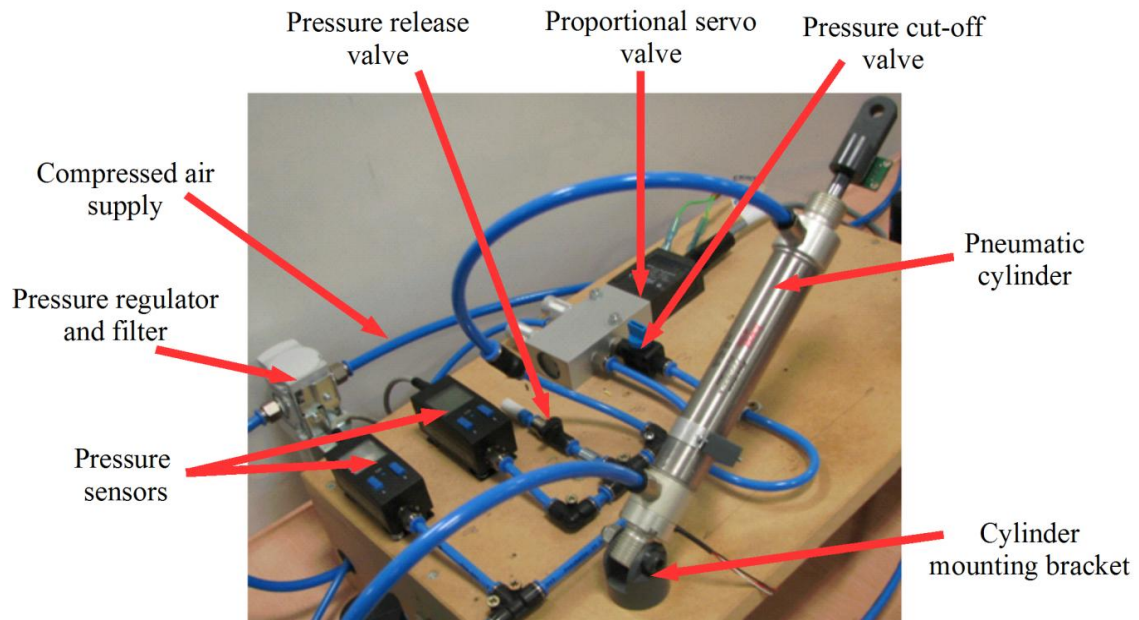
Figure 3.1: The single cylinder test rig set-up

3.1   Single cylinder set-up

The single cylinder test rig is shown in Figure 3.1, the individual components are described next and the overall rig operation is explained in section 3.1.5.

3.1.1   Pneumatic cylinder

For the set-up shown in Figure 3.1 a Bimba® Position Feedback Cylinder (part number PFC-094-XL) is used. The pneumatic cylinder has one moving component, which is the piston and rod assembly that converts the air-pressurized flow into linear motion. Figure 3.2 details the cylinder which is known as a double-acting pneumatic cylinder that has two ports through which air supply is reversed to cause displacement in both directions.
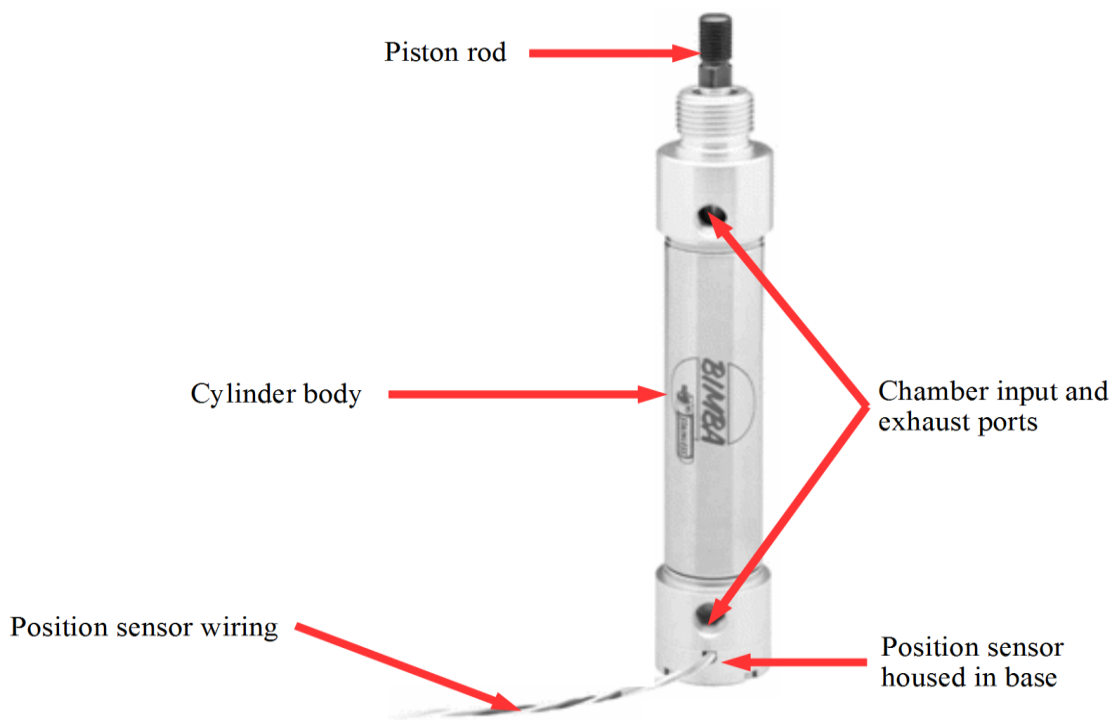
Figure 3.2: The Bimba® pneumatic cylinder

The pneumatic cylinder assembly contains a Linear Resistive Transducer (LRT) mounted in the cylinder rear section. The LRT probe which has a resistive element on one side and a collector strip on the other is contained inside the cylinder rod. A wiper assembly is installed in the piston; this is illustrated in Figure 3.3. As the piston moves, an

electrical circuit is created between the resistive element and collector strip. A variable resistance (approximately 1kΩ per 25mm of stroke) proportional to piston position in the cylinder is produced by the cylinder. The cylinder is set-up to produce an analogue signal compatible with 0-10 VDC PLC analogue inputs. The accuracy of an LRT is determined by three factors: resolution, linearity and repeatability.

- *Resolution* - refers to the smallest change that can be detected on the LRT. The Bimba LRT has infinite resolution. For example, for this project with a 12-bit, 4096-part controller, and the stroke is be divided into 4096 parts. When 10 VDC are placed on the 100mm cylinder, the smallest detectable increment would be 10 VDC ÷ 4096 = 2.4 millivolts or 0.062mm.

- *Linearity* - refers to the maximum deviation of the output voltage to a straight line. The Bimba LRT's linearity is ± 1 percent of stroke (± 1mm).

- *Repeatability* - is the ability of the LRT to provide the same output voltage relative to a unique cylinder position each time the cylinder is cycled. Mechanical repeatability of the Bimba® Position Feedback Cylinder is ± 0.0254mm.

The retaining ring or scraping ring is to prevent dirt particles from entering the components in pneumatic cylinders. The piston seals seal against the inner surface of the cylinder to prevent air leakage.
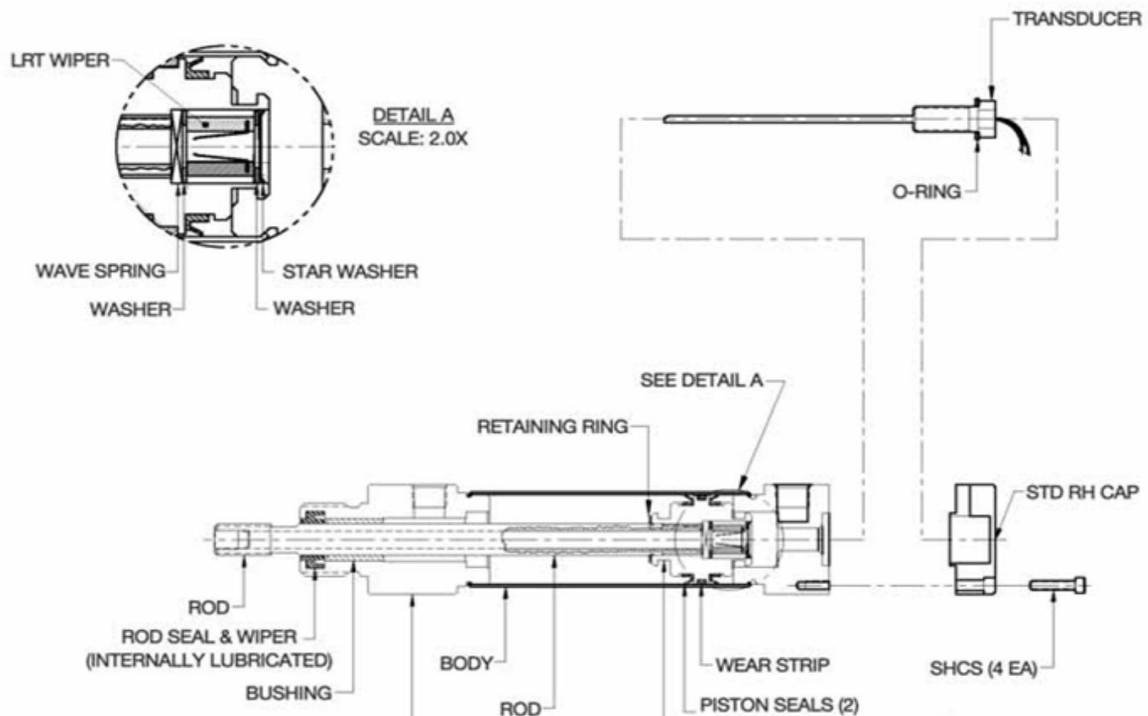
Figure 3.3: The Bimba® Position Feedback Cylinder

3.1.2   *Proportional control valve*

Proportional valves are used for control in pneumatics. For this work a Festo® 5/3-way proportional valve (part number MPYE-5-1/8-LF-010-B) is used to control the cylinder. The proportional valve in Figure 3.1, controls flow in response to an electrical (voltage or current) control signal. The proportional valve can be infinitely and precisely positioned to control the amount, pressure and the direction of the flow of air. The directly actuated proportional directional control valve has a position-controlled spool. This transforms an analogue input signal into a corresponding opening cross-section at the valve outputs. In combination with an integrated control algorithm and displacement sensor, a precise pneumatic positioning system is created. The valve motion is spring-centred. The outlet (exhaust) is located in the mid-position. The exhaust ports are fitted with silencers to reduce noise from exhausted air. A cross-sectional diagram of the valve is shown in Figure 3.4. The technical specifications of the proportional directional control valve are detailed in Appendix (C). This valve has the following features:

- Flow is blocked in the centre position so that the piston can be stopped at any position between the stops.
- The required direction of movement of the piston is preset by controlling the valve accordingly.
- The valve is constantly adjustable (= proportional valve) in order to be able to regulate the flow rate and, thus, the speed of movement of the piston.
- The valve is directly actuated and electrically controlled, with Integrated valve electronics

3.1.3   *Pressure sensor*

In order to detect the pressure in the pneumatic system pressure sensors are used (Figure 3.1). The sensors are located between the proportional valve and pneumatic cylinder chambers. This type of pressure sensor consists of a micro-machined silicon diaphragm with piezo-resistive strain gauges diffused into it, fused to a silicon back-plate. Four resistors are employed within a Wheatstone bridge arrangement, the output of which is directly proportional to the pressure. The resistors have a value of approx. 3.5 kOhm.

Electrical connection   Valve electronics   Plunger-armature drive   5/3-way valve

Load 4   Load 2

5 Exhaust   1   3 Exhaust

Spool valve   Air supply
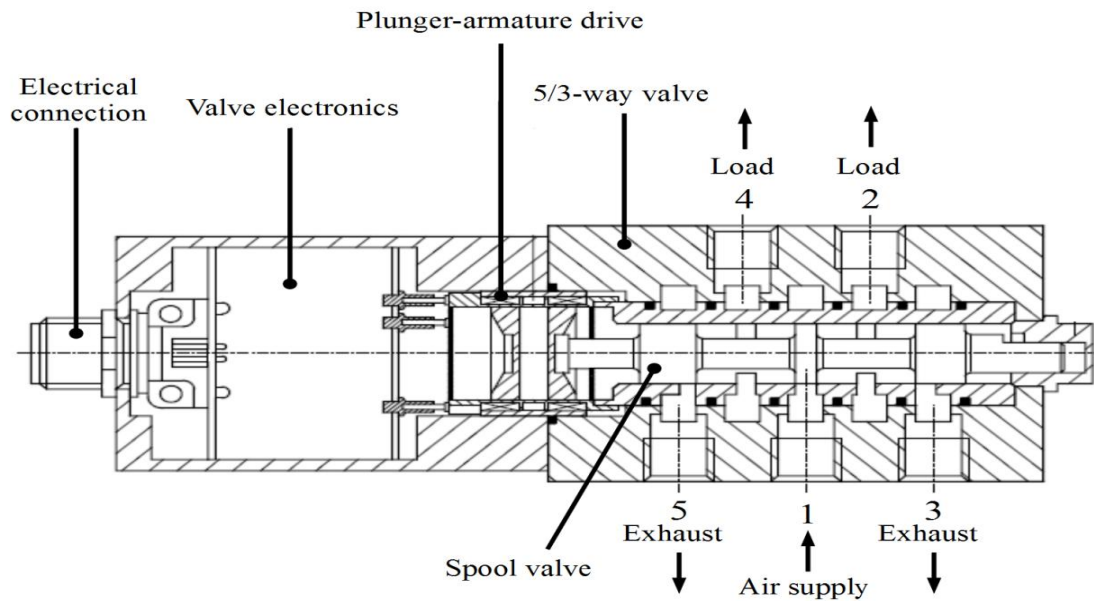
Figure 3.4: 5/3-way directional proportional control valve. Showing the valve closed in its mid-position

3.1.4 Additional test rig components

This includes high pressure piping and the necessary end fixings. In order to induce actual faults associated with pneumatic systems various valves are used (Figure 3.1). These include pressure release valves which are used to induce air loss within a pneumatic system and pressure cut-off valves, which are used to create blockages within a pneumatic system. Electrical power to the rig electrical components is supplied using a 10V and 24V power supply. The compressed air supply is via the main air supply and in order to store a certain amount of compressed air a 5 litre reservoir is used within a 4 bar working pressure range. In order to keep moisture and foreign particles from entering the pneumatic system the air supply is filtered using a 5 micron filter. The Filter set up is a filter/regulator which includes a manual drain relief valve and a pressure gauge to measure regulated air supply pressure.

3.1.5   Single cylinder test rig operation

The set-up of the single cylinder test rig is illustrated schematically in Figure 3.5. In order to move the cylinder piston to the desired position the system requires to the follow the following operation. The desired input is passed from the controller PC (1) to the proportional control valve (2). The proportional valve controls the air flow to the pneumatic cylinder (3) in proportion to the drive voltage received from the controller PC. The proportional valve receives the supply of air from the reservoir (4). The reservoir is used to store air in order to keep the 4bar air supply pressure constant. The reservoir in turn receives air from the main air supply which is regulated and filtered (5). The output of the pneumatic cylinder (position) is measured by the two position sensors, where one is used as a redundant signal (6). This feedback signal is compared with the command signal (demand), and the resulting error signal is used to obtain the control signal. Pressure between the proportional valve and the cylinder chambers is measured using pressure sensors (7). The flow control valves (8) are used to simulate a pressure block within the pneumatic system. The pressure release valves (9) are used to simulate an air leak within the pneumatic system. The pressure release valves and the flow control valves are operated manually.

3.1.6   Data acquisition and control hardware

The set-up (Figure 3.5) shows the xPC Target coupled with Matlab/Simulink, which provides a real-time environment (1). A host and a target computer are connected using a TCP/IP network. Matlab/Simulink is run on the host computer. This is where the control and FDI system is designed using xPC Target I/O blocks. Using external mode the system file is built and compiled within the host computer. Then once compiled it is downloaded to the target computer where it is executed using the real-time kernel. The sampling time for all the experiments is set as a result of the closed-loop bandwidth being measured at 14.3Hz, ideally the sample time should be set to 70 times the closed-loop bandwidth (1kHz). However, due to the capability of the computer the sampling time is set to 0.0025 seconds (400Hz), this is the fastest the computer capability allows. Analogue-to- digital and digital- analogue cards are used to send and receive signals between the target and the system. These boards provide a direct interface to the sensors, actuators, or other devices for real-time control or signal processing applications.
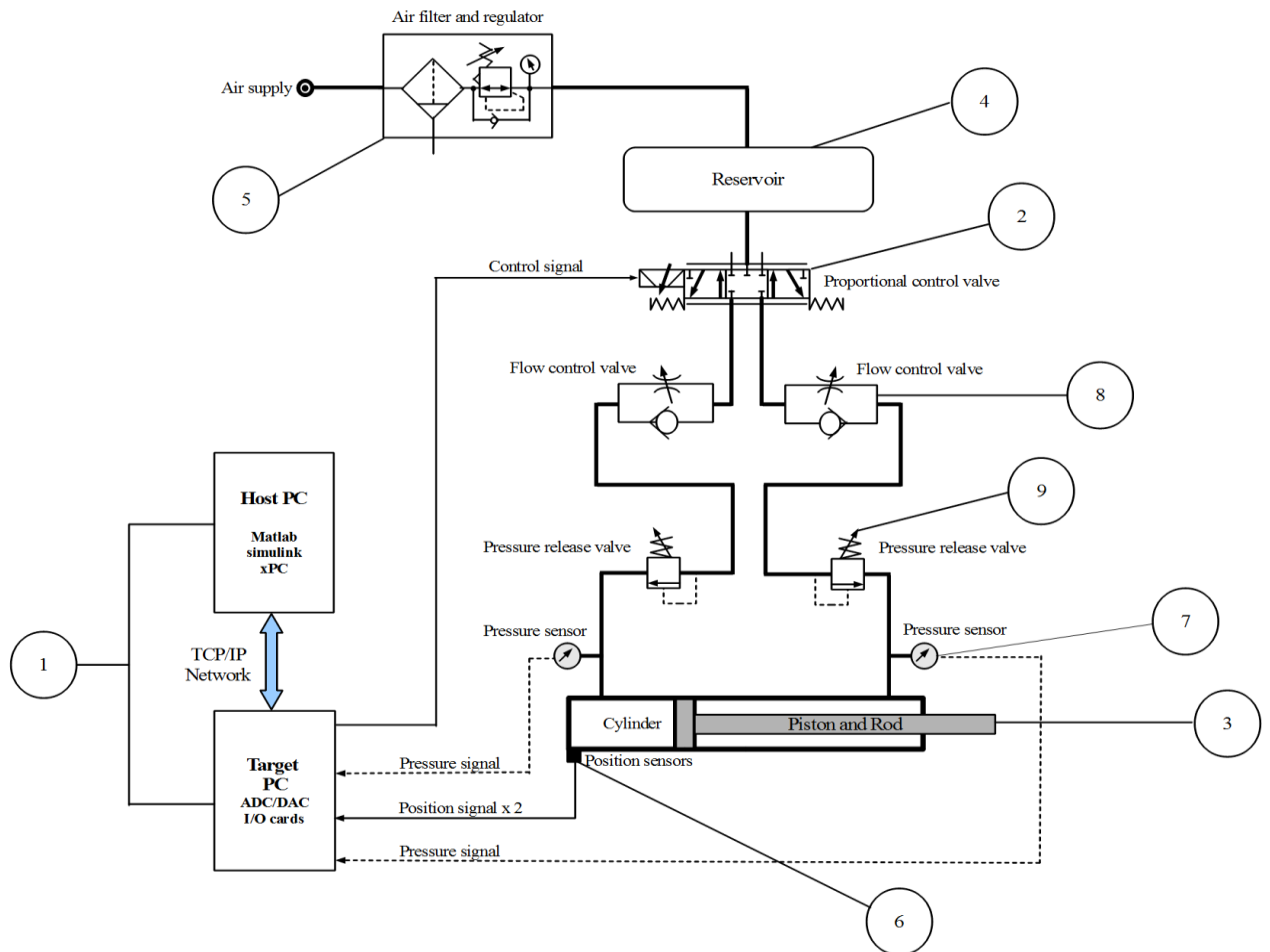
Figure 3.5: Schematic of single cylinder set-up

3.2   *Stewart-Gough platform set-up*

The Stewart platform also known as the "Stewart-Gough" platform was first introduced by Gough and Whitehall (1962) as a tyre-testing machine. This design was then applied by Stewart (1965) as an aircraft simulation mechanism. Since then, a wide variety of applications have benefited from this design. Current industries using the Stewart-Gough platform design include aerospace, automotive, defence, transportation, and machine tool technology. The Stewart-Gough platform design is also used for positioning of satellite communication dishes and telescopes. Shipbuilding and bridge construction also take advantage of this design. The design of the Stewart-Gough platform supports high load-carrying capabilities.

3.2.1. Basic configuration of a Stewart-Gough platform

Stewart-Gough platforms are generally of a mechanical design used mainly for position control. The design is a parallel mechanism consisting of a rigid body mobile plate, connected to a fixed base plate and is defined by at least three stationary points on the fixed (grounded) base connected to six independent legs. The six legs are connected to both the base and top plate by universal/ball joints in parallel located at both ends of the six legs. The legs are designed with an upper body and lower body that can be adjusted. This allows for the length of each leg to be varied. The linear extension and retraction of the six cylinders gives the platform six degrees of freedom positioning capabilities, the six degrees of freedom consisting of three translational and three rotational degrees of freedom. The linear actuation could be typically provided hydraulically, electrically or pneumatically. The great advantage of the Stewart-Gough platform is that no bending forces are applied to its six legs: they are in pure tension or pure compression (Merkle, 1997). For this project, the approach is to apply control to a pneumatic system. The aim is to control the pneumatic actuators (legs) using position control. The linear movement is achieved by varying the applied air pressure to either side of the actuator piston (double acting cylinder). The applied pressure to each side of the actuator piston is controlled through a proportional directional control valve (servo control valve). This device varies the output pressure proportional to the applied voltage. Rotational movement is achieved by attaching universal joints (top) and ball joints (bottom) to each end of the pneumatic actuator. Figure 3.6 shows the Stewart-Gough platform set-up. This illustrates the various component arrangement used to build the test-rig. The pneumatic cylinders used for the Stewart-Gough platform are similar to the one used in the single cylinder set-up (Figure 3.1). A schematic of the Stewart- Gough platform set-up is illustrated in Figure 3.7, where the FDI scheme is only applied to one pneumatic cylinder set-up. However, this can be extended to all six cylinders.
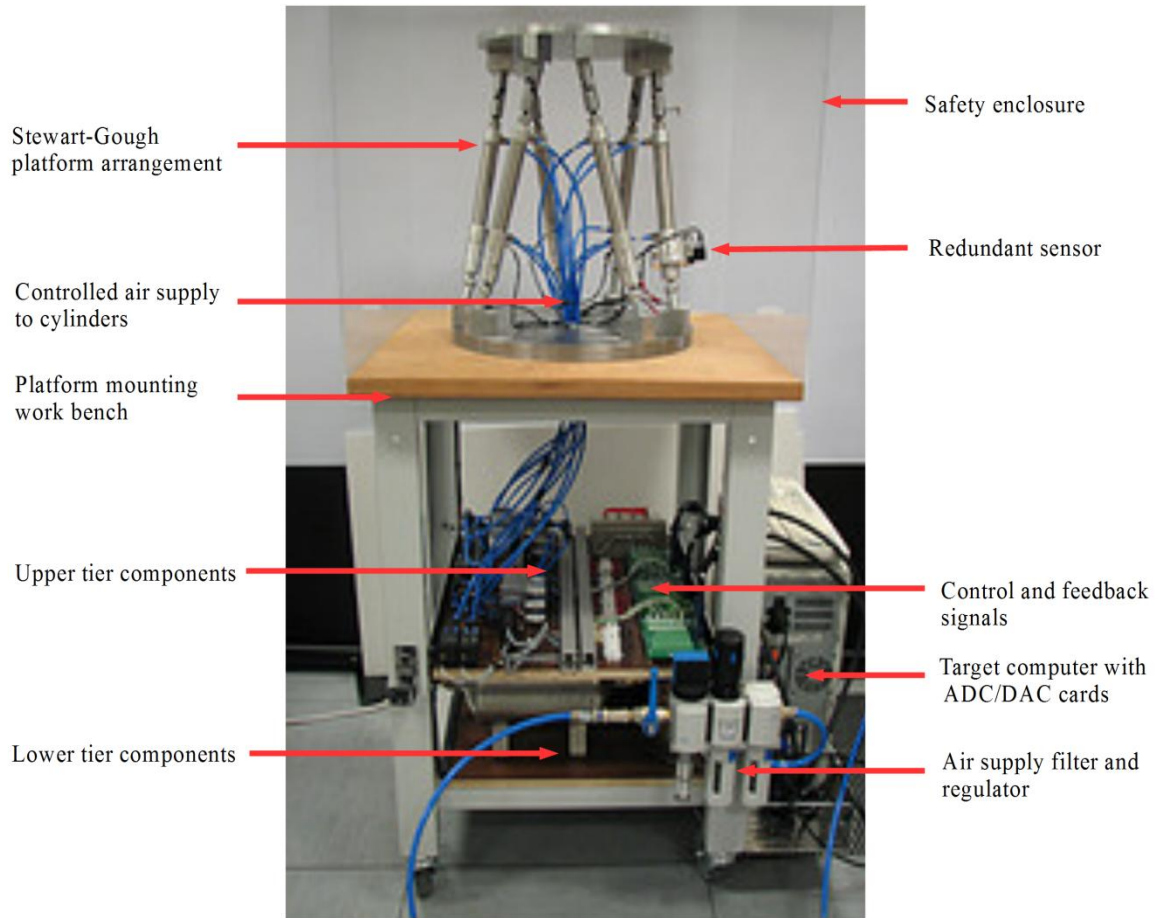
Figure 3.6: Stewart-Gough platform set-up

Although the cylinders and proportional valves used are identical to the ones used in the single cylinder set-up, this section details the components and arrangement (Figure 3.6) for the make-up of the Stewart-Gough platform set-up.
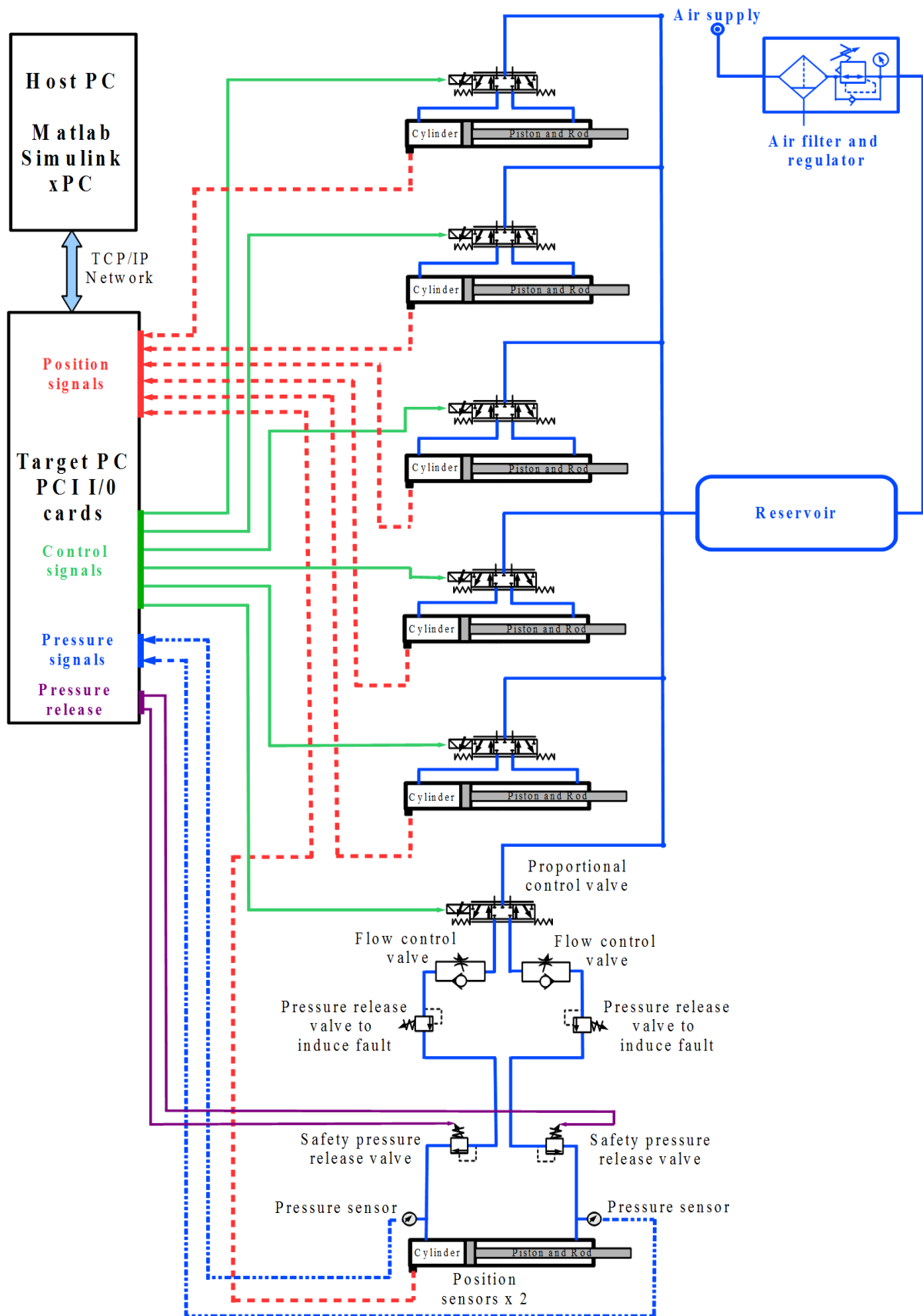
Figure 3.7: Schematic of Stewart-Gough platform set-up

3.2.2. *Top (moveable) plate and attachments*

The top arrangement of the Stewart-Gough platform is shown in Figure 3.8. This shows the top of the pneumatic cylinders attached to universal joints. The universal joints are connected to attachment blocks which in turn are fixed to the top aluminium moveable plate. All three components are assembled using M8 size threaded studs.
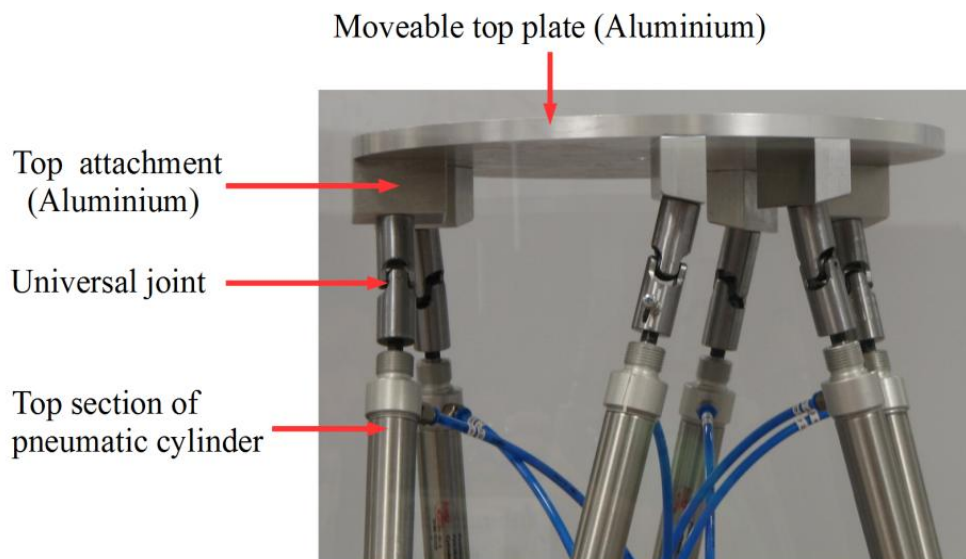
Figure 3.8: Top arrangement of the Stewart-Gough platform

The top plate (Figure 3.9) is manufactured from aluminium and has the dimensions of 300mm diameter, with a thickness of 15mm (The CAD drawings are detailed in Appendix A). The reason for the choice of aluminium for the top plate is to keep the moving component mass reasonably low, which allows the pneumatic cylinders to operate within their normal working range.
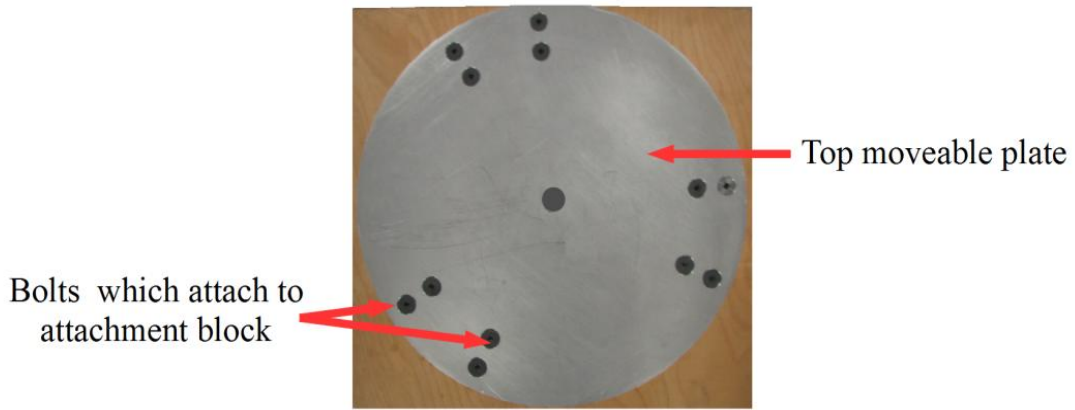
Figure 3.9: Plan view of the top moveable plate

The universal joints (Figure 3.8) are plain bearing type universal joints (Figure 3.10 details the relevant dimensions). The joints are manufactured from steel and are suitable for applications with a maximum speed of 1200rpm. The soft core enables easy machining of the joints to the required diameters. The universal joints have hardened journals with large bearing surfaces which help to reduce wear and prolong the operational life of the joint. The maximum working angle of the universal joint is 40 degrees. These particular types of plain bearing universal joints must be lubricated at regular intervals.
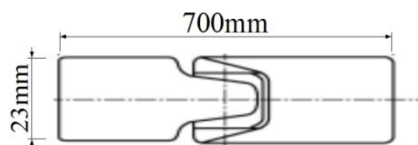
Figure 3.10: Universal joint dimensions

The top attachment blocks (Figure 3.11) are manufactured using aluminium. Three M8 threaded holes are machined to allow attachment to the top plate and universal joints.
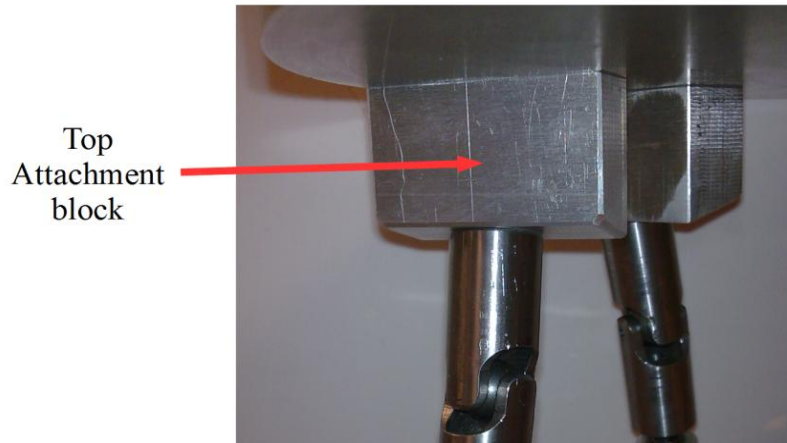
Figure 3.11: Top attachment block

3.2.3. *Base (fixed) plate and attachments*

The base arrangement of the Stewart-Gough platform is illustrated in Figure 3.12. The bases of the pneumatic cylinders are connected via machined attachments to the axial joints which in turn are fixed to attachment blocks. These attachment blocks are then secured to the base steel (fixed) plate.
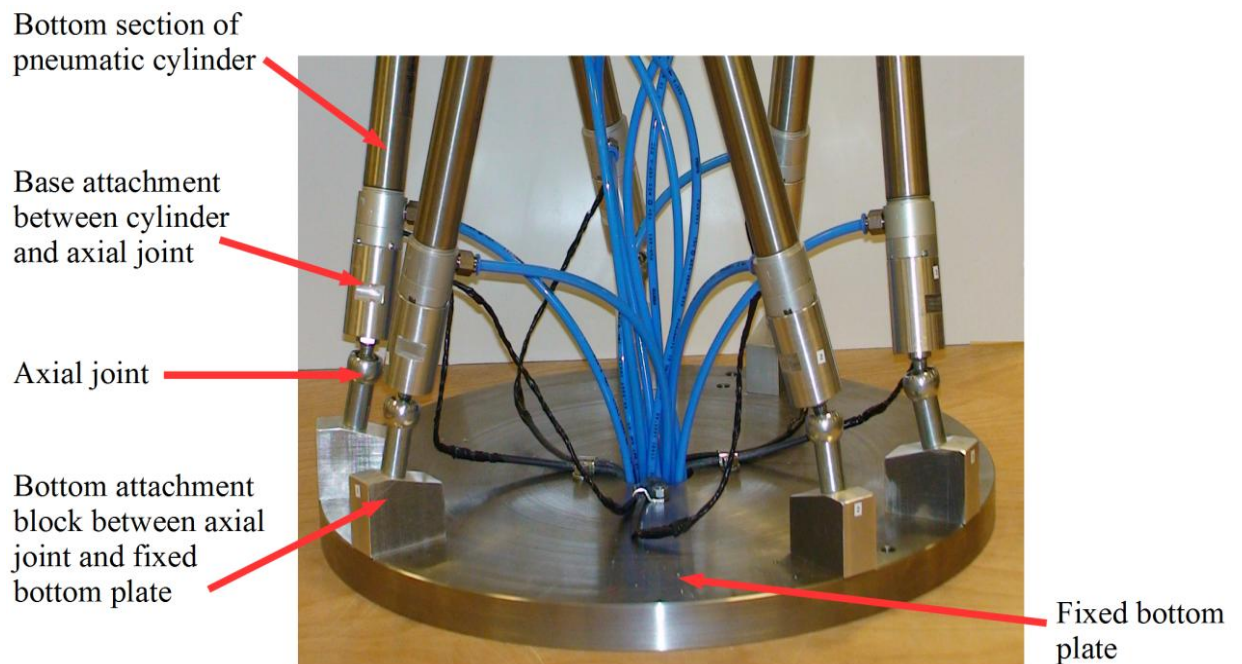
Figure 3.12: Base arrangement of the Stewart-Gough platform

The bases of the pneumatic cylinders are attached to specifically machined base attachments. This allows for the pneumatic cylinders to be connected to the axial joints. Figure 3.13 shows a closer view of this arrangement.
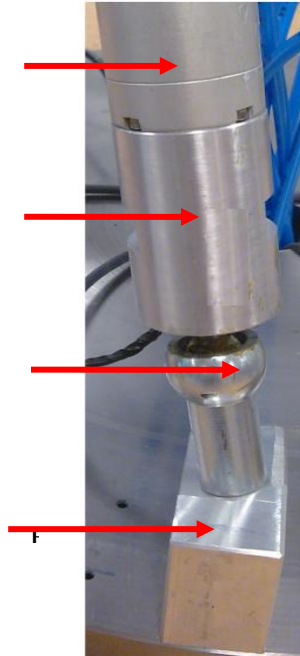
Figure 3.13: Base attachment arrangement

The machined base attachment is manufactured from aluminium (The CAD drawings are detailed in Appendix A). The attachment is secured to the pneumatic cylinder using a machined 7/8-14 UNF thread. The axial joint (part number C 13-M8 RH) is secured using a M10 thread. The axial joint is detailed in Figure 3.14.
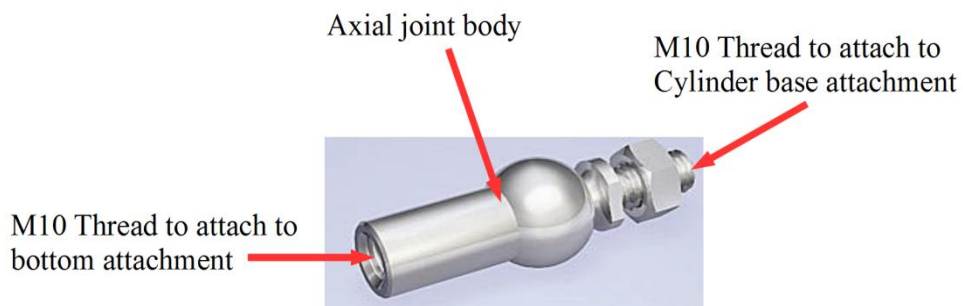
Figure 3.14: The Mbo Obwald GmbH & Co Axial joint

The Axial joint or sometimes called a ball joint is used as it can provide the Stewart-Gough platform freedom of movement with respect to all three Cartesian axes. However, in practice, this is not always true. The motion of the ball joint is always restricted because of its physical dimensions. The axial joint usually includes three main parts; the ball head, socket, and connecting leg (Yang and Lee, 1984). With reference to Figure 3.15, let the radii of the ball head be R_b, and the connecting leg be $d/2$.
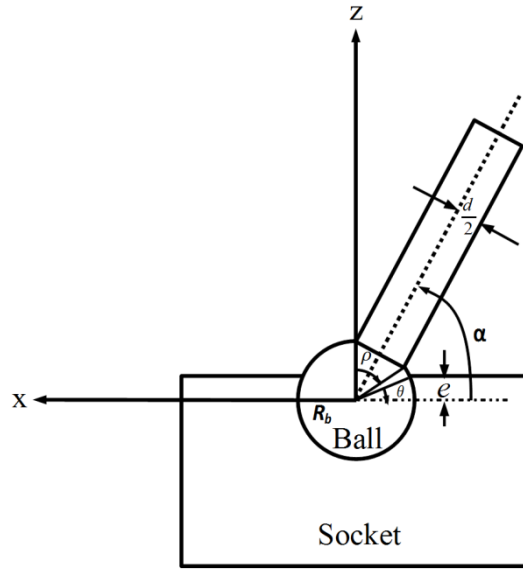
Figure 3.15: The principal cross-section of a ball and socket type joint

To physically hold the ball head in the socket, the holding width e, as shown in Figure 3.15, must be greater than zero. Let α denote the rotation angle of the joint on the *XZ* plane, the rotational limits of the angle α can be determined as follows:

$$\theta = sin^{-1} \frac{e}{R_b} \tag{5}$$

$$\rho = \left(\frac{\pi}{2} - \alpha\right) + sin^{-1} \frac{\frac{d}{2}}{R_b} \tag{6}$$

For free rotation, ρ should be less than or equal to $\pi/2 - \theta$; from equation (5) and (6)

$$\left(\frac{\pi}{2} - \alpha\right) + sin^{-1}\frac{\frac{d}{2}}{R_b} \leq \frac{\pi}{2} - sin^{-1}\frac{e}{R_b} \tag{7}$$

or

$$\alpha \geq sin^{-1}\frac{d}{2R_b} + sin^{-1}\frac{e}{R_b} \tag{8}$$

The complete rotational range of α on the *XZ* plane is then given as

$$\pi - \left(sin^{-1}\frac{d}{2R_b} + sin^{-1}\frac{e}{R_b}\right) \geq \alpha \geq sin^{-1}\frac{d}{2R_b} + sin^{-1}\frac{e}{R_b} \tag{9}$$

Equation (9) can be useful, as it represents the physical constraints of ball joints and provides some practical design guidelines. For the axial joint shown in Figures 3.13-3.14, the rotational limit as specified by the manufacturer is $\alpha = 18$ degrees. Then the total rotational angle is 2α or 36 degrees.

The fixed bottom plate (Figure 3.12) is manufactured from mild steel and has the dimensions of 400mm diameter, with a thickness of 20mm (Figure 3.16). The reason for the choice of mild steel is to provide a rigid base to attach the base components of the rig. The bottom plate is fastened to a solid 'I' section constructed work bench which is shown in Figure 3.6. The work bench has castor type wheels attached to each corner; this allows the whole rig set-up to be moved with increased ease.

The bottom attachment block (Figure 3.13) is machined from aluminium and is attached to the axial joint using a M10 threaded stud. The bottom attachment block is secured to the fixed bottom plate via through bolts.
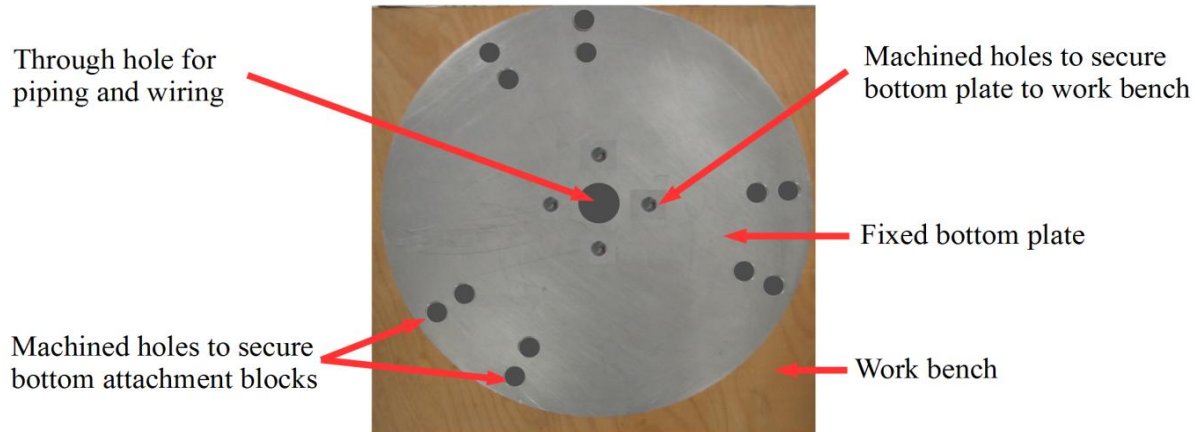
Figure 3.16: Fixed bottom plate arrangement

3.2.4   Redundant sensor arrangement

The experiments are carried out using a redundant sensor. This allows reconfiguration after a primary position sensor fault that could otherwise cause serious damage to the Stewart-Gough platform. Figure 3.17 describes the layout and location of the redundant position sensor within the Stewart-Gough platform.
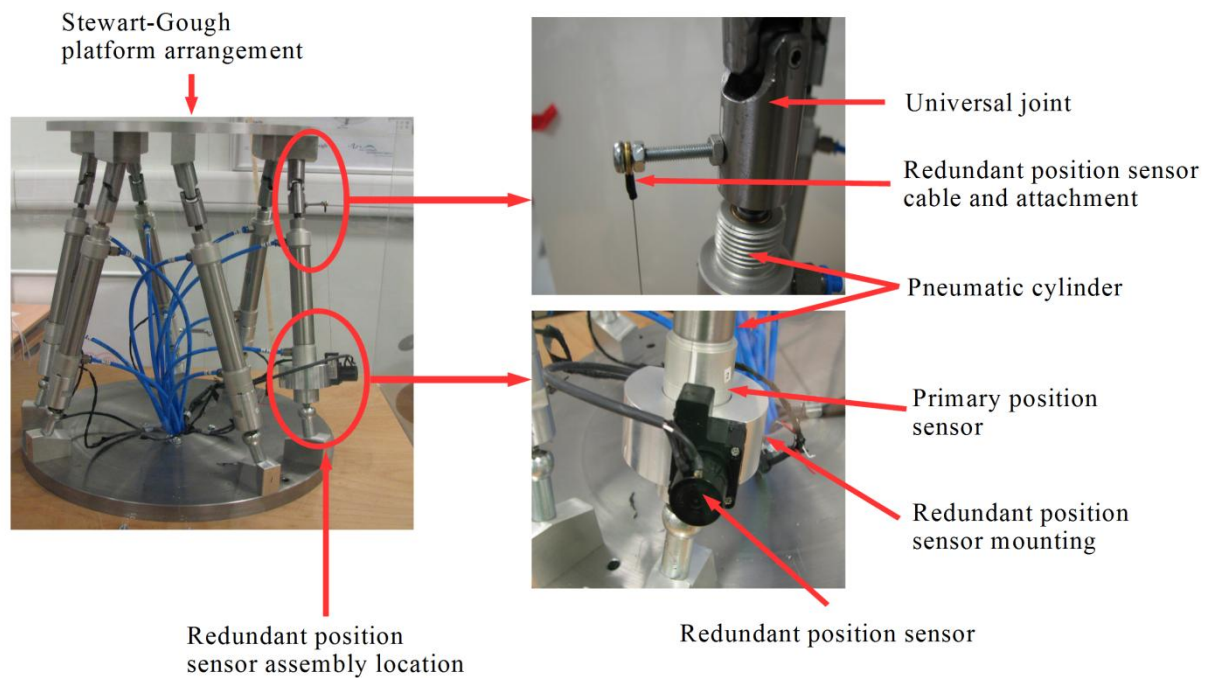
Figure 3.17: Redundant sensor location within platform arrangement.

The components of the Stewart-Gough platform are all located on various sections within the work bench. The work bench (Figure 3.6) is divided into four sections. Namely, (i) the top mounting surface, (ii) the upper tier, (iii) the lower tier, and (iv) side mounting bracket.

3.2.5. Upper tier set-up

Figure 3.18 shows a front view of the upper tier. This shows the upper tier incorporating the proportional servo valves, the pressure release valves, the pressure sensors, the wiring required to send and receive signals to the various components, the air flow valves, the pressure release valves (these include manual and electrically operated), and the fault switches. The fault switches are used to induce faults into the various components (i.e. disconnect position sensor feedback signal, disconnect control signal to proportional valve, and disconnect pressure sensor feedback signals). Figure 3.19 shows a side view of the upper tier and Figure 3.20 shows a schematic of the upper tier layout.
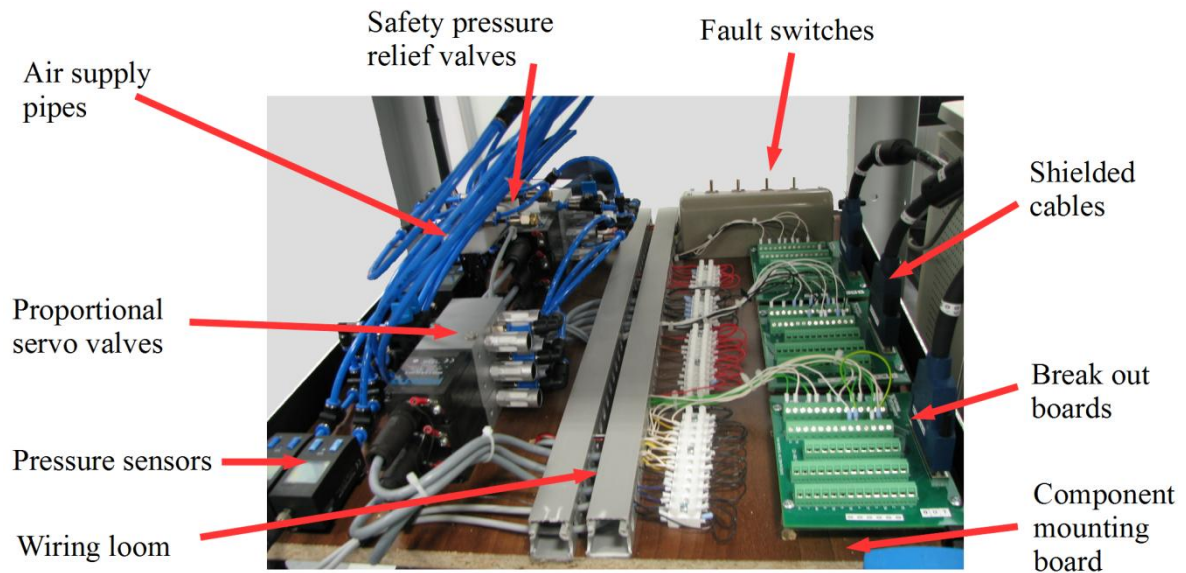
Figure 3.18: Upper tier component set-up front view
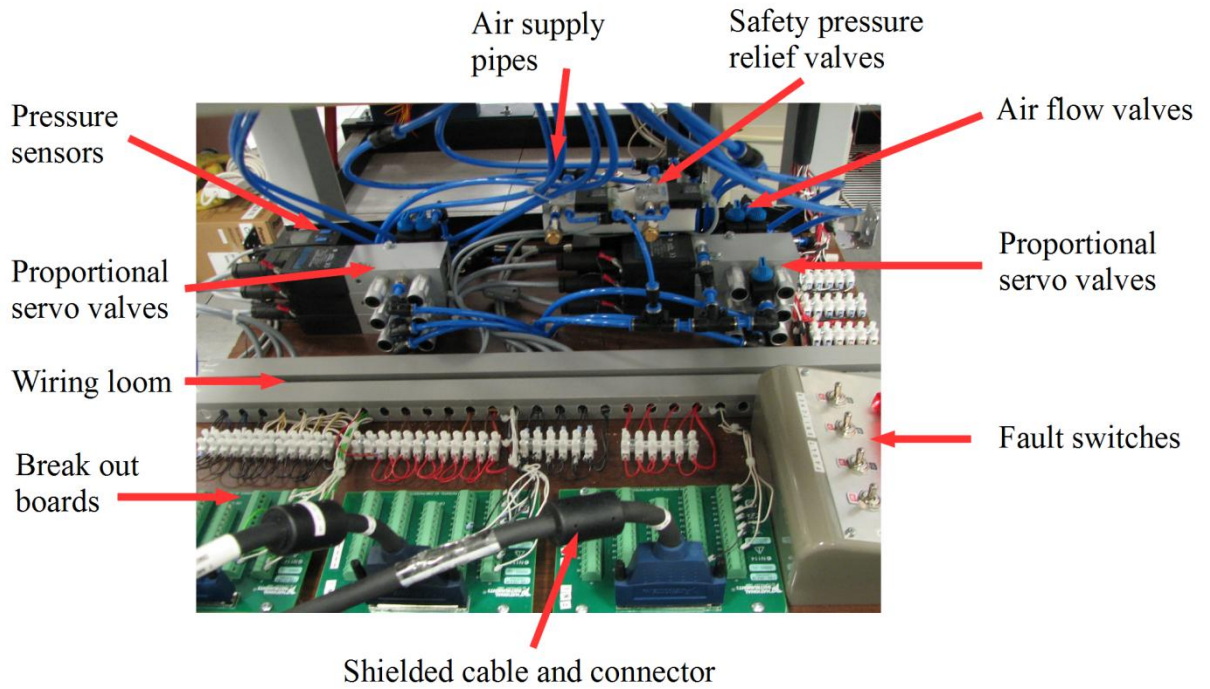
Figure 3.19: Upper tier component set-up side view
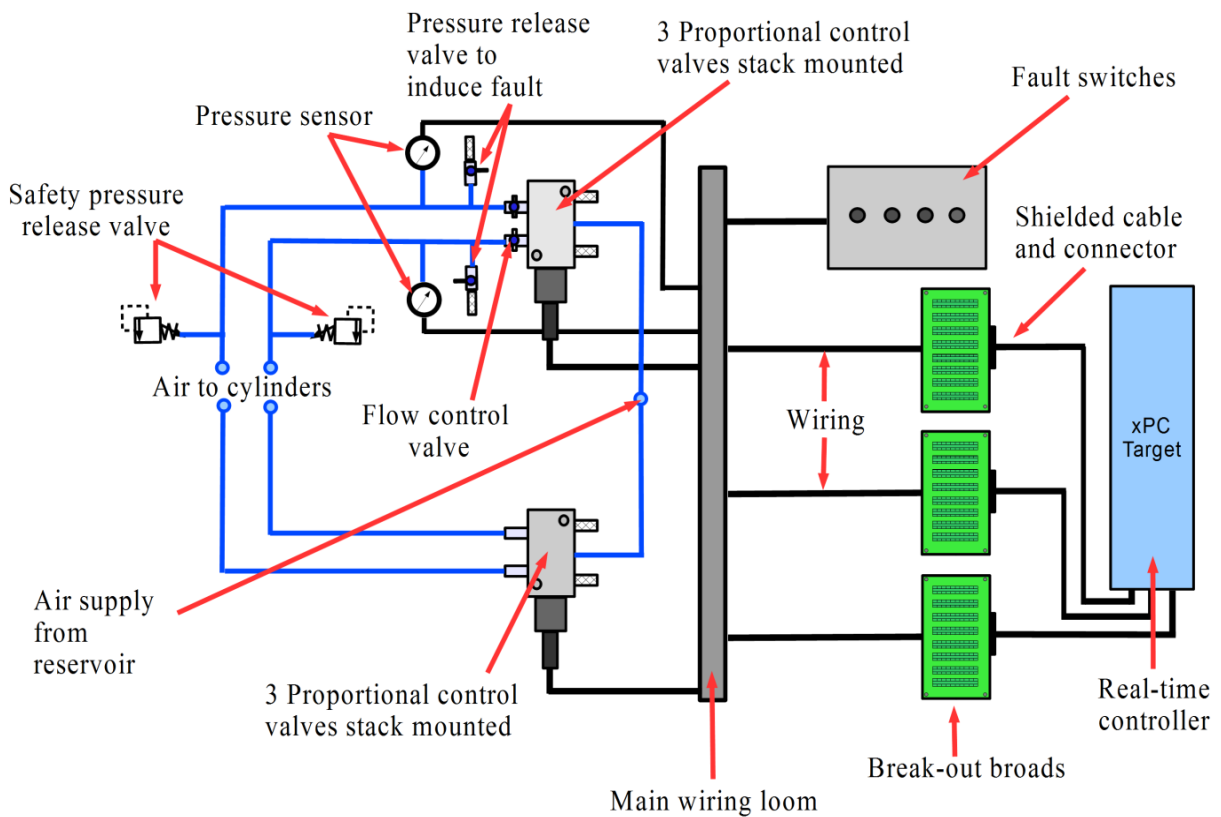
Figure 3.20: Schematic of the upper tier layout

Shown in Figures 3.19-3.20, the air flow valves are used to induce blockage type faults which may occur within a pneumatic system. The valves are used to induce a blockage in each chamber of the pneumatic cylinder. Figure 3.21 illustrates where the valve are located within the air supply system. The positioning of the air flow valves in the single cylinder test-rig and Stewart-Gough platform are also shown schematically in Figures 3.2 and 3.7 respectively.
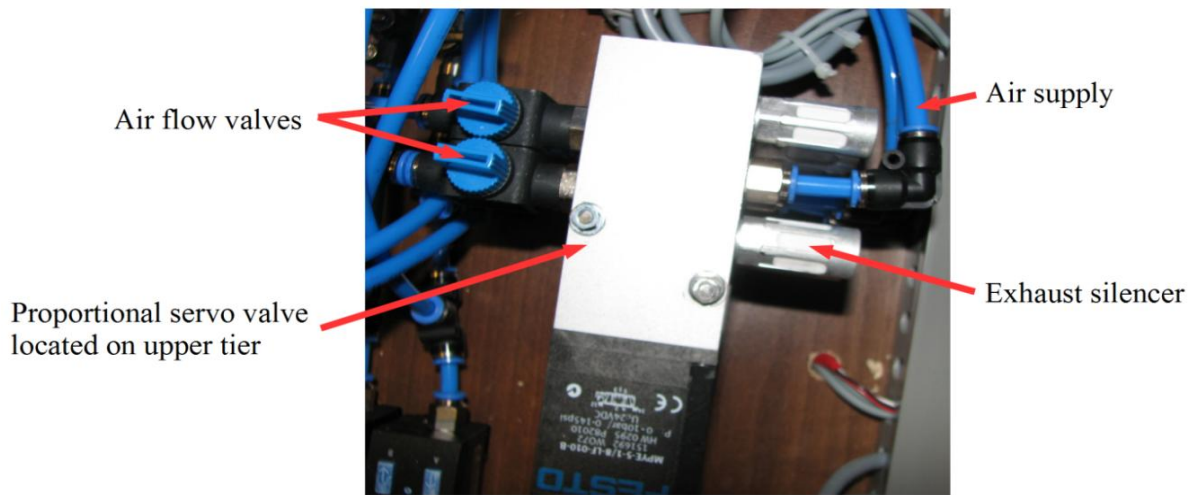
Figure 3.21: Location of air flow valves

In order to induce leak faults, manually operated pressure release valves are used. Figure 3.22 depicts where the release valves are positioned within the air supply system. The positioning of the release valves in the single cylinder test-rig and Stewart-Gough platform are also shown schematically in Figures 3.2 and 3.7 respectively.
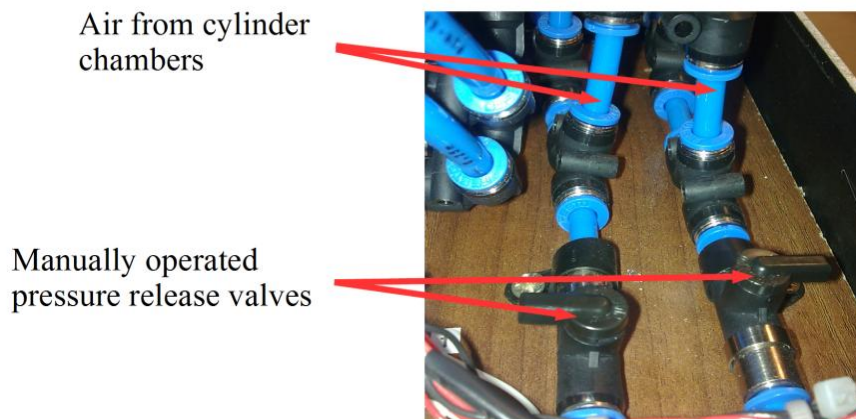
Figure 3.22: Location of manually operated pressure release valves

The safety pressure release valves are shown in Figures 3.18 and 3.19. These valves are incorporated as part of the fault tolerant scheme. Basically, the valves are used within the safety mode sequence. Whereby, if certain faults are detected which may result in the Stewart-Gough platform becoming unsafe, the pressure release valves are activated. The control and application of the safety release valves is outlined in chapter 7. This describes what fault scenarios trigger/activate the safety release valves into operation. Figure 3.23 shows a detailed view of the safety release valves set-up. The general technical specifications of the safety release valves are detailed in Appendix C.
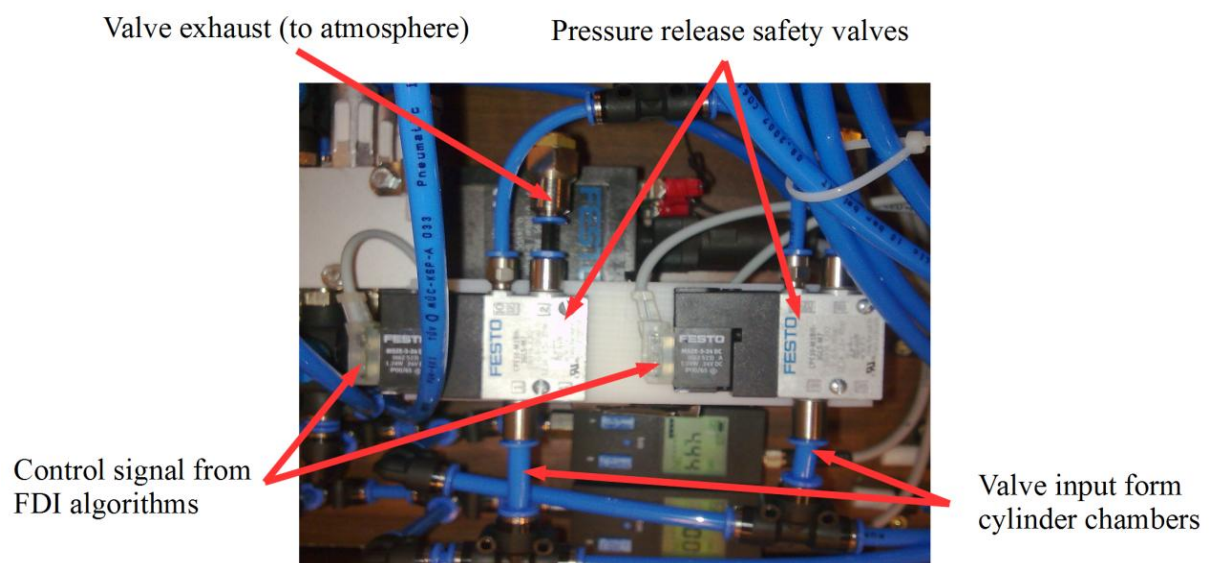
Figure 3.23: Safety release valves

3.2.6   *Lower tier arrangement*

The lower tier's location within the work bench is shown in Figure 3.6. The arrangement of the lower tier components are shown in Figure 3.24. This shows the lower tier incorporating the filter/ regulator housing, the air reservoir, the electrical power supplies, and the safety release valve switch and amplifier. Figure 3.25 shows a close-up of the reservoir and air supply connections. The arrangement is illustrated schematically in Figure 3.26. The compressed air supply is via the main air supply and in order to store a certain amount of compressed air a 5 litre reservoir is used within a 4 bar working pressure range. In order to keep moisture and foreign particles from entering the pneumatic system the air supply is filtered using a 5 micron filter. Electrical power to the rig electrical

components is supplied using 10V and 24V power supplies. Where the 10V supply is to power the position sensors and the 24V supply is to provide power to both proportional servo valves, pressure sensors, and safety pressure release valves.
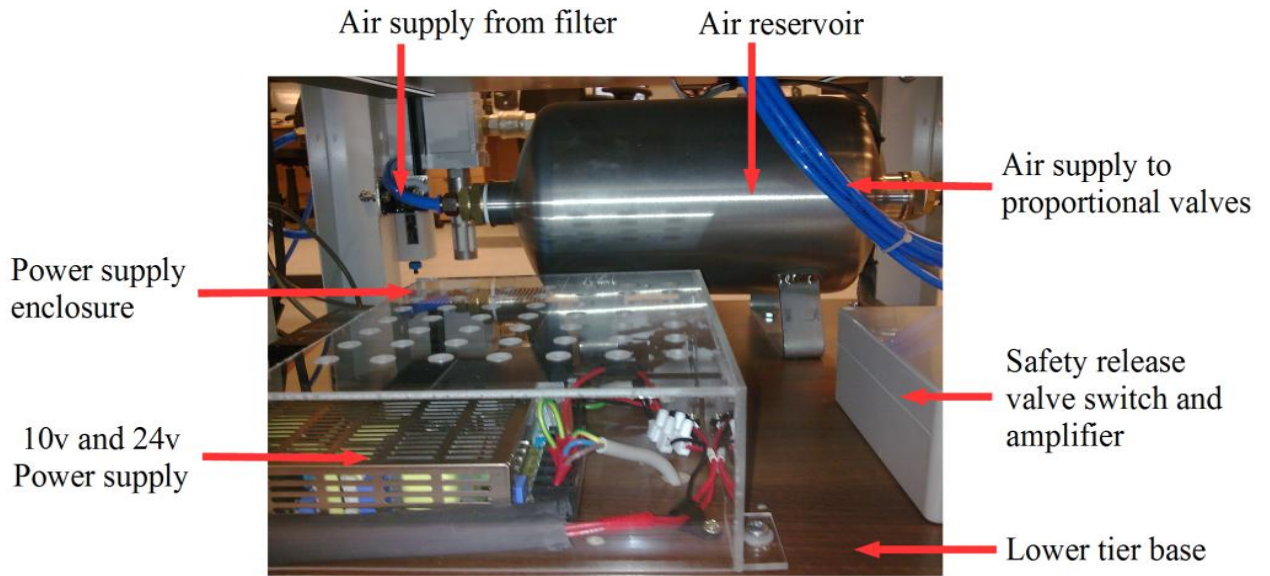
Figure 3.24: Shows the lower tier arrangement
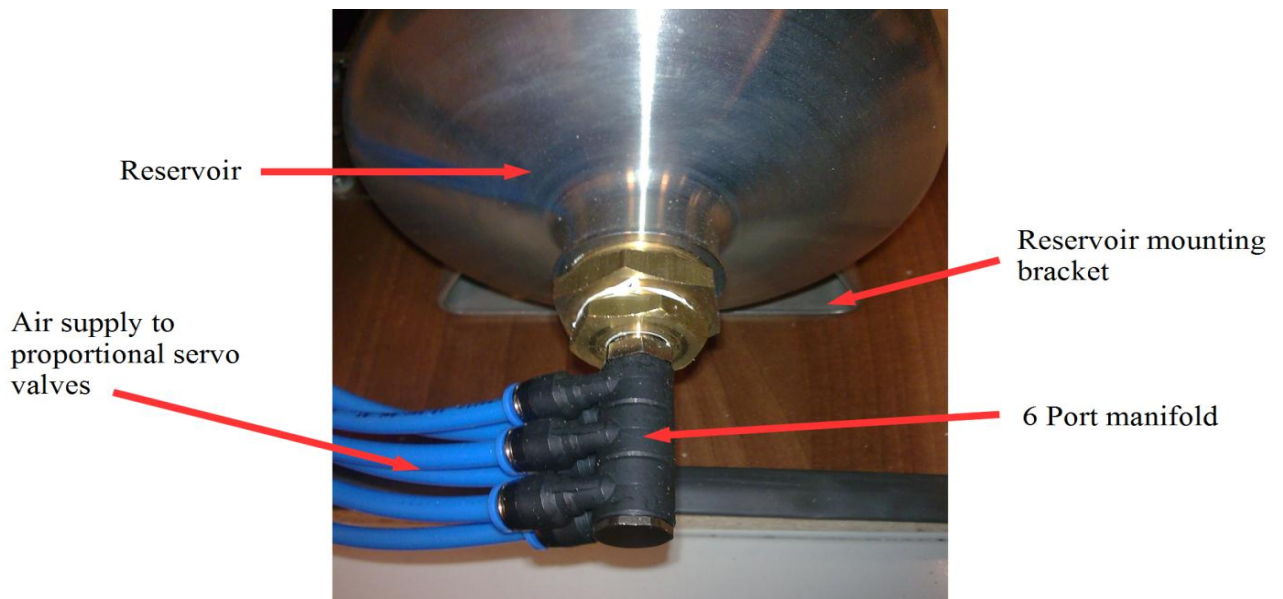
Figure 3.25: Reservoir and air supply manifold
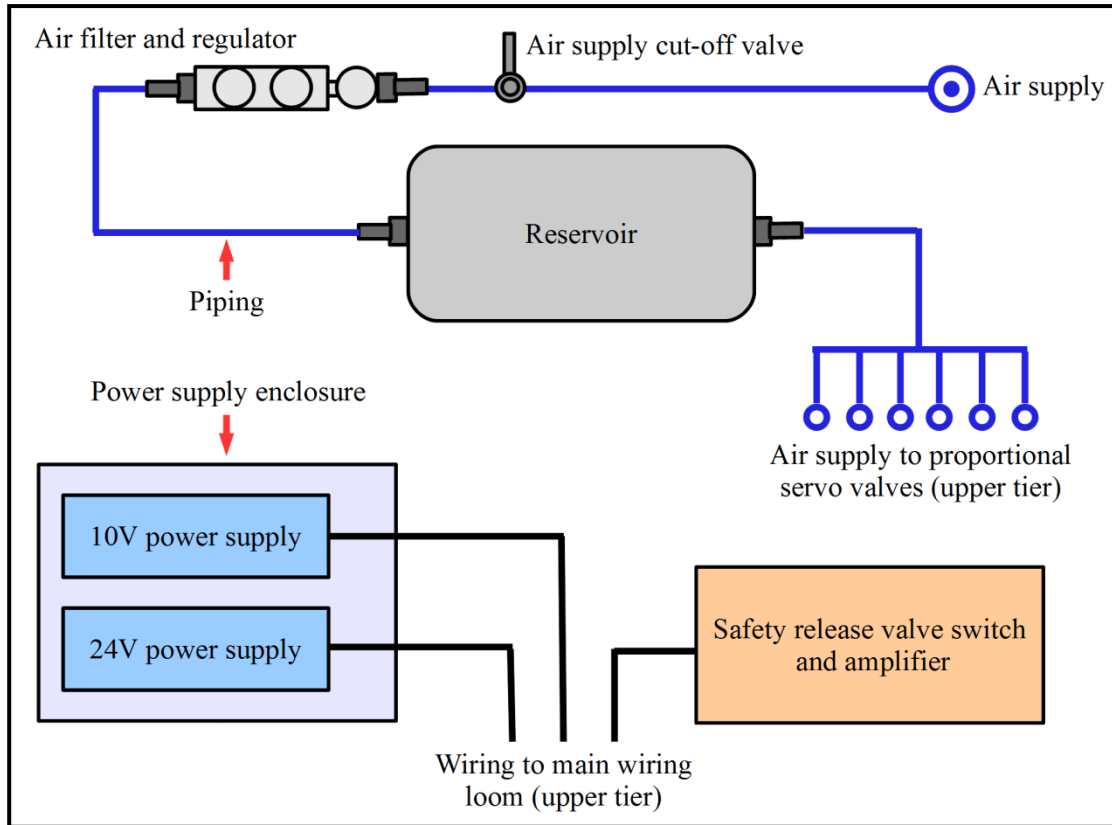
Figure 3.26: Schematic of the lower tier layout

3.2.7 Side mounting bracket

The side mounting bracket is attached to the main work bench frame. The side mounting bracket is used to house the target PC. With this arrangement the whole rig set-up can be made mobile excluding the host PC. However, if a laptop computer is used as the host computer, then this can be included as part of the mobile test-rig. Figure 3.27 illustrates the side mounted target PC arrangement.
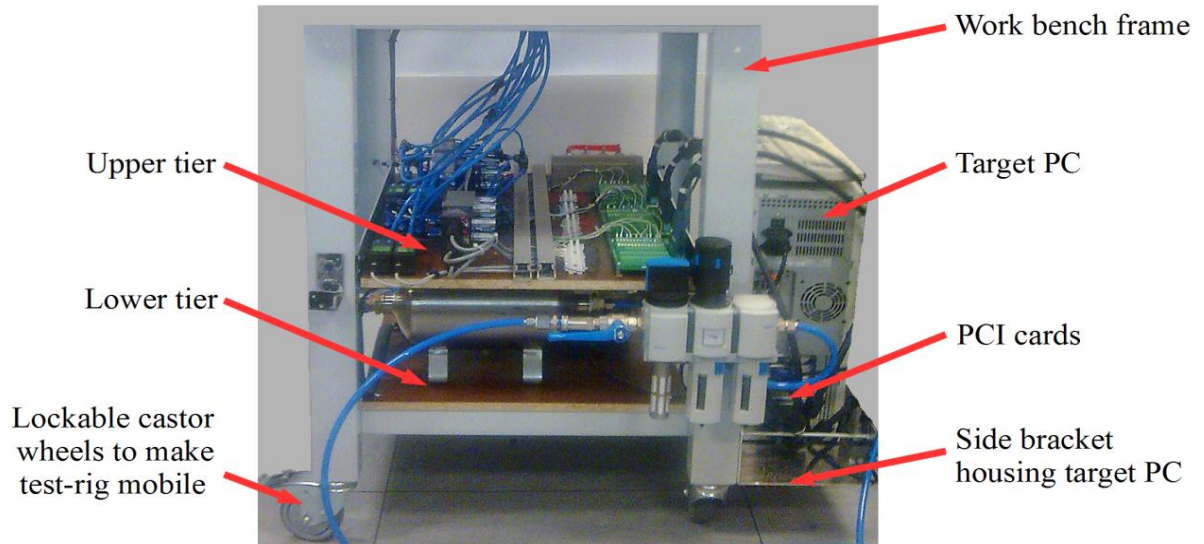
Figure 3.27: Side bracket arrangement

3.3. Conclusion

This chapter has detailed the experimental test rigs used for the experiments for the purpose of building a fault detection and fault isolation scheme. Two types of test rig set-ups have been discussed. These include (i) the single cylinder set-up and (ii) the Stewart-Gough platform set-up. The chapter defined the components used for both test-rigs and described their layouts and operation in detail. The single cylinder test rig will be used to design the initial fault detection and isolation scheme. The designing process includes designing and validating various control schemes for a single actuator set-up. The main reasons for using a single cylinder set-up is so a modular designed scheme can be applied using the single cylinder set-up, then apply this modular design to each cylinder of the Stewart-Gough platform arrangement. The control and kinematic equations that govern the movement of the Stewart-Gough platform are detailed in Chapter 6.

Chapter 4

System modelling

4.1. Introduction

The word *pneumatics* is a derivative of the Greek word *pneuma,* which means air, wind, or breath. Pneumatics can be defined as that branch of engineering science that pertains to gaseous pressure and flow. Pneumatics is the portion of fluid power in which compressed air, or other gas, is used to transmit and control power to actuating mechanisms. Some basic principles of pneumatics are that gases differ from liquids in that they have no definite volume; that is, regardless of size or shape of the vessel, a gas will completely fill it. Gases are highly compressible, while liquids are only slightly so. Also, gases are lighter than equal volumes of liquids, making gases less dense than liquids. Gases can be readily compressed and are assumed to be perfectly elastic. This combination of properties gives gas the ability to yield to a force and return promptly to its original condition when the force is removed. These are the properties of air that are used in pneumatic tyres, tennis balls, and other deformable objects whose shapes are maintained by compressed air.

To explain the compressibility of gases, consider the container shown in Figure 4.1 as containing a gas. At any given time, some molecules are moving in one direction, some are travelling in other directions, and some may be in a state of rest. The average effect of the molecules bombarding each container wall corresponds to the pressure of the gas. As more gas is pumped into the container, more molecules are available to bombard the walls, thus the pressure in the container increases. Increasing the speed with which the molecules hit the walls can also increase the gas pressure in a container. If the temperature of the gas is raised, the molecules move faster, causing an increase in pressure.

Pneumatic technology plays an important role in applications of modern industrial mechatronic systems. Pneumatics offers in many cases a cost-effective solution(s) for a wide range of intelligent motion applications. In most cases, applications of pneumatic actuators require only point-to-point control. Pneumatic actuators give suitable solutions for quickly transporting materials between workstations and for movements in automatic control and flexible manufacturing systems. However, if pneumatic actuators are given precision tracking ability in addition to their light weight, cleanliness, high-speed, and

simple working mechanism they can be used for many robot and medical applications. In this chapter the mathematical model of the pneumatic system is formulated and described in section 4.2. Section 4.3 describes the model parameters and in section 4.4 the model validation is described by directly comparing the model to the actual system.
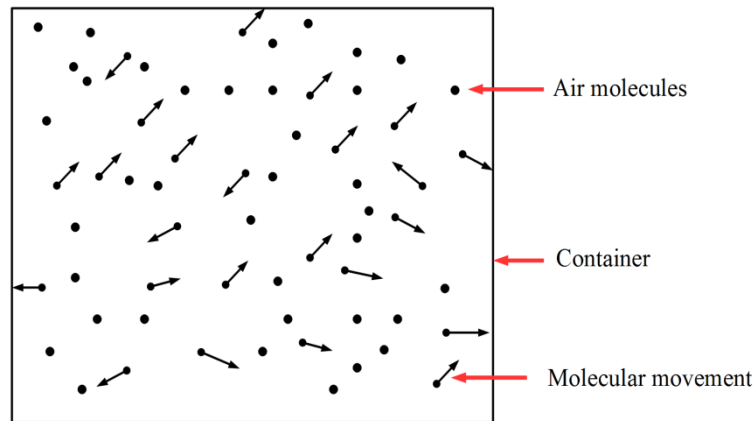
Figure 4.1: Molecular bombardment creating pressure

4.2. *Modelling of pneumatic system*

An early attempt to analyse pneumatic systems was reported by Shearer (1956). This was further extended by Burrows (1969), and Scavarda *et al* (1987). One of the main problems in pneumatic actuator position control is the highly non-linear equations that model the system. Of course these can be linearized for use within a restricted (linear) operating range. However, using approximations of the model allows the use of a restricted range of the optimum parameters that are selected with classical methods (Chillari *et al,* 2001).

In order to model an approximate linear transfer function, describing the dynamics of the pneumatic system shown in Figure 4.2 the thermodynamic analysis of the system is initially presented. The subsequent description model is comparable to that which is presented in (Kaitwanidvilai and Parnichkun, 2005; Lee *et al*, 2001; Hamiti *et al* 1996; and Grewal *et al* 2008). The dynamic model derived is developed based on the relationship between (i) the air mass flow rate and the pressure changes in the cylinder chambers, and (ii) the equilibrium of the forces acting at the piston, including the friction forces.
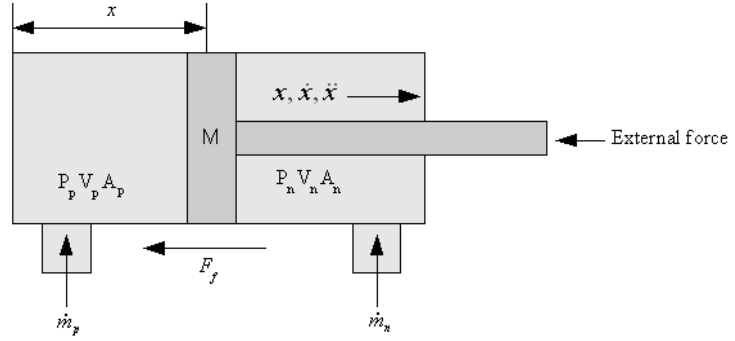
Figure 4.2: Schematic of the double acting cylinder.

Certain assumptions are considered for the construction of the model these include:

- The air is a perfect gas[2].
- Homogeneous (uniform) pressure and temperature in both chambers.
- Supply pressure variation not considered.
- Air loss is not considered.
- System undergoes an adiabatic process (the rate of heat exchange through the system boundary is ignored).

4.2.1. *Valve model*

From Lee *et al* (2001); and Grewal *et al* (2008) the following equation can express the mass flow rate through an orifice

$$\dot{m} = A_C \lambda_2 \frac{P_u}{\sqrt{RT_s}} \, f\left(\frac{P_d}{P_u}\right) \tag{10}$$

Where $\dot{m}$, P_u, P_d, R and T_s are the mass flow rate, pressures at the input and output ports (upstream and down stream), the gas constant and the absolute temperature respectively. A_c is the effective area of the valve orifice, which changes according to spool position. In Equation (10) the flow function f has the following expression:

---

[2] A perfect gas is one in which intermolecular forces are negligible due to the separation of the molecules and any particle collisions are elastic.

$$f\left(\frac{P_d}{P_u}\right) = \begin{cases} \frac{\lambda_1}{\lambda_2}\sqrt{(P_r)^{2/\gamma} - (P_r)^{(\gamma+1)/\gamma}}, & P_r > P_{Crit} \\ 1, & P_r < P_{Crit} \end{cases} \tag{11}$$

with

$P_r = P_d / P_u$

where γ is the ratio of specific heat (air: 1.4) and P_{Crit} is the critical pressure ratio having the following expression:

$$P_{Crit} = \left(\frac{2}{\gamma+1}\right)^{\frac{\gamma}{\gamma-1}} = 0.528 \tag{12}$$

For sonic and subsonic cases, where λ_1 and λ_2 are the constants given by

$$\lambda_1 = \sqrt{\frac{2\gamma}{\gamma-1}} = 2.645, \tag{13}$$

$$\lambda_2 = \sqrt{\gamma\left(\frac{2}{\gamma+1}\right)^{(\gamma+1)/(\gamma-1)}} = 0.684, \tag{14}$$

4.2.2. Cylinder model

The following equation is applicable to each of the cylinder chambers, assuming isentropic (without change in entropy[3]) behaviour of air.

$$P\left[\frac{V}{m}\right]^{\gamma} = \text{Constant} \tag{15}$$

---

[3] Entropy is a measure of the number of random ways in which a system may be arranged; often taken to be a measure of "disorder". Increases in entropy correspond to irreversible changes in a system, reducing the system's ability to do work as energy is lost to irretrievable heat.

Where *P*, *V* and *m* are pressure, volume, and mass of air in cylinder. Differentiating equation (15) with respect to time gives:

$$\dot{P}V + \gamma P\dot{V} = \left[\frac{\dot{m}}{m}\right]PV \tag{16}$$

Using equation (16) and the ideal gas law[4]

$$PV = mRT_s \tag{17}$$

A relationship between cylinder pressure and mass flow rate into the cylinder is obtained

$$\dot{P}V + \gamma P\dot{V} = \gamma \dot{m}RT_s \tag{18}$$

The relationship between the air mass flow and the pressure changes in the chambers is obtained using energy conservation laws (first law of thermodynamics), and the force equilibrium is given by Newton's second law. The relationship between the mass flow rate of air and the change of both pressure and volume in chambers can be written as:

$$\dot{m}_p = \frac{V_p}{\gamma RT_s}\frac{dP_p}{dt} + \frac{P_p}{RT_s}\frac{dV_p}{dt} \tag{19}$$

$$\dot{m}_n = \frac{V_n}{\gamma RT_n}\frac{dP_n}{dt} + \frac{P_n}{RT_s}\frac{dV_n}{dt} \tag{20}$$

P_p is the pressure in chamber *p*, P_n is the pressure in chamber *n*, V_p is the air volume in chamber *p*, V_n is the air volume in chamber in *n*, T_s is the operating temperature, $\dot{m}_p$ is the mass flow rate into chamber *p*, $\dot{m}_n$ is the mass flow rate into chamber *n*, γ is the ratio of specific heat, and *R* is the universal gas constant. The dynamics of the cylinder motion can be described by:

$$M\ddot{x} + F_f\dot{x} = A_pP_p - A_nP_n \tag{21}$$

where *M* is the piston mass, A_p is the area of the piston in chamber *P* , A_n is the area of the piston in chamber *n*, *x* is the position of the piston, and F_f represents the viscous friction coefficient and coulomb friction force.

---

[4] The Ideal gas law is the equation of state of a hypothetical ideal gas. It is an approximation to the behaviour of many gases under many conditions.

Equations (19)-(21) describe the non-linear mathematical model of the pneumatic system. To linearize the system, a small deviation from the initial equilibrium point is considered. The linearization is made at the equilibrium point (initial point of the linearization process), the pressure in the working chambers and their capacity undergo small changes. At this point the actuator has the following initial conditions: $x = 0, \dot{x} = 0, \ddot{x} = 0$, and $P_p = P_n$. These conditions designate that the piston moves a small distance closer to its centre position (50mm), the pressure in the working chamber only differ slightly from the initial value. The values of the state variables are $x=0$, $P_p = P_{p0}$, $P_n = P_{n0}$, $V_p = V_{p0}$, $V_n = V_{n0}$. Rewriting Equations (19)-(21) gives-

$$M\Delta\ddot{x} + F_f\Delta\dot{x} = A_p\Delta P_p - A_n\Delta P_n \tag{22}$$

$$\Delta\dot{m}_p = \frac{V_p}{\gamma RT_s}\Delta\dot{P}_p + \frac{P_p}{RT_s}\Delta\dot{V}_p \tag{23}$$

$$\Delta\dot{m}_n = \frac{V_n}{\gamma RT_n}\Delta\dot{P}_n + \frac{P_n}{RT_s}\Delta\dot{V}_n \tag{24}$$

where Δ denotes the small deviation value. The mass flow rate is identical (in magnitude) for both chambers and is proportional to the valve input voltage. Hence

$$\Delta\dot{m}_p = K\Delta v \quad \text{and} \quad \Delta\dot{m}_n = -K\Delta v \tag{25}$$

where K is the servo valve constant (kg.s^{-1}.V^{-1}) determined from the valve's data-sheet. By simple volume equation

$$\Delta\dot{V}_p = A_p\Delta\dot{x} \quad \text{and} \quad \Delta\dot{V}_n = -A_n\Delta\dot{x} \tag{26}$$

Substituting equation (25) and (26) into equation (23) and (24), then rearranging the equations for pressures in the chambers gives:

$$\Delta\dot{P}_p = -\frac{\gamma A_p P_p}{V_p}\Delta\dot{x} + K\frac{\gamma RT_s}{V_p}\Delta v \tag{27}$$

$$\Delta\dot{P}_n = \frac{\gamma A_n P_n}{V_n}\Delta\dot{x} - K\frac{\gamma RT_s}{V_n}\Delta v \tag{28}$$

Then rearranging equation (22) gives:

$$\Delta\ddot{x} = \frac{A_p\Delta P_p - A_n\Delta P_n}{M} - \frac{F_f}{M}\Delta\dot{x} \tag{29}$$

Equations (27), (28) and (29) can be represented in state space form (Equation 30), or block diagram (see Figure 4.3) form. The Simulink model representation of the pneumatic system is shown in Figure 4.4. The assumed state variables are pressure in chamber (p), pressure in chamber (n), position (x) and velocity($\dot{x}$).

$$X = \begin{bmatrix} \Delta P_p, & \Delta P_n, & \Delta x, & \Delta\dot{x} \end{bmatrix}^T$$

where

$$\dot{X} = AX + Bu \text{ and } y = CX + Du$$

$$\begin{bmatrix} \dot{P}_p \\ \dot{P}_n \\ \dot{x} \\ \ddot{x} \end{bmatrix} = \begin{bmatrix} 0 & 0 & 0 & -\dfrac{\gamma A_p P_p}{V_p} \\ 0 & 0 & 0 & \dfrac{\gamma A_n P_n}{V_n} \\ 0 & 0 & 0 & 1 \\ \dfrac{A_p}{M} & \dfrac{-A_n}{M} & 0 & \dfrac{-F_f}{M} \end{bmatrix} \begin{bmatrix} \Delta P_p \\ \Delta P_n \\ \Delta x \\ \Delta\dot{x} \end{bmatrix} + \begin{bmatrix} K\dfrac{\gamma RT_s}{V_p} \\ -K\dfrac{\gamma RT_s}{V_n} \\ 0 \\ 0 \end{bmatrix}\Delta v$$

$$\tag{30}$$

$$y = \begin{bmatrix} 0 & 0 & 1 & 0 \end{bmatrix}\begin{bmatrix} \Delta P_p \\ \Delta P_n \\ \Delta x \\ \Delta\dot{x} \end{bmatrix} + \begin{bmatrix} 0 \end{bmatrix}\Delta v$$
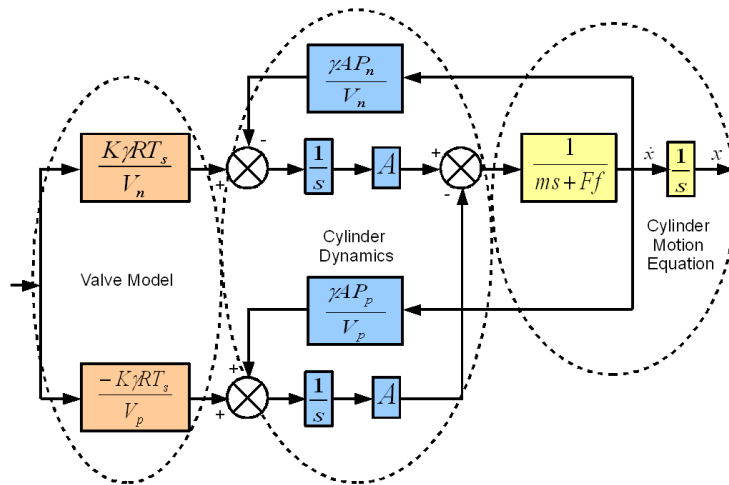
Figure 4.3: Block representation of the pneumatic system
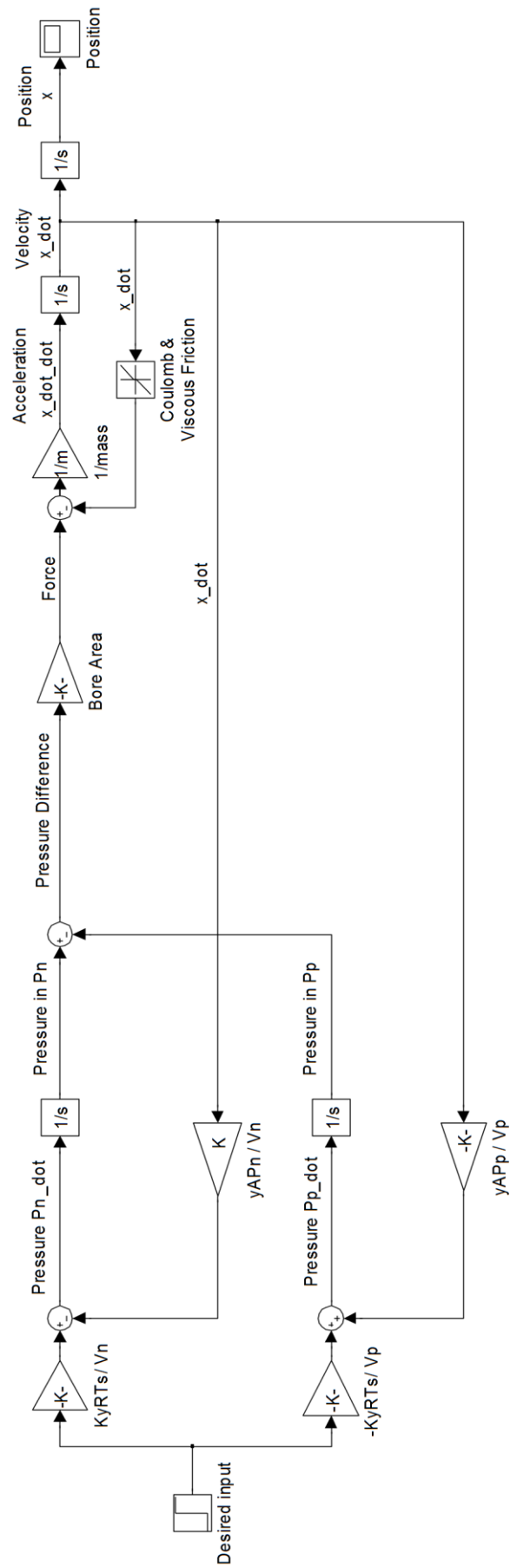
Figure 4.4: Simulink model of pneumatic system

4.3   System parameters

This section describes the pneumatic system parameters. Most of the pneumatic system parameters are determined from the manufacture's data sheet. The system parameters are shown in Table 4.1. However, certain parameters which are not available from the manufacturer need to be ascertained. These include the friction forces and the proportional servo valve constant. Section 4.3.1 details the friction force parameter identification and section 4.3.2 details the formulation of the proportional valve constant.

Table 4.1: Pneumatic system parameters

Parameter	Name	Value
T_s	Temperature	300Kelvin
γ	Ratio of specific heat	1.4
F_f	Friction forces	47N s/m
R	Universal gas constant	287
K	Servo valve constant	0.002 kg/s.V
M	Piston mass	0.1kg
A_p	Piston area (Chamber p)	5.72×10^{-4} m^2
A_n	Piston area (Chamber n)	4.94×10^{-4} m^2
P_p	Nominal pressure in chamber p	2.5×10^5 Pa
P_n	Nominal pressure in chamber n	2.5×10^5 Pa
V_p	Nominal volume in chamber p *	5.683×10^{-5} m^3
V_n	Nominal volume in chamber n *	5.285×10^{-5} m^3

* Nominal chamber volumes include air supply pipe volume

4.3.1   Friction parameter identification

Friction is the tangential reaction force between two surfaces in contact. Physically these reaction forces are the results of many different mechanisms, which depend on contact geometry and topology, properties of the bulk and surface materials of the bodies, displacement and relative velocity of the bodies and presence of lubrication.

Pneumatic actuators exhibit low stiffness due to the non-linear characteristics caused by compressibility of air, inherently non-linear behaviour and low damping of the actuators systems are which cause control difficulties (Andrighetto et al, 2006). According to Nouri *et al* (2000) the main non–linearities in pneumatic position servo systems are air flow-pressure relationship through valve orifices, the air compressibility and friction effects between contact surfaces in actuator seals. The most complex non-linearity in pneumatic systems is the actuator friction force Nouri *et al* (2000). The effects of friction forces increases the difficulty of position control, because it can cause steady-state position and

trajectory tracking errors, limit cycles around the desired position (hunting) and stick-slip movements.

Friction is considered as one of the most common non-linearities present in pneumatic systems. In order to achieve accurate position control an accurate estimation of frictional forces within the mechanical system is required. Friction is a very complex phenomenon which has various forms. These include stiction, Stribeck effect, viscous, and Coulomb friction.

Many pneumatic systems manufacturers supply insufficient information regarding frictional characteristics. This makes the selection and design of pneumatic systems difficult. However, some manufacturers (Festo, Parker) present friction force as a performance loss using an efficiency factor μ (Equation 31).

$$F_f = \mu.P.A \tag{31}$$

where

F_f = Friction force

P = Working pressure

A = Actuator area (bore area)

Many research efforts have been directed towards addressing these issues, more particularly in pneumatic systems. Dahl (1968) made early attempts to model the Coulomb and viscous friction model. Olsson *et al* (1998) and Valdiero *et al* (2005) describe the stiction and dynamic friction between two surfaces using the LuGre model. With this approach identifying the surface characteristics is difficult and assumptions have to be made (Perondi, 2002).

For this work in order to represent the friction in the pneumatic cylinders described in Chapter 3, a static friction-velocity map in steady state approach is used. These maps allow the four main static friction force coefficients to be formulated. The static friction-velocity maps are produced with a constant supply of pressure. The coefficients include static friction (F_s); Coulomb friction (F_c); viscous damping coefficient (B) and Stribeck velocity ($\dot{y}_s$). The coefficients are illustrated in Figure 4.5 (Andrighetto *et al* 2006). With these coefficients, Nouri *et al* (2000) modelled friction forces F_f using Equation (32).

$$F_f = F_c + B.v + (F_s + F_c)e^{-\left(\frac{v}{\dot{y}_s}\right)^2} \tag{32}$$

where, v is the actuator velocity.

The static map that represents the value of friction force with the corresponding steady-state velocity is obtained by using Newton's second law from the equilibrium of forces acting on the piston; i.e. the total applied force (F) on the piston is equal to the inertia force of the sliding body plus the friction force (F_f). This is shown as

$$F = M\ddot{x} + F_f \tag{33}$$
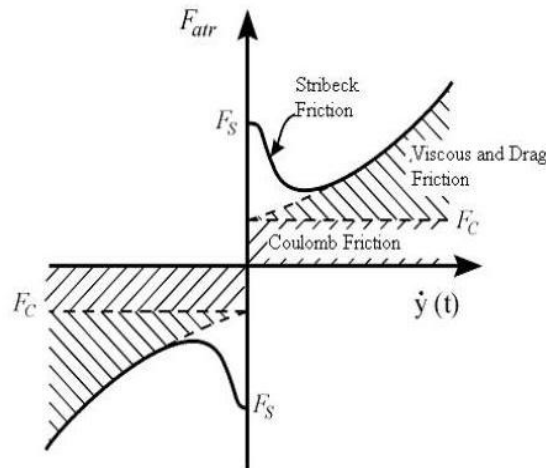
Figure 4.5: Friction force characteristics combined in steady state

Where, M is the mass of the piston. The total applied force (F) is equivalent to the chamber's differential pressure multiplied by the cross sectional area (A) of the cylinder bore. Inserting equation (32) into equation (33) gives

$$F = M\ddot{x} + F_c + B.v + (F_s + F_c)e^{-\left(\frac{v}{\dot{y}_s}\right)^2} \tag{34}$$

The actuator friction force F_f can be calculated using Equation (33)-(34) if the acceleration is known. If the tests are carried out with a constant actuator velocity, the acceleration is zero. Then the friction force in steady-state $F_{f,ss}$ is equivalent to the force produced in the actuator. This is shown as

$$F_{f,ss} = A_p.P_p - A_n.P_n = A_{pn}\Delta P \tag{35}$$

where it is assumed that $A_p = A_n = A_{pn}$, and $P_p - P_d = \Delta P$.

As the output (mass flow rate) of the proportional servo valve is proportional to the voltage applied, applying various voltage increments allows for different velocity outputs. Using equation (35) the friction forces are calculated and shown in Figure 4.6. The velocity is calculated in a region where the position output is in a straight line (i.e. constant velocity). Related pressure difference values (ΔP), are read in the same time interval for calculation of friction forces. From the obtained Friction-velocity maps the four friction parameters (F_s), (F_c), (B), and ($\dot{y}_s$) are calculated. The various pressure difference and position output plots are detailed in Appendix B. Figure 4.7 shows a close up of point of interest for the friction force calculations.
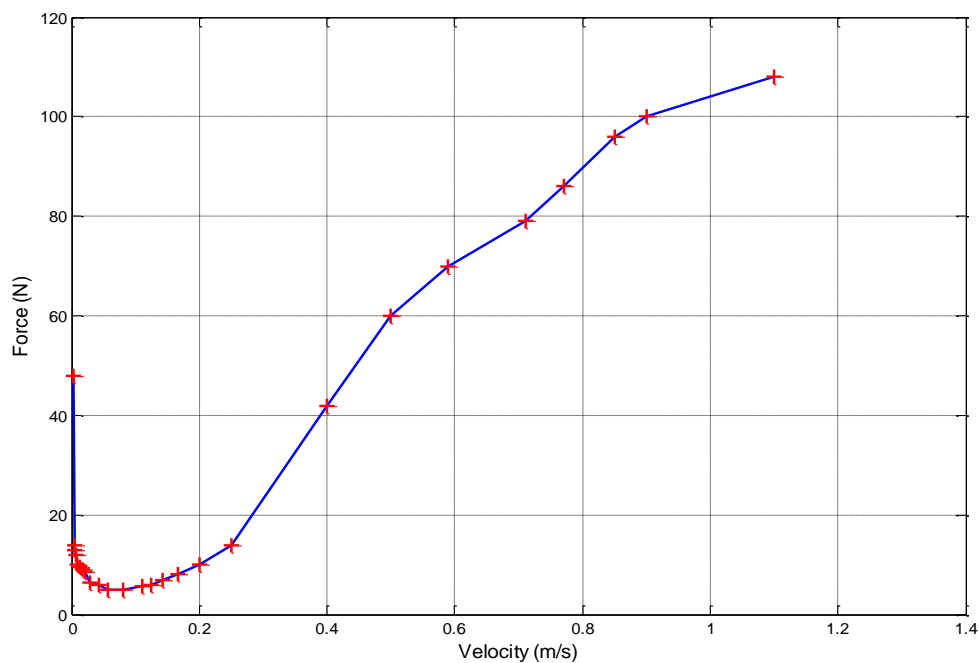
Figure 4.6: Friction-velocity map

From Figure 4.7 and equation (32) the pneumatic system friction is calculated as the following.

Where, $F_c = 4N$, $B = 71.5N$, s/m, $v = 0.6m/s$, $F_s = 48N$, and $\dot{y}_s = 0.01m/s$.

Then the friction force is

$$4 + (71.5 \times 0.6) + (48 - 4)e^{\left(\frac{0.6}{0.01}\right)^2} = 47N \tag{36}$$
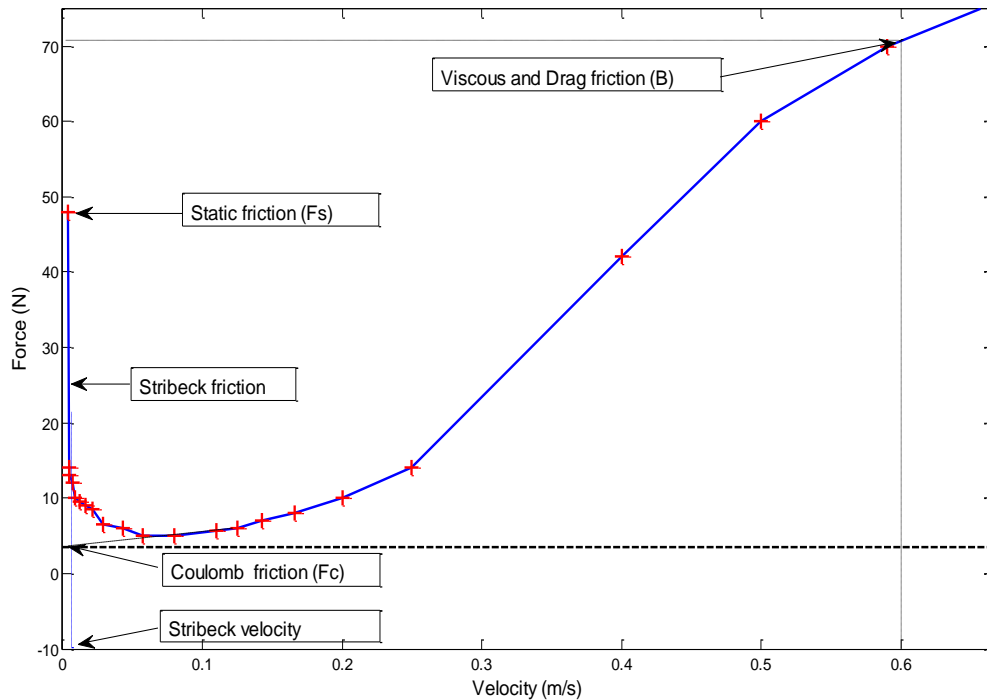
Figure 4.7: Friction-velocity map close up

4.3.2 *Determining the proportional servo valve constant (K)*

The servo valve constant (*K*) used Equation (30) is a function of the mass flow rate per Volt. From the manufactures data sheet for the proportional servo valve the flow of the valve is 700 litres per minute at a supply pressure of 7 kPa (7 bar). For the system in this work the working pressure is set to 4 kPa (4 bar). Then the flow rate can be calculated for the valve at 400 litres per minute.

In order to convert the volumetric flow rate to a mass flow rate. The SI derived unit for volumetric flow is cubic metre/second. 1 litre per minute is equal to 1. 667×10^{-5} m^3/s.

To convert the flow rate to a volumetric flow.

$$400 \; litres \; per \; min \times 1.667 \times 10^{-5} = 6.667 \times 10^{-3} \; m^3/s \tag{37}$$

Mass flow rate is given by the formula

$$\text{Density (kg/m}^3) \text{ x volumetric flow rate (m}^3\text{/s)} \tag{38}$$

Where density for air is given at 1.29 kg/m^3

Then

$$\text{Mass flow rate} = 1.29 \text{ kg/m}^3 \text{ x } 6.667 \text{ x}10^{-3} = 0.0086 \text{ kg/s} \tag{39}$$

From the manufactures data sheet looking at the mass flow rate per Volt (slope of graph)

$$\text{Valve constant} = \frac{0.0086 \text{ kg/s}}{4.3 \text{ V}} = 0.002 \text{ kg/s.V} \tag{40}$$

4.4   Model validation

In this section the derived model (Equations 27-29) is validated. The validation consists of comparing the model output against the actual system output. The validation set-up is shown in Figure 4.8. The validation is conducted in open-loop. Firstly, the validation is made with applying a square wave input to both system and model. Secondly, a frequency response comparison is taken with regards to Bode plots.

The results for a square wave input are shown in Figure 4.9. Here, the square wave input is set at 0.65V and the frequency set at 0.5Hz, and the position output responses are plotted alongside those predicted by the model.
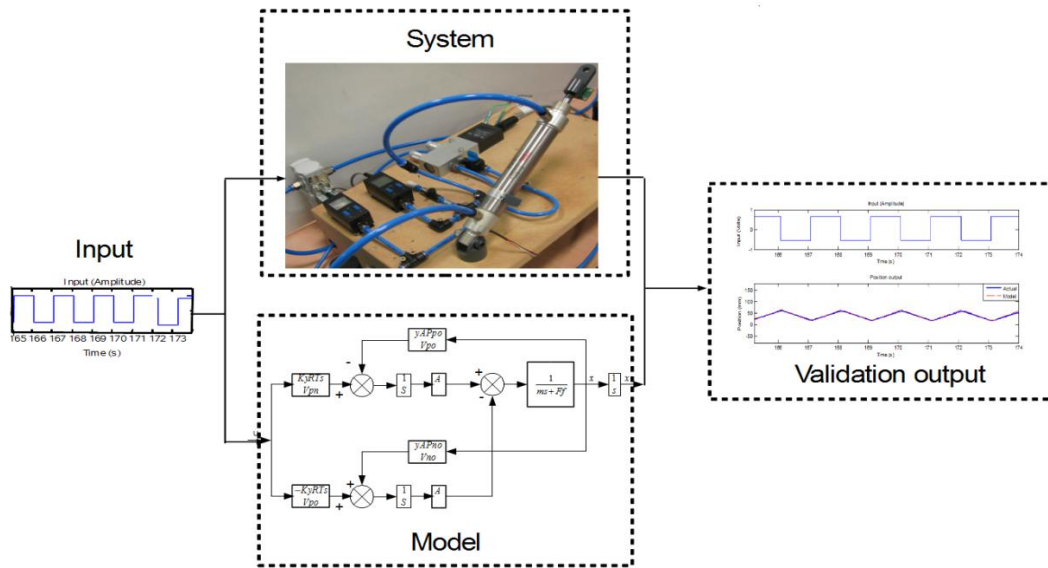
Figure 4.8: Model validation set-up
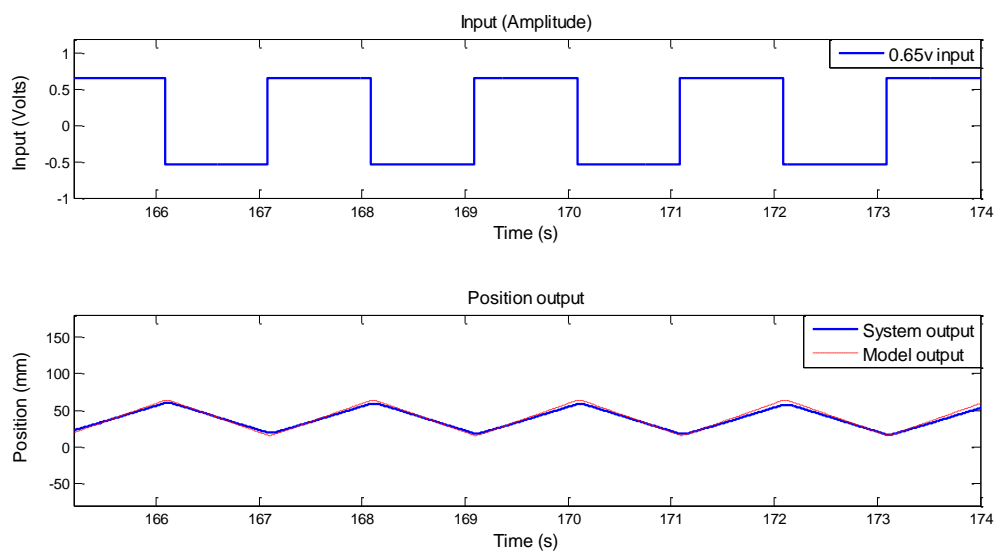
Figure 4.9: Validation plots for a square wave

The results illustrated in Figure 4.9 show reasonable agreement with those from the experiment. Indicating that the model is a good representation of the pneumatic system. Further validation is done with regards to frequency response. In order to validate the model against the actual system a frequency response of the actual system was obtained over a frequency range of 1-30 radians/second. A sinusoidal signal with its frequency manually varied is applied. The frequency response readings are taken with the piston

moving up and down the cylinder without the piston reaching the end stops. The input signal was adjusted to accommodate this. The Bode plot comparisons (Figure 4.10) of the pneumatic system and the model show that both the system outputs are similar within the measured frequency range. The comparisons show that the model is a good representation of the actual system. The discrepancies are insignificant and are consistent with expected levels of experimental/measurement error. Table 4.2 details the outputs of the bode diagrams and quantifies the differences between model and system measurements.
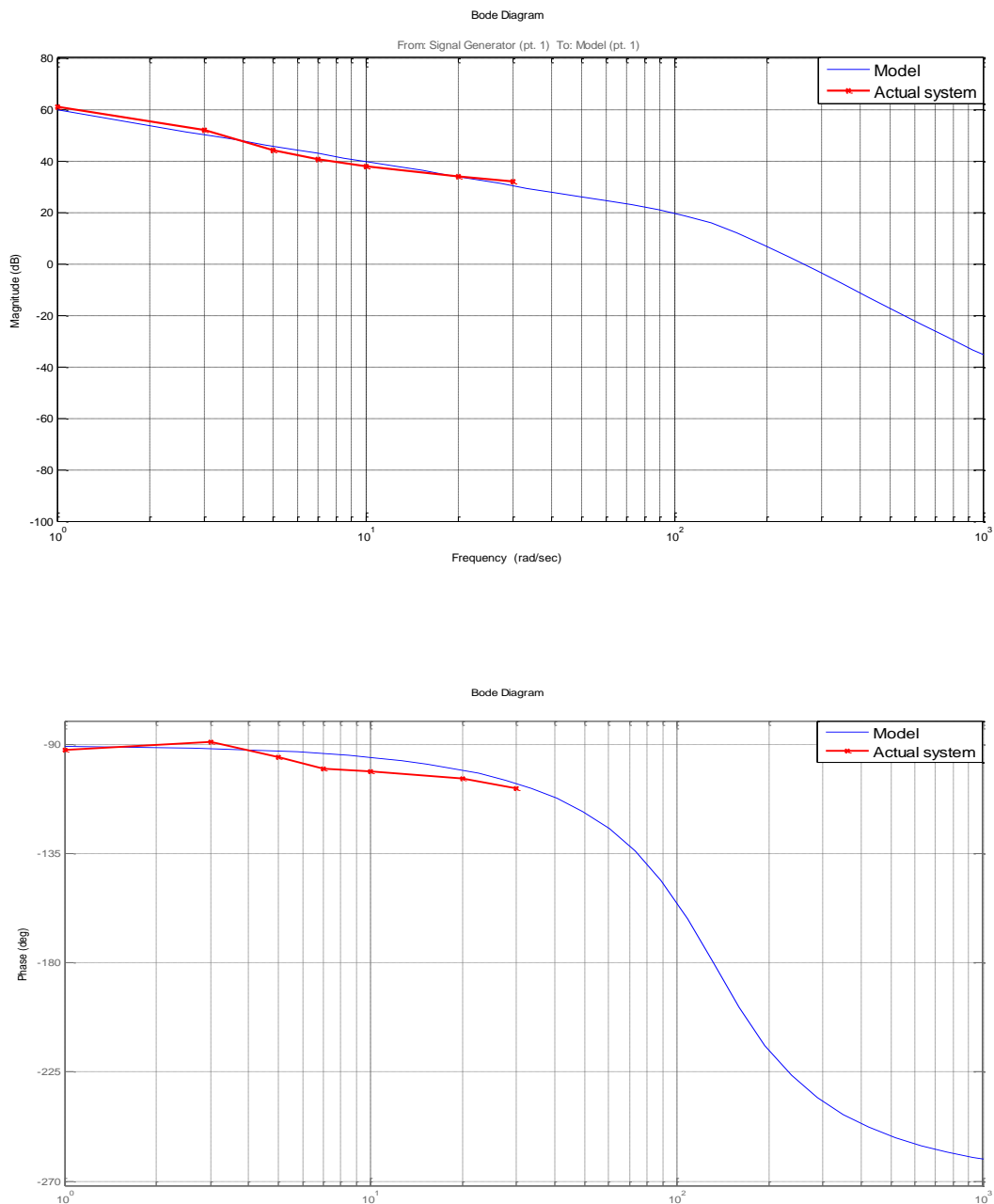
Figure 4.10: Bode plot comparison of the pneumatic system and model.

Table 4.2: Bode diagram comparisons between model and system

Frequency (rad/sec)	Magnitude (dB)			Phase (deg)		
	Model	System	Difference	Model	System	Difference
1	60	61	1	-90	-93	3
3	50	52	2	-92	-89	4
5	45	43	2	-93	-95	2
7	43	41	2	-94	-100	6
10	40	38	2	-95	-101	6
20	33	33	0	-100	-104	4
30	31	32	1	-106	-107	1

4.5   Conclusion

In this chapter pneumatic principles have been described. Reference has been made to work conducted by previous authors in modelling pneumatic systems. A mathematical model of the pneumatic system has been formulated. Various parameters have been identified using experimental data. The model has been validated by directly comparing it to the actual pneumatic system. The results have showed that the model is a good representation of the actual system.

This model can now be used as the foundation on which to design both the control strategies and the model-based fault tolerant scheme.

Chapter 5

Pneumatic control

5.1   Introduction

Pneumatic actuating control systems, similar to actuating systems of other types, can usually be divided into two groups: namely, open-loop and closed loop control. Open-loop pneumatic systems remain widely used in manufacturing and processing industry. This is due to the sturdiness, versatility, and ease of use of pneumatic systems and low set-up costs. Open-loop pneumatic actuator systems are often used in positioning applications. In such systems the final positioning of the actuator is provided by a manually adjusted hard stop. Position sensors, usually attached to the outside of the actuator or the hard stop, indicate the position. These types of actuators contain air-cushioning units or shock absorbers, which provide the absorption and dissipation of actuators kinetic energy. Due to these absorber devices, deceleration of the actuator is reduced to a tolerable level and positioning is carried out without impact and has high repeatability.

However, the performance obtainable using open-loop control has limitations. Open-loop control systems are sensitive to initial condition (Krivts and Krejnin, 2006). For actuators with repeated stops in the same locations this drawback is not critical, but for multi-location applications, where the initial conditions vary significantly, this factor is very important. In such cases, closed-loop control systems are usually used. The basic reasons for using closed-loop systems in contrast to open-loop systems are the need to improve transient response times, reduce the steady-state errors, and reduce the sensitivity to load parameters.

In section 5.2, control strategies for pneumatic systems are discussed with reference to previous work by other authors. Then, two closed-loop control strategies are designed for the pneumatic system. Namely, PI control (section 5.3) Linear Quadratic Gaussian (LQG) and state-feedback control (section 5.4). In section 5.5, the two designed control schemes are compared. Finally, section 5.6 concludes by giving reference to the best control method to be used for controlling the pneumatic system.

5.2   Control strategies

Until the 1980's, pneumatic systems were used purposely for two-ended position control. Sporadic positioning was achieved by incorporating mechanical limit stops or brakes. This led to difficult fine positioning when users attempted to close the feedback loop. Pneumatic actuators are of particular interest for robotic applications because of their large power output at a relatively low cost.   Increasing requirements in terms of independent positioning and accurate control has led to several approaches in pneumatic system control. A number of researchers have tried controlling air cylinders using various methods. Wang *et al* (1999) based a control strategy on a PID controller with acceleration feedback and non-linear compensations for servo-pneumatic actuator systems. Van Varseveld and Bone (1997) implemented a PID controller with added friction compensation and position feedforward. Hamiti *et al* (1996) applied a control scheme consisting of two components, which included an analogue proportional controller scheme as the first component. This was known as the inner loop. The second component was a digital proportional- integral controller scheme this was known as the outer loop. The inner loop was used to stabilise the system, which initially contains an integrator, and to reduce the effects of the non-linearities in the system. The outer loop was used to specify the characteristics of the whole system and used to cope with the problems caused by stick-slip friction. Other investigations include studies by Liu and Bobrow (1988), who investigated proportional-derivative (PD) as well as optimal linear quadratic Gaussian (LQG) controls. Paul *et al,* (1994) and Shunmuham and Hayakawa*,* (1997) investigated sliding mode control. Gross *et al,* (1998)., Choi *et al,* (1998)., Hesselroth *et al,* (1994) studied Neural networks as a means of pneumatic control. Belforte *et al,* (1992)., Muscato and Trovato, (1998) implemented Fuzzy control. Kaitwanidvilai and Parnichkun, (2005) used a combination of Neural networks and Fuzzy control techniques in order to control pneumatic systems. Chillari *et al* (2001) favoured Fuzzy logic, as well as Neuro-Fuzzy as a means of pneumatic control. This study included an experimental comparison between several pneumatic position control methods. The study investigated the performance of different methodologies in terms of both error and complexity of design and cost. The results obtained from the study confirm that with suitable control strategies pneumatic actuators can be a valid alternative to other actuation methodologies at a lower cost and high power-to-weight ratio with out decreasing the precision in trajectory following.

For this work two control strategies are used. Firstly, classical control is applied using Proportional–integral (PI) control algorithms. Secondly, a modern control technique is implemented; the control strategy is based on a Linear Quadratic Gaussian Regulator (LQG) controller.

5.3   *Proportional-integral controller (PI)*

A   Proportional-integral controller algorithm is one of the most popular feedback controllers used in industry (Kraus and Myron, 1984). It is robust, and the algorithms are easily understood which provide excellent control performance despite the varied dynamic characteristics of a process plant. The PI approach is easy to implement and relatively simple to tune. Figure 5.1 represents a schematic diagram of the PI algorithm (controller).
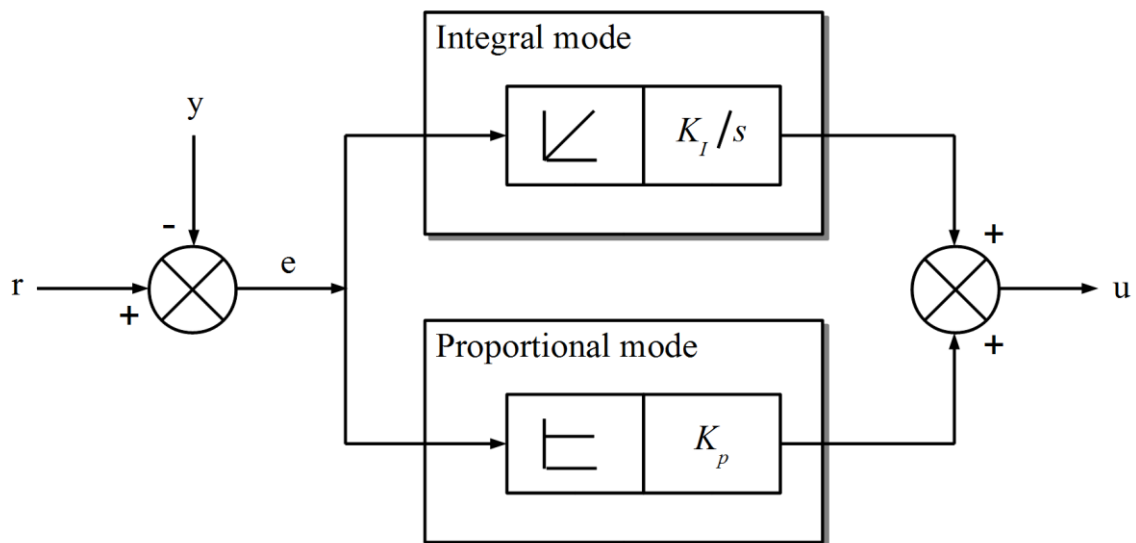
Figure 5.1: Schematic of PI controller.

In general, a PI controller takes as its input ($e = r - y$) the error signal (difference) between the desired set point (r) and the output (measured) signal (y). It then acts on the input such that a drive signal (u) is generated. The gains K_P and K_I are the proportional

and integral gains of the controller which to act on error and integral of the error. The PI control signal can be expressed as:

$$u = K_P \cdot e + K_I \cdot \int e \cdot dt \tag{41}$$

Equation (41) can be also written as

$$u(t) = K \left[e(t) + \frac{1}{T_i} \int_0^t e(t) dt \right] \tag{42}$$

Where the transfer function can be represented as:

$$C(s) = K_p \left(1 + \frac{1}{T_i s} \right) \tag{43}$$

Where K_p is the proportional gain and T_i is the integration time constant. Note that, K_i is related to K_p and T_i by $K_i = K_p / T_i$. This form of PI compensator lends itself to classical frequency design methods.

The Simulink model of the pneumatic system with PI control is shown in Figure 5.2.
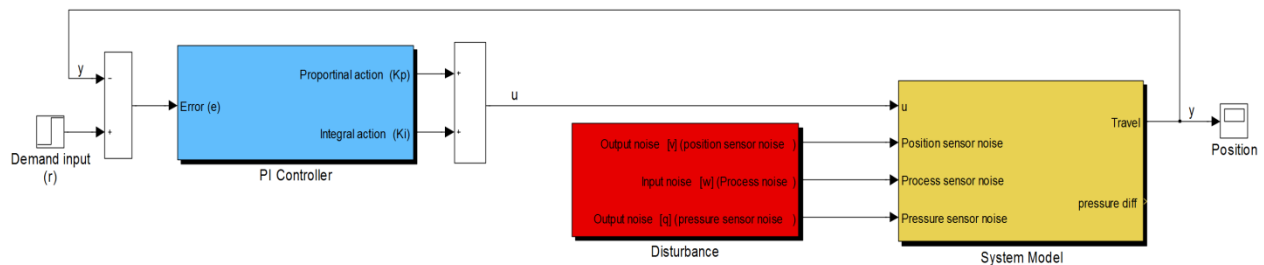
Figure 5.2: Simulink model of pneumatic system with PI control

5.3.1   *Design of Proportional-integral controller*

The PI controller is designed using classical frequency domain design methods. The model described in chapter 4 is used to calculate the system open-loop frequency response. Initially, setting the proportional gain to 1 and the integral gain to zero, the Nichols plot (Figure 5.3) shows the phase and gain margins.
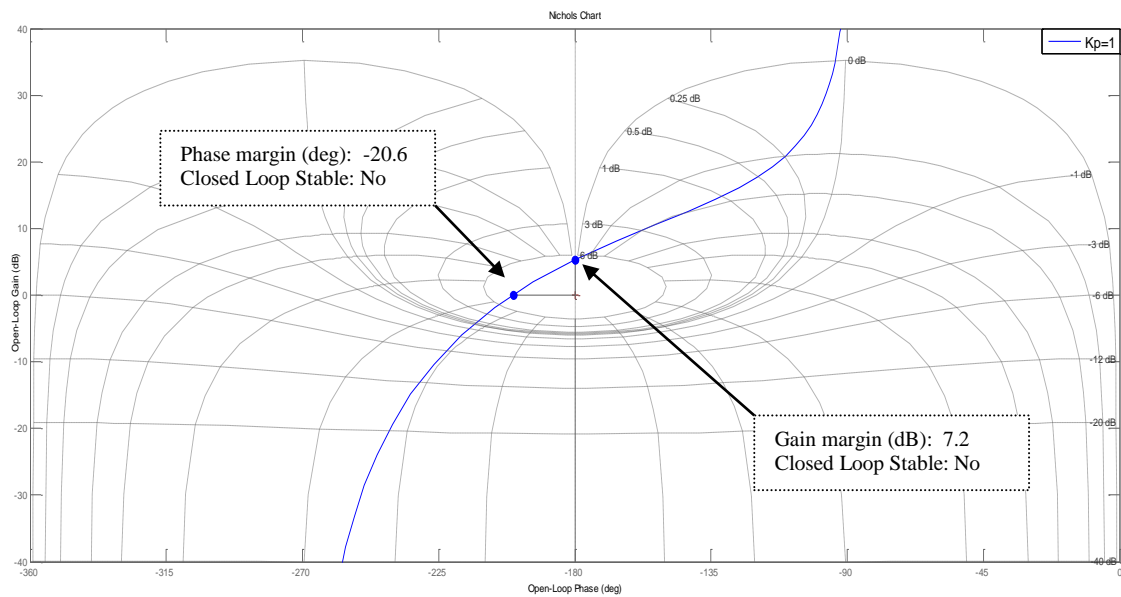
Figure 5.3: Nichols plot with $K_p = 1$

It is clear from Figure 5.3, that with a gain margin of 7.2dB and the phase margin at 20.2^0 degrees, the system is unstable. To obtain a stable system and meet the control requirements described earlier the curve needs to be brought down approximately -18dB. Then,

Gain reduction factor $= alog(-18/20) = K_p = 0.125V$

Plotting the Nichols plot with K_p set to 0.125V. Figure 5.4 shows that the phase margin is 66^0 and gain margin is 10 dB. In order to achieve the required phase margin (60^0) and gain margin (8 dB) an integral action is applied (Figure 5.4). The integral gain is tuned by adjusting the Nichols plot at the lower frequency end, where T_i is calculated to 0.7, and the integral gain is calculated to 0.1. The following control algorithm is produced

$$C(s) = \frac{0.125 + 0.1}{s}$$

(44)
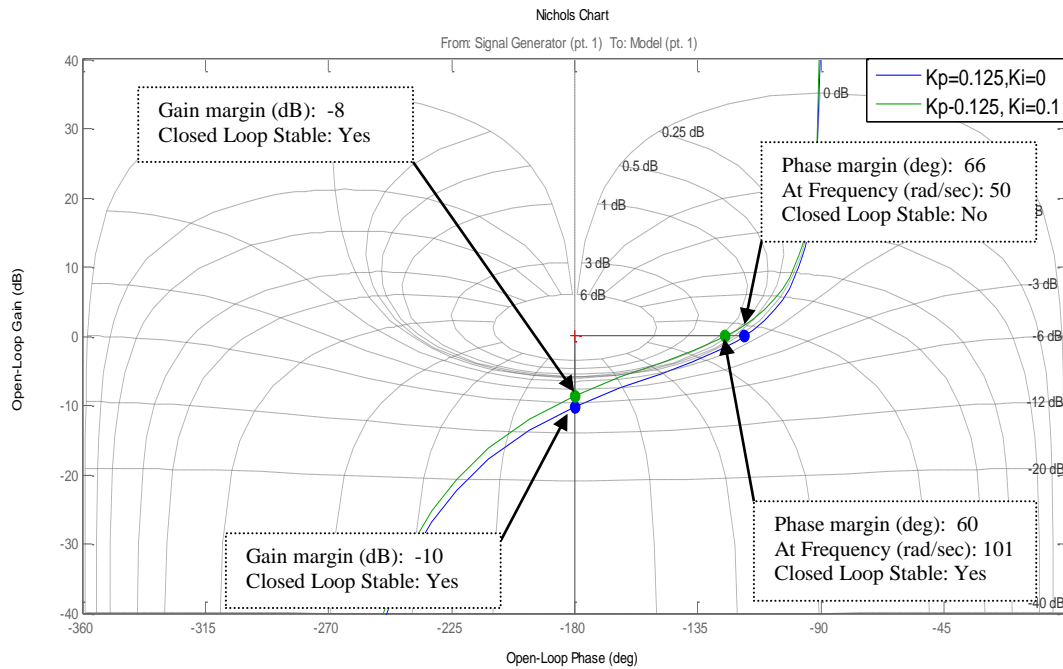
Figure 5.4: Nichols plot

5.3.1.1 *PI controller with Antiwindup*

In any control system the output of the actuator can saturate because the dynamic range of the actuators is limited (Franklin, Powell & Emami-Naeini 2002). Whenever actuator saturation happens, the control signal to the process stops changing and the feedback path is effectively opened. If the error continues to be applied to the integrator input under these conditions, the integrator stored value will grow (windup) until the sign of the error changes and the integration turns around. This can result in large overshoot due to the output growing to produce the necessary unwinding error. In order to overcome this, an antiwindup scheme is integrated within the PI control scheme. The purpose of anti-windup is to improve the controller's ability to recover from output saturation. When the output saturates, the error is likely to be large, since the process is unable to provide power fast enough to recover the process output. The integrator contribution may not account for the full amount of controller output (Astrom and Rundqwist, 1989). In this case, the integrator continues to integrate the error until the integrator output saturates. This 'winding up' characteristic of integral control becomes a problem when the process recovers and the error level passes through zero (Grimm *et al*, 2003). This is because the error must move significantly beyond zero for the integrator to unwind from saturation. In addition, once

the controller output is fixed at a limit, nothing is gained by driving it harder into that set limit by more integration. This usually results in large swings back and forth from limit to limit. There is a variety of anti-windup strategies to alleviate this effect, see for example (Kothare *et al*, 1994; Zheng *et al*, 1994; and Edwards and Postlethwaite, 1999). One simple way is to implement anti-windup is to switch off the integrator whenever the output saturates. For this project, to prevent the integrator from winding up, an anti-windup mechanism can be implemented within the PI controller as a subtractive term from the integral contribution. Figure 5.5 illustrates a schematic diagram of the pneumatic system showing the PI control with anti-windup.

As displayed in Figure 5.5 the feedback signal e_s (saturation error) is defined as:

$$e_s = U_s - U_c \tag{45}$$

Where U_c is the magnitude of the control action requested by the control system, and U_s is the magnitude of the same control signal coming out from the saturation element. T_t is the saturation time constant. Where $T_t \leq \tau_i$ (Astrom and Rundqwist, 1989).
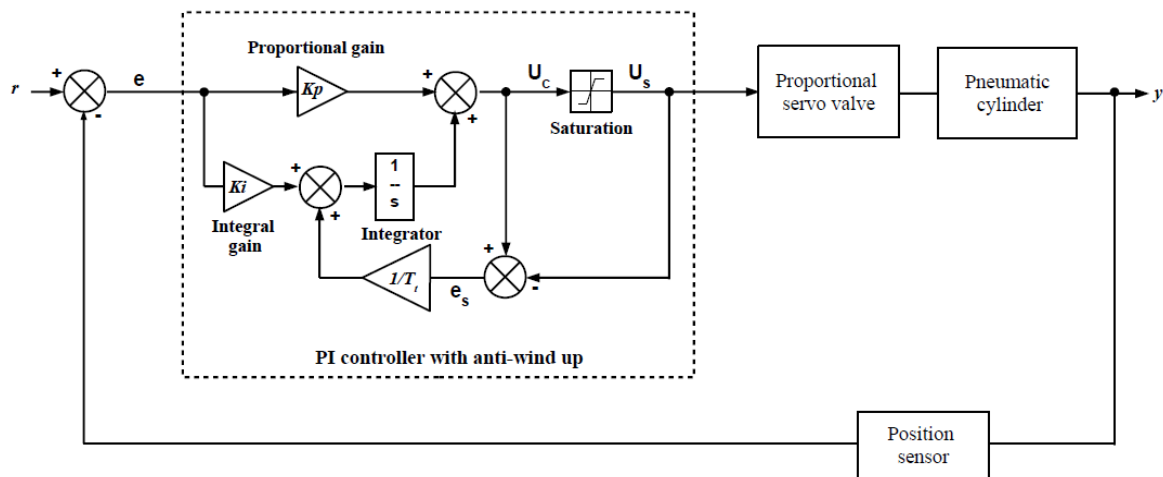
Figure 5.5: Pneumatic system using a PI controller with an anti-windup scheme.

Under saturation conditions the integral part *I* of the control system will be given by the following:

$$I = K_i \int_0^t e(t)dt + \frac{1}{T_t} \int_0^t e_s(t)dt \tag{46}$$

$$I = \int_0^t \left(K_i e(t) + \frac{1}{T_t} e_s(t) \right) dt \tag{47}$$

When there are no saturation problems within the system then:

$$U_C = U_S \tag{48}$$

Therefore $e_s = 0$ and the action of the anti-windup control scheme will be cancelled and conventional feedback is continued.

In accommodating integrator windup the actions are described below.

- If the control action happens to hit its upper bound then $U_C > U_S$ and the sign of the saturation error (e_s) will be negative leading to a reduction in magnitude of the controller integral action (I) and the combined control action (U_C).
- If the control action hits its lower bound then $U_C < U_S$ and the sign of the saturation error (e_s) will be positive contributing to reduce the magnitude of the controller integral action (I) and increasing the combined control action (U_C).

Figure 5.6 shows the step response to the PI controller (with antiwindup) for the system model, this shows that all the desired control specifications have been achieved.
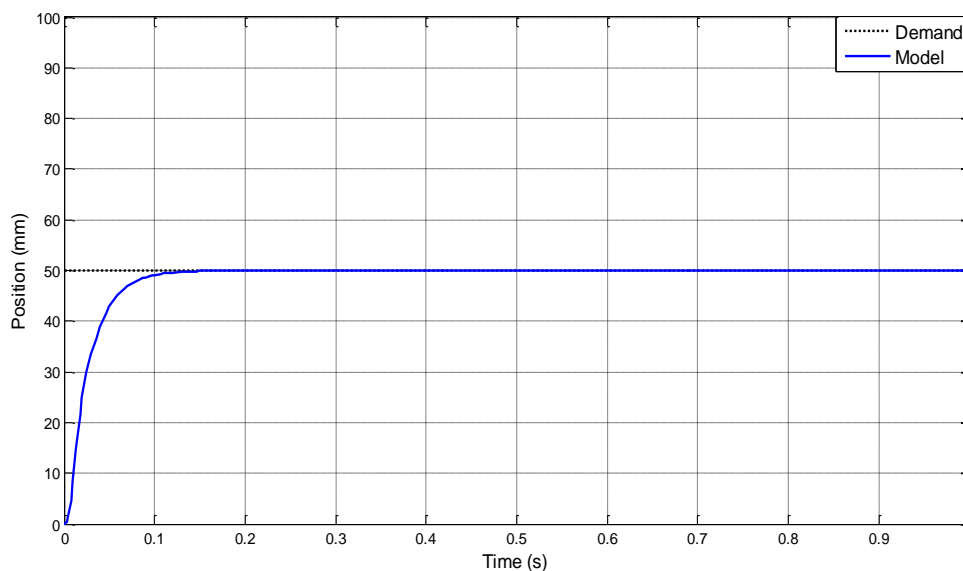
Figure 5.6: Step input response for model with PI controller

$(K_p = 0.125$ and $K_I = 0.1)$

Figure 5.7 shows the Simulink model of the pneumatic system with PI control and the incorporated antiwindup scheme.
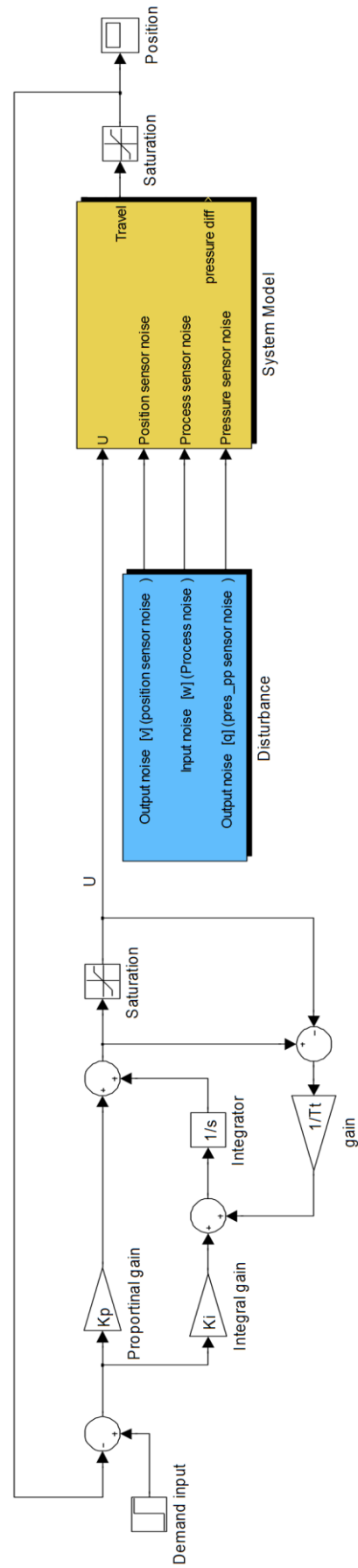
Figure 5.7: Simulink model of pneumatic system with PI control with antiwindup

5.3.2   *Implementation of Proportional-integral controller*

The designed PI controller (with antiwindup) is implemented on the single actuator test (Chapter 3). The xPC target controller is compiled with a sampling time 0.0025seconds and downloaded to run on the target system. The result for a step response can be seen in Figure 5.8, which illustrates the comparison between the model, system and demand after applying a step input of 50mm. When comparing the model and actual output from the pneumatic system the required objectives for settling-time, overshoot, and steady-state error are satisfied.
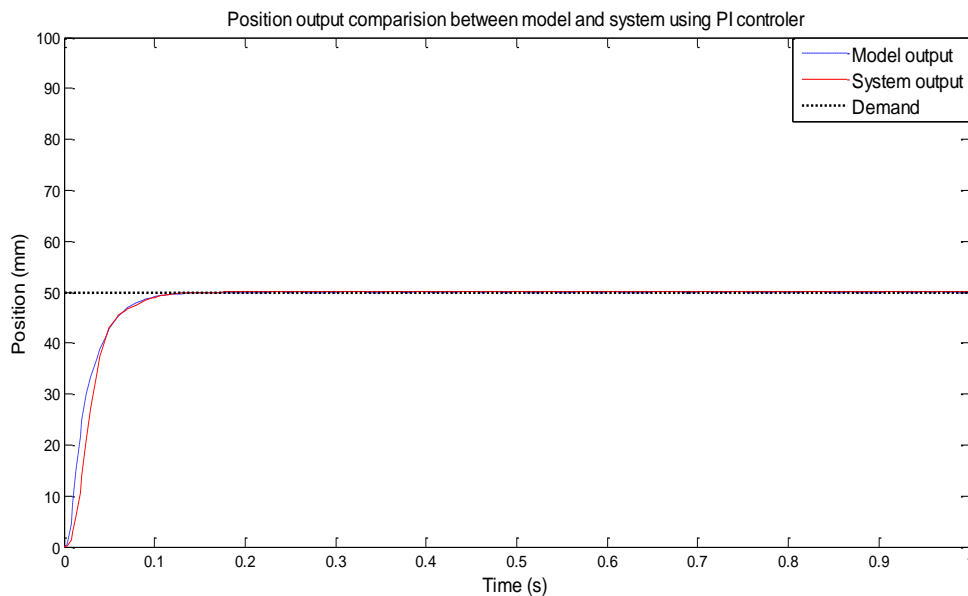
Figure 5.8: Comparison between model and system using PI controller

5.4   *Linear Quadratic Gaussian Control (LQG)*

The controller is based on the model described in Section 4 using Linear Quadratic Gaussian (LQG) optimal control theory. The control strategy is based on a LQG controller for the pressure servo valve controlled pneumatic actuator system shown in Figure 3.1. The LQG method is designed to satisfy the previously specified requirements for steady state error, transient response, stability margins or closed loop pole location.

The LQG design consists of two steps, undertaken separately making use of the separation principle[4]. The first design step is to seek a state feedback control gain that minimizes the cost function of regulation performance, which is measured by a quadratic performance criterion with tuning weighting matrices. The second design step is to derive a state estimator using a Kalman filter because the optimal state-feedback controller cannot be implemented without reducing disturbances that perturb the system. The LQG controller is the combination of a <u>Kalman filter</u> i.e. a Linear-Quadratic Estimator (LQE) with a <u>Linear-Quadratic Regulator</u> (LQR).

5.4.1   Step 1, regulator design

To realize the controller design, the pneumatic system must satisfy the following conditions:

1. The system is controllable.

2. The system is observable

These conditions are applicable to the state space model of the pneumatic system derived in equation (30). The plant model is written in state-space form as per Equation (30) where, to ensure observability of all states, Equation (30) has been manipulated. Equation (49) shows the observable state space representation, where it is assumed $A_p = A_n = A_{pn}$, and $P_p - P_n = P_d$.

$$
\begin{bmatrix} \dot{P}_d \\ \dot{x} \\ \ddot{x} \end{bmatrix} = \begin{bmatrix} 0 & 0 & a-b \\ 0 & 0 & 1 \\ \dfrac{A_{pn}}{M} & 0 & \dfrac{-F_f}{M} \end{bmatrix} \begin{bmatrix} P_d \\ x \\ \dot{x} \end{bmatrix} + \begin{bmatrix} c-d \\ 0 \\ 0 \end{bmatrix}
$$

$$
y_{pos} = \begin{bmatrix} 0 & 1 & 0 \end{bmatrix} \begin{bmatrix} P_d \\ x \\ \dot{x} \end{bmatrix}
$$

$$(49)$$

Where

$$
P_d = P_p - P_n, \;\; A_p = A_n = A_{pn}, \;\; a = -\frac{\gamma A\, P_p}{V_p}, \;\; b = \frac{\gamma A P_n}{V_n}, \;\; c = K\frac{\gamma RT_s}{V_p}, \;\; d = -K\frac{\gamma RT_s}{V_n}
$$

---

[4] In control theory, a separation principle (more formally known as a principle of separation of estimation and control) states that under some assumptions the problem of designing an optimal feedback controller for a stochastic system can be solved by designing an optimal observer for the state of the system, which feeds into an optimal deterministic controller for the system. Thus the problem can be broken into two separate parts, which facilitates the design.

The LQG control consists of a technique for designing optimal dynamic regulators, based on the state-space system modelling (Equation 49). This technique is based on the search for the trade off between regulation performance and control efforts and takes into account process disturbances and measurement noises. Basically, the LQG approach addresses the problem where the considered dynamic model is perturbed by a dynamical noise *w*, and a state observation corrupted by measurement noise *v*.

As the LQG regulator comprises of an optimal state-feedback gain and Kalman filter estimate or the technique requires a slight modification to Equations (49) with the addition of the noise effect as shown in equation (50). The dynamic model is given by:

$$\dot{x} = Ax + Bu + w_d \tag{50}$$

$$y = Cx + Du + w_n$$

Where w_d and w_n are the disturbance (process noise) and measurement noise respectively, and are modelled as white noise.

The LQG design consists of obtaining the feedback control law in the form $u = -Kx$, which optimises the regulation index given by a quadratic performance criterion.

$$J = \int_0^\infty (x^T Q x + u^T R u)dt \tag{51}$$

Where *Q* and *R* are weighting matrices that define the trade-off between regulation performance and control efforts (design parameters), i.e. the relative weight of how fast the state *x*(t) goes to zero and the magnitude of the control efforts *u*.

For a time invariant system, the gain matrix *K* is obtained by solving the algebraic Riccati equation (equation 52) and taking $K = R^{-1}B^T S$.

Where *S* is the unique positive semi-definite solution of the algebraic Riccati equation

$$A^T S + SA - SBR^{-1}B^T S + Q = 0 \tag{52}$$

In addition to the state-feedback gain *K*, The Matlab function *lqr* returns the solution *S* of the associated Riccati Equation as shown in (52). This is done by choosing two parameter values, input *R* and *Q=C'xC* where *C* is from state Equation (49).

5.4.2 Step 2, Estimator design (Kalman Filter)

The state vector estimate, $\hat{x}(t)$ is calculated using the following well known state-space observer formulation (equation 53).

$$\dot{\hat{x}} = A\hat{x} + Bu + L(y - C\hat{x} - Du) \tag{53}$$

Where $\char94$ indicates that the vector is an estimate, and L is the optimal gain matrix (Kalman gain) obtained using Matlab function *lqe*

With L calculated in this way, equation 53 represents a steady-state Kalman-Bucy filter. The function *lqe*, basically solves for L such that,

$$L = PC^T R^{-1} \tag{54}$$

where P is the unique positive semi-definite solution of the algebraic Riccati equation

$$AP + PA^T - PC^T R^{-1}CP + Q = 0 \tag{55}$$

In which $Q = E(ww^t), R = E(vv^T)$ are covariance matrices for the plant disturbance and measurement noise respectively. In the above, the weightings for the process and measurement noise (Q and R respectively) are chosen based either on knowledge of the noise signals or, more commonly, on engineering judgement. The block diagram of a basic LQG controller is shown in Figure 5.9.
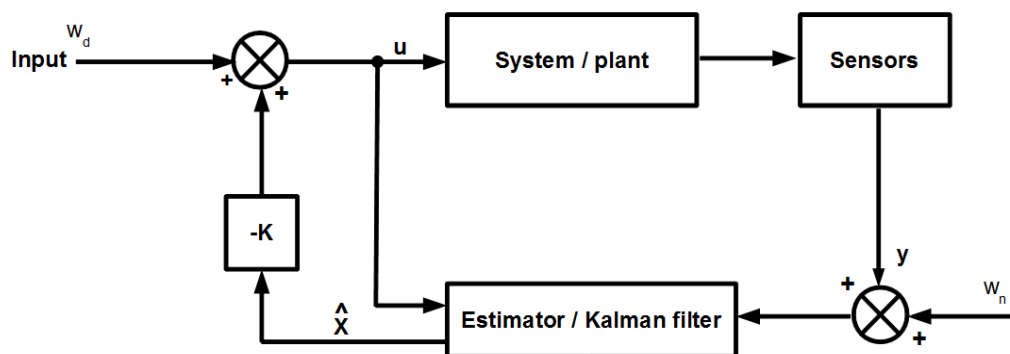
Figure 5.9: Basic LQG control scheme

5.4.3   *Reference signal tracking*

Using the controller scheme combined with the estimator is essentially a LQG regulator design. Typically, this design approach does not consider the reference input. In turn not providing any command following (reference tracking). Many approaches in literature are mentioned regarding robust reference tracking techniques. See for example Franklin *et al,* (2002). For this work an integral control structure is used to obtain robust tracking. Figure 5.10 shows the integral control scheme.
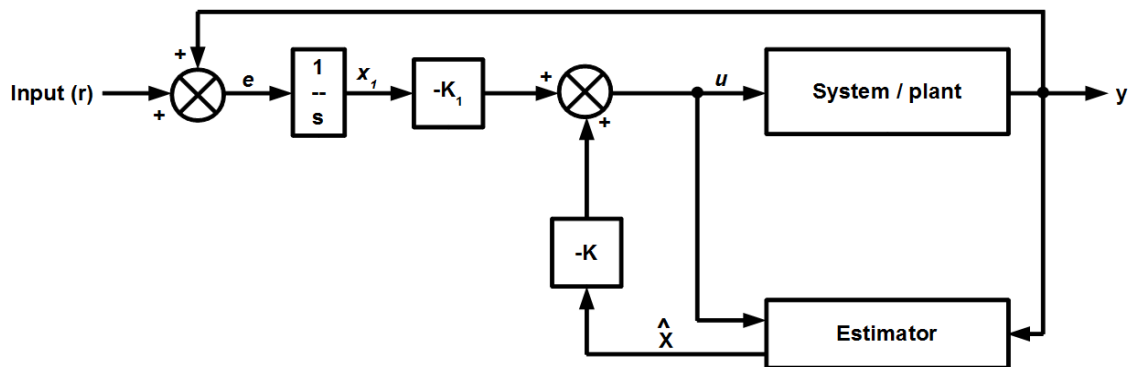
Figure 5.10: Tracking LQG control scheme

For a system

$$\dot{x} = Ax + Bu + B_1 r \tag{56}$$

$$y = Cx \tag{57}$$

Where r is the set point or command input. The state of the system (x) as well as the integral of the error (e) can be fed back, by augmenting the system state with the extra (integral of the error) state x_1, which is shown in Figure 5.10 and represented by the equation.

$$\dot{x}_1 = r - Cx \ (= e) \tag{58}$$

The augmented state equations then become

$$\begin{bmatrix} \dot{x}_1 \\ \dot{x} \end{bmatrix} = \begin{bmatrix} 0 & -C \\ 0 & A \end{bmatrix} \begin{bmatrix} x_1 \\ x \end{bmatrix} + \begin{bmatrix} 0 \\ B \end{bmatrix} u + \begin{bmatrix} 1 \\ 0 \end{bmatrix} r \tag{59}$$

The feedback law is

$$u = -[K_1 \quad K]\begin{bmatrix} x_1 \\ x \end{bmatrix}, \text{ or } u = -K\begin{bmatrix} x_1 \\ x \end{bmatrix} \tag{61}$$

5.4.3.1   LQG controller with Antiwindup scheme

As robust reference tracking is applied using an integral control scheme, it is important to include an anti-windup scheme similar to the scheme applied to the PI controller scheme. Figure 5.11 shows the reference tracking with anti-windup using a LQG control strategy.
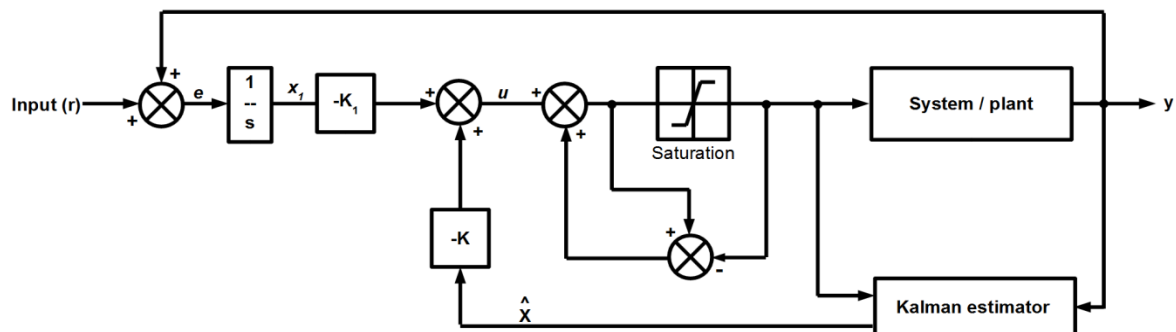
Figure 5.11: LQG control with reference tracking and an anti-windup scheme

The Simulink model for the LQR control with reference integral action including anti-windup is shown in Figure 5.12. The Nichols plot shown in Figure 5.13 depicts the required control objectives for phase and gain margins respectively are satisfied and the closed loop response is stable.
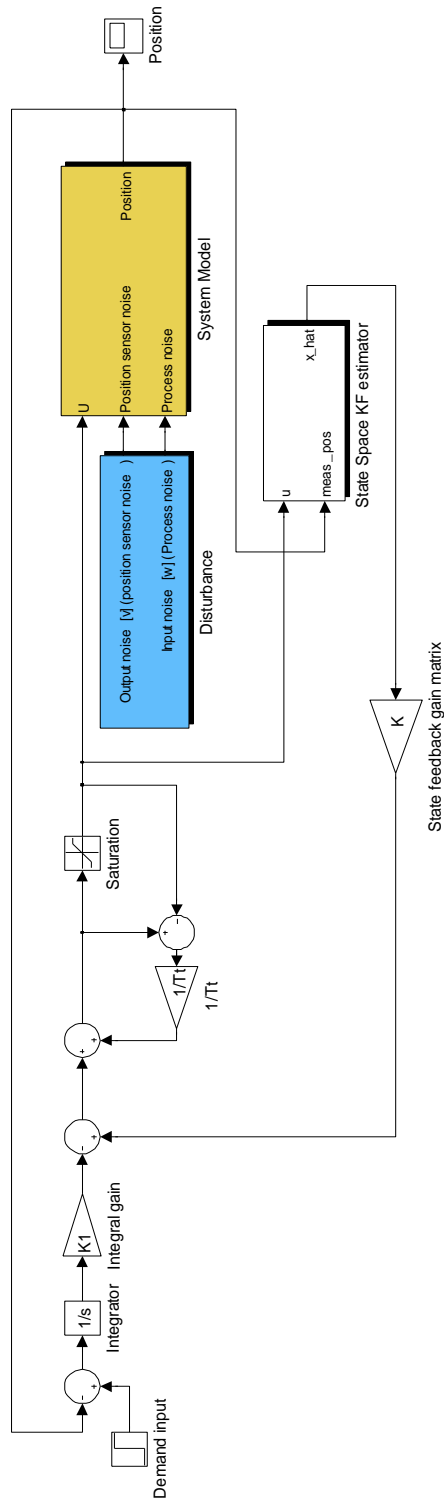
Figure 5.12: Simulink model for the Pneumatic system using LQG control with anti-windup
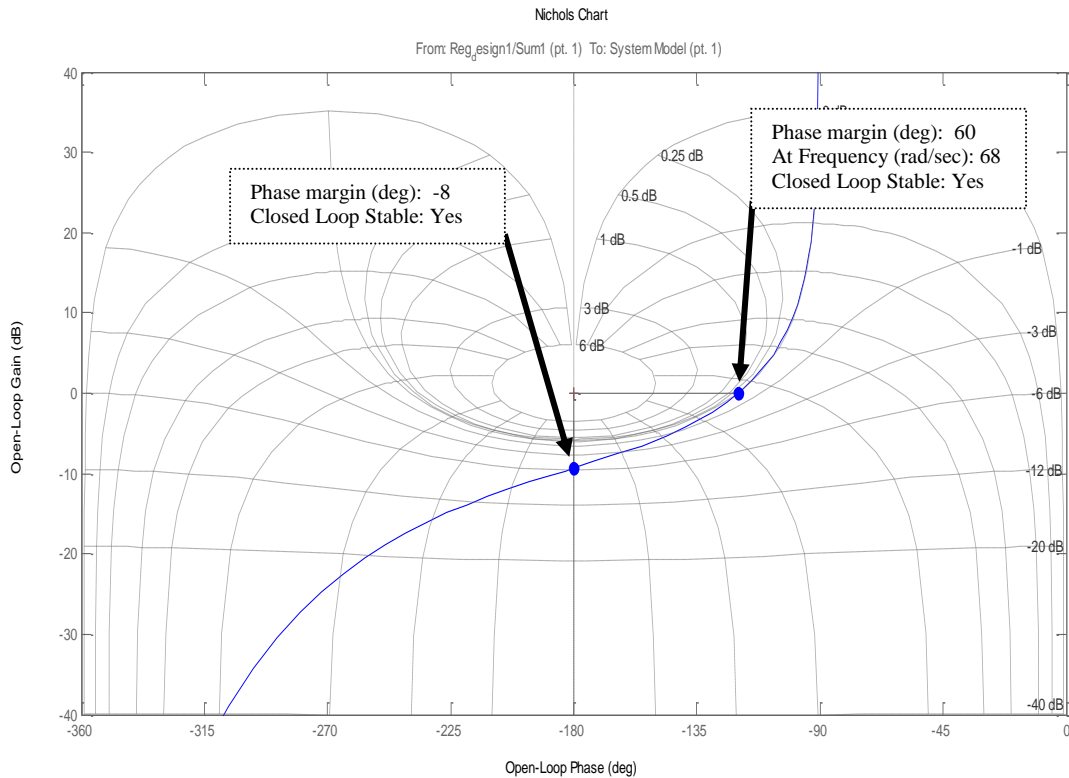
Figure 5.13: Nichols chart

5.4.4 *Implementation of LQG controller*

In this section the designed LQG controller scheme is implemented on to the pneumatic system. For a step input (50mm), Figure 5.14 illustrates the step response comparing the model and actual output from the pneumatic system. This shows that the required objectives for settling-time, overshoot, and steady-state error are satisfied and again the predicted closed-loop time response closely matches that achieved in practice.
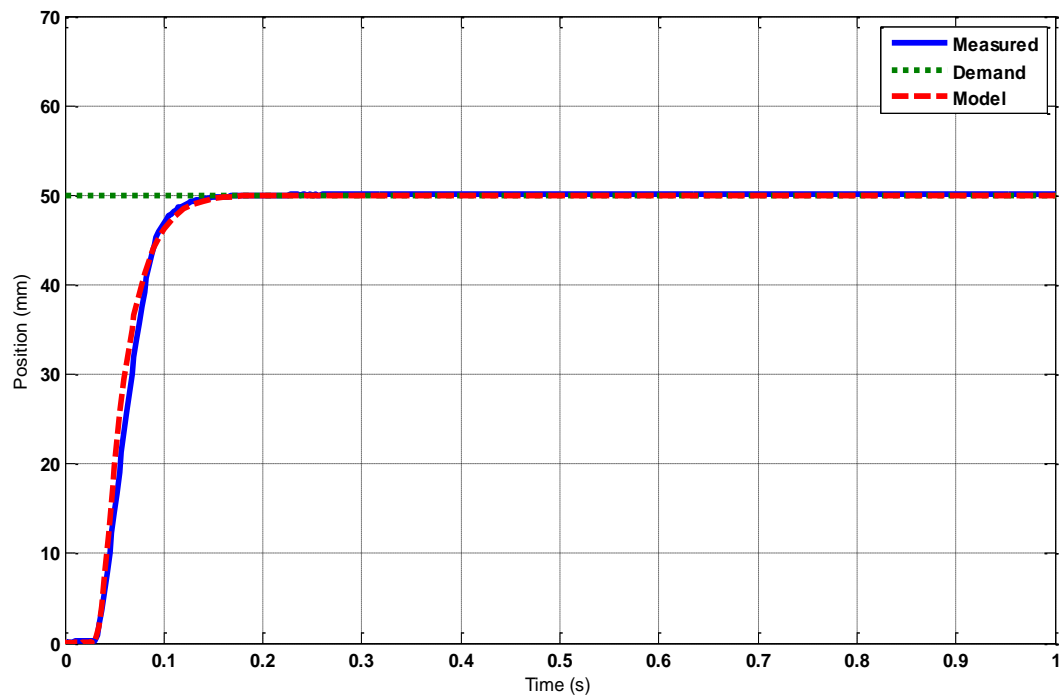
Figure 5.14: Step response comparison between model and system using LQR control

5.5   *Comparison of control methods*

In this section the designed control strategies described in the previous sections are compared. The comparison is carried out in order to assess which type of control scheme will be used (with regards to performance) to control the pneumatic system for the single actuator set-up and the Stewart-Gough platform.

Although both control schemes meet the required control specifications, assessing both schemes will allow evaluating the performances of each control scheme. The evaluation is carried out as a direct comparison. The comparisons are carried out using the single actuator set-up to different step responses. The outputs for various step inputs are shown in Figure 5.15.
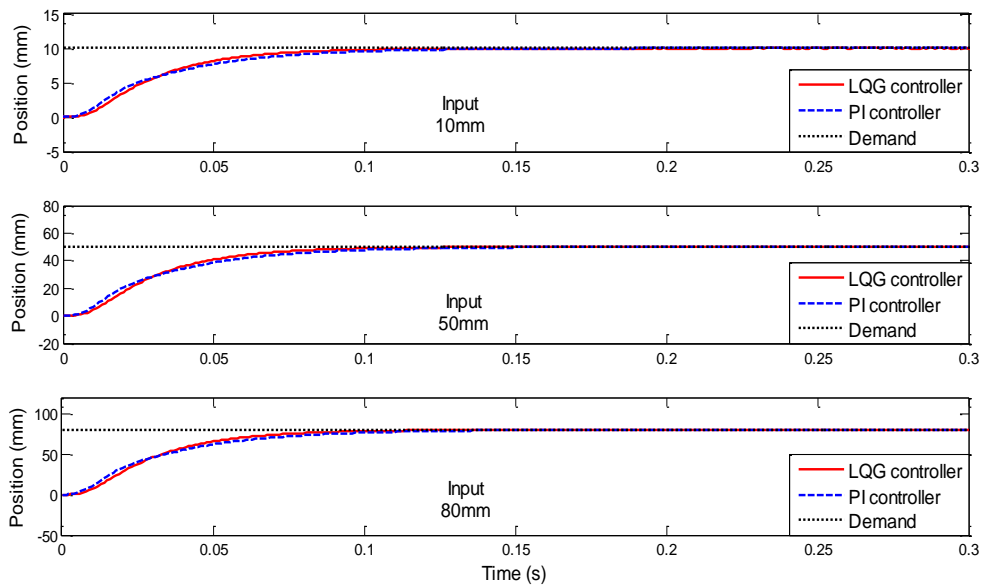
Figure 5.15: Comparison of controllers for various step inputs

From Figure 5.15, various step inputs are applied for both control strategies. It can be seen that both strategies are within the control specifications described in section 5.2. However, the LQG control scheme shows to be reaching the steady-state value quicker (settling time). The performance of both strategies show to be adequate for controlling the pneumatic system, with the LQG controller showing slightly better performance.

5.6   Conclusion

In this chapter a brief review of various control techniques applied to pneumatic systems has been presented. For this work two control strategies have been designed in order to successfully meet the desired control specifications. Namely, (i) PI control, and (ii) LQG control.

The designed PI controller was implemented on the test rig in an antiwindup form and the closed-loop performance was found to be adequate (closely matching that of the design).

For the LQG controller strategy the outputs show that this approach also achieved the desired control objectives. In order to give tracking capability with this strategy, an integral control structure was implemented with reference input. This approach gave slightly better tracking of the input reference signal, when compared to the PI controller.

In order to evaluate the designed control schemes a direct comparison was made. The results depicted that the performance of both strategies is adequate for controlling the pneumatic system (the LQG controller showed slightly better performance with regards to settling time). Of course, both could be slightly redesigned to change this result. Though the LQG approach has more flexibility to further improve response time whereas the PI structure is on its limit (any increase in K_P requires an increase in T_i (less K_i) to maintain stability margins. So having evaluated the performance of the designed control strategies, it is clear that either control scheme can be successfully applied to both test rig experiments. For the experiments in this thesis, the PI controller will be used for the single actuator test rig and the LQG controller will be used for the Stewart-Gough platform. It should be noted that for the reasons discussed above either control scheme can be used for the single actuator test rig or the Stewart-Gough platform test rig.

Chapter 6

Stewart-Gough platform kinematics

This chapter discusses the kinematics and control (algorithm) used to provide motion for the Stewart-Gough platform described in chapter 3. A Stewart-Gough platform is a six degrees of freedom mechanism consisting of a movable platform, fixed base, 12 spherical joints, and six links whose length is adjustable. Much effort has been devoted to finding an efficient algorithm for giving an accurate kinematic solution, where the kinematic solution establishes the relationship between the lengths of the six cylinders and the position and configuration of the mobile platform. In literature two main approaches are considered. (i) The inverse kinematic solution and, (ii) The forward kinematics solution. Both methods are discussed below.

6.1   The inverse kinematic solution

The inverse kinematic solution of the Stewart-Gough platform provides a means to obtain the link (cylinder) lengths as a function of the position, (x, y, z - linear motions) and orientation, (α, β, γ – angular motions), (see for example Stewart, 1965; Yang and Lee, 1984; Nguyen and Pooran, 1988; Zanganek *et al,* 1997; Wang and Gosselin, 1998). The linear motions consist of the longitudinal (surge), lateral (sway), and vertical (heave) motion, whereas angular motions are expressed as Eulerian angle rotations with respect to the x-axis (roll), y-axis (pitch), and z-axis (yaw) illustrated in Figure 6.1.
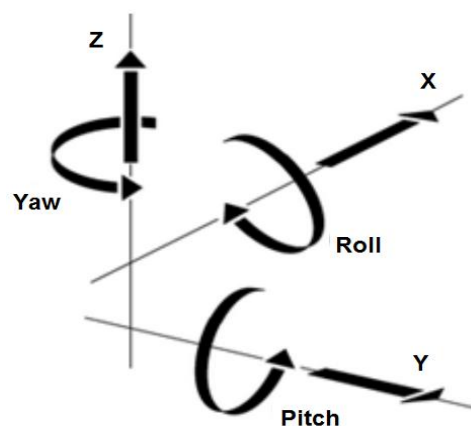
Figure 6.1: Linear and angular motions.

Inverse kinematics deals with the determination of a set of joint variables, which yield a set of Cartesian variables, usually composed of Cartesian position and orientation of the Stewart-Gough platform with respect to a reference frame. For the Stewart-Gough platform the lengths of the pneumatic cylinders are linearly variable, and therefore are chosen to be the joint variables. Following from Yang and Lee (1984); Craig (1989), and Nguyen and Pooran (1988) in order to define the Cartesian variables two coordinate frames {A}, and {B} are assigned to the moveable and fixed base platforms, respectively. Figure 6.2 illustrates, the origin of Frame {A} is chosen to be the centroid A of the moveable platform (this is also called the payload platform), the z_A-axis is pointing upwards and the x_A-axis passes through the joint attachment point A_1. The angle between A_1 and A_2 is denoted by θ_A, and in order to obtain a symmetrical distribution of joints on the moveable platform the angles between A_1 and A_3 and between A_3 and A_5 are at 120 degrees.

Frame {B} has its origin at the centroid B of the base frame. The x_B-axis passes through the joint attachment point B_1 and the angle between B_1 and B_2 is denoted by θ_B. Where, the angles between B_1 and B_3 and between B_3 and B_5 are at 120 degrees. This maintains a symmetrical distribution of joints on the base platform (Nguyen and Pooran, 1988). The Cartesian variables are chosen to be the relative position and orientation of Frame {A} with respect to Frame {B}, where the position of Frame {A} is specified by the position of its origin with respect to Frame {B}.
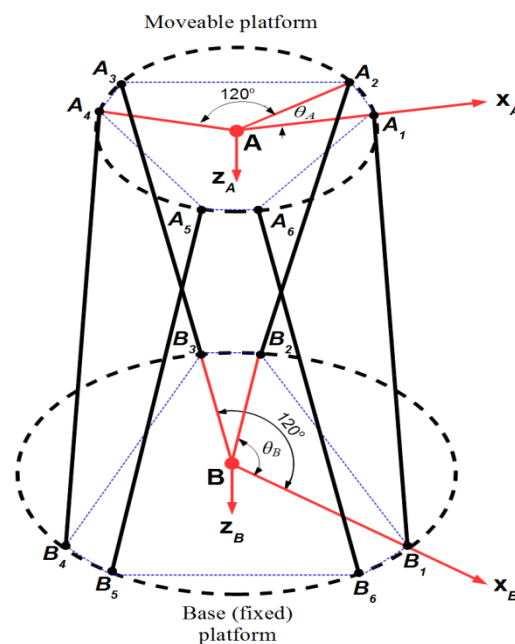
Figure 6.2: Stewart-Gough platform frame assignment

Denoting the angle between AA_i and x_A by λ_i, and the angle between BB_i and x_B by Λ_i for $i = 1, 2, 3, 4, 5, 6$, then by inspection of Figure 6.2, the following can be obtained.

$$\lambda_i = 60(i-1)^o; \quad \Lambda_i = 60(i-1)^o \qquad i = 1, 3, 5 \tag{62}$$

and

$$\lambda_i = \lambda_{i-1} + \theta_A \ ; \quad \Lambda_i = \Lambda_{i-1} + \theta_B \qquad i = 2, 4, 6 \tag{63}$$

In addition, if the Vector $^A a_i = \begin{pmatrix} a_{ix} & a_{iy} & a_{iz} \end{pmatrix}^T$ describes the position of the attachment point A_i with respect to Frame $\{A\}$, and Vector $^B b_i = \begin{pmatrix} b_{ix} & b_{iy} & b_{iz} \end{pmatrix}^T$ the position of the attachment point B_i with respect to Frame $\{B\}$, these can be expressed as

$$^A a_i = \begin{bmatrix} r_A \cos(\lambda_i) \\ r_A \sin(\lambda_i) \\ 0 \end{bmatrix} = \begin{bmatrix} a_{ix} \\ a_{iy} \\ a_{iz} \end{bmatrix} \tag{64}$$

And

$$^B b_i = \begin{bmatrix} r_B \cos(\Lambda_i) \\ r_B \sin(\Lambda_i) \\ 0 \end{bmatrix} = \begin{bmatrix} b_{ix} \\ b_{iy} \\ b_{iz} \end{bmatrix} \tag{65}$$

For $i = 1, 2, 3, 4, 5, 6$. Where r_A and r_B represent the radii of the moveable and base platforms, respectively.

Figure 6.3 shows a vector diagram for the ith actuator. The length vector $^B q_i = \begin{pmatrix} q_{ix} & q_{iy} & q_{iz} \end{pmatrix}^T$, expressed with respect to Frame $\{B\}$ can be found by

$$^B q_i = {}^B a_i - {}^B b_i \tag{66}$$

Where Vector $^B\text{a}_i$ and Vector ^Bd describe the positions of A_i and A, respectively both in terms of Frame {B} (Nguyen and Pooran, 1988). Vector ^Bd contains the Cartesian coordinates x, y, z of the origin, A of the Frame {A} with respect to Frame {B} such that

$$^B\text{d} = (x\ y\ z)^T \tag{67}$$
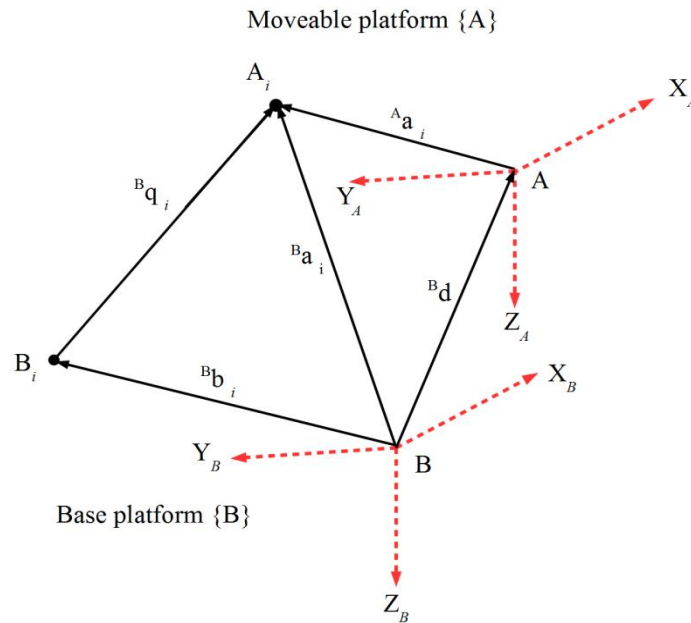
Figure 6.3: Vector diagram for the ith actuator

Assigning $^B_A R$ as the orientation matrix. This represents the orientation of Frame {A} with respect to Fame {B}. This can be shown as:

$$^B_A R = \begin{bmatrix} r_{11} & r_{12} & r_{13} \\ r_{21} & r_{22} & r_{23} \\ r_{31} & r_{32} & r_{33} \end{bmatrix} \tag{68}$$

For $i = 1, 2, 3, 4, 5, 6$, then $^B\text{a}_i$ can be computed by

$$^B\text{a}_i = {}^B_A R\ {}^A\text{a}_i + {}^B\text{d} \tag{69}$$

90

Now substituting equation (69) into equation (66) gives

$$^{B}q_i = {}_{A}^{B}R\, {}^{A}a_i + {}^{B}d - {}^{B}b_i \quad \text{for } i = 1, 2, 3, 4, 5, 6 \tag{70}$$

Where ${}_{A}^{B}R\, {}^{A}a_i$ can be written as

$$_{A}^{B}R\, {}^{A}a_i = \begin{bmatrix} r_{11}\, a_{ix} + r_{12}a_{iy} + r_{13}a_{iz} \\ r_{21}\, a_{ix} + r_{22}a_{iy} + r_{23}a_{iz} \\ r_{31}\, a_{ix} + r_{32}a_{iy} + r_{33}a_{iz} \end{bmatrix} \tag{71}$$

Then equation (68) can be rewritten as the following

$$^{B}q_i = \begin{bmatrix} r_{11}\, a_{ix} + r_{12}a_{iy} + r_{13}a_{iz} + x - b_{ix} \\ r_{21}\, a_{ix} + r_{22}a_{iy} + r_{23}a_{iz} + y - b_{iy} \\ r_{31}\, a_{ix} + r_{32}a_{iy} + r_{33}a_{iz} + z - b_{iz} \end{bmatrix} \tag{72}$$

The length of Vector $^{B}q_i$, l_i can be computed from the vector components as

$$l_i = \sqrt{q_{ix}^2 + q_{iy}^2 + q_{iz}^2} \tag{73}$$

Using equation (72) equation (73) can be rewritten as the following

$$l_i{}^2 = x^2 + y^2 + z^2 + a_{ix}^2(r_{11}^2 + r_{21}^2 + r_{31}^2) + a_{iy}^2(r_{12}^2 + r_{22}^2 + r_{32}^2)$$

$$+a_{iz}^2(r_{13}^2 + r_{23}^2 + r_{33}^2) + b_{ix}^2 + b_{iy}^2 + b_{iz}^2 + 2a_{ix}a_{iy}(r_{11}r_{12} + r_{21}r_{22} + r_{31}r_{32})$$

$$+2a_{ix}a_{iz}(r_{11}r_{13} + r_{21}r_{23} + r_{31}r_{33}) + 2a_{iy}a_{iz}(r_{12}r_{13} + r_{22}r_{23} + r_{32}r_{33})$$

$$+2(r_{11}a_{ix} + r_{12}a_{iy} + r_{13}a_{iz})(x - b_{ix}) + 2(r_{21}a_{ix} + r_{22}a_{iy} + r_{23}a_{iz})(y - b_{iy})$$

$$+2(r_{31}a_{ix} + r_{32}a_{iy} + r_{33}a_{iz})(z - b_{iz}) - 2(xb_{ix} + yb_{iy} + zb_{iz}) \tag{74}$$

From the properties of orientation matrix

$$r_{11}^2 + r_{21}^2 + r_{31}^2 = r_{12}^2 + r_{22}^2 + r_{32}^2 = r_{13}^2 + r_{23}^2 + r_{33}^2 = 1 \tag{75}$$

Also

$$r_{11}r_{12} + r_{21}r_{22} + r_{31}r_{32} = 0$$

$$r_{11}r_{13} + r_{21}r_{23} + r_{31}r_{33} = 0$$

$$r_{12}r_{13} + r_{22}r_{23} + r_{32}r_{33} = 0 \tag{76}$$

From equation (62) and equation (63) it can be noted that

$$a_{iz} = b_{iz} = 0 \tag{77}$$

$$a_{ix}^2 + a_{iy}^2 + a_{iz}^2 = r_A^2 \tag{78}$$

$$b_{ix}^2 + b_{iy}^2 + b_{iz}^2 = r_B^2 \tag{79}$$

Therefore equation (74) can be simplified to

$$l_i^{\,2} = x^2 + y^2 + z^2 + r_A^2 + r_B^2 + 2(r_{11}a_{ix} + r_{12}a_{iy})(x - b_{ix})$$

$$+2(r_{21}a_{ix} + r_{22}a_{iy})(y - b_{iy}) + 2(r_{31}a_{ix} + r_{32}a_{iy})z - 2(yb_{iy}) \tag{80}$$

For $i = 1, 2, 3, 4, 5, 6$.

Equation (80) represents the inverse kinematics solution for a given Cartesian configuration, composed of the position and orientation specified by equation (67) and equation (68). The actuator lengths l_i for $i = 1, 2, 3, 4, 5, 6$, can be calculated using equation (80). In equation (68) nine variables are needed to describe the orientation of

Frame {A}, where six of them are redundant because only three are needed to specify an orientation (Fichter, 1986). There are several methods to represent an orientation by three variables (see for example Craig 1989). The most widely used method is the Euler Angles α, β, and γ, which represent the orientation of Frame {A}, obtained after the following sequence of rotations from Frame {B}:

1. A rotation of α about the z_B-axis (Roll)
2. A rotation of β about the y_B-axis (Pitch)
3. A rotation of γ about the x_B-axis (Yaw).

The orientation represented by α, β, and γ, can be given by

$$R_{xyz}(\alpha, \beta, \gamma) = \begin{bmatrix} c\alpha & -s\alpha & 0 \\ s\alpha & c\alpha & 0 \\ 0 & 0 & 1 \end{bmatrix} \begin{bmatrix} c\beta & 0 & s\beta \\ 0 & 1 & 0 \\ -s\beta & 0 & c\beta \end{bmatrix} \begin{bmatrix} 1 & 0 & 0 \\ 0 & c\gamma & -s\gamma \\ 0 & s\gamma & c\gamma \end{bmatrix} \tag{81}$$

Where $c\alpha = cos\alpha$ and $s\alpha = sin\alpha$. Multiplying out equation (81) gives

$$R_{xyz}(\alpha, \beta, \gamma) = \begin{bmatrix} c\alpha c\beta & c\alpha s\beta s\gamma - s\alpha c\gamma & c\alpha s\beta c\gamma + s\alpha s\gamma \\ s\alpha c\beta & s\alpha s\beta s\gamma + c\alpha c\gamma & s\alpha s\beta c\gamma - c\alpha s\gamma \\ -s\beta & c\beta s\gamma & c\beta c\gamma \end{bmatrix} \tag{82}$$

6.2   The forward kinematics solution.

Forward kinematics deals with determining the position and orientation of the moving platform when the actuator lengths are known. To solve for the position of the top moveable platform in terms of given lengths, 30 non-linear algebraic equations must be solved simultaneously (Liu *et al* 1991). Due to the time-consuming nature of this procedure, it is impossible to compute the kinematic solutions on-line. Waldron *et al* (1989) and Nanua *et al* (1990) made efforts to solve the 30 equations as 24th-order polynomials and 16th-order respectively in a single variable. These approaches made for high computational complexity in solving such high order polynomials, the multiple solutions alone (64 possible solutions) make this an impossible approach to use practically.

Generally, there exists no closed-form solution for the forward kinematics solution. However, a brief explanation of one method is described. Many authors have used iterative

numerical methods to solve non-linear equations. One widely used method for solving the non-linear equations has been the Newton-Raphson method (Fichter, 1986).

Although the Newton-Raphson method is a popular technique to solve the derivation problem, it suffers from repetitive steps before solution convergence and hence fails to become a real-time solution. Moreover, this technique can lead to infinite looping in the case of wrong selection of the initial values. Nevertheless, the general form (Song and Kwon, 2001 and Nguyen and Pooran, 1988) of expression can be made by rewriting equation (80) so that

$$f_i(x, y, z, \alpha, \beta, \gamma) = x^2 + y^2 + z^2 + r_A^2 + r_B^2 + 2(r_{11}a_{ix} + r_{12}a_{iy})(x - b_{ix})$$

$$+ 2(r_{21}a_{ix} + r_{22}a_{iy})(y - b_{iy}) + 2(r_{31}a_{ix} + r_{32}a_{iy})z - 2(yb_{iy}) - {l_i}^2 = 0$$

$$(83)$$

6.3   Kinematic equation validation through simulation

In order to validate the inverse kinematic equation (80), a comparison with the direct kinematic solution can be made. The validation approach is shown in Figure 6.4.
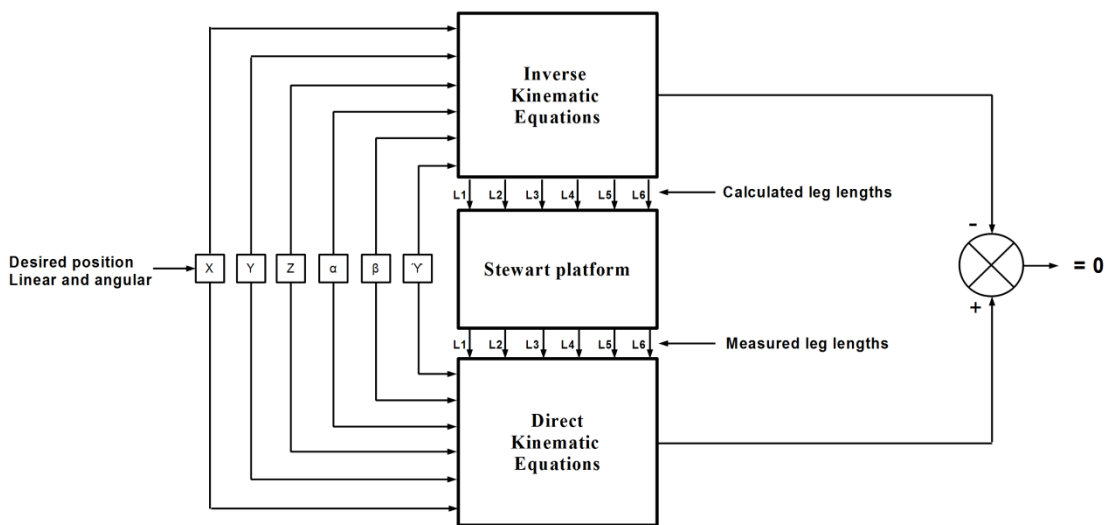
Figure 6.4: Inverse kinematic equations validation

Figure 6.4 shows the desired position in terms of translational and rotation is inputted into both inverse and forward kinematic equations. The inverse kinematics calculates the required leg lengths of the pneumatic cylinders. The measured leg lengths are then inserted into the forward kinematic equations. The output from the inverse kinematic equations is then subtracted from the forward kinematic equations output, where if there is no discrepancy the results should be zero. The validation equation is shown in equation (84).

$$[[x^2 + y^2 + z^2 + r_A^2 + r_B^2 + 2(r_{11}a_{ix} + r_{12}a_{iy})(x - b_{ix}) + 2(r_{21}a_{ix} + r_{22}a_{iy})(y - biy+2r31aix+r32aiyz-2ybiy]-[x2+y2+z2+rA2+rB2$$

$$+2r11aix+r12aiyx-bix+2r21aix+r22aiyy-biy+2r31aix+r32aiyz-2ybiy]=0$$

Where $i = 1, 2, 3, 4, 5, 6.$ (84)

Simulations are carried out using Matlab. The code used for this is detailed in Appendix D. Different value of linear motions (x, y, z) and orientation, (α, β, γ − angular motions) are inserted into the equations and the output in terms of actuator lengths are calculated and shown graphically. Figure 6.5 shows the graphical display with the Cartesian coordinates set at $x = 0$, $y = 0$, $z = 353$, $\alpha = 0$, $\beta = 0$, $\gamma = 0$. These setting are when the platform is at rest position. Applying these setting the lengths of the actuators (l_i =1, 2, 3, 4, 5, 6) are calculated to 364.95mm for each actuator. This length is also confirmed from the length of the actuators of the Stewart-Gough platform test rig.
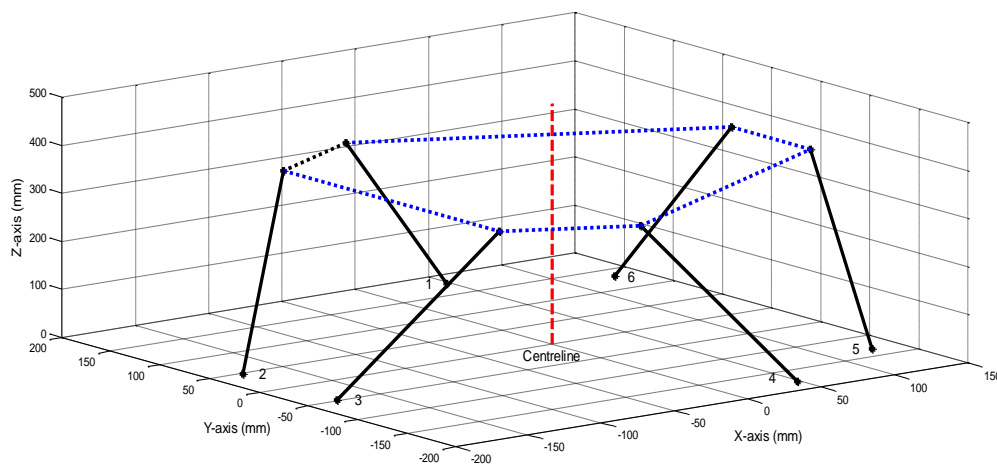
Figure 6.5: Platform in rest position

$$x = 0, \ y = 0, \ z = 353, \ \alpha = 0, \ \beta = 0, \ \gamma = 0 \text{ (Rest position)}$$

Figure 6.6 shows the graphical display with the Cartesian coordinates set at $x = 0, \ y = 0, \ z = 440$mm, $\alpha = 0, \ \beta = 0, \ \gamma = 0$. Applying these setting the lengths are calculated as

$$l_1 = 449.6481 \text{ mm}$$
$$l_2 = 449.6481 \text{ mm}$$
$$l_3 = 449.6481 \text{ mm}$$
$$l_4 = 449.6481 \text{ mm}$$
$$l_5 = 449.6481 \text{ mm}$$
$$l_6 = 449.6481 \text{ mm}$$
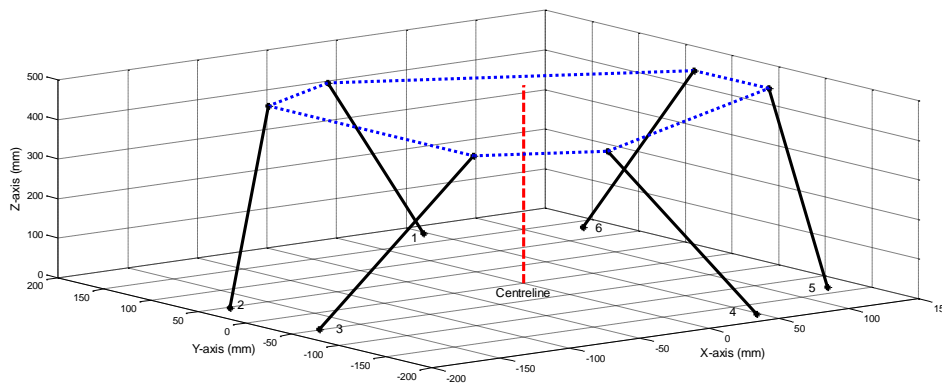
Figure 6.6: Platform movement in z direction

$$x = 0, \ y = 0, \ z = 440\text{mm}, \ \alpha = 0, \ \beta = 0, \ \gamma = 0.$$

Figure 6.7 shows the graphical display with the Cartesian coordinates set at $x = 50, \ y = 0, \ z = 420$mm, $\alpha = 0, \ \beta = 0, \ \gamma = 0$. Applying these setting the lengths are calculated as

$$l_1 = 422.7098 \text{ mm}$$
$$l_2 = 440.9001 \text{ mm}$$
$$l_3 = 440.9001 \text{ mm}$$
$$l_4 = 422.7098 \text{ mm}$$
$$l_5 = 435.1710 \text{ mm}$$
$$l_6 = 435.1710 \text{ mm}$$
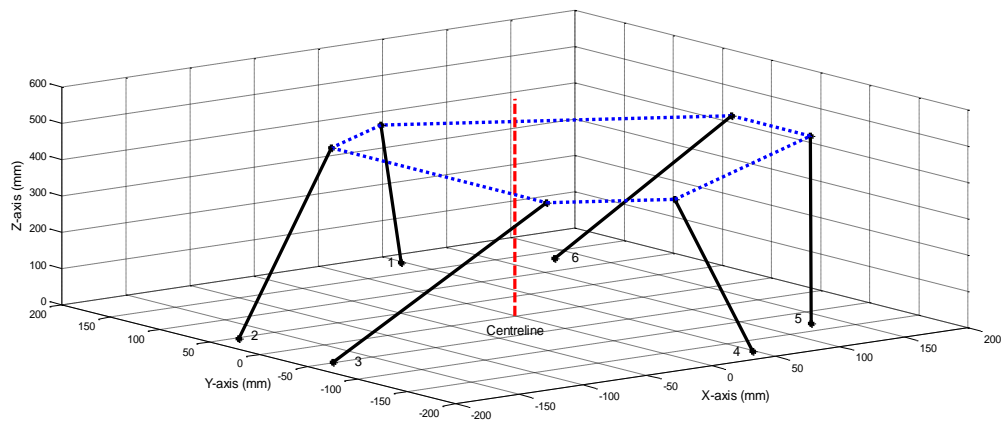
Figure 6.7: Platform position in x direction

$$x = 50\text{mm}, y = 0, z = 420\text{mm}, \ \alpha = 0, \beta = 0, \gamma = 0$$

Figure 6.8 shows the graphical plot with the Cartesian coordinates set at $x = 0$, $y = 50\text{mm}$, $z = 420\text{mm}$, $\alpha = 0$, $\beta = 0$, $\gamma = 0$. The lengths of the actuators are calculated as

$$l_1 = 429.6343 \text{ mm}$$
$$l_2 = 440.0630 \text{ mm}$$
$$l_3 = 425.8068 \text{ mm}$$
$$l_4 = 436.3270 \text{ mm}$$
$$l_5 = 443.3432 \text{ mm}$$
$$l_6 = 422.3904 \text{ mm}$$
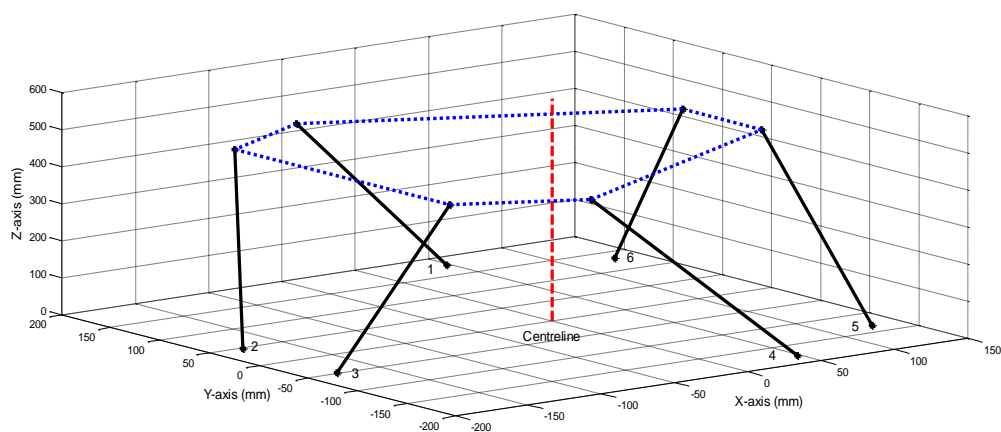
Figure 6.8: Platform position in y direction

$$x = 0, \ y = 50\text{mm}, \ z = 420\text{mm}, \ \alpha = 0, \ \beta = 0, \ \gamma = 0.$$

97

Figure 6.9 shows the graphical plot with the Cartesian coordinates set at $x = 0$, $y = 0$, $z = 420$mm, $\alpha = 0.35$, $\beta = 0$, $\gamma = 0$. The lengths of the actuators are calculated as

$$l_1 = 444.7777 \text{ mm}$$
$$l_2 = 422.0924 \text{ mm}$$
$$l_3 = 444.7777 \text{ mm}$$
$$l_4 = 422.0924 \text{ mm}$$
$$l_5 = 444.7777 \text{ mm}$$
$$l_6 = 422.0924 \text{ mm}$$

Figure 6.10 shows the graphical display with the Cartesian coordinates set at $x = 0$, $y = 0$, $z = 420$mm, $\alpha = 0$, $\beta = 20^0$ (0.35 rad), $\gamma = 0$. Applying these setting the lengths of the actuators are calculated as

$$l_1 = 443.0639 \text{ mm}$$
$$l_2 = 467.8966 \text{ mm}$$
$$l_3 = 467.8966 \text{ mm}$$
$$l_4 = 443.0639 \text{ mm}$$
$$l_5 = 443.0639 \text{ mm}$$
$$l_6 = 379.7818 \text{ mm}$$
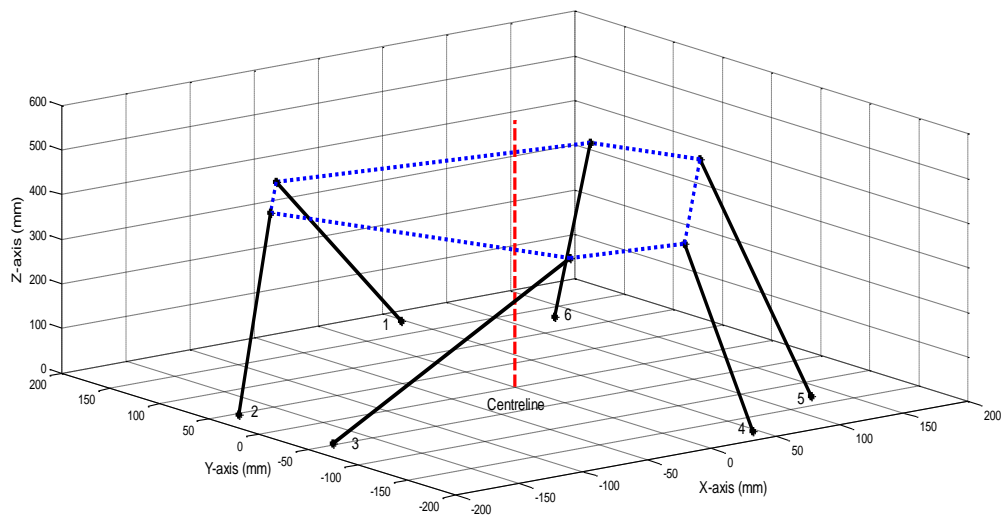
Figure 6.9: Platform position in α (yaw) rotation

$x = 0$, $y = 0$, $z = 420$mm, $\alpha = 20^0$ (0.35 rad), $\beta = 0$, $\gamma = 0$
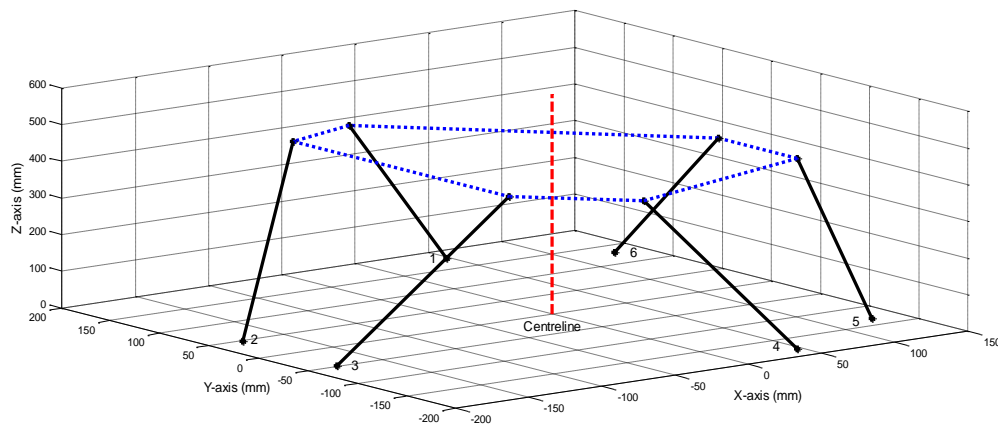
Figure 6.10: Platform position in β (pitch) rotation

$$x = 0, \ y = 0, \ z = 420\text{mm}, \ \alpha = 0, \ \beta = 20^0(0.35 \text{ rad}), \ \gamma = 0$$

Figure 6.11 shows the graphical display with the Cartesian coordinates set at $x = 0$, $y = 0$, $z = 420$mm, $\alpha = 0$, $\beta = 0$ $\gamma = 20^0$ (0.35 rad). Applying these setting the lengths of the actuators are calculated as

$$l_1 = 480.9902 \text{ mm}$$
$$l_2 = 466.0352 \text{ mm}$$
$$l_3 = 392.4930 \text{ mm}$$
$$l_4 = 380.9245 \text{ mm}$$
$$l_5 = 417.2106 \text{ mm}$$
$$l_6 = 444.0437 \text{ mm}$$
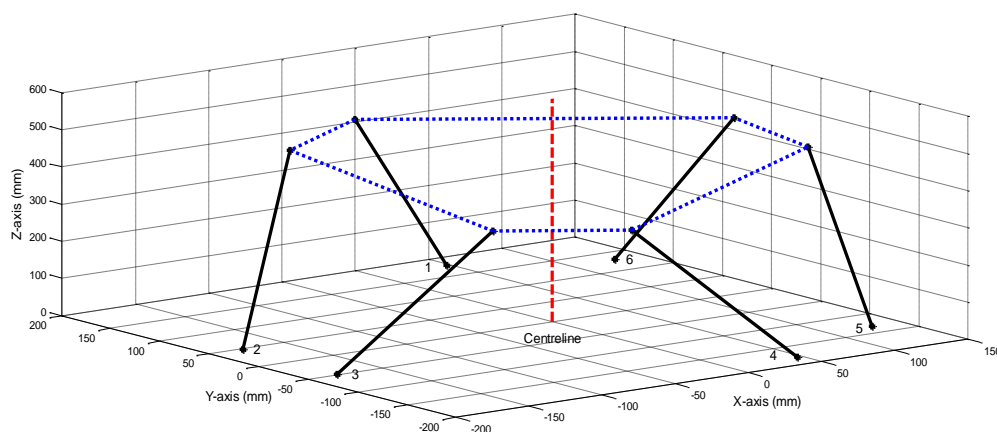
Figure 6.11: Platform position in γ (roll) rotation

$$x = 0, \ y = 0, \ z = 420\text{mm}, \ \alpha = 0, \ \beta = 0, \ \gamma = 20^0(0.35 \text{ rad})$$

Figure 6.12 shows the graphical plot of applying multi-inputs with regards to the Cartesian coordinates. The Cartesian coordinates are set at $x = 0$, $y = 50$mm, $z = 420$mm, $\alpha = 11.45^0$ (0.2 rad), $\beta = 0$ $\gamma = 20^0$ (0.35 rad) . Applying these setting the lengths of the actuators are calculated as

$$l_1 = 465.7947 \text{ mm}$$
$$l_2 = 447.9538 \text{ mm}$$
$$l_3 = 374.6688 \text{ mm}$$
$$l_4 = 363.2451 \text{ mm}$$
$$l_5 = 424.1204 \text{ mm}$$
$$l_6 = 414.0833 \text{ mm}$$
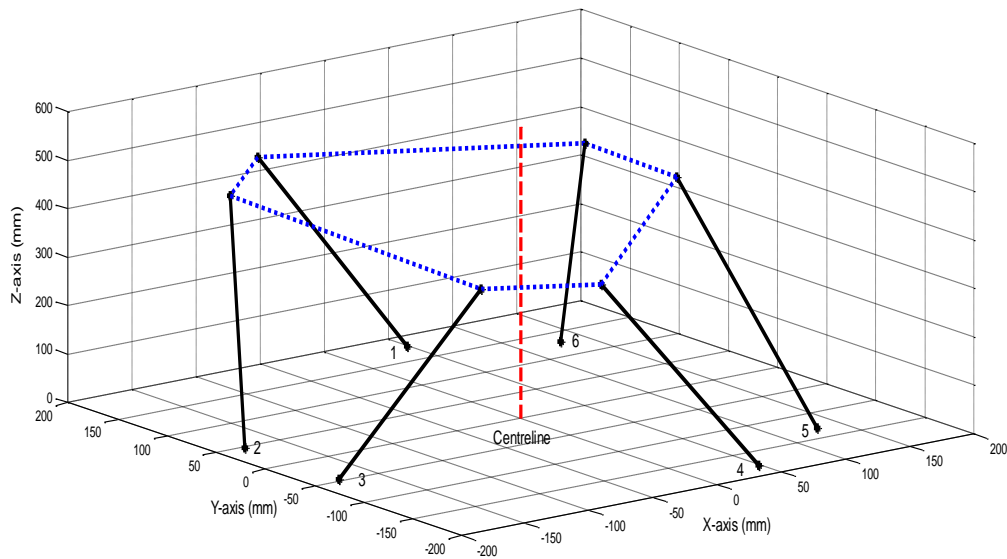
Figure 6.12: Platform position for γ (roll), α (yaw) rotation and z (vertical) and y (lateral) movement. $x = 0$, $y = 50$mm, $z = 420$mm, $\alpha = 11.45^0$ (0.2 rad), $\beta = 0$, $\gamma = 20^0$ (0.35 rad).

6.4   Stewart-Gough platform control strategy

Due to the relative simplicity and with its low computational requirements the inverse kinematic approach will be used within the control strategy. As described in Chapter three in order to control the movement of the Stewart-Gough platform, all six pneumatic cylinders have to be controlled simultaneously. Previously described in chapter 3 is the Stewart-Gough platform hardware set-up. Figure 6.13 describes the control system arrangement. This shows the input is the required position (pose) of the Stewart-Gough platform in terms of the linear motions which consist of the longitudinal (surge), lateral (sway), and vertical (heave) motion, whereas angular motions are expressed as Eulerian angle rotations with respect to the x-axis (roll), y-axis (pitch), and z-axis (yaw). The required motion is then passed through the inverse kinematic solution (equations 80 and 82). The inverse kinematic solution converts the desired position and orientation of the platform into the required pneumatic cylinder lengths. These calculated lengths are then compared with the measured output lengths of the pneumatic cylinders. The comparison difference (error) is then fed through the controller (the two control approaches are described in chapter 4) the controller then applies the necessary control action, which in turn is applied to each pneumatic cylinder, achieving the correct lengths.

6.5   Conclusion

In conclusion, this chapter has discussed the kinematics and control (algorithm) used to provide motion for the Stewart-Gough platform. Two types of kinematic solutions have been discussed, namely, inverse kinematics and forward kinematics. In comparison the inverse kinematic solution was found to be simpler to implement and to require less computational effort. The formulated equations for the inverse kinematics were simulated using Matlab and the plots show the position (pose) of the platform in terms of cylinder lengths to the desired position and orientation. The control strategy of the Stewart-Gough platform was also discussed. This described where in the control loop the kinematic equations are located in order to calculate the desired pneumatic cylinder lengths. For this set-up both PI and LQG control could be used as a means of providing the local position control action for the Stewart-Gough platform.
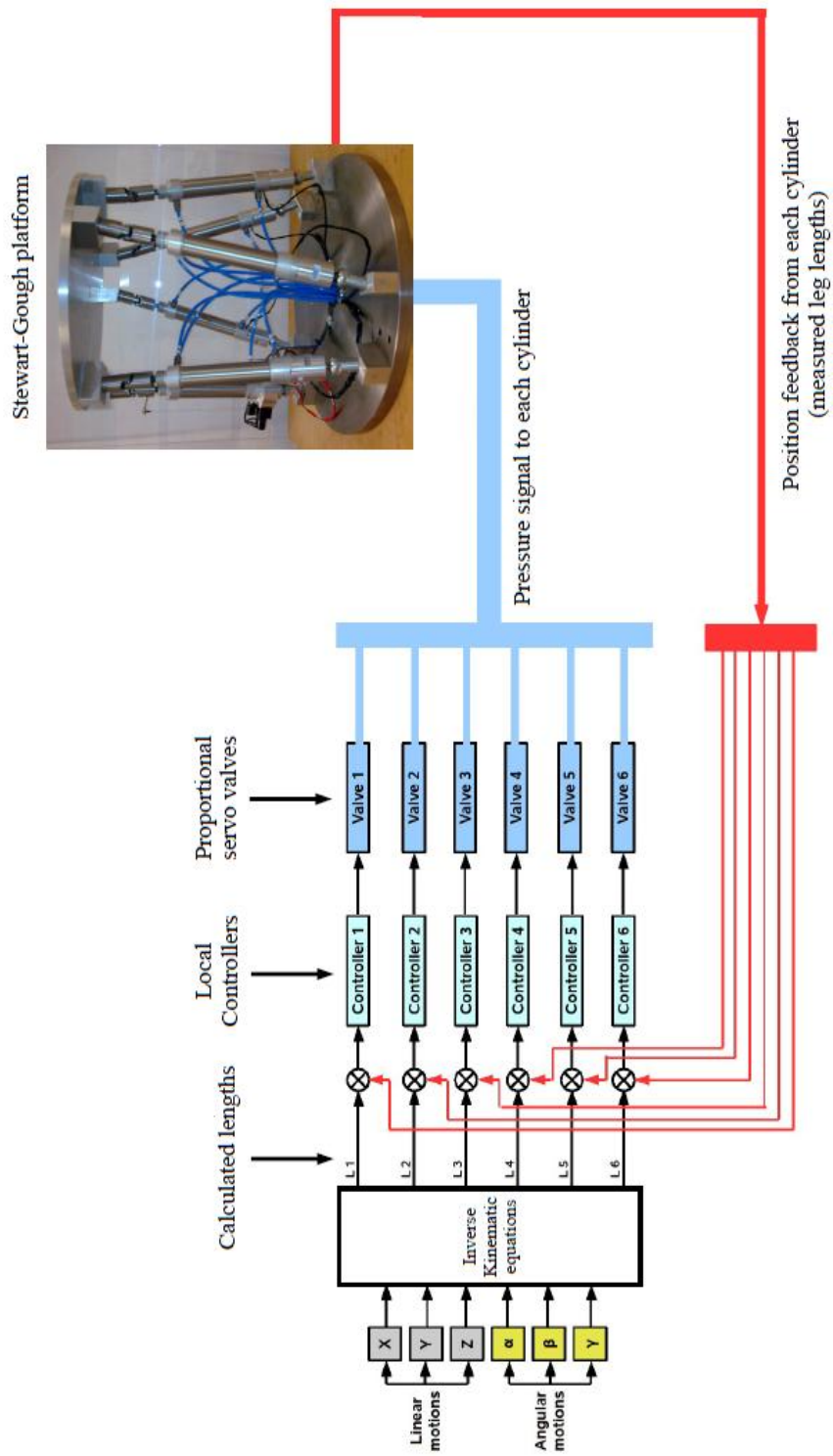
Figure 6.13: Stewart-Gough platform control system arrangement

Chapter 7

Design of fault detection and isolation scheme

7.1   Introduction

In this chapter a model-based fault detection and isolation strategy is developed for the Stewart-Gough platform. The main reasons for a model-based approach were highlighted in chapters 1 and 2. They include, firstly as a model is already available (chapter 4) it seems that a co-designed control and fault detection and isolation (FDI) scheme is practical solution and secondly, using a hardware redundancy approach will increase the cost of the necessary equipment, including increased complexity of the Stewart-Gough platform design and structure. Thirdly, as no prior knowledge in terms of time histories for normal and fault operation of the pneumatic system are known (new system), therefore qualitative models or process history based schemes are difficult to employ.

The approach adopted for this work is to design the FDI scheme on the single cylinder set-up. Then utilize this modular design and apply this to the full Stewart-Gough platform system. In this chapter, subsection 7.1.1 describes typical fault associated with pneumatic systems. Section 7.2 describes the general FDI approach and describes the formulation of the parity and Kalman filter equations. Section 7.3 describes the FDI scheme used. In section 7.4, the FDI scheme is tested initially on the single actuator model. In section 7.5, the application of the redundant signal and voting scheme is described. Section 7.6 describes the FDI scheme for the Stewart-Gough platform model. This includes testing the FDI scheme for the Stewart-Gough platform. Section 7.7 concludes the chapter. Typical pneumatic system faults are discussed below.

7.1.1   Typical pneumatic system faults

Air leaks may occur during normal operating conditions. Leaks can contribute to a decreased performance of a pneumatic system. Leaks cause a drop in system pressure, which can make air driven equipment function less efficiently, adversely affecting performance. Leaks can appear from any part of the pneumatic system, the most common problem area include:

- Pipes, Couplings and fittings,

- Pressure regulators and actuators,

- Pipe joints, pipe disconnects and thread sealants.

In pneumatic systems a major fault can be blockages caused by restrictions formed within the compressed air pathways. One major cause can be damaged pipes. Another cause of blockages is rust. Simply put, atmospheric air contains water vapour. The air's ability to hold water vapour is dependent upon its temperature. As temperature increases, the level of water vapour held by the air increases during compression, air temperature is increased significantly, which allows the air to retain incoming moisture. After the compression stage, air is typically cooled to a usable temperature, reducing the air's ability to retain water vapour. A proportion of the water vapour condenses into liquid water and can be removed by a drain fitted to the reservoir. Condensed water can cause corrosion to the storage (reservoir) and distribution system (piping), as well as damage to pneumatic components (proportional valve and cylinder). Liquid water can also wash away pre-lubricants on the cylinders and valves, decreasing their operational life. Water in a compressed air system also reduces production efficiency and increases maintenance costs. It must be noted that blockage faults due to water/particles in the pathways of the airways can be adequately dealt with when appropriate filtration systems are employed

Harsh working conditions along with the gradual build up of dirt on the sensor and faulty circuitry can cause the effect of sensor drift. Sensor drift can take effect over a long period of time, and occurs gradually and incrementally, however, it will not be evident on the system output. Sensors drift occurs without any obvious system changes or indications, therefore fault detection and isolation methods are of a particular importance to this type of fault.

Sensor signal loss can be caused mainly by two causes. (i) Sensor circuitry damage (i.e. damaged connections, loose connections) or (ii) Faulty sensor unit. In position feedback control systems or safety critical systems, sensor loss can have an adverse effect on the control signal, often making the system uncontrollable or unstable.

7.2 FDI Approach

Figure 7.1 shows the generic structure of the model-based fault detection scheme. The method consists of detecting faults in the process, which includes actuators, components and sensors, based on measuring the input signal *U(t)* and the output signal *Y(t)*. The detection method uses models to generate residuals *R(t)*. The residual evaluation examines the residuals for the likelihood of faults and a decision rule is applied to determine if faults have occurred. Referring to the pneumatic system depicted in Figure 3.1 (and with reference to Figure 7.1) the proportional valve would be described as the actuator and the pneumatic cylinder would be described as the plant. The sensors are self-evident. In this work the process model can be based on either parity equations or Kalman filters. Both are discussed below.
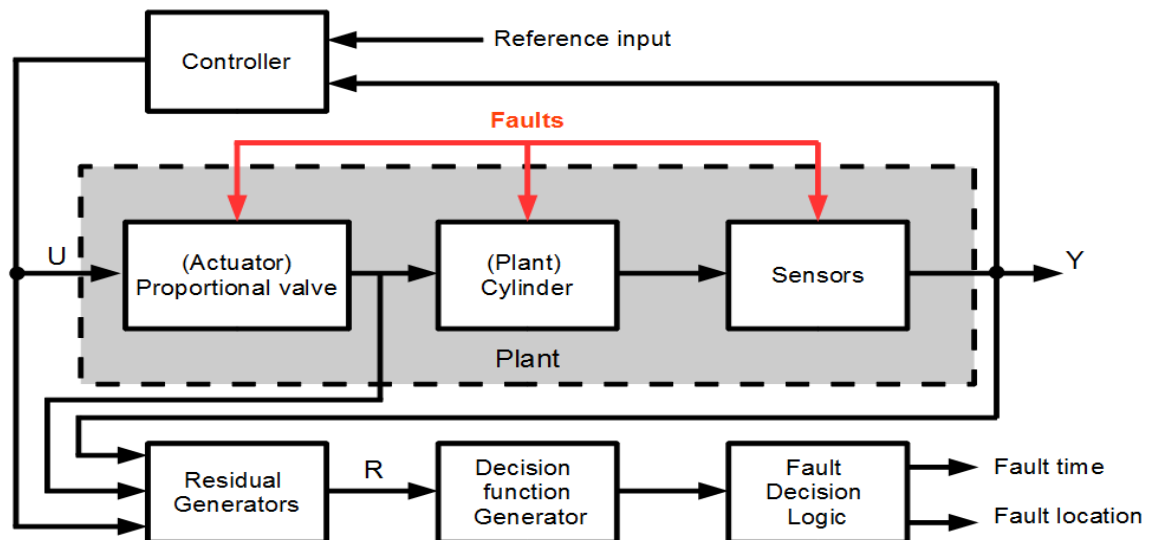
Figure 7.1: Generic structure of the model-based fault detection scheme

7.2.1 The Parity Equation Method

The parity equation method was first proposed by Chow and Willsky, (1984) using the redundancy relations of the dynamic system. The basic idea is to provide a proper check of the parity (consistency) of the measurements for the monitored system. Parity equations are rearranged and usually transformed variants of the input-output or space-state models of the system (Venkatasubramaniam *et al* 2003). In effect this means making use of known mathematical models that describe the relationships between system variables. In theory,

under normal operating conditions, the residual or value of the parity equations is zero mean. However, in real situations, the residuals will be nonzero. This is due to measurement and process noise, model inaccuracies and faults in sensors, actuators and plant(s). The idea of the parity approach is to rearrange the model structure to achieve the best fault isolation (i.e. so that the effect of faults is far greater than that of the other uncertainties). The residual generator scheme used hereafter is a model-based methodology using the parity space approach. The desired properties for the residual signal are ***R(t) ≠ 0*** if ***f(t) ≠ 0,*** where ***R*** is the residual and *f* is the fault. The residual is generated based on the information provided by the system input and output signals and the plant equation. Figure 7.2 shows the pneumatic control loop scheme, which contains the following elements: The controller *C(s),* the proportional valve *GA(s)*, the pneumatic actuator *GP(s)*, and the sensor *GS(s)*. The proportional valve fault *Fa(s)* and the sensor fault *FS(s)* can have dynamics, which are modelled by the transfer functions *Ha(s),* and *HS(s).* In addition to the position (feedback) sensor, pressure sensors are included in the system to read pressure from each chamber of the actuator. These are not included in the closed loop system, and are shown as *Pp(s)* and *Pn(s)* respectively. With the pressure sensor faults, shown as *FPp(s)* and *FPn(s)*, again having dynamics modelled by the transfer functions *HPp(s)* and *HPn(s).* Using the description of the system shown in Figure 7.2 the following relationships (equations) can be derived.

$$XS(s) = [GS(s)+HS(s)FS(s)][GA(s)U(s)\ GP(s)+Ha(s)Fa(s)\ GA(s)\ GP(s)] \tag{85}$$

$$Pn_{act}= [U(s)GA(s)+Ha(s)Fa(s)][Pn(s)+HPn(s)FPn(s)] \tag{86}$$

$$Pp_{act}= [U(s)GA(s)+Ha(s)Fa(s)][Pp(s)+HPp(s)FPp(s)] \tag{87}$$

$$U(s)=C(s)(V(s)-XS(s)) \tag{88}$$

With the current experimental set-up (Figure 3.1) the pneumatic plant output can only be measured with the position sensor. Therefore the actuator and plant faults cannot be isolated. Residuals are formulated from equations (85) to (88) as follows,

$$R_1=XS(s)-GS(s)GP(s)GA(s)U(s)=HS(s)FS(s)+Ha(s)Fa(s) \tag{89}$$

106

$$R_2 = Pn_{act} - U(s)GA(s)Pn(s) = Ha(s)Fa(s) + HPn(s)FPn(\text{s}) \qquad (90)$$

$$R_3 = Pp_{act} - U(s)GA(s)Pp(s) = Ha(s)Fa(s) + HPp(s)FPp(\text{s}) \qquad (91)$$

To represent the pneumatic process shown in Figure 7.2, *GA(s)* is modelled by the equations (28) and (29) and *GP(s)* by equation (30). It is assumed that the fault and sensor transfer functions are all instantaneous i.e. *Ha(s)*, *HS(s), HPn(s), HPp(s), Pn(s), Pp(s)* and *GS(s)* =1.
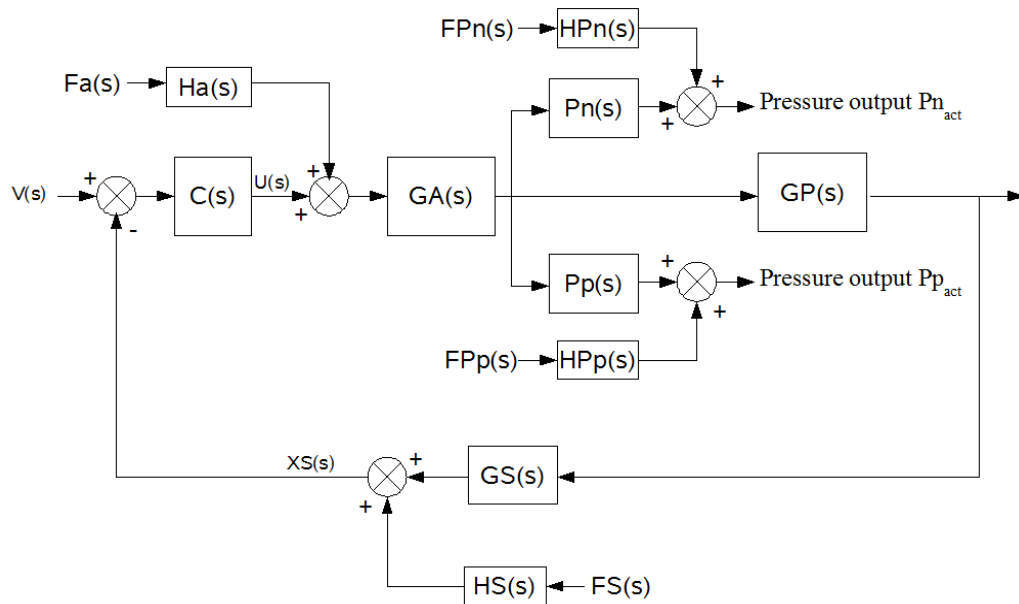
Figure 7.2: Pneumatic closed loop scheme with intended faults

7.2.2 *Observer approach (Kalman filter)*

Many authors have approached the FDI problem by directly starting with a single or banks of observers; see for example Frank and Ding (1997). The basic idea of the observer approach is to reconstruct the outputs of the system from the measurements or subsets of measurements with the aid of observers or Kalman filters using the estimation error or innovation (Frank, 1990), (It should noted, that the Kalman filter was also used in chapter

5 in the LQG control, in this case it was used as a state estimator). In fault detection, this estimation error or innovation is used as a residual for the detection and isolation of faults. Kalman filters are often used for the stochastic case, as noise can be considered directly in the problem formulation. See e.g. Kalman, (1960) for more details. In general, a Kalman filter processes all available measurements regardless of their precision, to estimate the current value of the variable of interest. Given a system:

$$\dot{x} = Ax + Bu + Gw \qquad \text{(State equations)} \qquad (92)$$

$$y = Cx + Du + Hw + v \qquad \text{(Measurement equations)} \qquad (93)$$

Where u is the input, w is the process noise, v is the measurement white noise with E $(ww^T) = Q$, and E $(vv^T) = R$. It is also assumed that the state and measurement noise is uncorrelated, that is, E $(wv^T) = 0$. An optimal estimate of y, $\hat{y}$ can be provided by the Kalman filter equations:

$$\dot{\hat{x}} = A\hat{x} + Bu + L(y - C\hat{x} - Du) \qquad (94)$$

and

$$\hat{y} = C\hat{x} + Du \qquad (95)$$

Where in practice the weightings for process and measurement noise (Q and R respectively) are chosen heuristically using engineering judgement to provide a trade-off between sensitivity to faults, and the likelihood of false alarms. The Kalman filter gain L is determined by solving an algebraic Riccati equation. This estimator uses the known inputs u and the measurement y to generate the output and state estimates $\hat{y}$ and $\bar{x}$. The Kalman estimator is depicted in Figure 7.3. In order to make the system model equations observable, equation (30) is manipulated and to achieve system observability the model is reduced from a fourth order equation to a third order equation. Equation (96) shows the observable state space representation.
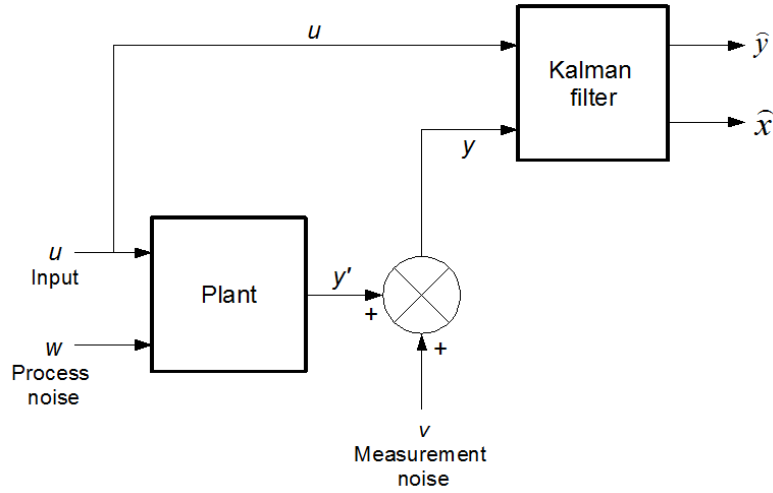
Figure 7.3: Schematic of the Kalman filter estimator

$$\dot{X}\begin{bmatrix} \dot{P_d} \\ \dot{x} \\ \ddot{x} \end{bmatrix} = \begin{bmatrix} 0 & 0 & a-b \\ 0 & 0 & 1 \\ \dfrac{A_{pn}}{M} & 0 & \dfrac{-F_f}{M} \end{bmatrix}\begin{bmatrix} P_d \\ x \\ \dot{x} \end{bmatrix} + \begin{bmatrix} c-d \\ 0 \\ 0 \end{bmatrix}v$$

$$y_{pos} = \begin{bmatrix} 0 & 1 & 0 \end{bmatrix}\begin{bmatrix} P_d \\ x \\ \dot{x} \end{bmatrix}$$

$$y_{P_d} = \begin{bmatrix} 1 & 0 & 0 \end{bmatrix}\begin{bmatrix} P_d \\ x \\ \dot{x} \end{bmatrix} \tag{96}$$

where

$$P_d = P_p - P_n, \quad A_p = A_n = A_{pn}, \quad a = -\frac{\gamma A \, P_p}{V_p}, \quad b = \frac{\gamma A P_n}{V_n}, \quad c = K\frac{\gamma R T_s}{V_p}, \quad d = -K\frac{\gamma R T_s}{V_n}$$

In designing the Kalman filter approach only the sensed outputs are considered. These are position and pressure difference outputs. Figure 7.4 illustrates the Kalman filter set up; where the residuals (R_4 and R_5) are given by two separate Kalman filters. The residual equations are:

$$R_4 = y_{pos} - C_{pos}\hat{x}_1 \tag{97}$$

$$R_5 = y_{P_d} - C_{P_d}\hat{x}_2 \tag{98}$$

where $\hat{x}_1$ and $\hat{x}_2$ are the state estimates from the two Kalman filters. The first $(\hat{x}_1)$ uses the position feedback. Whilst, the second $(\hat{x}_2)$ is based on the pressure difference feedback.

$$C_{pos} = \begin{bmatrix} 0 & 1 & 0 \end{bmatrix}, C_{P_d} = \begin{bmatrix} 1 & 0 & 0 \end{bmatrix} \tag{99}$$
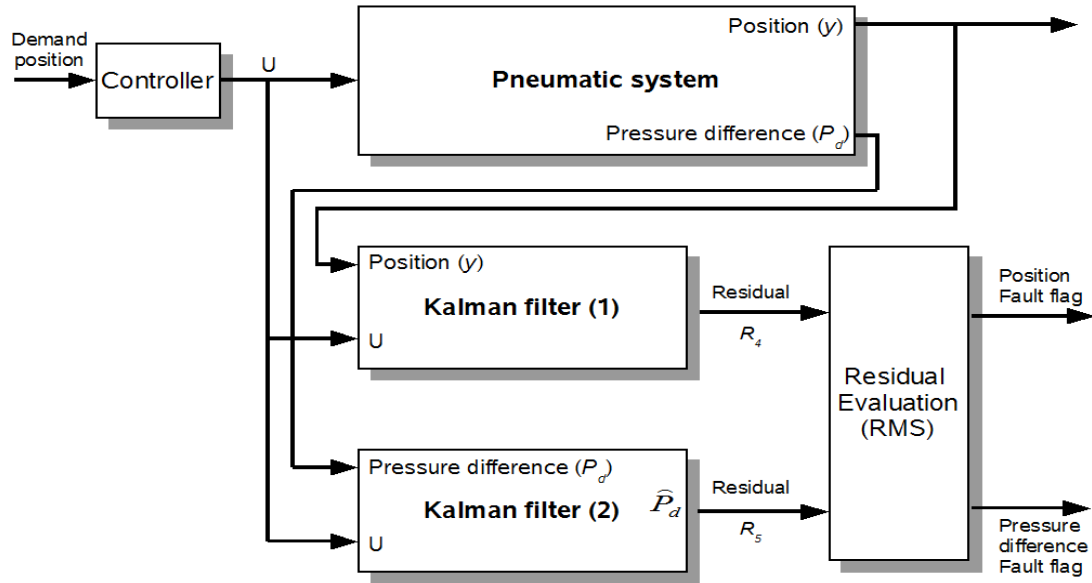
Figure 7.4: Overview of the Kalman filter scheme

7.2.3 *Residual Evaluation and Thresholds*

The purpose of residual evaluation is to generate a fault decision by processing the residuals. A fault decision is the result of all the tasks fault detection and isolation, (Kiencke and Nielsen, 2005). Residual evaluation is essentially to check if the residual is responding to a fault. The residual evaluation can in its simplest form be a threshold applied to the residual, i.e. a fault is assumed present if $| R_i(t) | > J_i(t)$ where $J(t)$ is the threshold applied to the ith residual. Another method may consist of statistical sequential probability ratio testing (Patton *et al*, 2000). In the present case the residuals are processed to acquire the root mean square (RMS) of the value over a moving window of N samples (Dixon, 2003) as shown:

$$R_{i_{RMS}}(k) = \sqrt{\frac{\sum_{j=k-N}^{k} R_{ij}^2}{N}} \quad i = 1, 2, 3, 4, 5 \tag{100}$$

where $R_i(k)$ is the value of the residual at the k_{th} sample. Subsequently, the residual RMS value is compared with a predetermined fault detection threshold. Table 7.1 shows the theoretical fault signatures using the parity equations and Kalman filter approaches of the pneumatic Stewart platform system for various faults. These signatures arise from the formulation of parity equations and the structure of the observer scheme, where the parity equations residuals (R_1, R_2 and R_3), are given in equations (89), (90), and (91). The Kalman filter residuals (R_4 and R_5) are given by equations (96), (97), and (98). For this work once a fault has been detected the fault flag remains high as triggering is set so that once the threshold is exceeded the flag remains raised.

Table 7.1   Theoretical fault signatures for the various faults

Residuals	Faults				
	Actuator	Plant	Position sensor	Pressure sensor P_p	Pressure sensor P_n
R_1	1	1	1	0	0
R_2	1	1	0	1	0
R_3	1	1	0	0	1
R_4	1	1	1	0	0
R_5	1	1	0	1	1

7.3   Fault detection scheme

Utilizing the residual generation and fault isolation equations from parity and Kalman filter approaches, a fault detection and isolation scheme is proposed. Figure 7.5 illustrates the proposed FDI scheme for the pneumatic system. This shows the desired input is applied and the difference (error) between the desired and actual measurement is passed through to the controller. The controller applies the necessary control action to the system. This control action is also passed to the Kalman filters and parity equation schemes. The position output from the pneumatic system is fed directly into Kalman filter (1) and the parity equations. The pressure difference output from the pneumatic system is fed directly into Kalman filter (2). The two pressure readings from the pneumatic system (both cylinder chambers) are passed through to the parity equations. The parity equations and Kalman filters are used to detect any differences between their outputs and actual system. If a fault occurs within the system a residual is generated. This residual passes through the residual evaluation scheme (discussed above) and if any threshold is exceeded a fault flag

is raised. From the fault flags shown in Figure 7.5 there are two position fault flags, one for Kalman filter (1) and one for the parity equations, with this certain advantages arise. For instance, false alarms can be reduced by having two separate residual schemes for the same output. Also if the residual is available it makes sense to employ this as part of the fault detection and isolation scheme.
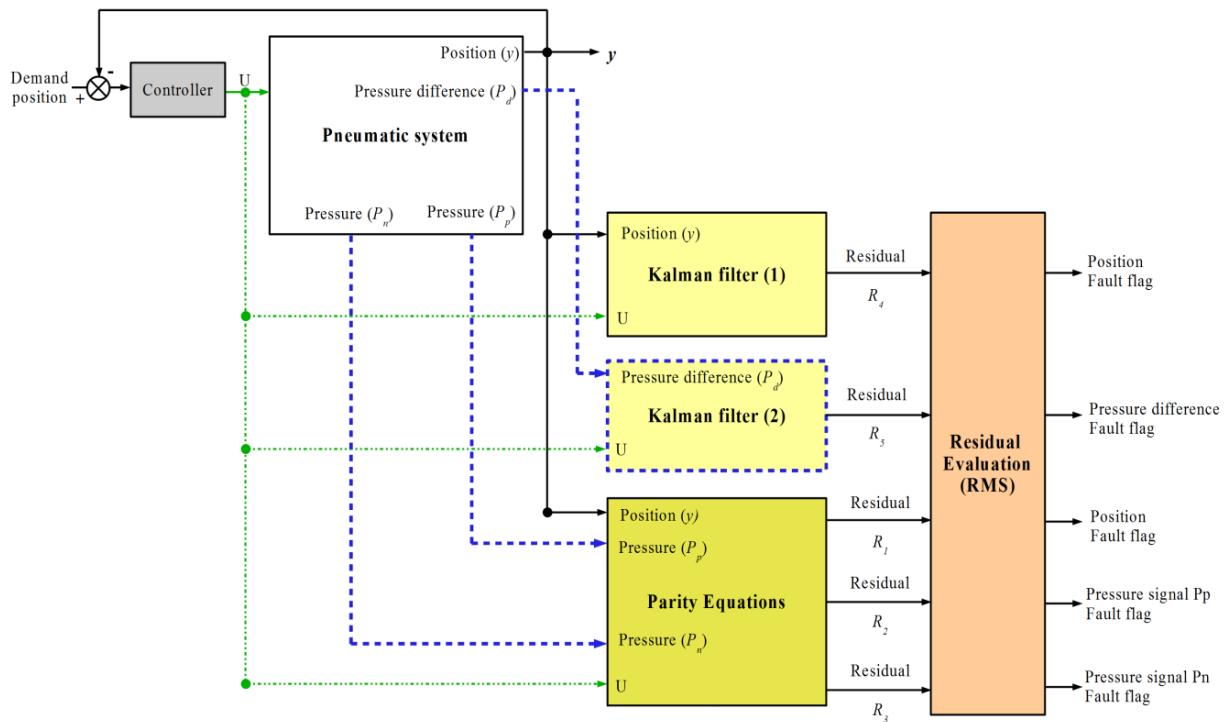
Figure 7.5: FDI scheme for the single cylinder pneumatic system.

7.4   *Testing designed FDI scheme (single actuator)*

In this section using the parity equations and Kalman filter approaches the designed FDI scheme shown in Figure 7.5 is tested within a Matlab/Simulink environment. A number of simulation experiments are carried out firstly, on the model of the pneumatic single cylinder system, and then secondly, to the Stewart-Gough platform model. The faults presented are actuator and position/pressure sensor faults (signal loss and signal drift), including air leaks. Figure 7.6 shows the top level of the Simulink model of the designed FDI scheme for the single cylinder set-up. This shows the pneumatic model, the Kalman filter and parity equation arrangement. Also shown are the faults that are applied.
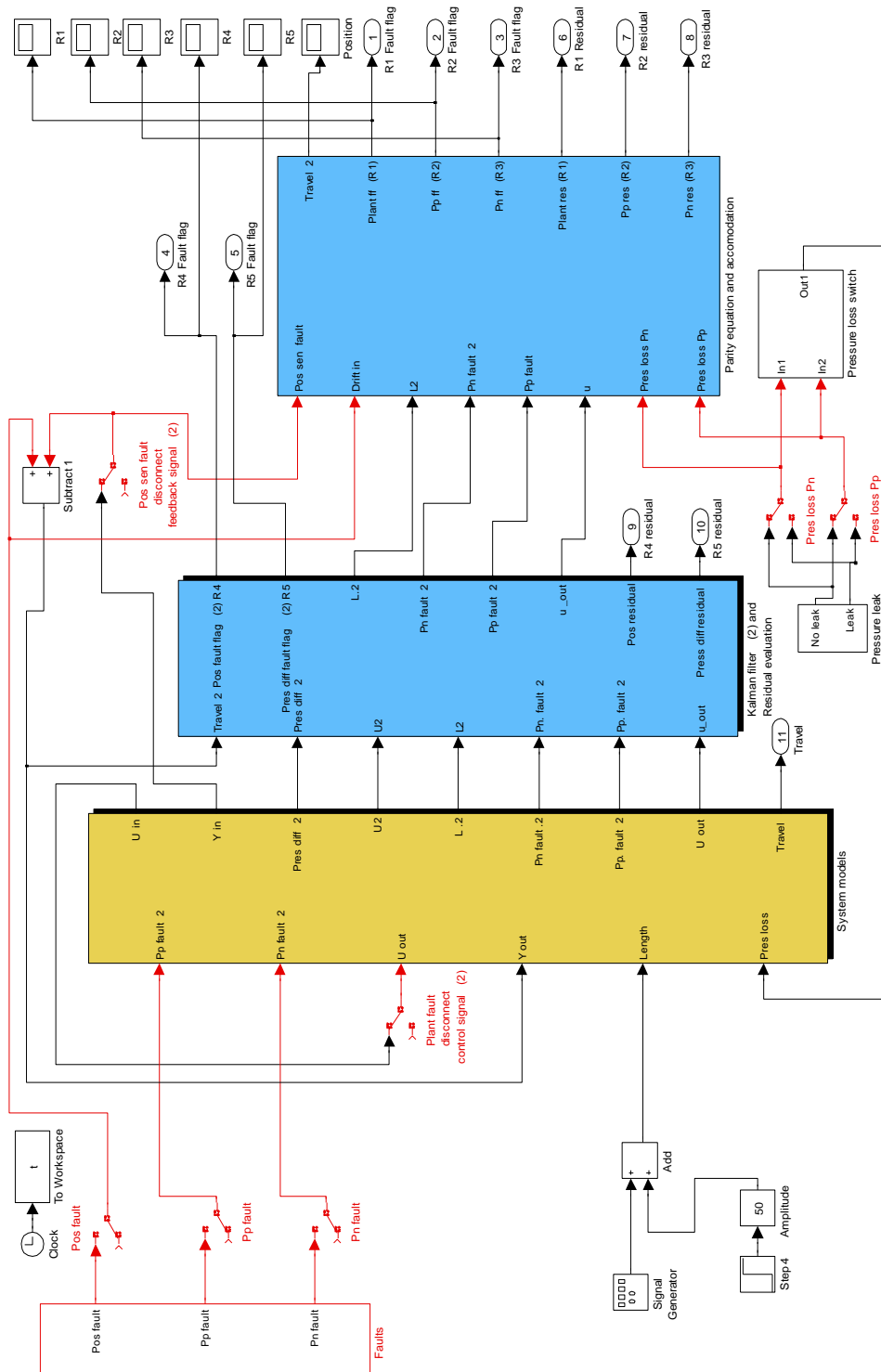
Figure 7.6: Single actuator Simulink model with FDI scheme

7.4.1. *Position sensor fault (Single actuator)*

A fault FS(s) (see Figure 7.2) is applied to position sensor GS(s). The fault injected is that the position signal has been disconnected. This is achieved by means of a switch as shown in Figure 7.6. Figures 7.7-7.9 show the time histories of this simulation experiment (position sensor signal loss) for the parity equation scheme. Figures 7.10-7.11 show the time histories of this simulation experiment (position sensor signal loss) for the Kalman filter scheme.
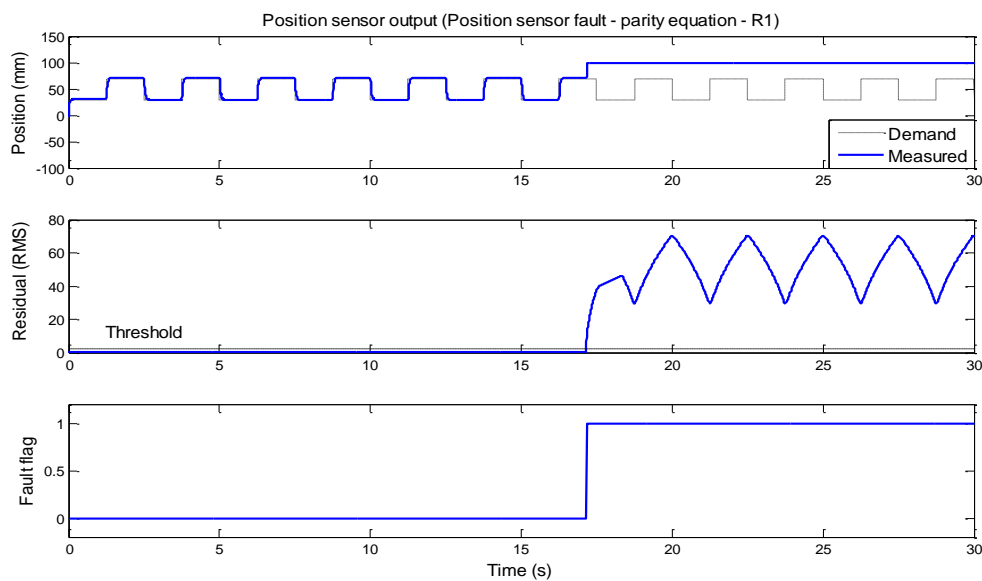
Figure 7.7: Position sensor fault (signal loss), parity equation - position sensor output (R_1)
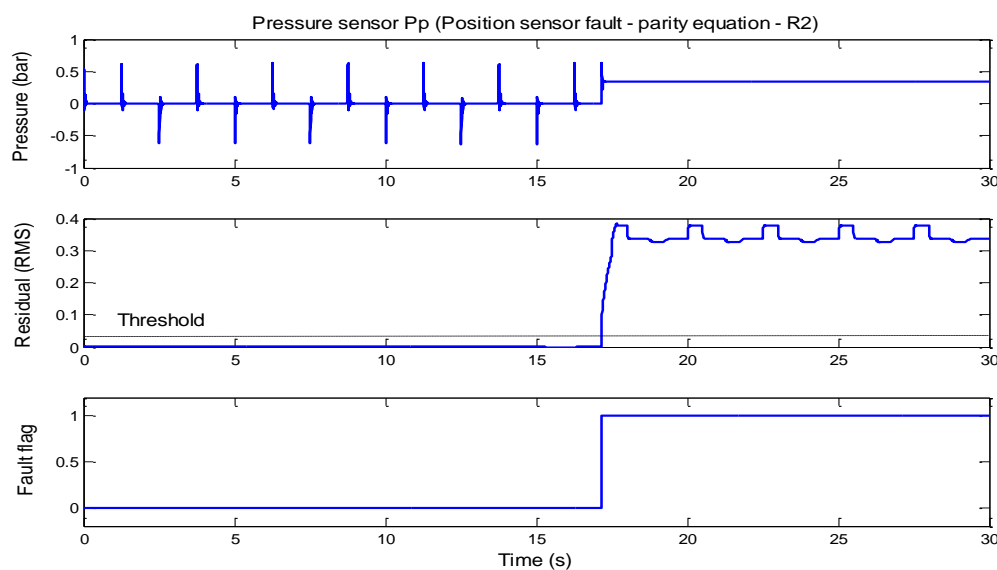
Figure 7.8: Position sensor fault (signal loss), parity equation - Pressure sensor Pp (R_2)

114
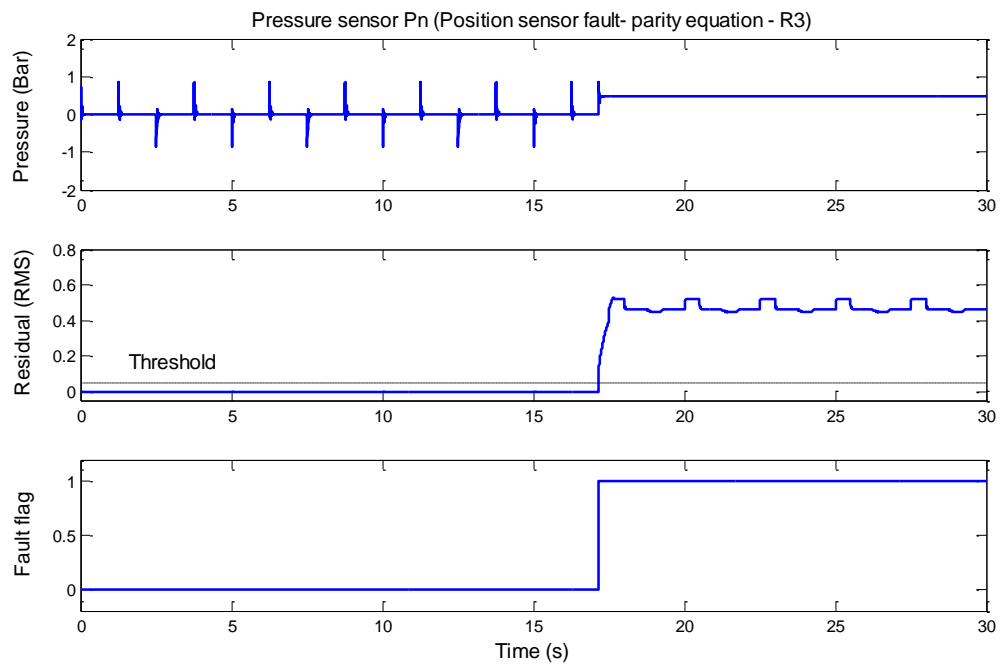
Figure 7.9: Position sensor fault, parity equation - Pressure sensor Pn (R_3)
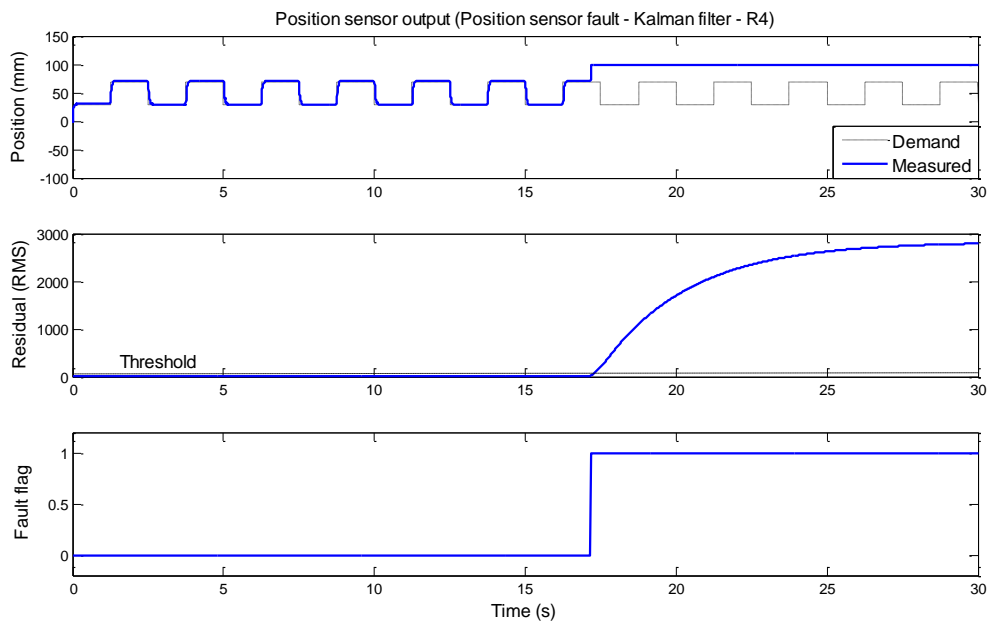
Figure 7.10: Position sensor fault (signal loss), Kalman filter - Position sensor output (R_4)
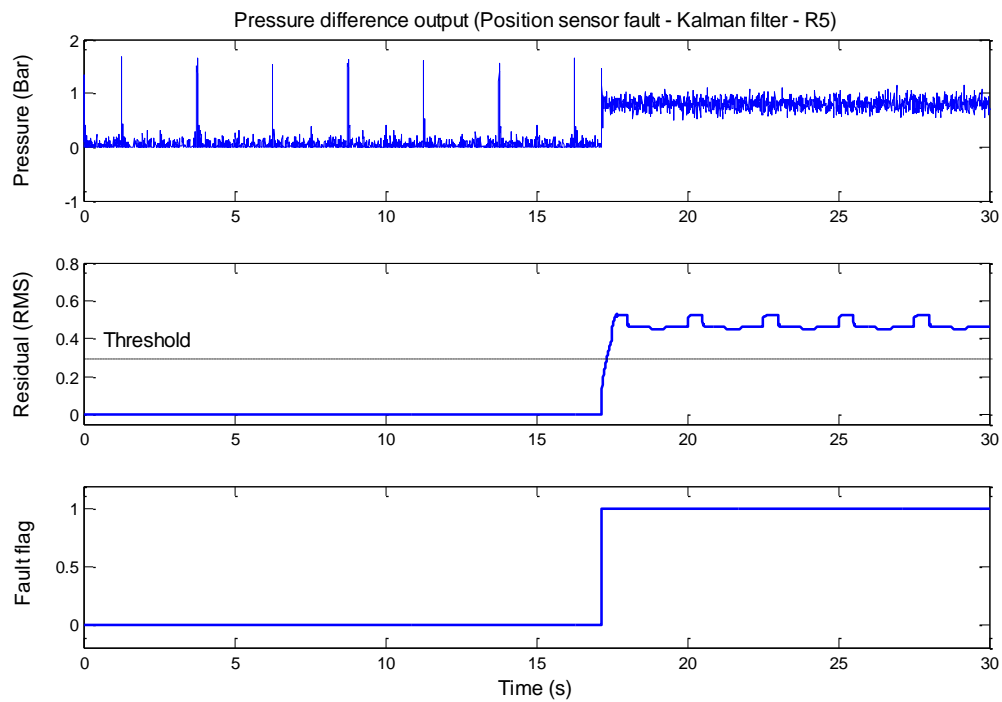
Figure 7.11: Position sensor fault (signal loss), Kalman filter -Pressure difference outputs (R_5)

7.4.1.1 Parity equations – Position sensor fault (sensor signal loss)

From Figure 7.7, at approximately 17s the fault is applied. From residual R_1 the fault is detected at 17.01s and the fault flag is raised. The RMS Residual R_2 exceeds its respective threshold at 17.05s (Figure 7.8). The fault flag is raised. The RMS Residual R_3 exceeds its respective threshold at 17.05s (Figure 7.9), where the fault flag is raised.

7.4.1.2 Kalman filter - Position sensor fault (sensor signal loss)

For same fault scenario as above, Figure 7.10 illustrates the outputs for the Kalman filter approach for the RMS residual R_4, the fault is detected at 17.01s and the fault flag is raised. The pressure difference residual (R_5) exceeds its respective threshold at 17.10s (Figure 7.11) and the fault flag is raised.

7.4.1.3   Discussion - Position sensor fault (sensor signal loss)

Applying the disconnection fault to the position sensor signal has an affect on the parity RMS residual (R_1), this raises the fault flag. The fault has an effect on the pressure sensor parity RMS residuals (R_2 and R_3). Both position and pressure difference Kalman residuals (R_4 and R_5) are affected by the position sensor fault and their fault flags are raised. However, these results do not agree with Table 7.1. In accordance with Table 7.1 only residuals R_1 and R_4 should be raised, and residuals R_2, R_3, and R_5 respectively should remain low. The reason for residuals R_2, R_3, and R_5 being raised are that applying this fault causes the control system to go into open-loop (no feedback) and this control scenario drives the pneumatic cylinder's piston to the maximum position (fully extended[6]). The system reacts instantaneously once the feedback signal is disconnected. The residuals R_2, R_3, and R_5 are generated as a result of this fault. In order to show that the residuals R_2, R_3, and R_5 correspond with the theoretical fault signatures of Table 7.1. A redundant signal is applied in order to simulate the effect of a redundant sensor. From these simulation results a loss of the position sensor produces an undesirable effect on the pneumatic system. Once the signal is disconnected the piston hits the end stop uncontrollably. This may cause damage the system components and more importantly there is no control of the system.

7.5   Applying redundant signal and voting scheme

In order to compute a correct output signal for the two position signals and to determine a continuous smooth function of the redundant input(s) a voting scheme is applied. The voter scheme is used to minimize switching transients since the isolation of faulty signals is achieved through a continuous numerical weighting (Broen, 1975). The voter scheme continuously determines the output in a manner which discriminates against the erroneous signal in favour of the other channels. The general form of the voter scheme (Figure 7.12) is determined using a weighted average of its inputs.   Shown as:

---

[6] It should be noted that end stops are included in the model (i.e. fully retracted = 0mm and fully extended = 100mm)
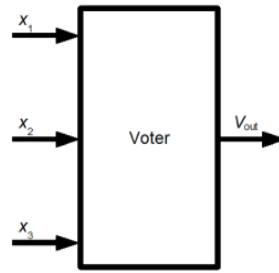
Figure 7.12: General Form of voting scheme

Where V_{out} is defined as

$$V_{out} = \frac{w_1 x_1 + w_2 x_2 + w_3 x_3}{w_1 + w_2 + w_3} \qquad (98)$$

This functional form of the voted output, V_{out}, could be utilized to produce the mean of those input signals which are close together and to discriminate against any out of tolerance signal. For these experiments other methods have been considered which include median voters and simple switching schemes. With the median voters the scheme simply selects the mid-value of all its redundant inputs whereas a weighted average voter generates weights w_1, w_2, …w_n that scale the contribution of each input, x_1, x_2, …x_n, to the output result. Applying switching technique shows a delay between deactivating the faulty sensor and activating the redundant sensor. This delay between switching is relatively large when compared to the reaction time of the system. This delay causes the pneumatic cylinder to reach its end stop almost immediately. Eventually, the redundant signal is initialised causing the pneumatic cylinder to oscillate until the controller brings the system under control. The switching scheme may not be desirable for a lot of applications as safety maybe an issue.

The numerical properties of the voting scheme are given by letting

$$\widehat{w_j} = \frac{w_j}{w_1 + w_2 + w_3}, j = 1, 2, \text{and } 3 \qquad (99)$$

118

where w_j is given by

$$w_1 = \left[1 + \left(\frac{x_1 - x_2}{a}\right)^2 \left(\frac{x_1 - x_2}{a}\right)^2\right]^{-1} \tag{100}$$

$$w_2 = \left[1 + \left(\frac{x_2 - x_1}{a}\right)^2 \left(\frac{x_2 - x_3}{a}\right)^2\right]^{-1} \tag{101}$$

$$w_3 = \left[1 + \left(\frac{x_3 - x_1}{a}\right)^2 \left(\frac{x_3 - x_2}{a}\right)^2\right]^{-1} \tag{102}$$

Where a is the tolerance parameter and is the measure of allowable noise level in a given channel. The tolerance parameter is chosen heuristically using engineering judgement (Broen, 1975).

It should be noted as the above voting scheme deals with three sensor inputs. The primary signal and the redundant signal, the third signal is taken from the Kalman filter estimate from the position feedback Kalman filter ($\hat{x}_1$). Although in this set-up the parity equations model may also be employed as an estimate for the position output. The Kalman filter set-up is described previously. The voter scheme (Figure 7.13) for the experimental set-up is determined using a weighted average of its inputs.

From Equations (100), (101), and (102) further residuals can be generated. Basically, if no faults occur the weighted output is 1 and if a fault occurs in either of the three signals (x_1, x_2 and x_3) ($\hat{w}_j$) →0. With the introduction of these newly formed residuals (w_1, w_2, and w_3) Table 7.1 can be updated to incorporate these. In order to comply with the fault signatures of Table 7.1 (i.e. fault =1, and no fault = 0) the weighted outputs are inverted. Table 7.2 shows the full set of fault signatures. For this work only faults on the primary position sensor (x_3) are considered.
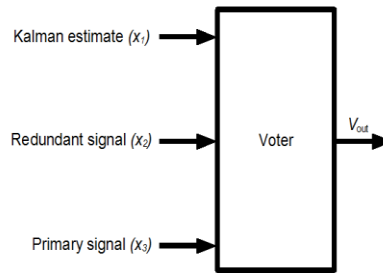
Figure 7.13: Voting scheme for experimental set-up

Table 7.2: Revised fault signatures

Residuals	Faults						
	Actuator	Plant	Position sensor (x_3)	Redundant sensor (x_2)	Estimated position signal (x_1)	Pressure sensor P_p	Pressure sensor P_n
R_1	1	1	1	1	1	0	0
R_2	1	1	0	0	0	1	0
R_3	1	1	0	0	0	0	1
R_4	1	1	1	1	1	0	0
R_5	1	1	0	0	0	1	1
w_1	0	0	0	0	1	0	0
w_2	0	0	0	1	0	0	0
w_3	0	0	1	0	0	0	0

7.5.1. *Position sensor fault (Single actuator) using redundant sensor*

Figure 7.14 shows the revised single actuator Simulink model with the incorporated redundant signal and voting scheme. The simulation experiments are repeated with the redundant sensor installed and applying the voting scheme described previously. Figures 7.15-7.17 show the time histories of this simulation experiment (position sensor signal loss) for the parity equation scheme using the redundant sensor and voting scheme. Figures 7.18-7.19 show the time histories of this simulation experiment (position sensor signal loss) for the Kalman filter scheme using the redundant sensor and voting scheme. Figure 7.20 depicts the time history of the weighted average outputs of the voting scheme.
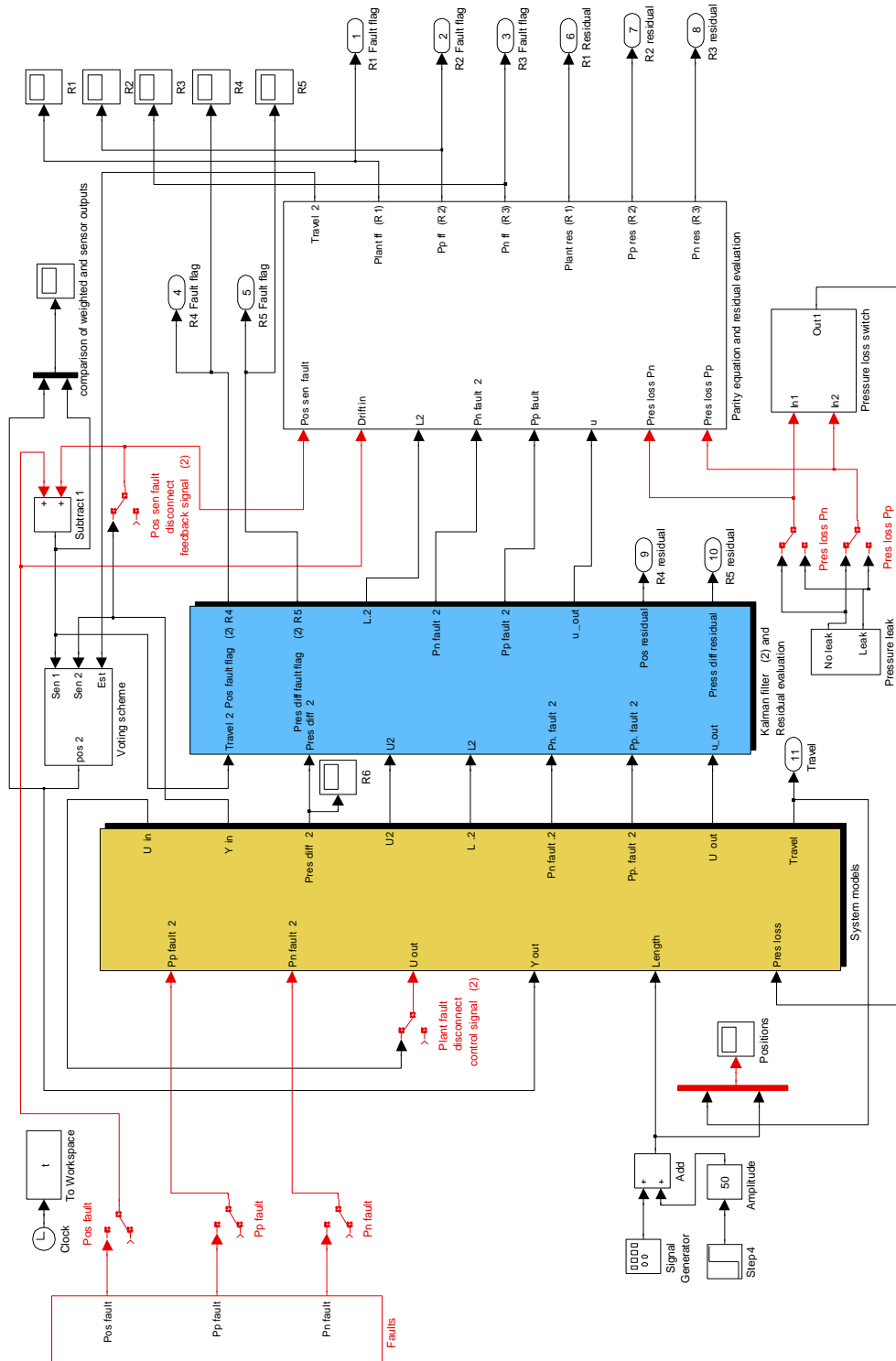
Figure 7.14: Simulink model with FDI scheme
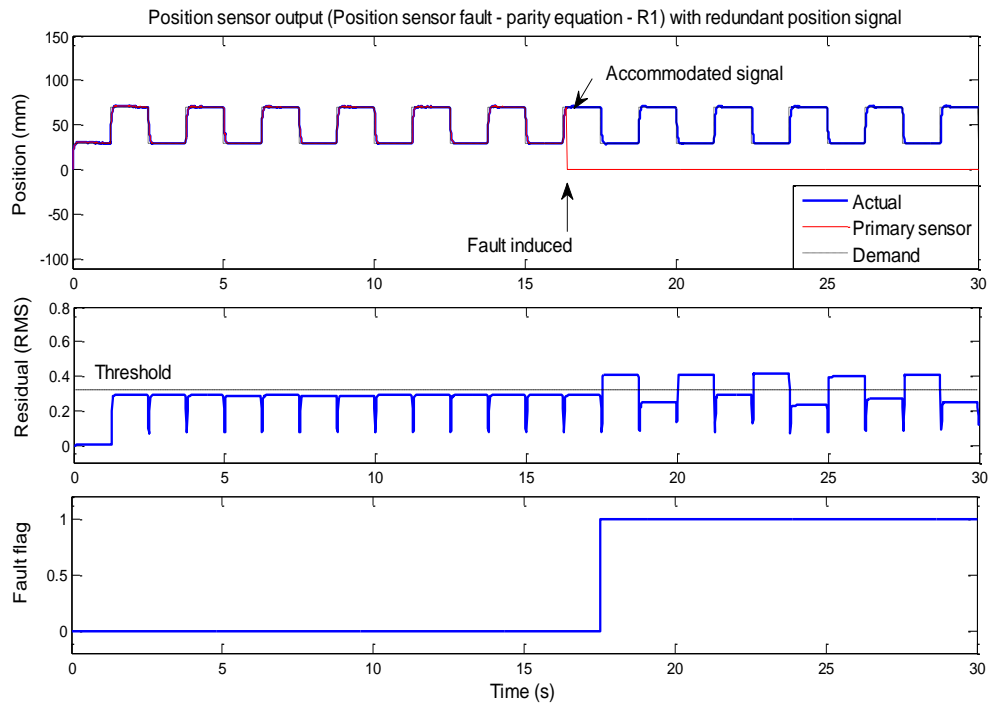
Figure 7.15: Position sensor fault (signal loss), Parity equation – Position sensor output (R_1) using the redundant sensor and voting scheme
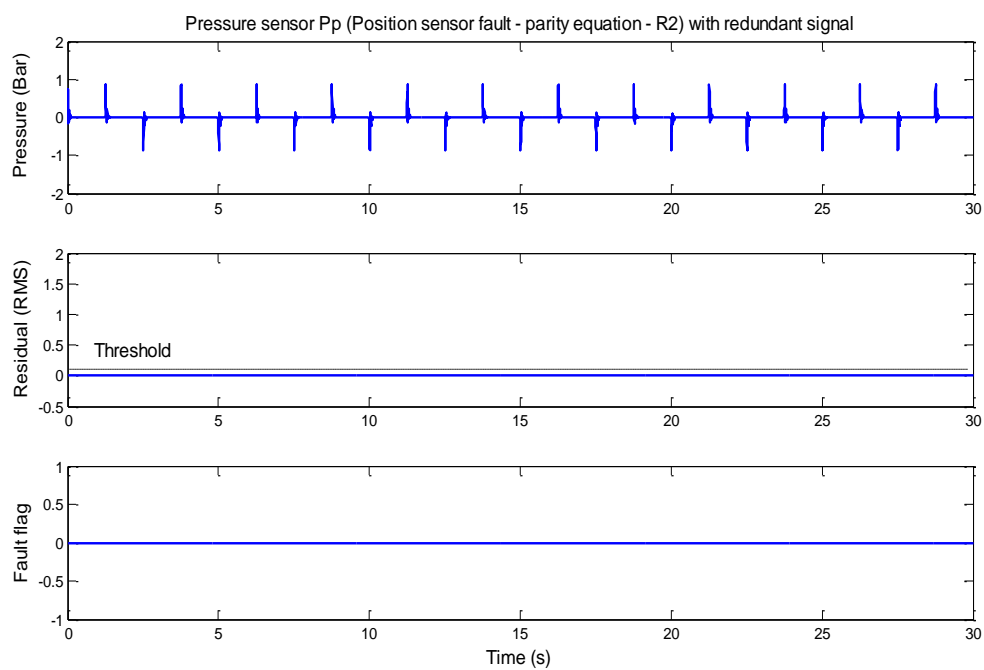
Figure 7.16: Position sensor fault (signal loss), Parity equation – Pressure sensor Pp (R_2) using the redundant sensor and voting scheme.
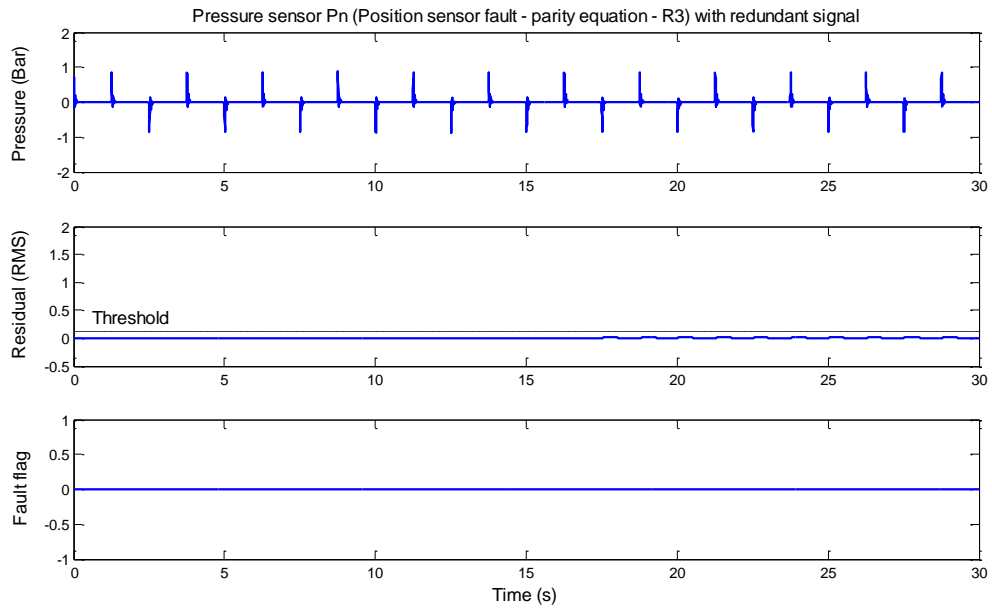
Figure 7.17: Position sensor fault (signal loss), Parity equation– Pressure sensor Pn (R_3) using the redundant sensor and voting scheme
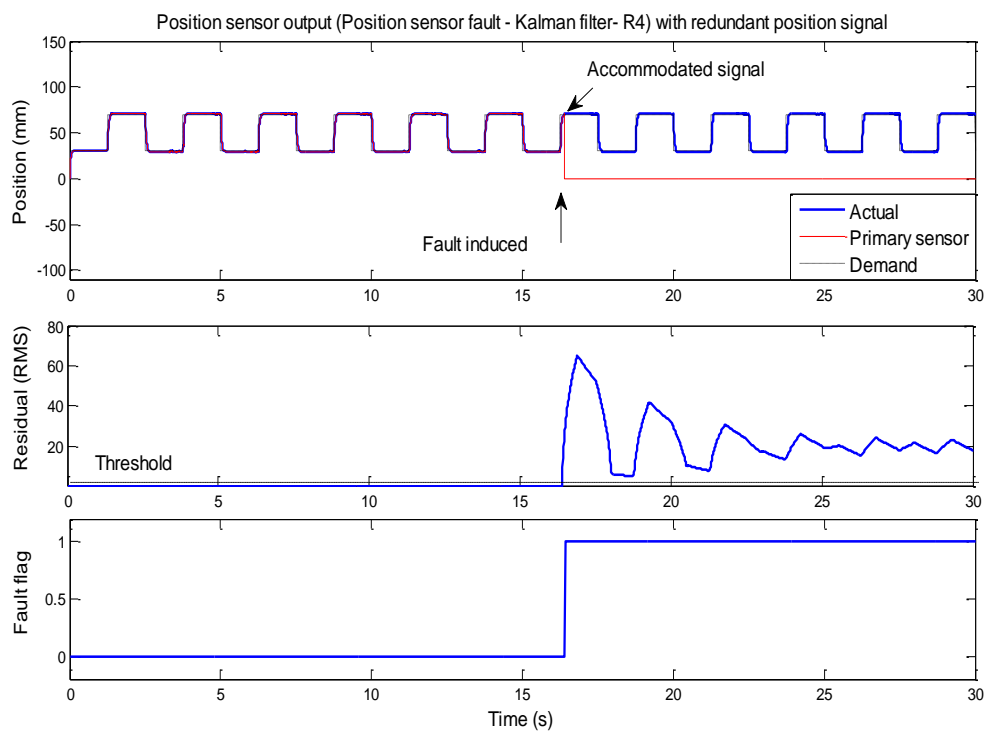
Figure 7.18: Position sensor fault (signal loss), Kalman filter - Position sensor output (R_4)
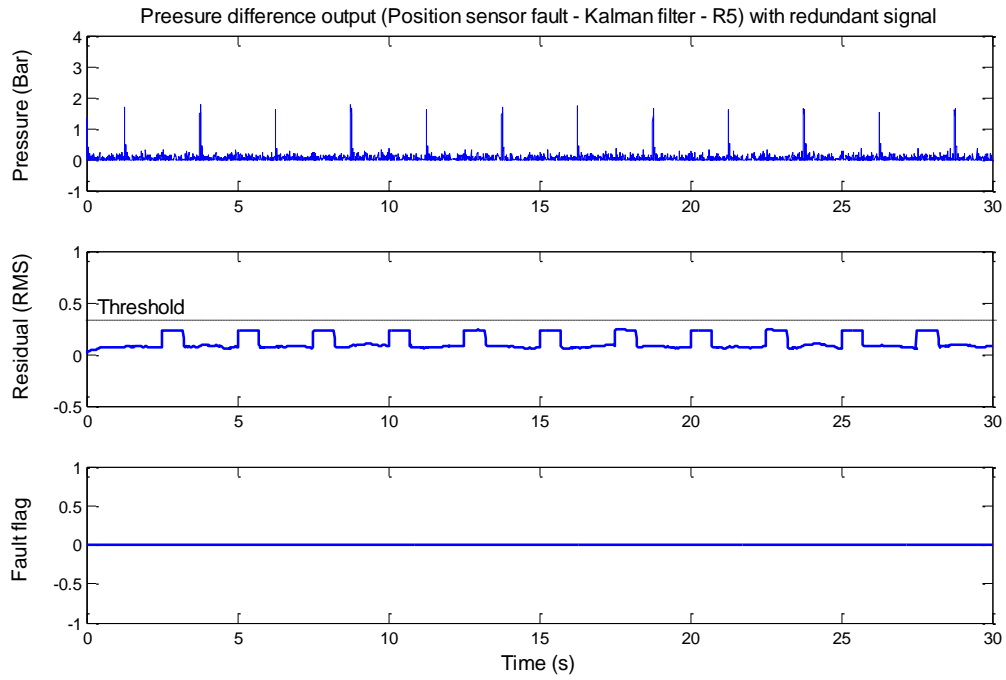
Figure 7.19: Position sensor fault (signal loss), Kalman filter - Pressure difference outputs

(R_5)
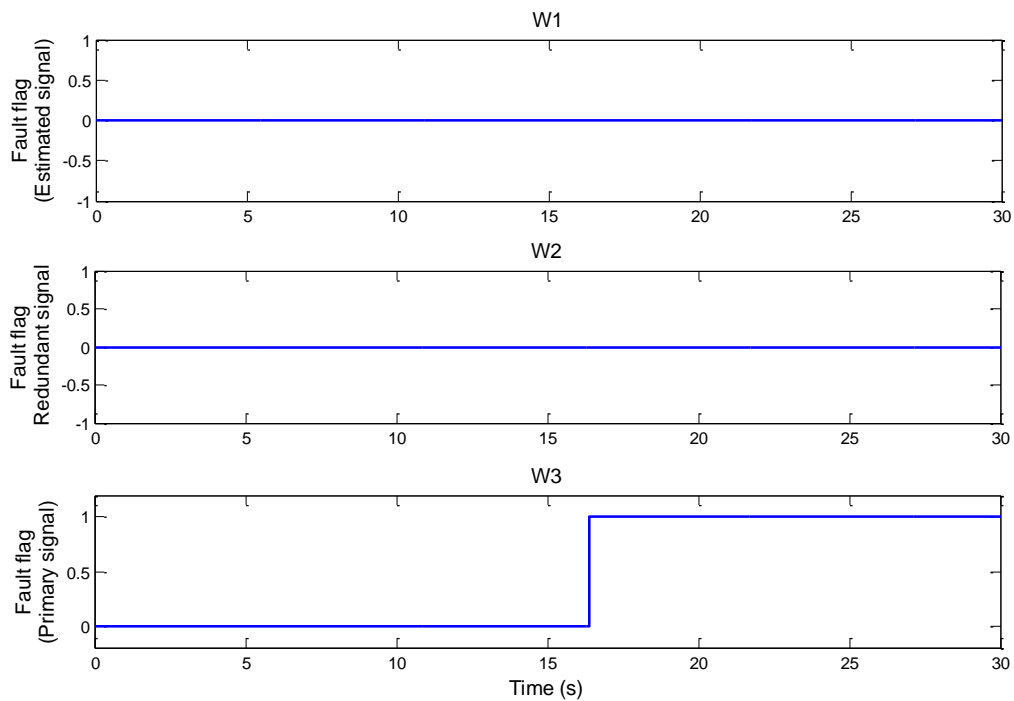
Figure 7.20: Weighted average outputs for a position (primary) sensor fault

7.5.1.1   Discussion - Position sensor fault (sensor signal loss)

Employing a redundant signal and applying the disconnection fault to the position sensor signal has an effect on the parity RMS residual (R_1). The fault is applied at 16.5s and the fault flag is raised at 16.5s (Figure 7.15). The fault has no effect on the pressure sensor parity RMS residuals R_2 and R_3 (Figure 7.16-7.17) respectively. The Kalman residual R_4 is affected and raises the fault flag at 16.5s (Figure7.18). There is no effect on the pressure difference Kalman residual R_5 (Figure 7.19). These results agree with the fault signatures detailed in Table 7.1. The results are also in agreement with Table 7.2 this shows that RMS residuals R_1, R_4 and w_3 (Figure 7.20) fault flags are raised and RMS residuals R_2, R_3 and R_5 are unaffected. From the plot of residual R_1 (Figure 7.15) and residual R_4 (Figure 7.18) it can be seen by using the redundant sensor along with the voting scheme, a continuous smooth function of the redundant input is achieved. The system functions normally under this fault, and successful detection, isolation and accommodation with regards to a position sensor fault is achieved. With incorporating the voting scheme within the FDI system, Figure 7.5 can be modified to show this. Figure 7.21 shows schematically the designed FDI scheme for the single actuator. The results for the other (faults) simulation experiments are detailed in Appendix E.
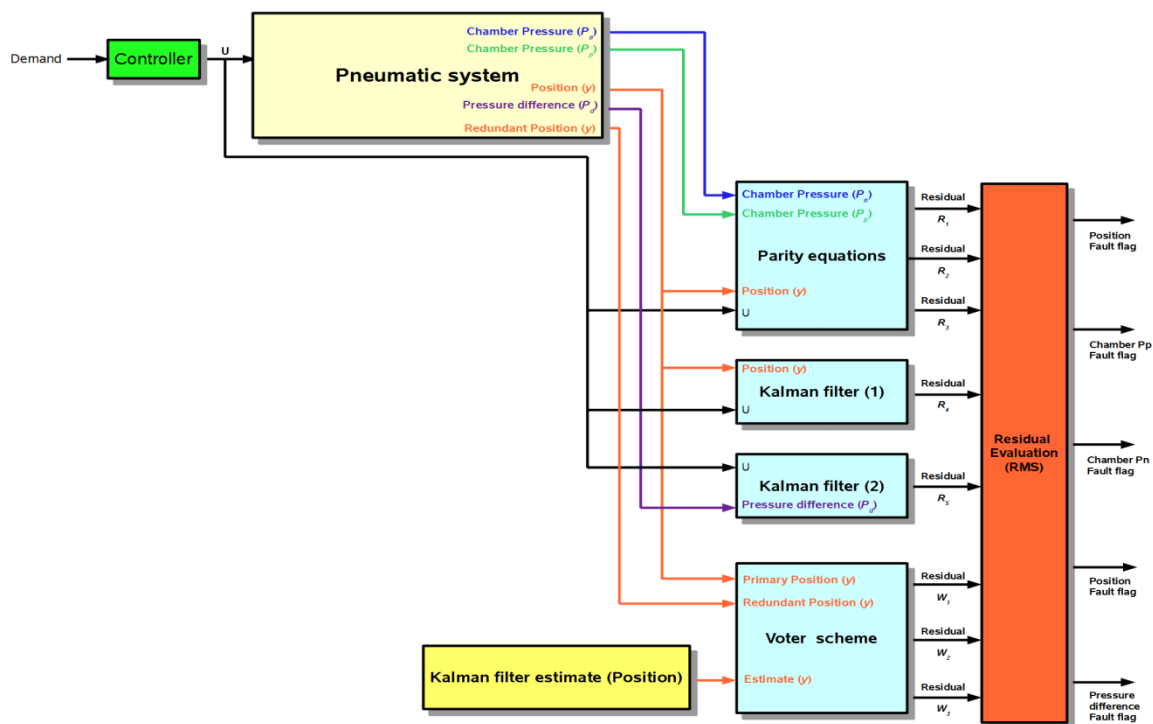
Figure 7.21: FDI scheme for single pneumatic cylinder set-up

7.6   *FDI scheme for Stewart-Gough platform*

The modular FDI scheme (Figure 7.21) employed with the single cylinder set-up is used for the Stewart-Gough platform set-up. The approach used is to apply each single cylinder FDI scheme (modular) to the 6 legs of the Stewart-Gough platform. This approach means that each leg has a FDI scheme incorporated within its control scheme. Therefore faults on each leg system of the Stewart-Gough platform can be detected, isolated and in some cases accommodated. For the sake of repeating the simulation experiments for each platform leg, the simulation experiments are only considered for one leg.

As the Stewart-Gough platform is a more complex design (kinematically) some design considerations have to be made. Depending on the fault type, the Stewart-Gough platform can become unsafe if these faults occur. In particular the faults in question are pneumatic faults, such as leaks, blockages and control signal loss. The reason why considerations have to be made is that with these faults no redundancy is available. For example if an air leak arises there is no method to accommodate this, the problem being locating where the leak fault has occurred. The same applies for the blockage fault. Firstly, determining where the blockage occurs is a very difficult problem, as the blockage could be anywhere within the pneumatic system. Secondly, if the blockage source was located, again accommodating the blockage is virtually impossible as determining where to locate the redundant air supply is again tricky from a practical perspective.

In the case of the control signal loss fault, this fault can be considered to be a pneumatic fault. As the control signal drives the proportional servo valve, if the control signal is lost the proportional servo valve will not function. Therefore, resulting as a pneumatic system fault (i.e. no pressure signal to pneumatic cylinders). If the pneumatic faults mentioned occur within the system, the system (Stewart-Gough platform) becomes unsafe. This is due to the complex kinematic arrangement, as the movement of the platform (movable base orientation) depends entirely on each leg operating correctly to its desired length (see chapter 6). Any pneumatic fault (i.e. pneumatic cylinder not at desired length) in any leg will jeopardise the required position of the platform.

With these pneumatic faults, certain fault management considerations (actions) have to be applied. A logic scheme is designed in order to distinguish between a pneumatic fault and particular sensor faults. Then using this knowledge an action can be taken in order to either accommodate the fault or to activate the safety scheme so that the system is brought back to its rest position from whatever position it is in. This is achieved by taking into

account the different fault scenarios and using their respective residuals. The categorisation of the various types of faults is shown in Table 7.3. Using Table 7.3 a safety scheme can be designed. Figure 7.22 shows a schematic of the applied logic, incorporating the actions taken and the integrated safety scheme.

Table 7.3. Residuals/fault flags for the various faults

Faults	Fault category	Residuals/fault flags							
		R_1	R_2	R_3	R_4	R_5	w_1	w_2	w_3^*
Control signal loss (Actuator)	Pneumatic	1	1	1	1	1	0	0	0
Pressure leak	Pneumatic	1	1	1	1	1	0	0	0
Pressure pipe blockage	Pneumatic	1	1	1	1	1	0	0	0
Signal loss (Pressure sensor Pp)	Sensor	0	1	0	0	1	0	0	0
Signal drift (Primary position sensor)	Sensor	1	0	0	1	0	0	0	1
Signal loss (Primary position sensor)	Sensor	1	0	0	1	0	0	0	1

*Fault only applied to primary sensor.

Figure 7.22 describes what actions are taken with respect to what residuals are raised. When residuals R_1, R_2, R_3, R_4 and R_5 are raised (i.e. pneumatic fault) the action taken is that the pressure from the faulty cylinder chambers is released, along with this the safety scheme is activated. The safety scheme once activated immediately sets the inputs to the system (platform) to 0. Therefore if

$$R_1, R_2, R_3, R_4 \text{ and } R_5 = 1 \text{ then inputs } (x, y, z, \alpha, \beta, \gamma) = 0$$

With the inputs set to 0, the platform is brought back to its rest position. From there the fault can be rectified. With the two pressure sensor faults when residuals $R_2 + R_5$ or $R_3 + R_5$ are raised the respective warning lights are activated. With the pressure sensor faults there is no loss in system performance and the platform can operate and complete its given task, once the task is completed the fault can be rectified.
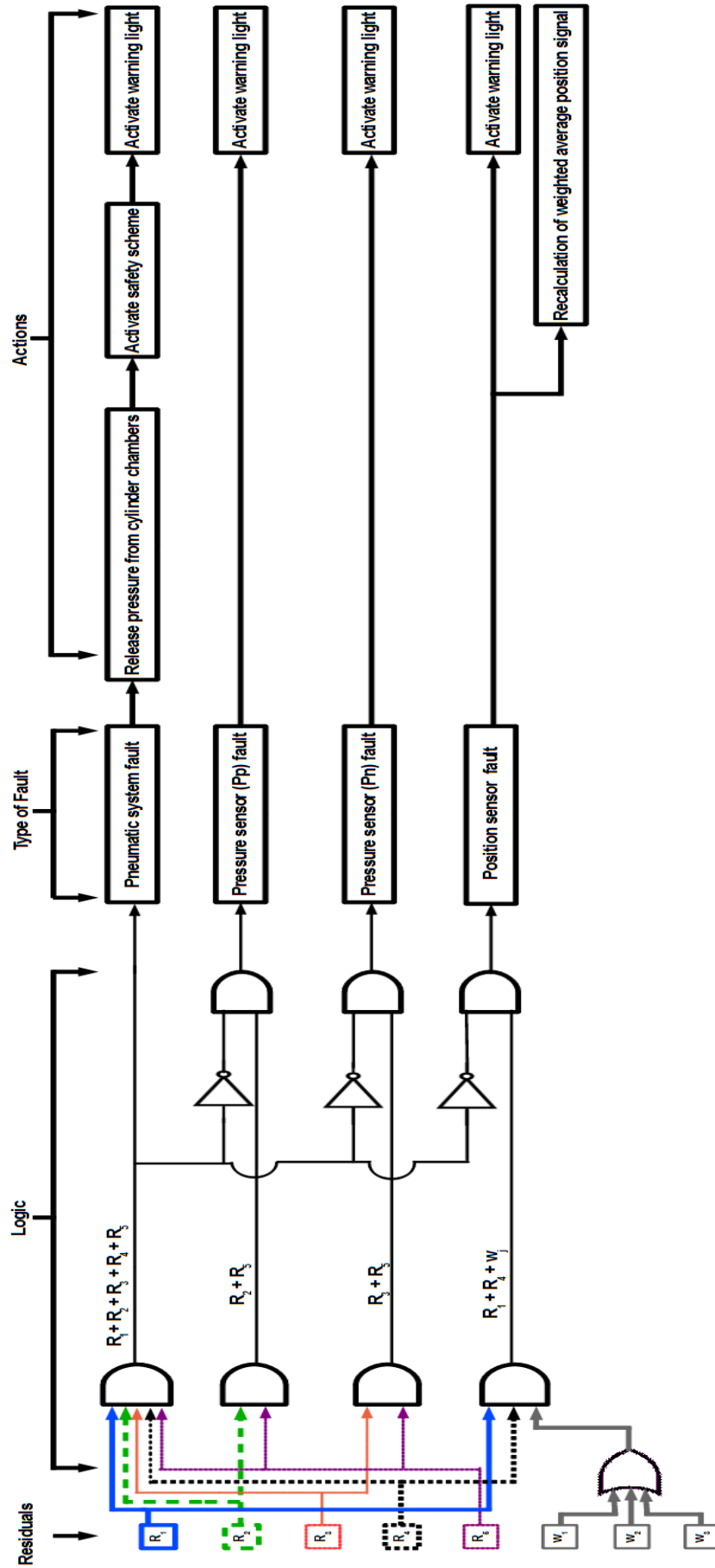
Figure 7.22: Logic diagram categorising a pneumatic fault and particular sensor faults with actions.

For the primary position sensor fault residuals $R_1 + R_4 + w_3$ are raised. With this the action taken is that the warning light is activated and the faulty signal is accommodated by recalculation of the weighted average voting output. As the faulty signal is accommodated no loss is system performance is encountered. Therefore, the platform can complete its given task. On completion of task, once the platform is in its rest position the fault can be rectified.

7.6.1   *Air leak (Stewart-Gough platform)*

In order to show the effectiveness of the proposed FDI scheme shown in Figure 7.23 for the Stewart-Gough platform, a leak fault is applied to the Stewart-Gough platform system model (one pneumatic cylinder). This is achieved by reducing the pressure in the system to one side of the cylinder chamber. The pressure in the chamber is reduced to 80% capacity (i.e. 20% air loss). The demand input to the system is a series of motions that utilise the 6-degrees of movement, i.e. the longitudinal (surge), lateral (sway), and vertical (heave) motion, whereas angular motions are expressed as Eulerian angle rotations with respect to the x-axis (roll), y-axis (pitch), and z-axis (yaw).

Figures 7.23-7.25 shows the time histories of this simulation experiment (leak fault) for the parity equation scheme. Figure 7.26-7.27 shows the time histories of this simulation experiment (leak fault) for the Kalman filter scheme. The time history of the weighted average outputs of the voting scheme is shown in Figure 7.28.

7.6.1.1   *Parity equations – Air leak*

The leak fault is applied at 28.5s. From the RMS residual R_1 (Figure 7.23) the fault is detected at 29.5s where the fault flag is raised and remains raised. The RMS residual R_2 (Figure 7.24) exceeds its respective threshold at 29.75s, where the fault flag is raised. The RMS residual R_3 (Figure 7.25) exceeds its threshold at 29.75s and the fault flag is raised.

7.6.1.2   *Kalman filter - Air leak*

From Figure 7.26, using the Kalman filter scheme, the RMS residual R_4 exceeds its threshold at 29s and the fault flag is raised. Residual R_5 (Figure 7.27) cross its respective threshold at 29.75s and the fault flag is raised.

7.6.1.3   *Weighted average outputs – Air leak*

The weighted average outputs shown in Figure 7.28 indicate that residuals w_1, w_2 and w_3 are not effected by the air leak fault and the respective fault flags remain low.
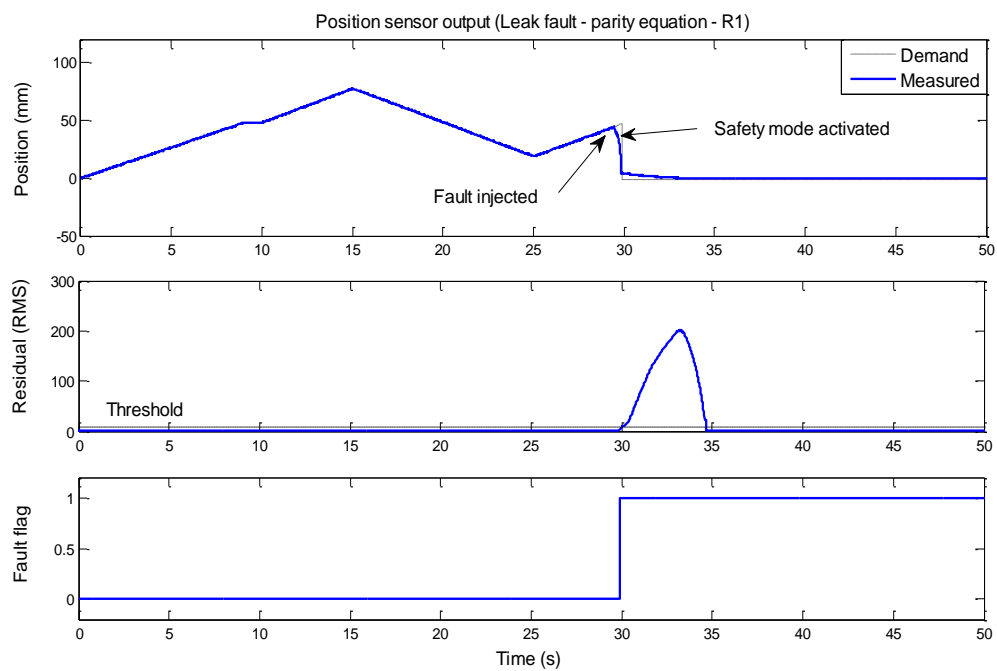
Figure 7.23: Air leak, parity equation result - Position sensor output (R_1)
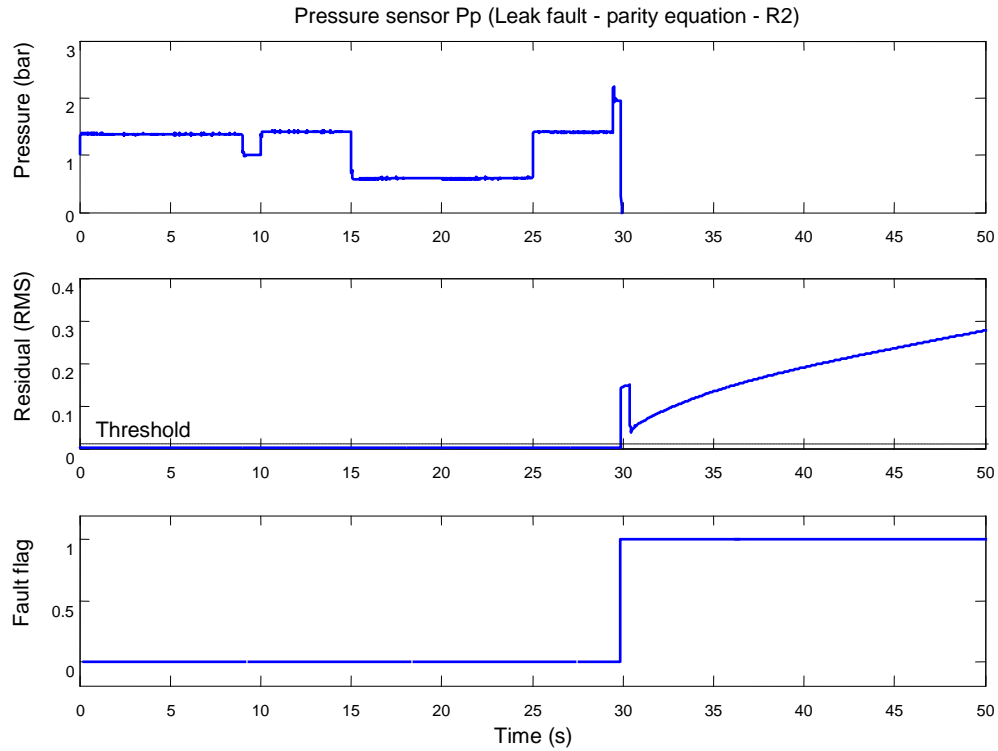
Figure 7.24: Air leak, parity equation - Pressure sensor Pp (R_2)
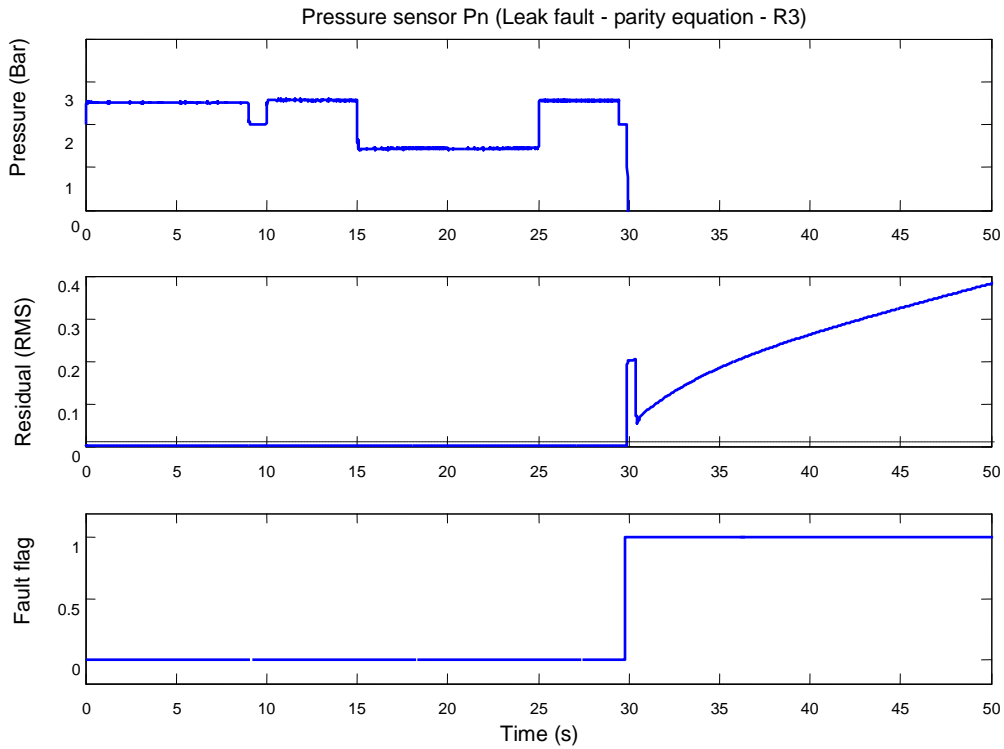
7.25: Air leak, parity equation - Pressure sensor Pn (R_3)
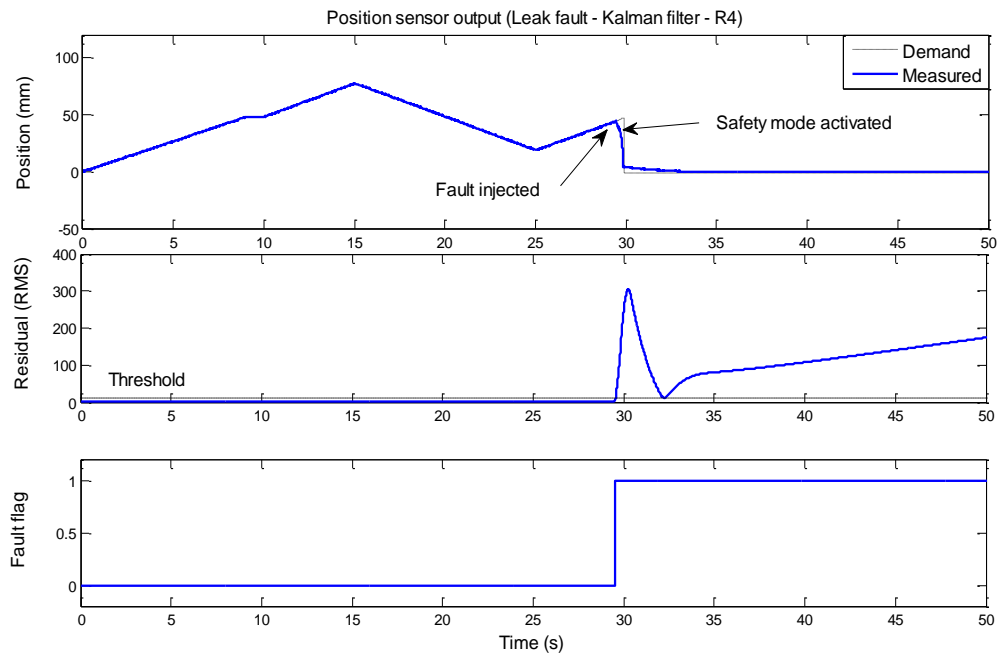
7.26: Air leak, Kalman filter - Position sensor output (R_4)
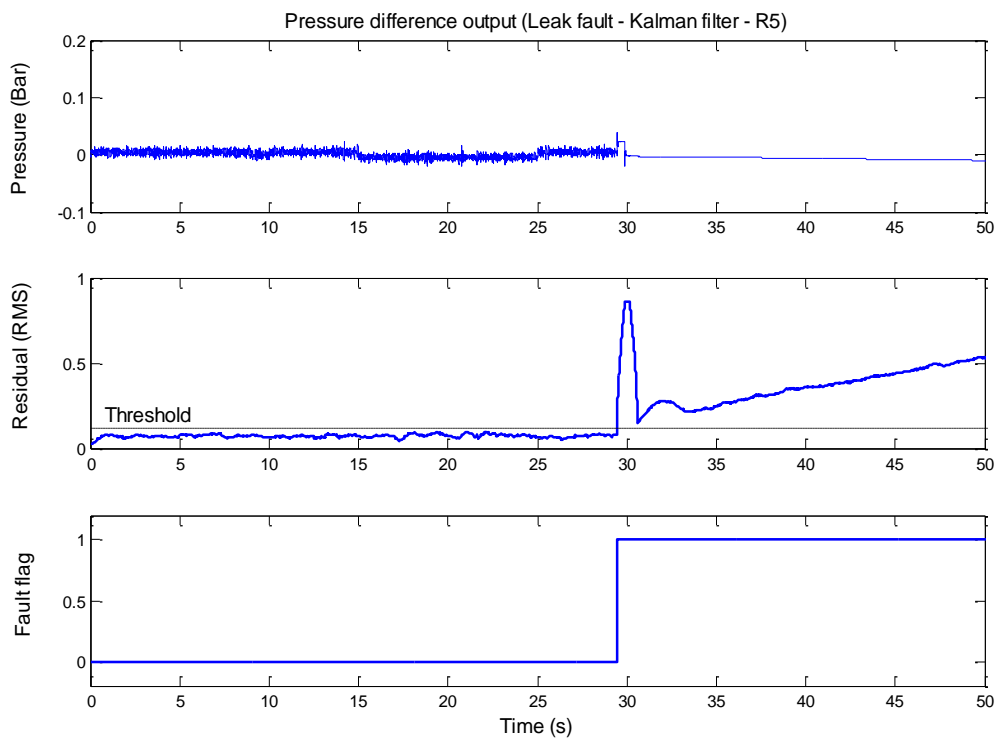
7.27: Air leak, Kalman filter – Pressure difference output (R_5)
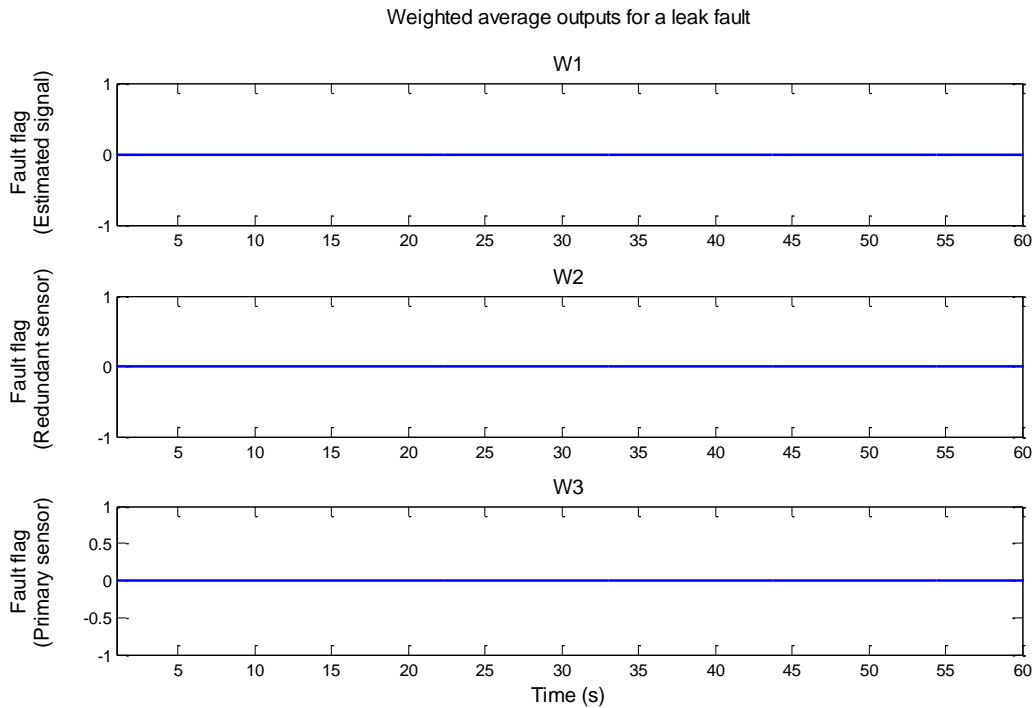
Figure 7.28: Weighted average outputs for a leak fault

7.6.1.4 Discussion - Air leak

Applying the leak fault to the pneumatic cylinder has an effect on the parity residual (R_1), this raises the fault flag. The fault also has an effect on the pressure sensor parity residuals (R_2 and R_3). The fault affects the position residual R_4 and the pressure difference residual R_5. Residuals w_1, w_2 and w_3 are not affected and the respective fault flags remain low. This agrees with the fault signatures detailed in Table 7.2. With this type of fault, accommodation is not available as pressure is lost between the servo valve and pneumatic cylinder. This means that the desired positional movement of the rig is not achievable. Once the residual fault flags (R_1-R_5) are raised the safety sequence is activated and the platform is made safe (i.e. brought back to its rest position). Figure 7.29 shows the FDI scheme for the Stewart-Gough platform, where the FDI scheme incorporates the fault management scheme described in Figure 7.22. Figure 7.30 shows the Simulink model for the Stewart-Gough platform. The results for the other (faults) simulation experiments for the Stewart-Gough platform are detailed in Appendix E.
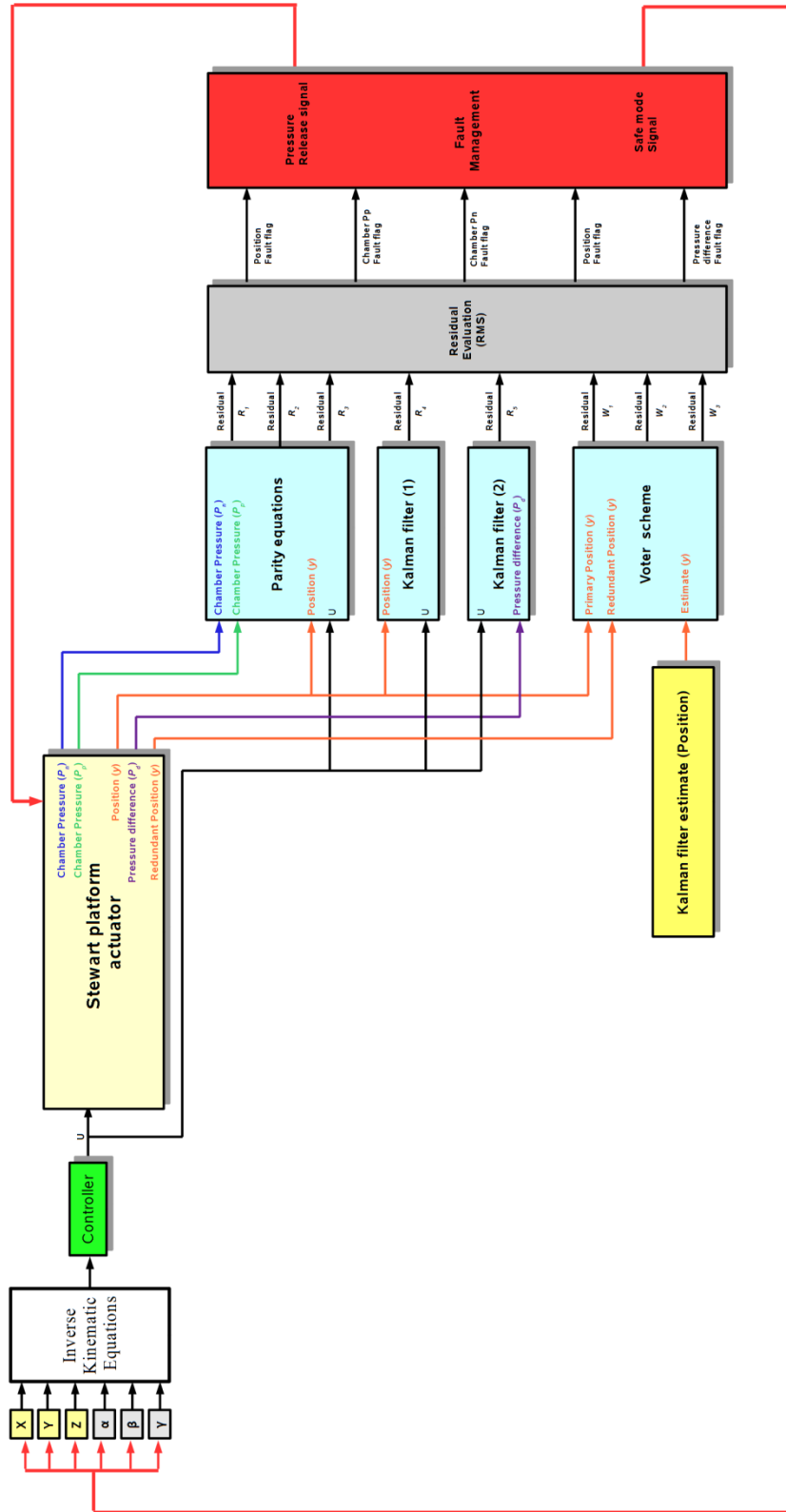
Figure 7.29: FDI scheme with incorporated fault management scheme for Stewart-Gough platform pneumatic cylinder set-up
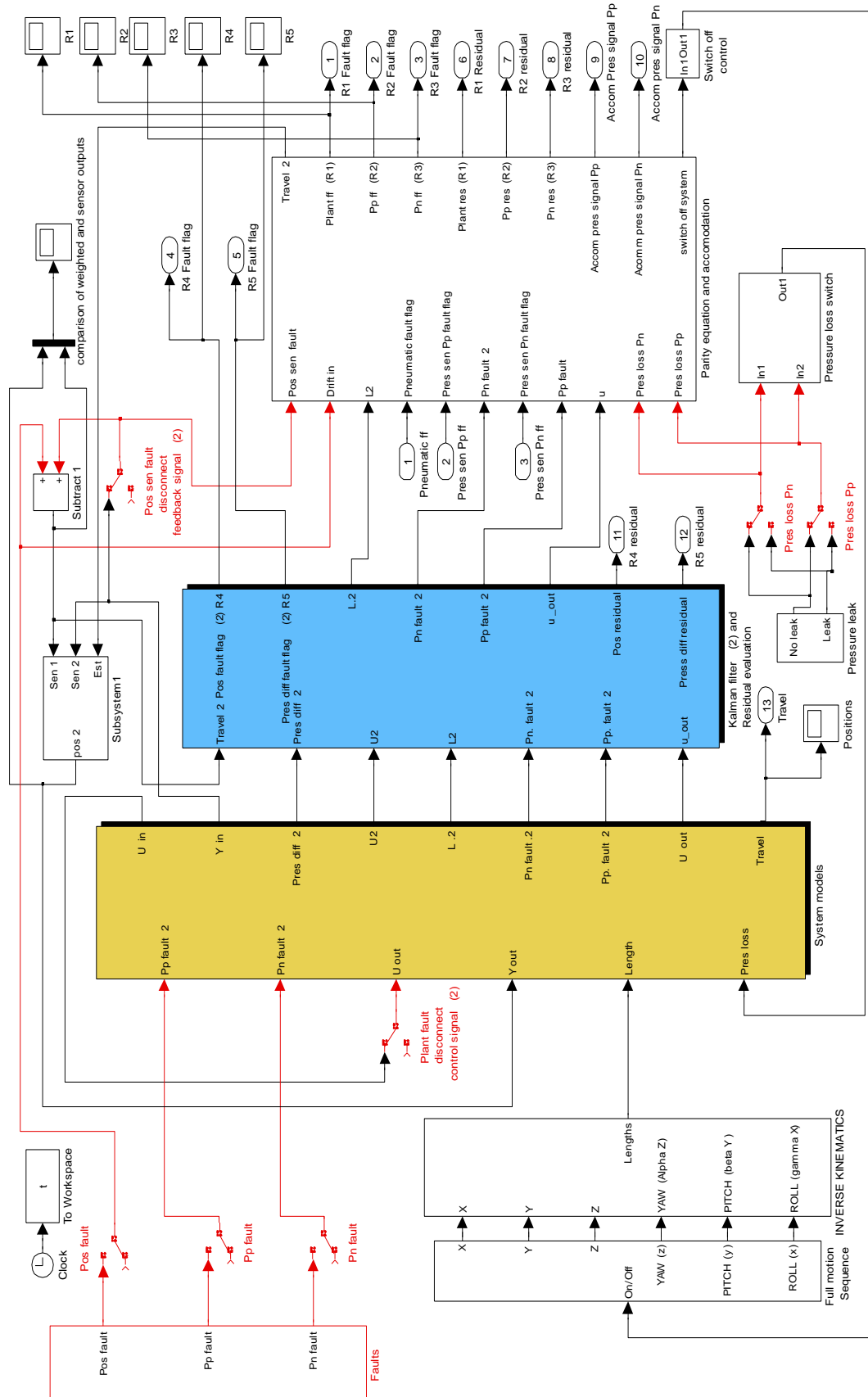
Figure 7.30: Simulink model for Stewart-Gough platform with FDI and fault management scheme

7.7   Conclusion

In this chapter typical faults associated with pneumatic systems have been described. A fault detection and isolation scheme has been designed for the pneumatic system described in chapter 3. The FDI scheme is based on combining parity equation and Kalman filter based techniques. The parity and Kalman filter equations were formulated and used to generate residuals that in turn, are analysed to determine whether faults are present in the pneumatic system. In order to accommodate position sensor faults a redundant signal has been applied with a weighted average voting scheme. The designed FDI scheme has been applied initially to the single actuator model, where faults through simulation associated with pneumatic systems have been applied and the results recorded. The designed FDI scheme was incorporated within the control scheme of the Stewart-Gough platform model. Due to the kinematic complexity of the Stewart-Gough platform certain faults can only be detected (pneumatic faults). These particular faults when applied made the system unsafe. In order to prevent system damage, a safe mode scheme has been designed and incorporated within the FDI scheme. By incorporating the safe mode scheme, if a pneumatic fault is detected this activates the safe mode scheme by initially releasing the pressure from the cylinder chambers and then setting the demand inputs to zero in order to bring the platform back to a safe position (rest position). A series of simulation experiments were carried out by applying various faults to the system and the results recorded. From the results shown, the designed FDI and fault management scheme proved to be effective when dealing with the various fault scenarios applied. The next phase of the work is to apply the designed FDI scheme initially to the actual single cylinder test-rig; the results are shown in chapter 8. Then the FDI scheme and fault management scheme is applied to the actual Stewart-Gough platform test-rig, the results for this are shown in chapter 9.

Chapter 8

Experimental results – Single actuator test-rig

8.1 Introduction

In order to demonstrate the designed FDI scheme (chapter 7) using parity equations and Kalman filter approaches a number of experiments were carried out on the pneumatic single cylinder system described in chapter 3. The faults presented include air leaks, pipe blockages, control signal loss and position/pressure sensor faults (signal loss and signal drift). The faults are applied physically by means of either disconnecting a signal or operating a switch or flow valve. These methods are intended to replicate actual faults associated with pneumatic systems. Typical pneumatic system faults have been described in chapter 7.

8.2 Experimental results (Single cylinder test-rig)

In this section the results and analysis of the experimental results for the single actuator test-rig are presented and described using the designed FDI scheme detailed in chapter 7. The position demand input to the system is a saw tooth input with amplitude of 60mm peak-to-peak at a frequency 0.2 Hertz. The starting point of the pneumatic cylinder is at mid position (50mm). For these experiments the PI control scheme is employed (see chapter 5).

8.2.1 Actuator fault

A fault Fa(s) (see Figure 7.2) is applied to the proportional valve at 13.3s. The fault injected is that the control signal has been disconnected. This is physically achieved by means of a switch. Figures 8.1-8.3 show the time history of this experiment (actuator fault) for the parity equation scheme. Figures 8.4-8.5 show the time history of this experiment (actuator fault) for the Kalman filter scheme.

Figure 8.1: Actuator fault Fa(s), parity equation results- Position sensor output (R_1)
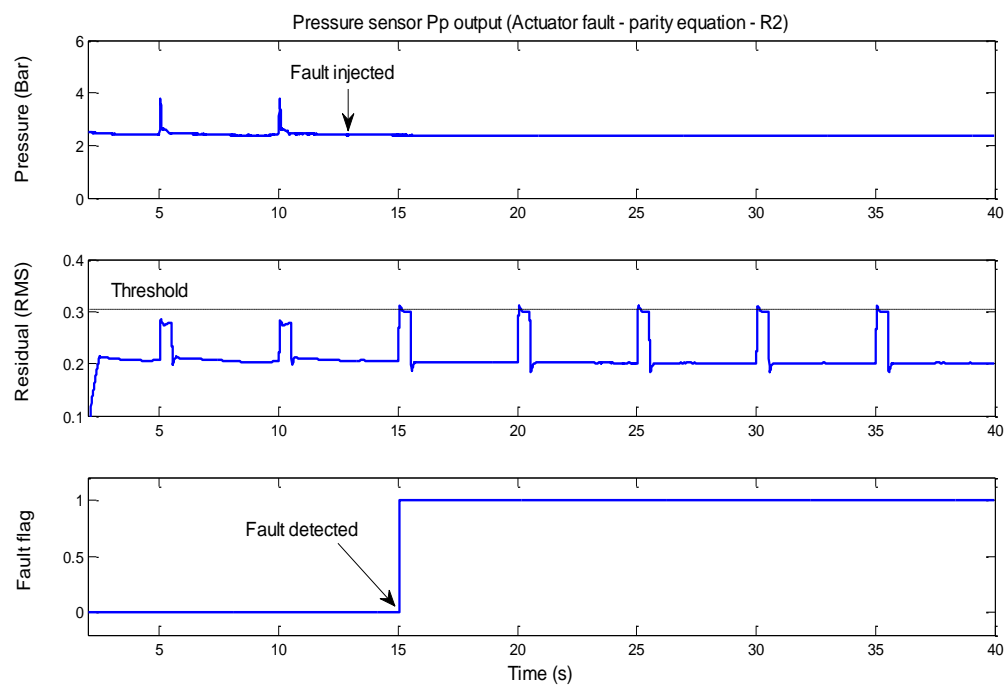
Figure 8.2: Actuator fault Fa(s), parity equation results- Pressure sensor Pp (R_2)
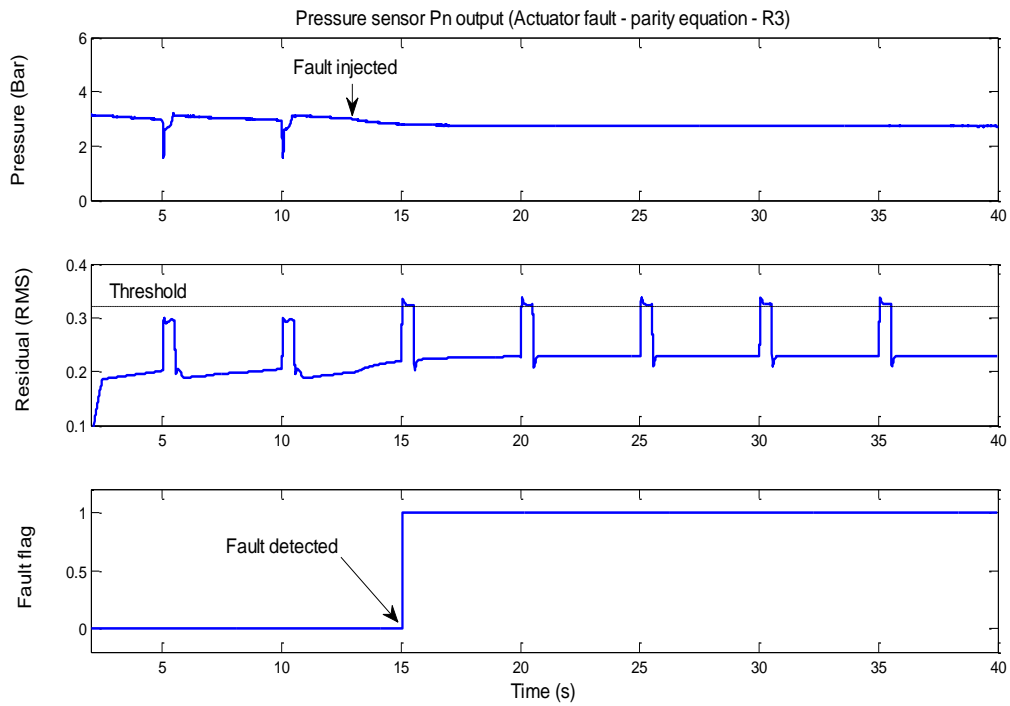
Figure 8.3: Actuator fault Fa(s), parity equation results-Pressure sensor Pn (R_3)
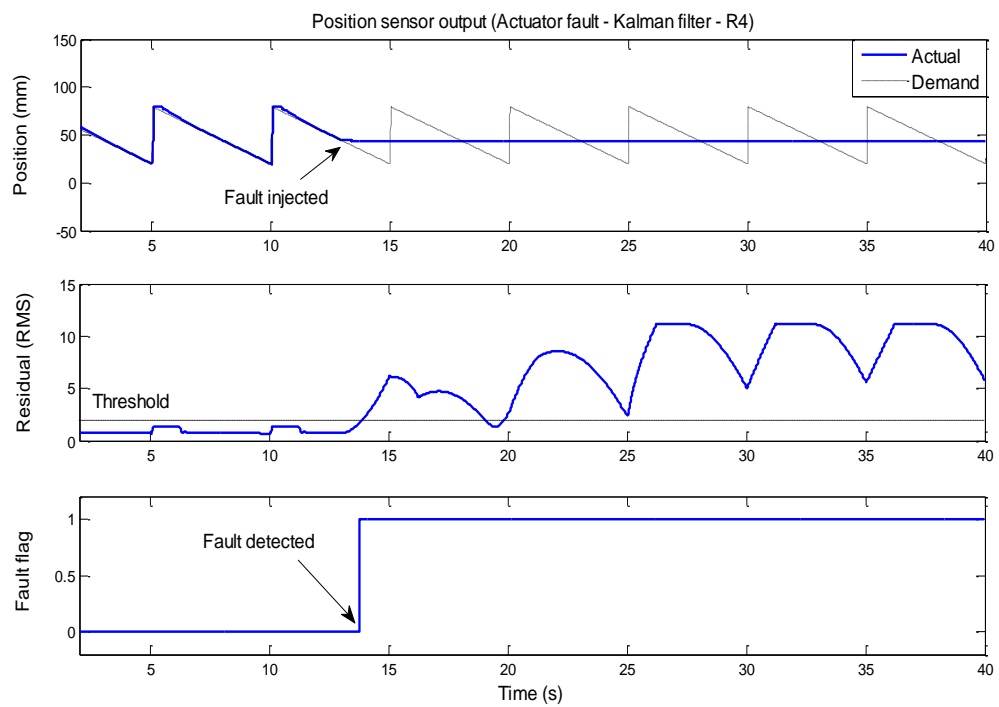
Figure 8.4: Actuator fault Fa(s), Kalman filter results-Position sensor output (R_4)
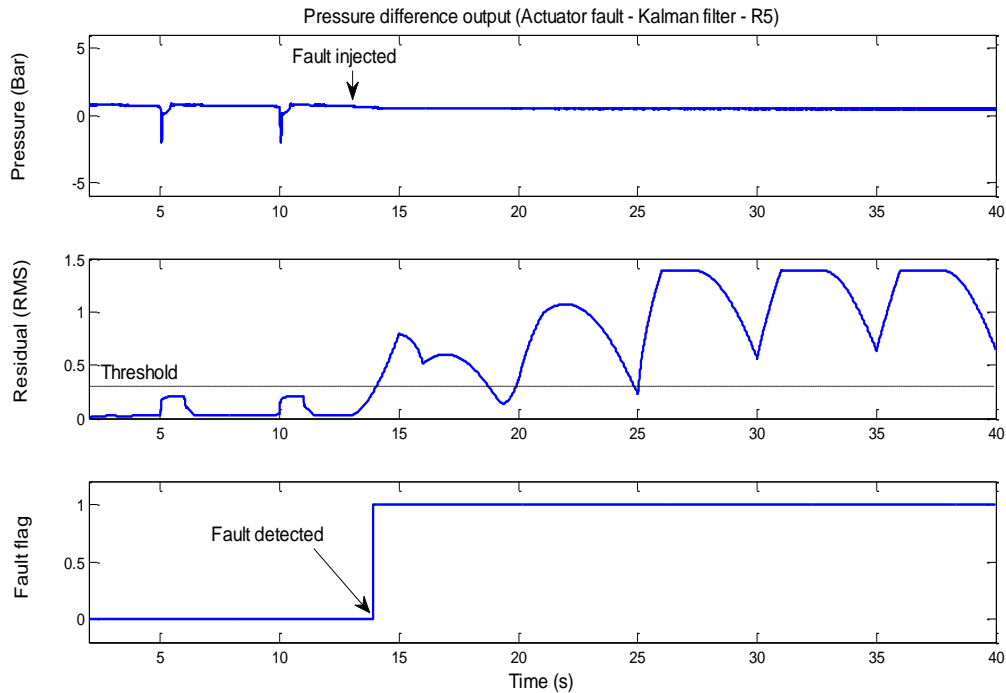
Figure 8.5: Actuator fault Fa(s), Kalman filter results-Pressure difference outputs (R_5)

8.2.1.1   Parity equations - Actuator fault

From Figure 8.1, at 13.3s the fault is applied. From residual R_1 the fault is detected at 13.83s and the fault flag is raised. At 18.5s the residual RMS falls below the threshold, which is due to the position output coinciding with the model output. This trend is apparent throughout the fault period. However the fault flag remains high as triggering is set so that once the threshold is exceeded the flag remains raised. Residual R_2 (Figure 8.2) exceeds its respective threshold at 15s and the fault flag is raised. Residual R_3 (Figure 8.3) exceeds its respective threshold at 15s and the fault flag is raised. Once triggered the fault flag remains raised.

8.2.1.2   Kalman filter - Actuator fault

For the same fault scenario as above, Figure 8.4 illustrates the outputs for the Kalman filter approach. From residual R_4 the fault is detected at 13.73s and the fault flag is raised and remains raised. The pressure difference residual (R_5) exceeds its respective threshold at 13.9s (Figure 8.5), where the fault flag is raised.

8.2.1.3   Discussion - Actuator fault

Applying the disconnection fault to the control signal of the proportional valve has an effect on the actuator fault parity residual (R_1), this raises the fault flag. The fault has an effect on the pressure sensor parity residuals (R_2 and (R_3). Both position and pressure difference Kalman residuals (R_4 and R_5) are affected by the actuator fault and their fault flags are raised. From both methods the Kalman approach tracks the fault better with a faster fault detection response time. Overall, it is clear that the parity equations and the Kalman filter approach can detect an actuator fault. However, using both methods an actuator or plant fault cannot be isolated. This agrees with the fault signatures detailed in Table 7.1 (chapter 7).

8.2.2   Air leak fault (between Proportional servo valve and pneumatic cylinder)

A leak fault is applied by means of opening a pressure release valve between the proportional servo valve and the pneumatic cylinder at time 11.6s. Figures 8.6-8.8 show the time histories of this experiment (leak fault) for the parity equation scheme. Figures 8.9-8.10 show the time histories of this experiment (leak fault) for the Kalman filter scheme.
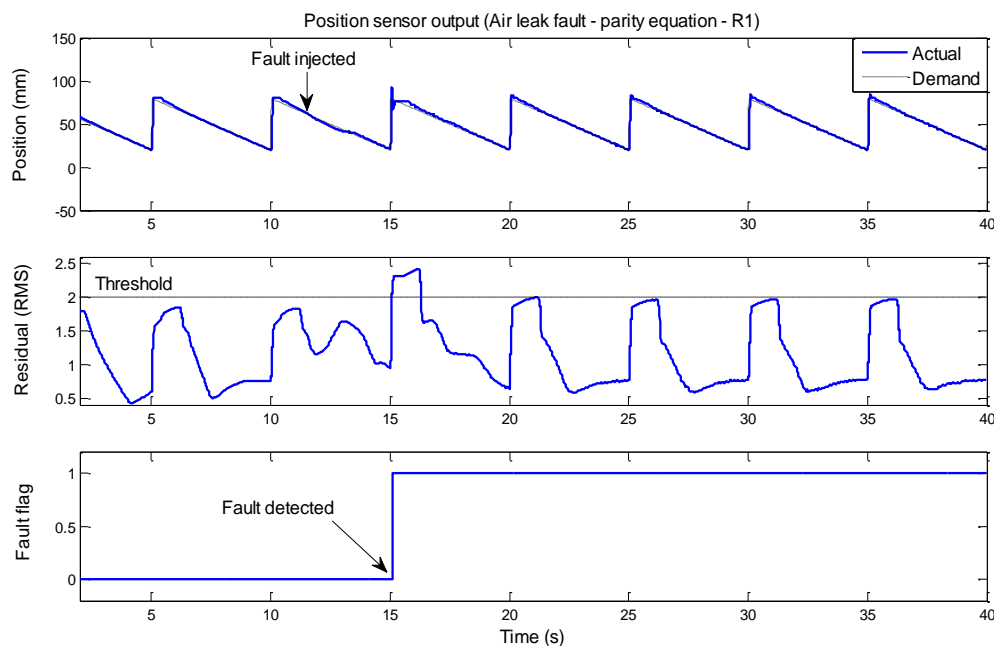
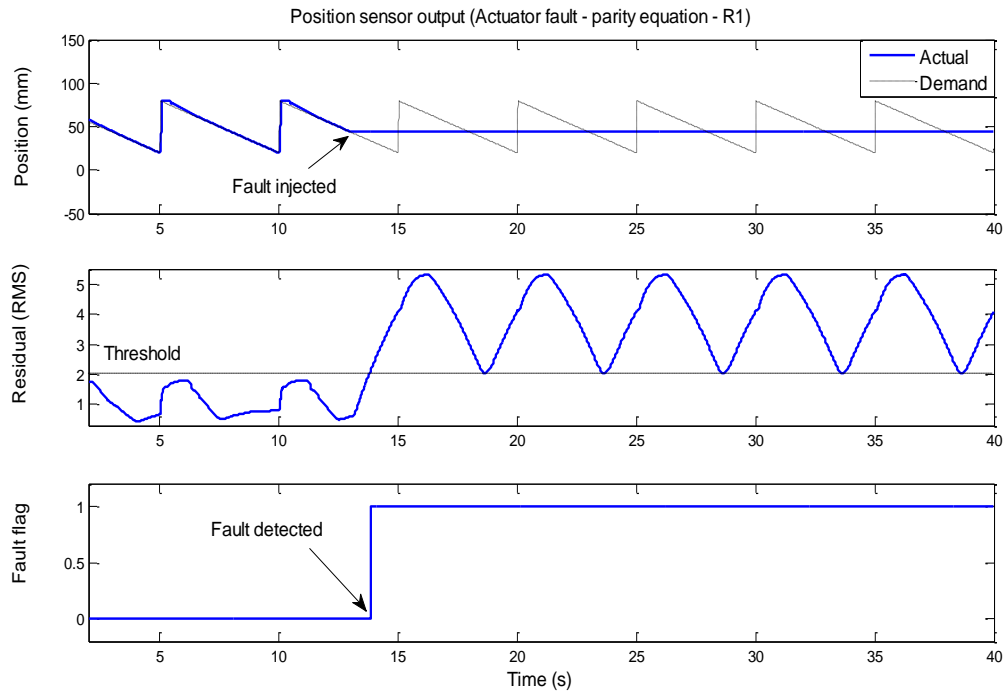Figure 8.6: Air leak fault, parity equation results - Position sensor output (R_1)

Figure 8.7: Air leak fault, parity equation results - Pressure sensor Pp (R_2)

Figure 8.8: Air leak fault, parity equation results - Pressure sensor Pn (R_3)

Figure 8.9: Air leak fault, Kalman filter results - Position sensor output (R_4)

Figure 8.10: Air leak fault, Kalman filter results - Pressure difference outputs (R_5)

143

8.2.2.1 Parity equations – Leak fault

The fault is applied at 11.6s. From the RMS residual R_1 (Figure 8.6) the fault is detected at 15.1s where the fault flag is raised and remains raised. The RMS residual R_2 (Figure 8.7) exceeds its respective threshold at 20s and the fault flag is raised. The RMS residual R_3 (Figure 8.8) exceeds its threshold at 12.5s and the fault flag is raised.

8.2.2.2 Kalman filter -Leak fault

From Figure 8.9, using the Kalman filter scheme, the RMS residual R_4 exceeds its threshold at 15s and the fault flag is raised. The RMS Residual R_5 (Figure 8.10) crosses its respective threshold at 15s and the fault flag is raised.

8.2.2.3 Discussion - Leak fault

Applying the leak fault to the pneumatic cylinder has an effect on the parity residual (R_1), this raises the fault flag. The fault also has an effect on the pressure sensor parity residuals (R_2 and R_3). The fault affects the position residual R_4 and the pressure difference residual R_5. Using both methods an actuator or plant fault cannot be isolated, this agrees with the fault signatures detailed in Table 7.1.

8.2.3 Pressure sensor fault (chamber Pp)

A fault FPp(s) (see Figure 7.2) is applied to pressure sensor (Pp). The fault injected is that the pressure signal to Chamber Pp has been disconnected. This is physically achieved by means of a switch. Figures 8.11-8.13 show the time history of this experiment (pressure sensor fault) for the parity equation scheme. Figures 8.14-8.15 show the time history of this experiment (pressure sensor fault) for the Kalman filter scheme.

Figure 8.11: Pressure sensor Pp fault [FPp(s)], parity equation results - Position sensor output (R_1)
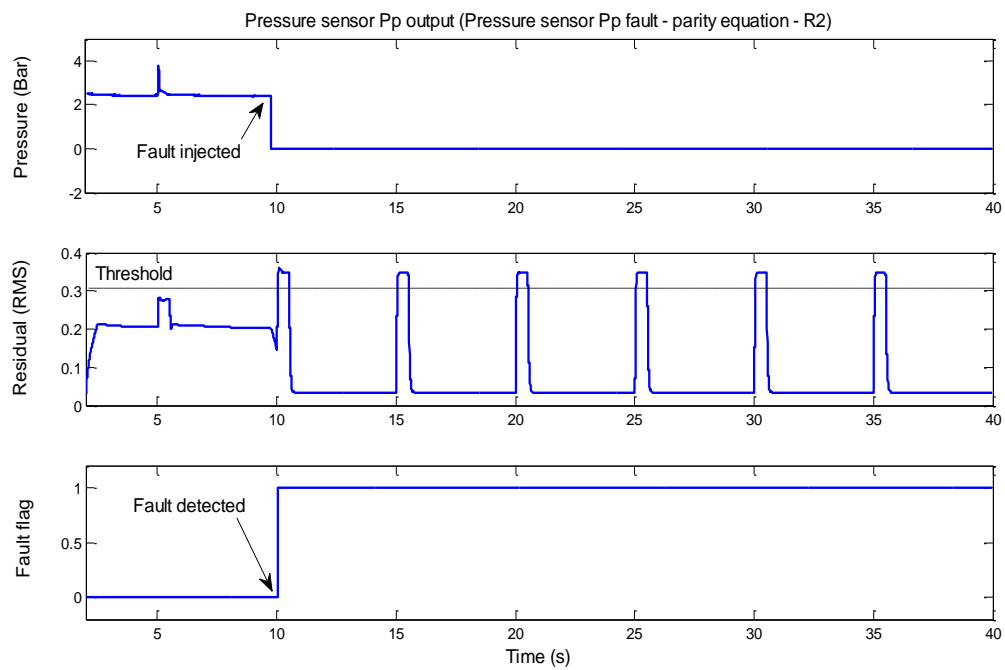
Figure 8.12: Pressure sensor Pp fault [FPp(s)], parity equation results - Pressure sensor Pp output (R_2)
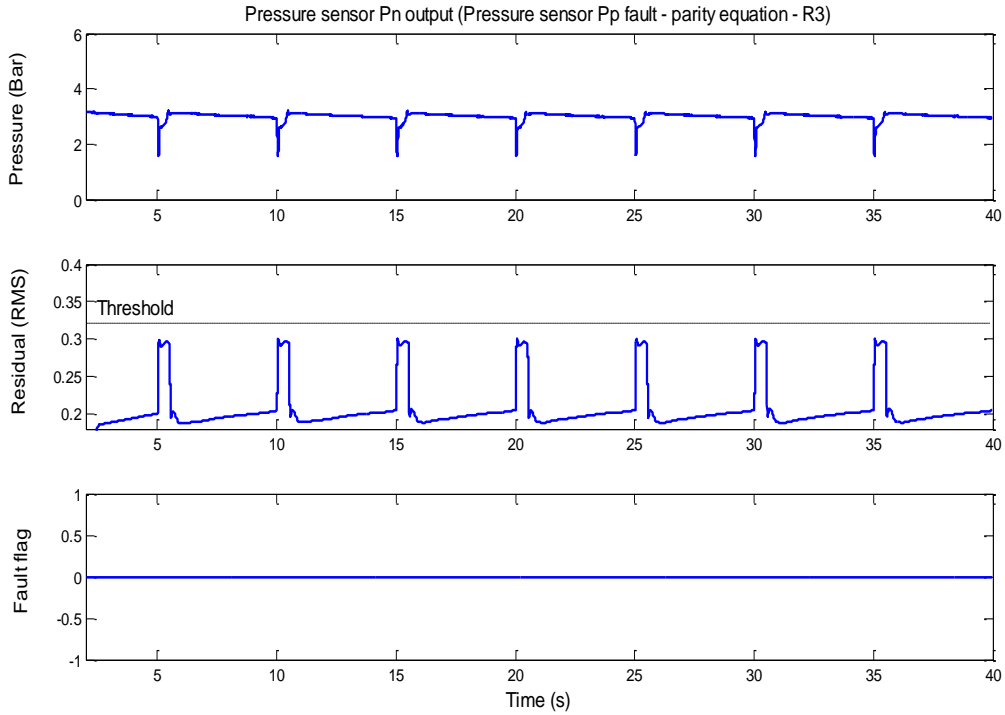
Figure 8.13: Pressure sensor Pp fault [FPp(s)], parity equation results - Pressure sensor Pp output (R_3)
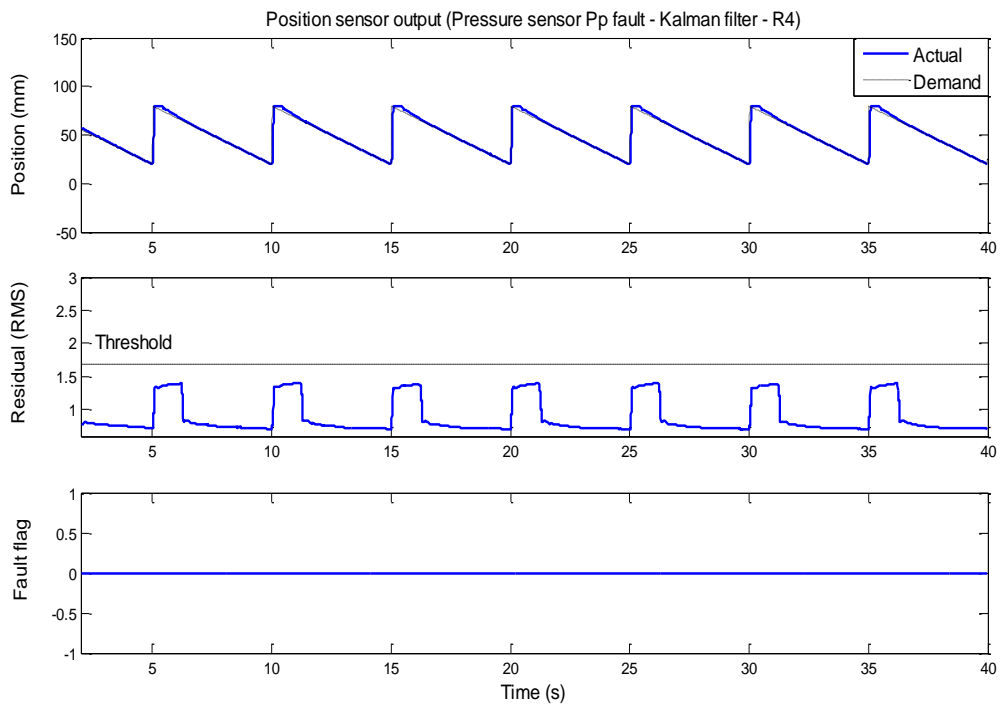
Figure 8.14: Pressure sensor Pp fault [FPp(s)], Kalman filter results - Position sensor output (R_4)
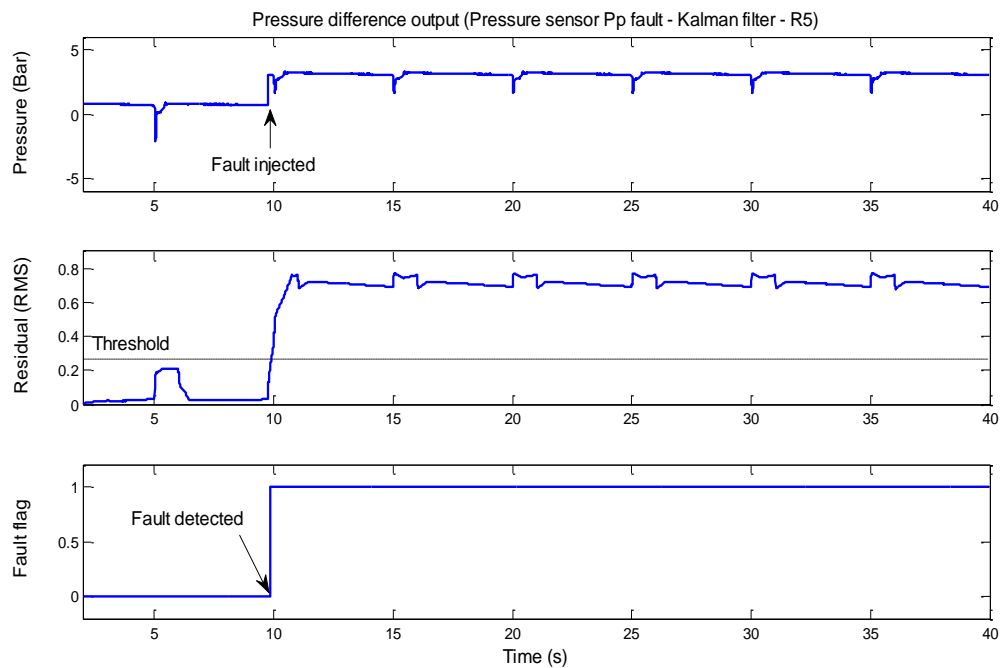
Figure 8.15: Pressure sensor Pp fault [FPp(s)], Kalman filter results - Pressure difference output (R_5)

8.2.3.1   Parity equations – Pressure sensor fault (chamber Pp)

From Figure 8.11 a fault is applied to the pressure sensor of chamber Pp at 9.75s. Using the parity equation scheme the RMS residual R_1 is unaffected by this fault. However, the RMS residual R_2 exceeds its threshold (Figure 8.12) at 10.05s and the fault flag is raised. The RMS residual R_3 plot (Figure 8.13) shows that this residual is unaffected by this fault.

8.2.3.2   Kalman filter - Pressure sensor fault (chamber Pp)

The outputs from the Kalman filter scheme (Figure 8.14) show that the residual R_4 is not affected by a fault applied to the pressure sensor for chamber Pp and the R_4 fault flag remains false. For the same fault the RMS residual R_5 exceeds its threshold at 9.87s (Figure 8.15) and the fault flag is raised.

8.2.3.3   *Discussion – Pressure sensor fault (chamber Pp)*

Applying a fault to the pressure sensor (Pp) has no affect on the parity RMS residual (R_1). The fault affects the pressure sensor RMS residual (R_2). However, this fault does not have an effect on the RMS residual R_3. The fault again having no affect on the position RMS residual R_4. The RMS residual R_5 is affected by this fault. These results concur with the fault signatures detailed in Table 7.1. Comparing parity and Kalman schemes, the Kalman filter approach has a faster detection response time.

8.2.4   *Air blockage fault*

Here, a blockage fault is applied to the system at 17.2s. This is physically achieved by means of a cut-off valve located between the proportional valve and chamber Pn of the pneumatic cylinder. Figures 8.16-8.18 show the time histories of this experiment (blockage fault) for the parity equation scheme. Figures 8.19-8.20 show the time histories of this experiment (blockage fault) for the Kalman filter scheme.
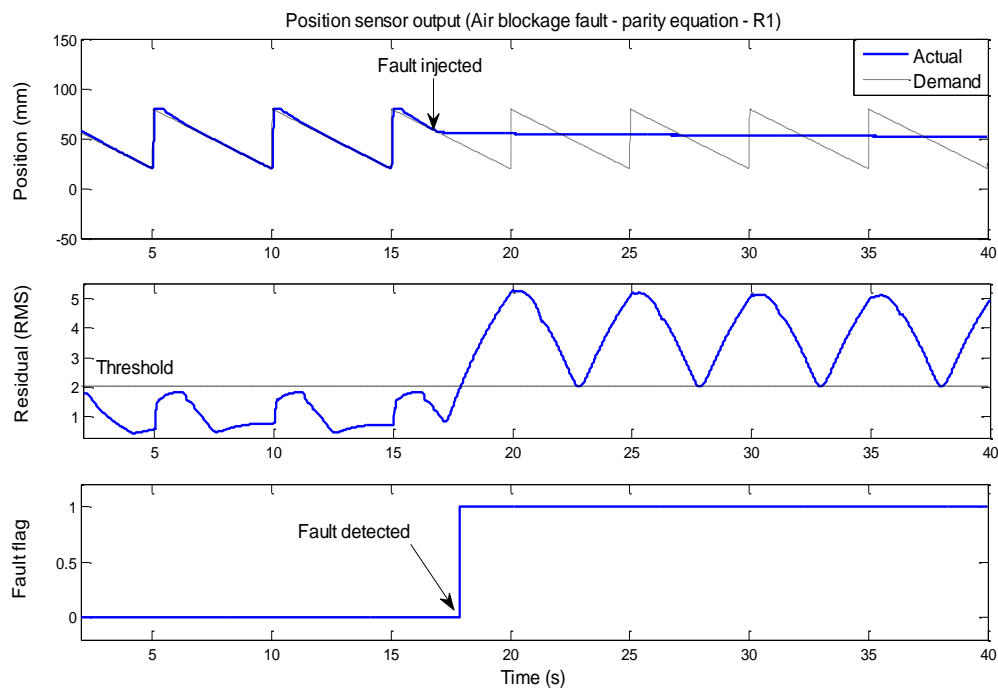
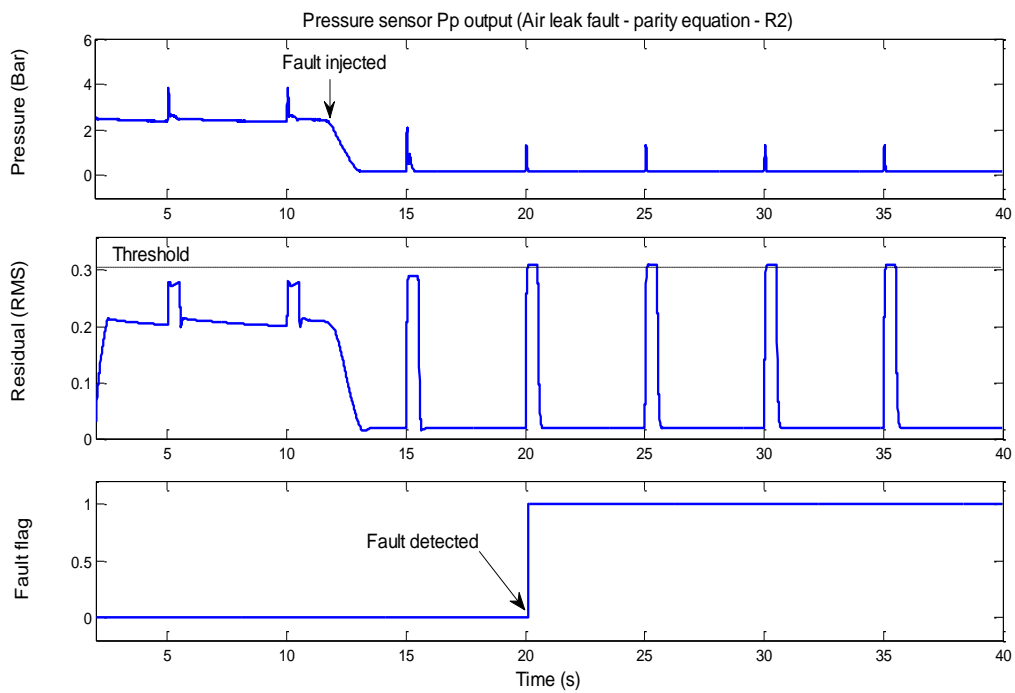Figure 8.16: Air blockage fault, parity equation results- position sensor output (R_1)
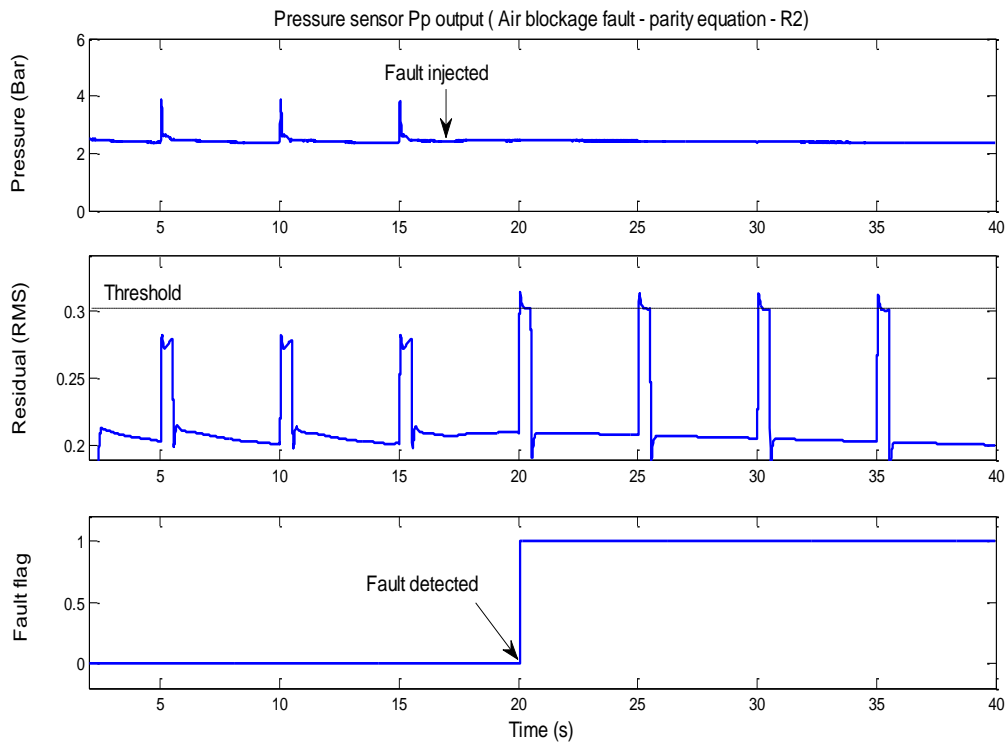
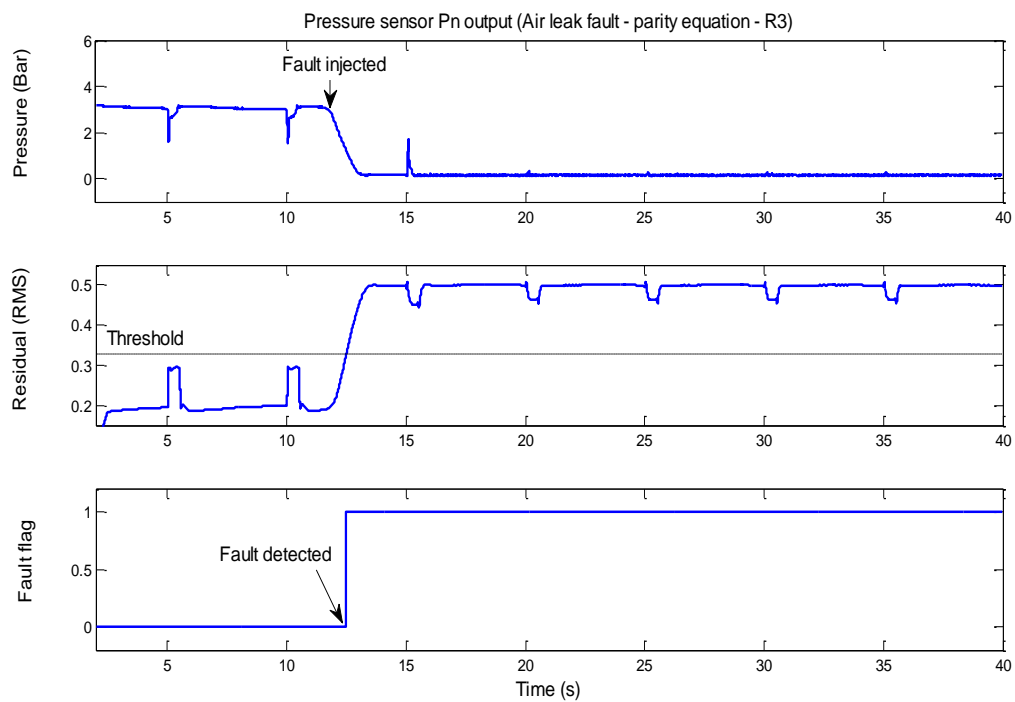Figure 8.17: Air blockage fault, parity equation results- Pressure sensor Pp output (R_2)
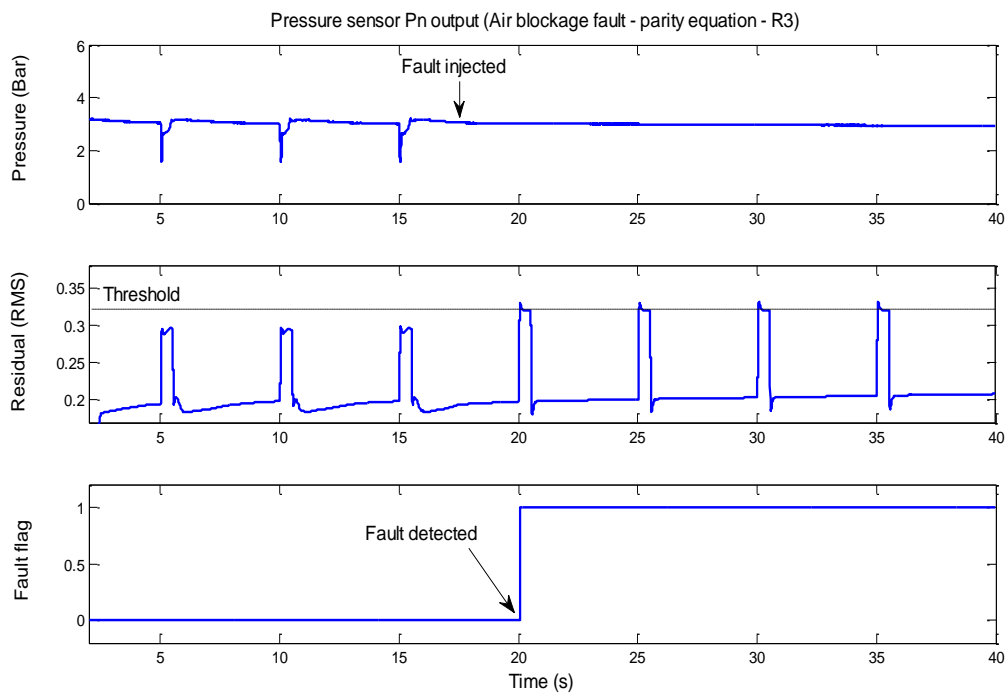
Figure 8.18: Air blockage fault, parity equation results- Pressure sensor Pn output (R_3)
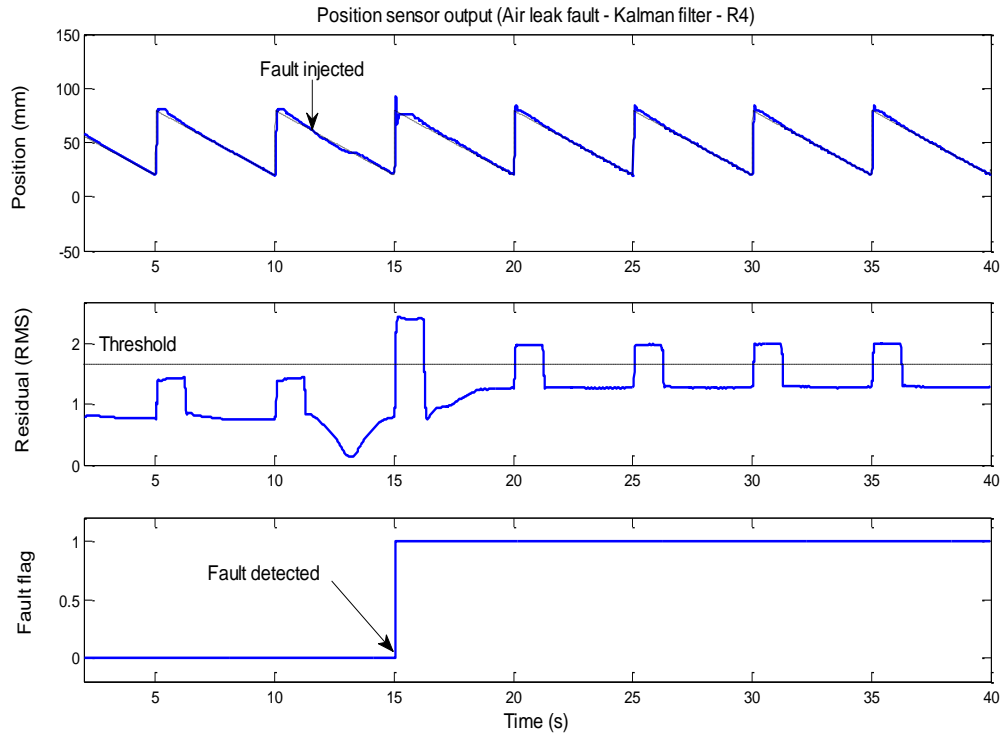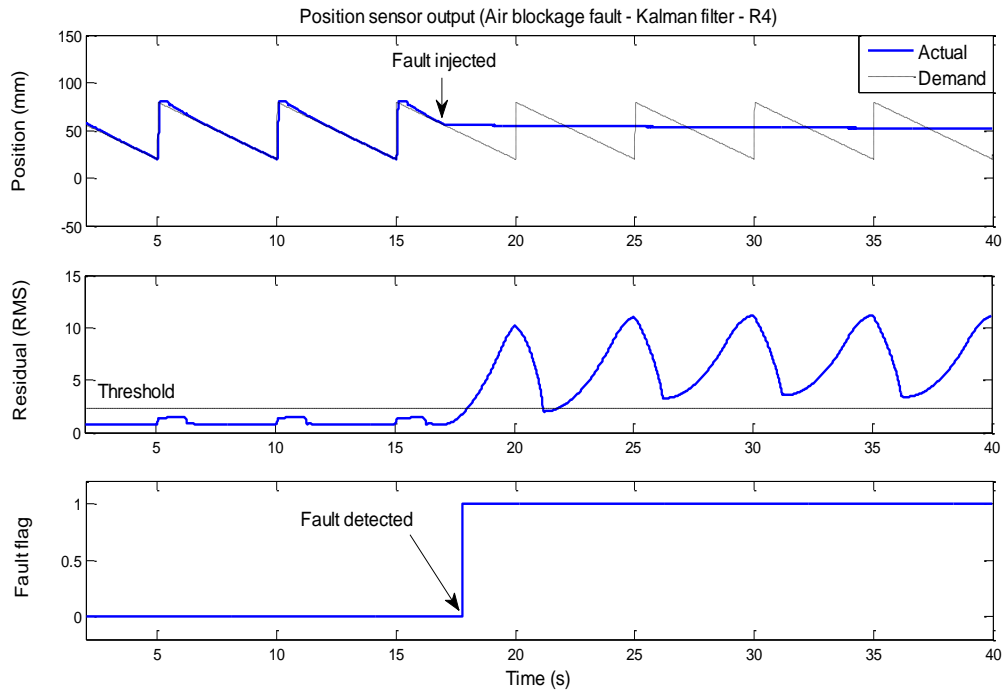
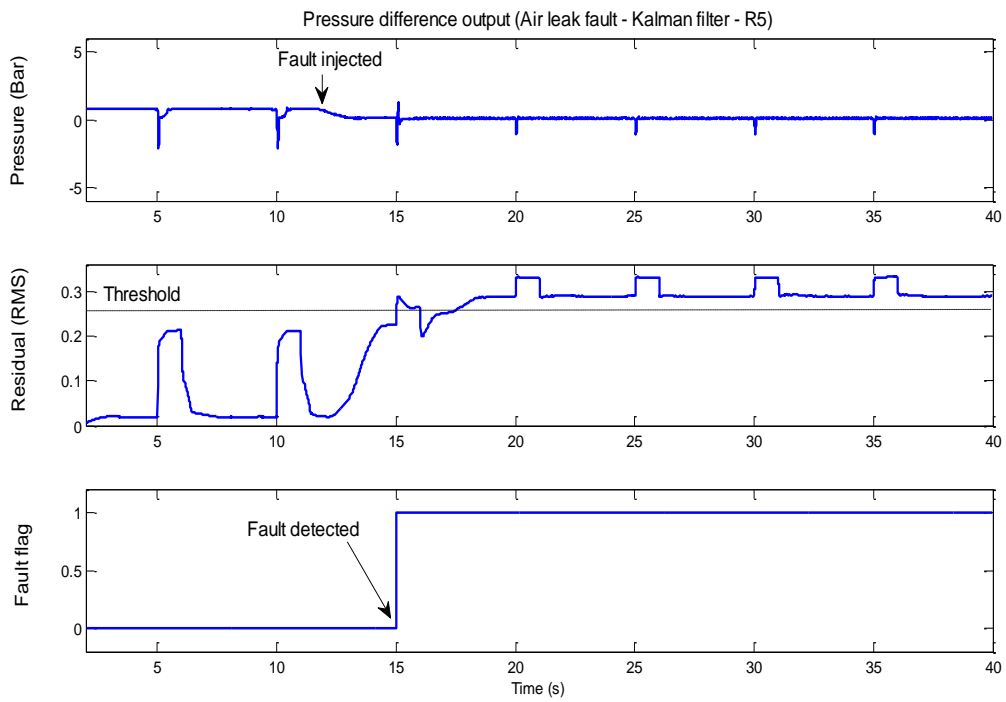Figure 8.19: Air blockage fault, Kalman filter results - position sensor output (*R₄*)
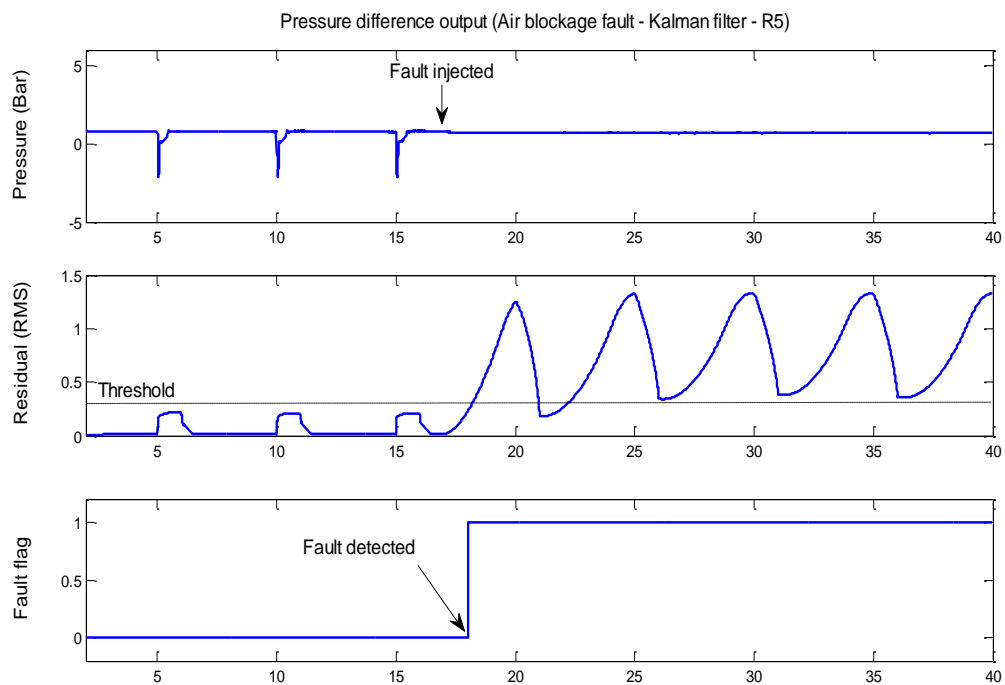
Figure 8.20: Air blockage fault, Kalman filter results - Pressure difference outputs (*R₅*)

8.2.4.1   Parity equations – Air blockage fault

From Figure 8.16 a blockage fault is applied at time 17.2s. Using the parity equation scheme the RMS residual R_1 exceeds its threshold at 17.86s and the fault flag is raised and remains raised. RMS residuals R_2 (Figure 8.17) and R_3 (Figure 8.18) both exceed their respective thresholds at 20s respectively, and raise their fault flags.

8.2.4.2   Kalman filter - Air blockage fault

The outputs from the Kalman filter scheme (Figure 8.19) show that the residual R_4 is affected by a blockage applied to the system. The fault flag is raised at 17.77s. For the same fault, the RMS residual R_5 exceeds its threshold at 18.02s (Figure 8.20) and the fault flag is raised.

8.2.4.3   Discussion – Air blockage fault

Applying a blockage fault to the pressure pipe has an effect on the parity RMS residual (R_1). The blockage also affects residuals R_2, R_3, R_4 and R_5. These results concur with the fault signatures detailed in Table 7.1. Comparing parity equation and Kalman filter schemes, the Kalman filter approach has a faster detection response time.

8.2.5   Position sensor fault (sensor signal loss)

A fault FS(s) (see Figure 7.2) is applied to position sensor GS(s) at 15.56s. The fault injected is that the position signal has been disconnected. This is physically achieved by means of a switch. Figures 8.21-8.23 show the time histories of this experiment (position sensor signal loss) for the parity equation scheme. Figures 8.24-8.25 show the time histories of this experiment (position sensor signal loss) for the Kalman filter scheme.
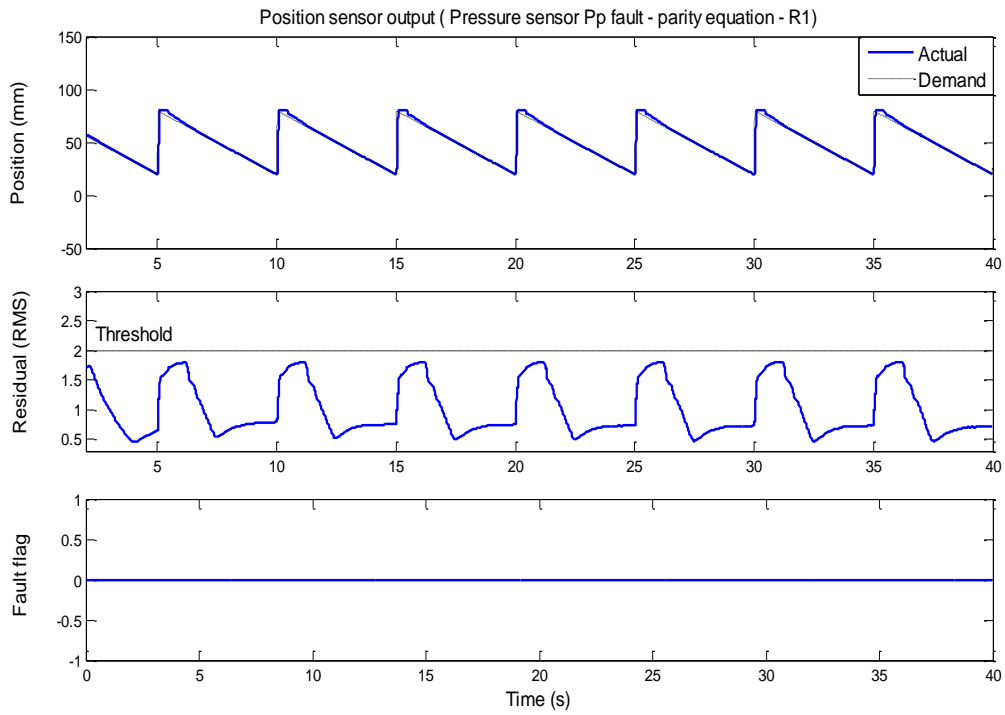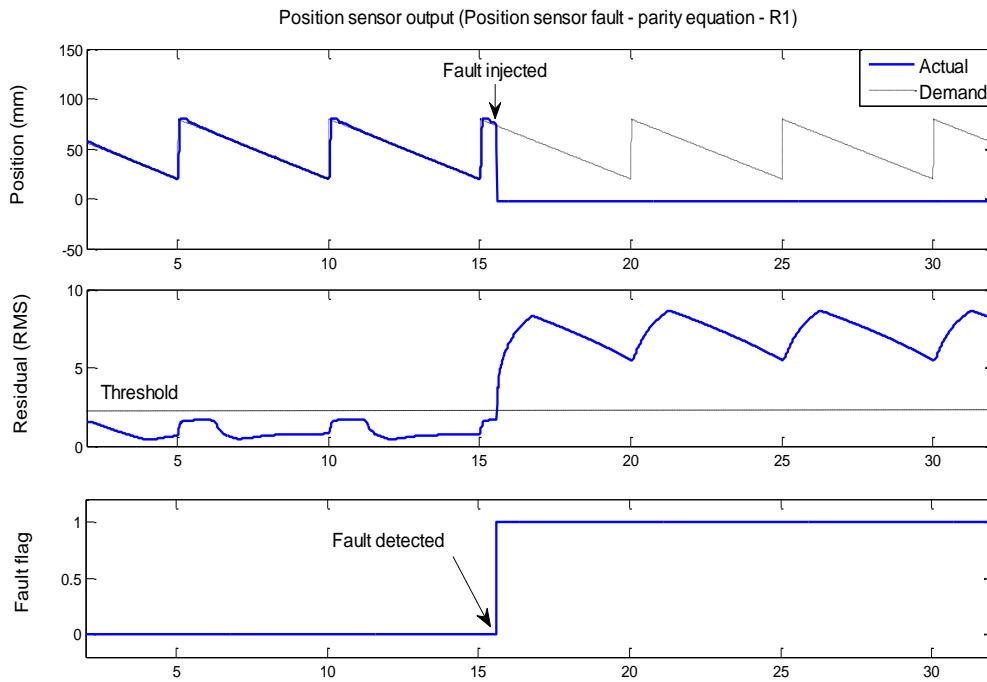
Figure 8.21: Position sensor fault Fs(s) (signal loss), parity equation results- position sensor output (R_1)
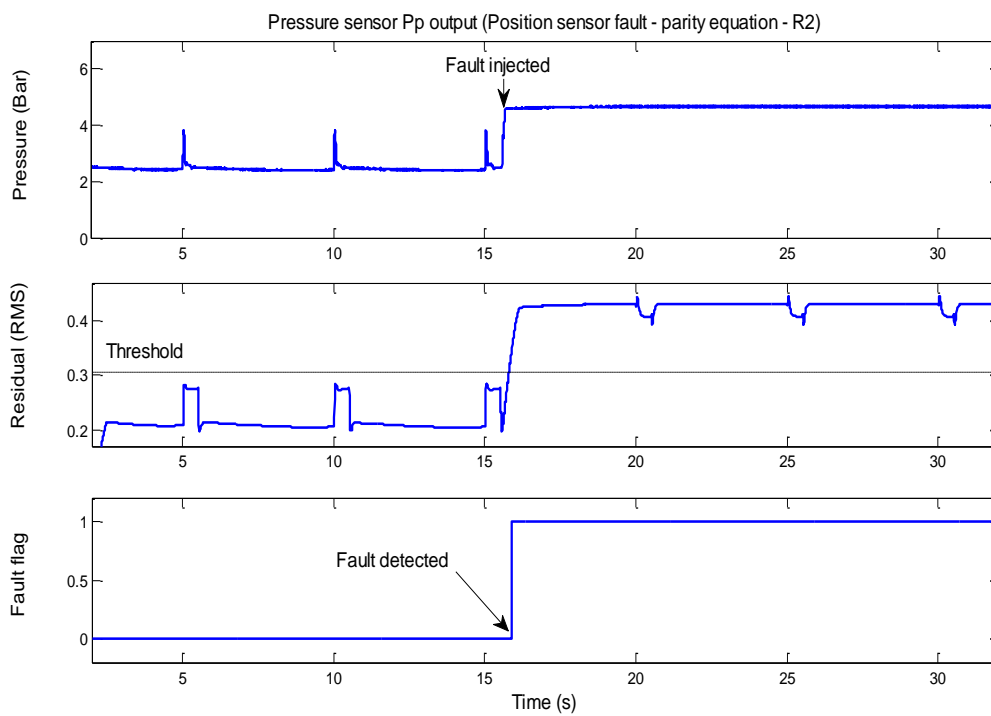
Figure 8.22: Position sensor fault Fs(s) (signal loss), parity equation results- Pressure sensor Pp output (R_2)
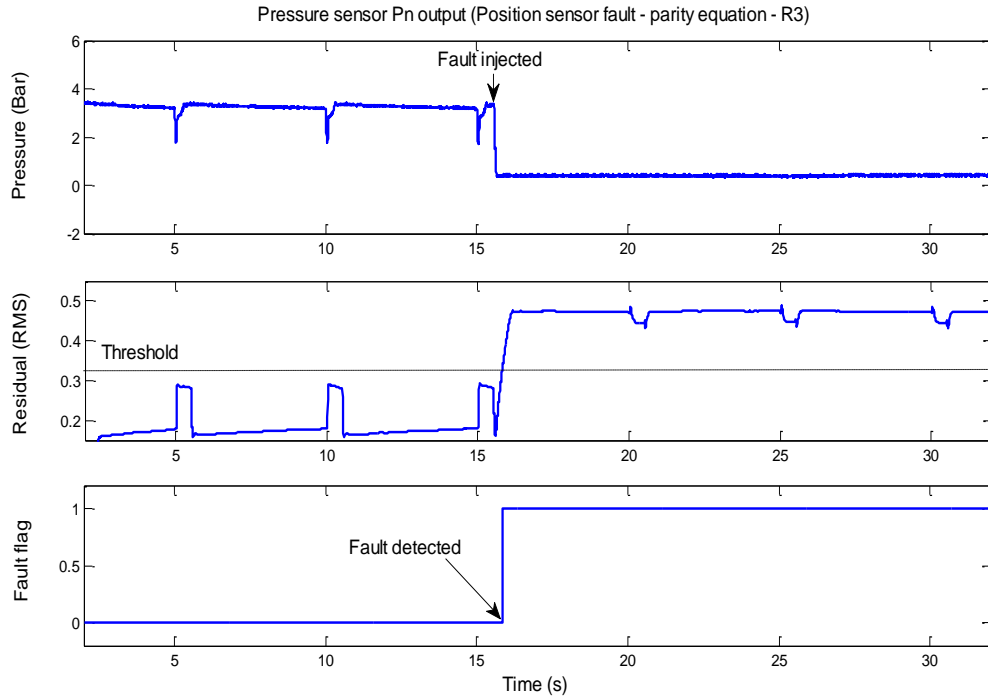
Figure 8.23: Position sensor fault Fs(s) (signal loss), parity equation results- Pressure sensor Pn output (R_3)
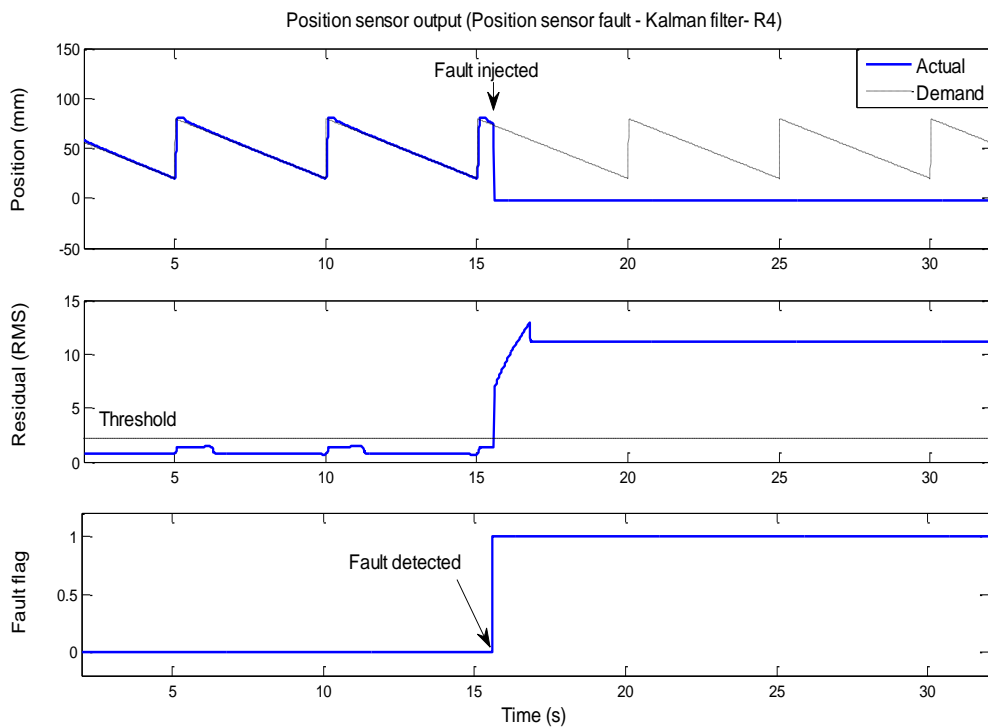
Figure 8.24: Position sensor fault Fs(s) (signal loss), Kalman filter results - Position sensor output (R_4)
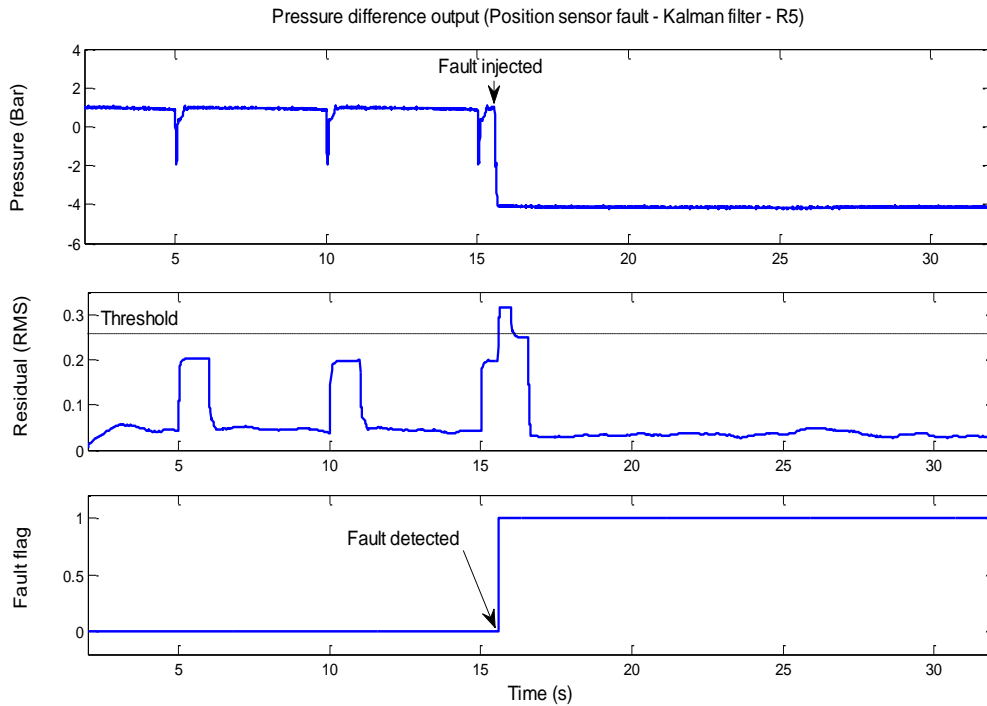
Figure 8.25: Position sensor fault Fs(s) (signal loss), Kalman filter results -Pressure difference outputs (R_5)

8.2.5.1   *Parity equations – Position sensor fault (sensor signal loss)*

From Figure 8.21 a fault is applied at time 15.56s. Using the parity equation scheme the RMS residual R_1 exceeds its threshold at 15.57S and the fault flag is raised and remains raised.. The RMS Residual R_2 exceeds its respective threshold at 15.9s (Figure 8.22). The fault flag is raised. The RMS Residual R_3 exceeds its respective threshold at 15.84s (Figure 8.23), where the fault flag is raised.

8.2.5.2   *Kalman filter - Position sensor fault (sensor signal loss)*

Applying the same fault scenario as above, Figure 8.24 illustrates the outputs for the Kalman filter approach for the RMS residual R_4, the fault is detected at 15.57s and the fault flag is raised .The pressure difference residual (R_5) exceeds its respective threshold at 15.58s (Figure 8.25) and the fault flag is raised.

154

8.2.5.3   Discussion - Position sensor fault (sensor signal loss)

Applying the disconnection fault to the position sensor signal has an effect on the parity RMS residual (R_1), this raises the fault flag. The fault has an effect on the pressure sensor parity RMS residuals (R_2 and R_3). Both position and pressure difference Kalman residuals (R_4 and R_5) are affected by the position sensor fault and their fault flags are raised. However, these results do not agree with Table 7.1. In accordance with Table 7.1 only residual's R_1 and R_4 should be raised, and residual's R_2, R_3, and R_5 respectively should remain low. The reason for residual's R_2, R_3, and R_5 being raised are that applying this fault causes the control system to go into open-loop (no feedback) and this control scenario drives the pneumatic cylinder's piston to the start position (fully retracted). The system reacts rapidly once the feedback signal is disconnected. The residual's R_2, R_3, and R_5 are raised as faults because the outputs of the system, in terms of position, pressure and pressure difference outputs do not correspond with the parity and Kalman equations outputs. These differences cause the faults to be raised. In order to show that the residuals R_2, R_3, and R_5 correspond with the theoretical fault signatures of Table 7.1. A redundant sensor is mounted on the end of the pneumatic cylinder (plant) as described in chapter 3. A voting scheme is applied to compute a correct output signal from the two position signals and the estimated signal (described in chapter 7) to determine a continuous smooth function of the redundant input(s).

The experiments are repeated with the redundant sensor installed. The fault is injected at 17.44s. Figures 8.26-8.28 show the time histories of this experiment (position sensor signal loss) for the parity equation scheme using the redundant sensor and voting scheme. Figures 8.29-9.30 show the time histories of this experiment (position (primary) sensor signal loss) for the Kalman filter scheme using the redundant sensor and voting scheme. Figure 8.31 depicts the time history of the weighted average outputs of the voting scheme.
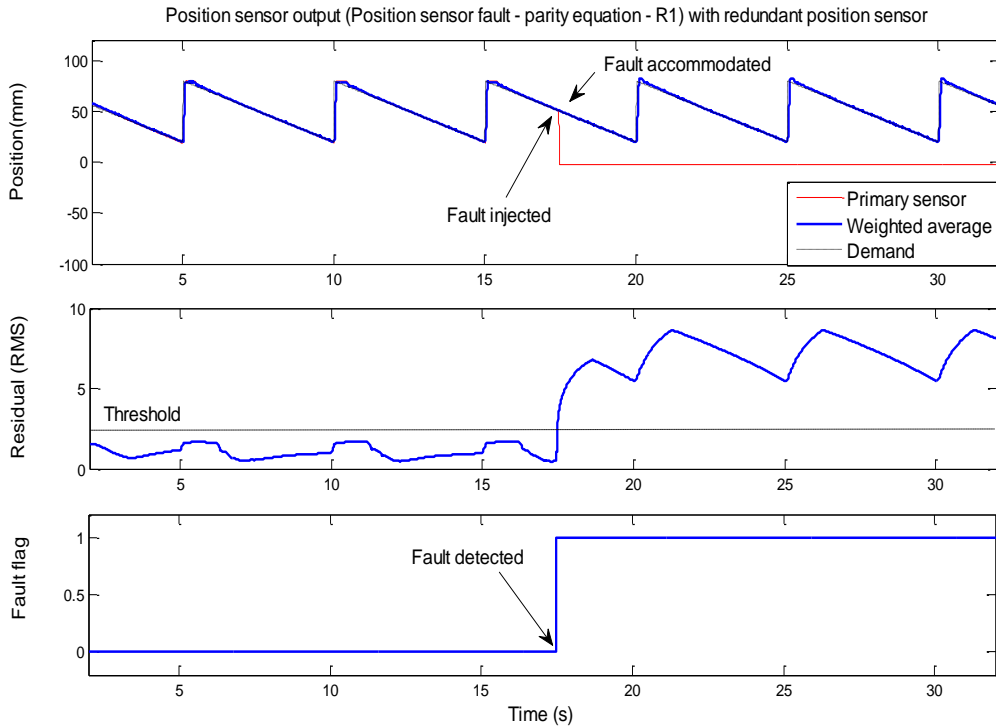
Figure 8.26: Position (primary) sensor fault Fs(s) (signal loss), Parity equation results –
Position sensor output (R_1) using the redundant sensor and voting scheme
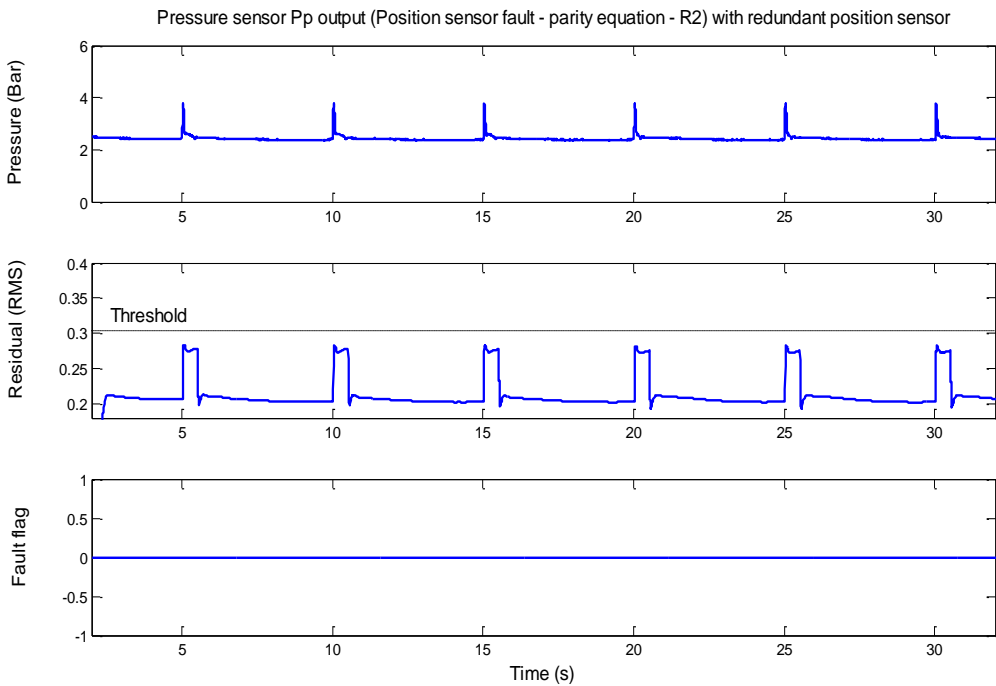
Figure 8.27: Position (primary) sensor fault Fs(s) (signal loss), Parity equation results –
Pressure sensor Pp (R_2) output using the redundant sensor and voting scheme
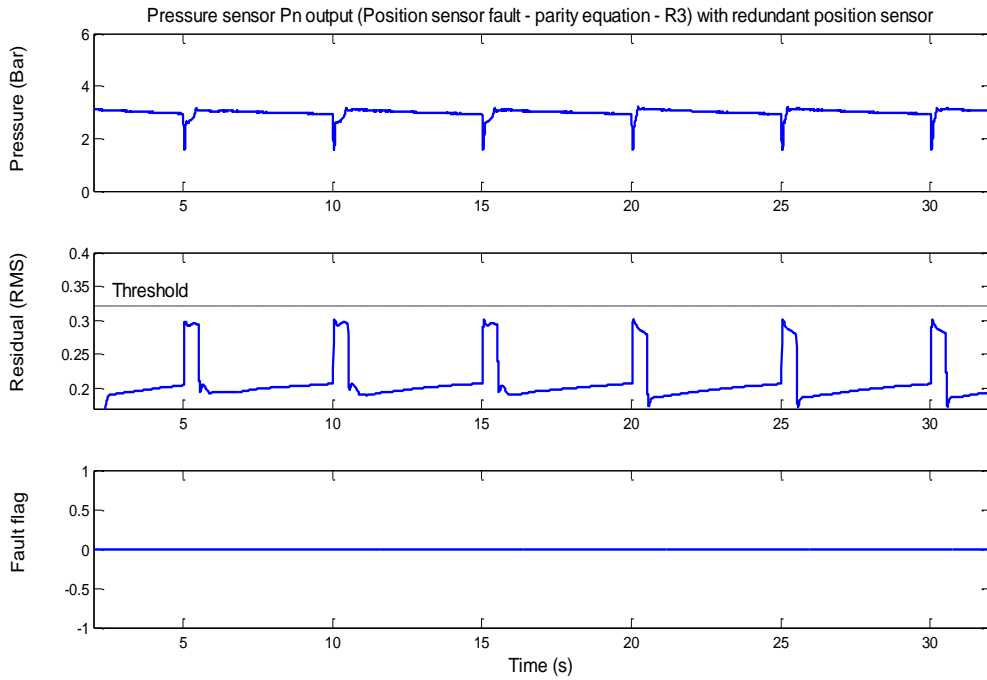
Figure 8.28: Position (primary) sensor fault Fs(s) (signal loss), Parity equation results – Pressure sensor Pn output (R_3) using the redundant sensor and voting scheme
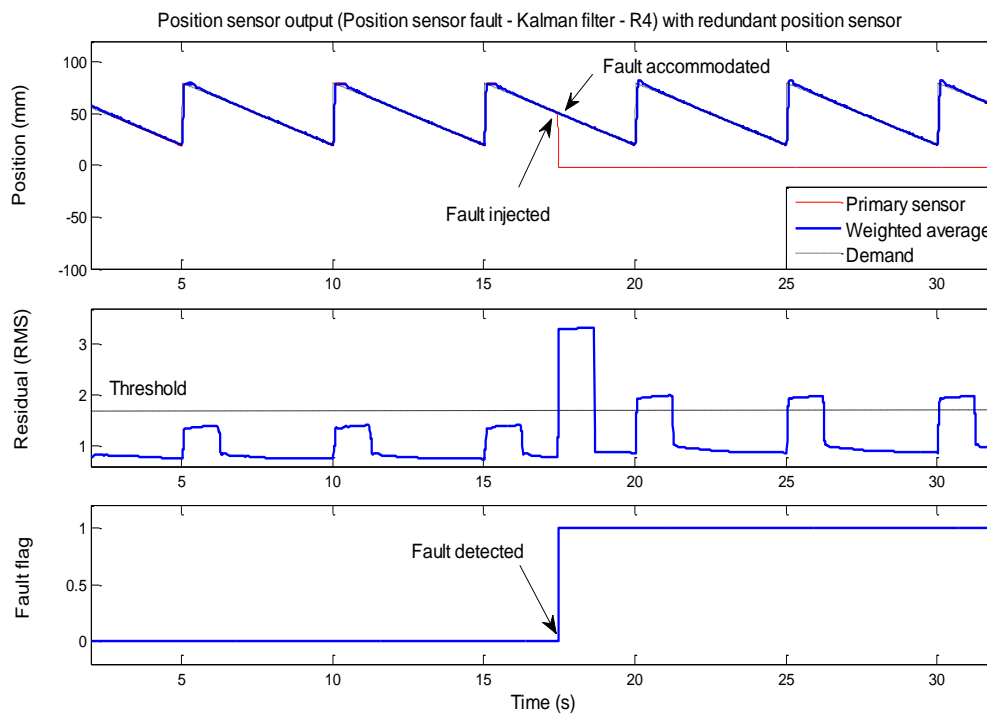
Figure 8.29: Position (primary) sensor fault Fs(s) (signal loss), Kalman filter results - Position sensor output (R_4) using the redundant sensor and voting scheme

157
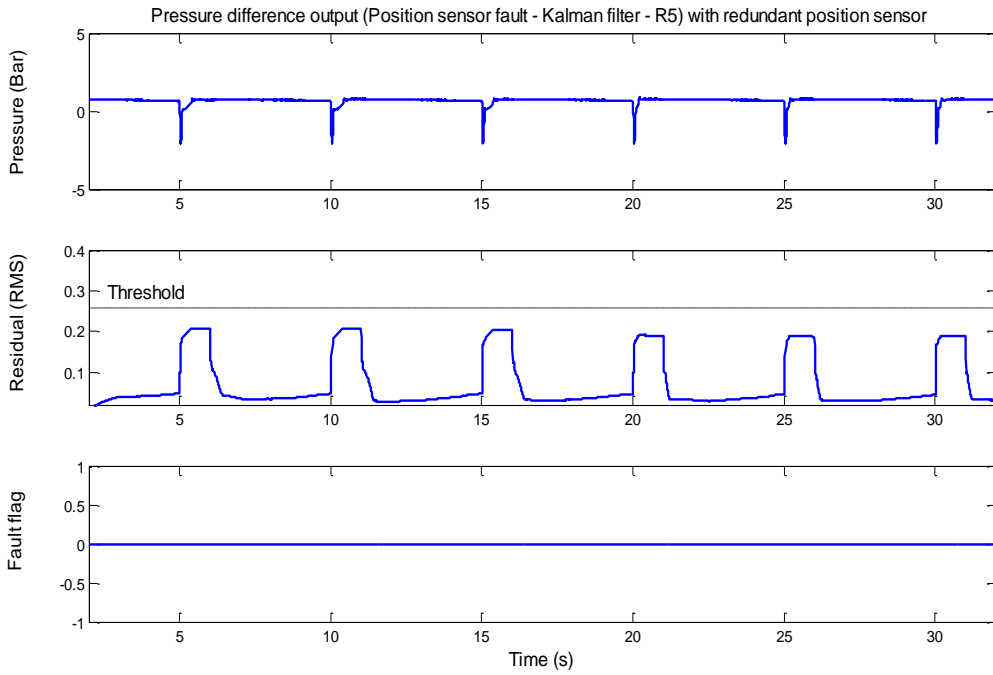
Figure 8.30: Position (primary) sensor fault Fs(s) (signal loss), Kalman filter results -
Pressure difference outputs (R_5) using the redundant sensor and voting scheme
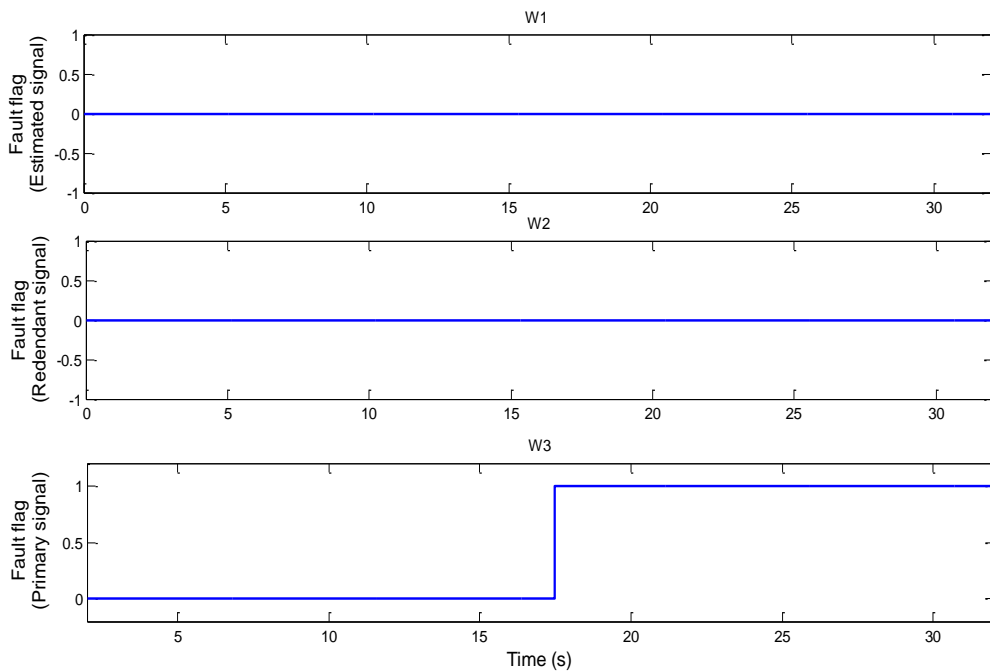
Figure 8.31: Weighted average outputs for a position (primary) sensor fault using the
redundant sensor and voting scheme

158

8.2.5.4 Discussion - Position sensor fault (sensor signal loss) with redundant sensor

Employing a redundant sensor scheme and applying the disconnection fault to the position sensor signal has an effect on the parity RMS residual (R_1). The fault is applied at 17.5s and the fault flag is raised at 19s (Figure 8.26). The fault has no effect on the pressure sensor parity RMS residuals R_2 and R_3 (Figure 8.27-8.28) respectively. The Kalman residual R_4 is affected and raises the fault flag at 19s (Figure 8.29). There is no effect on the pressure difference Kalman residual R_5 (Figure 8.30). These results agree with the fault signatures detailed in Table 7.1. The results are also in agreement with Table 7.2 this shows that RMS residuals R_1, R_4 and w_3 (Figure 8.31) all exceed their respective thresholds each flags a fault. From the plot of residual R_1 (Figure 8.26) and residual R_4 (Figure 8.29) it can be seen by using the redundant sensor along with the voting scheme, a continuous smooth function of the redundant input is achieved. The system functions normally under this fault, and successful detection, isolation and accommodation with regards to a position sensor fault is achieved. Comparing both residual schemes, the parity equations and Kalman filter approaches have the same response time when detecting this type of fault.

8.2.6 Pressure sensor fault (sensor drift)

A bias is added to the pressure sensor of chamber Pn, so that a drift fault is applied at 20.5s. Figures 8.32-8.34 show the time histories for the parity equation scheme. Figures 8.35-8.36 show the time histories of these experiments for the Kalman filter scheme. The redundant sensor scheme is used in this experiment. Figure 8.37 depicts the time history of the weighted average outputs of the voting scheme.

8.2.6.1 Parity equations – Pressure sensor drift fault

At 20.5s a drift bias is added to the pressure signal. From the RMS residual R_1 (Figure 8.32) the pressure sensor drift fault has no effect. The RMS residual R_2 (Figure 8.33) is not affected by the pressure sensor fault. The RMS residual R_3 (Figure 8.34) exceeds its threshold at 22.82s, where the fault flag is raised and remains raised.
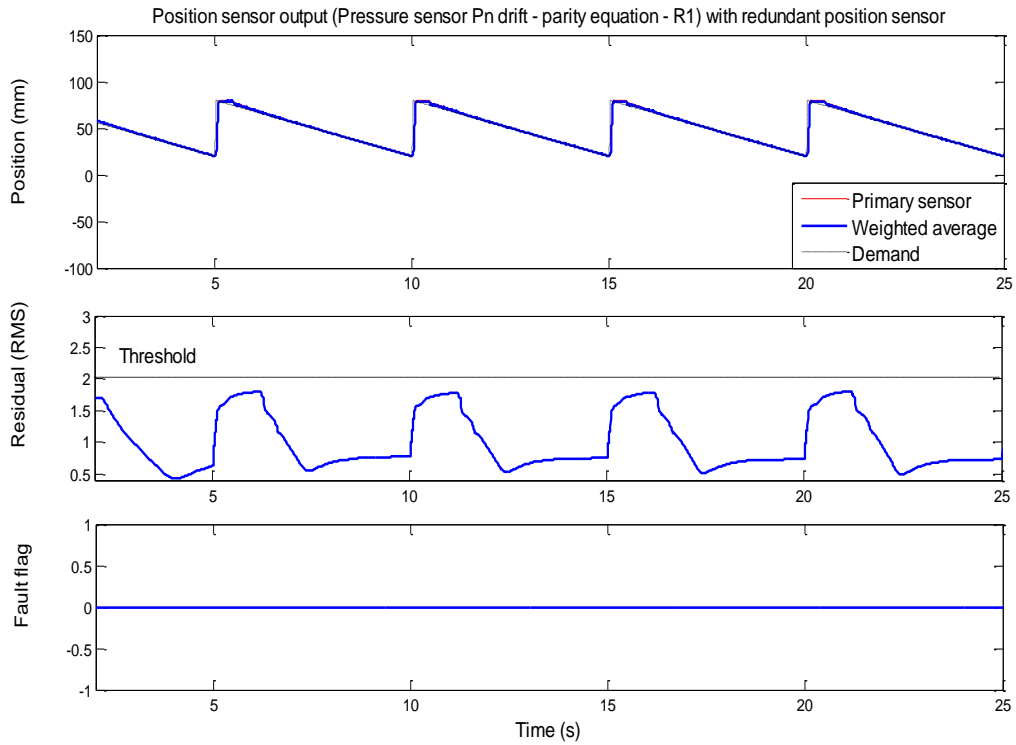
Figure 8.32: Pressure (Primary) sensor drift fault FPn(s), Parity equation results - Position sensor output (R_1)
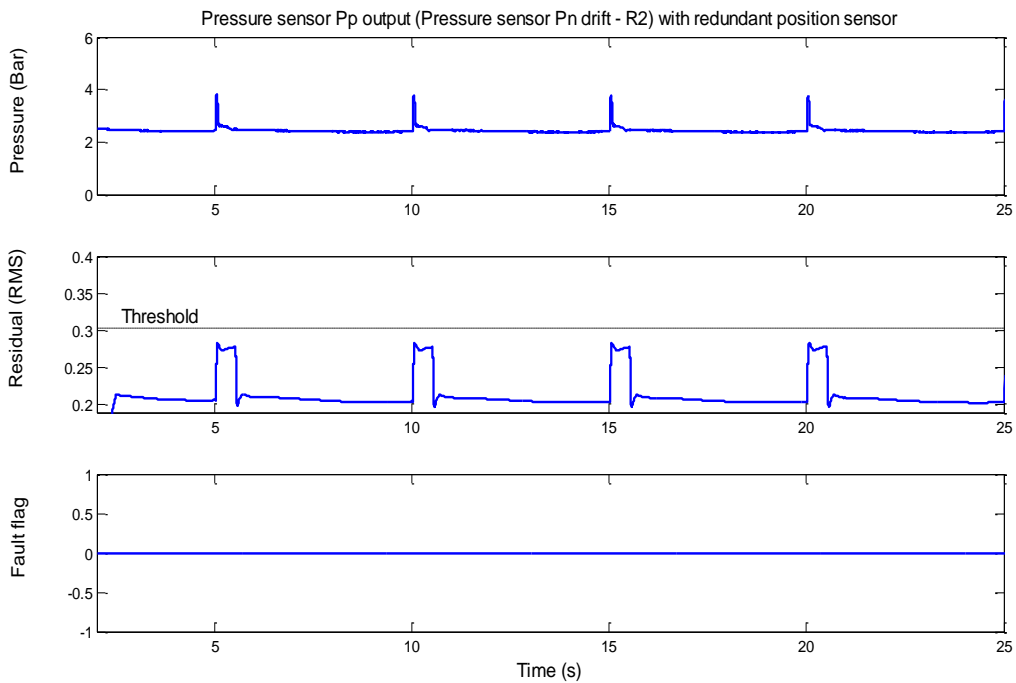
Figure 8.33: Pressure (Primary) sensor drift FPn(s), parity equation results - Pressure sensor Pp output (R_2)
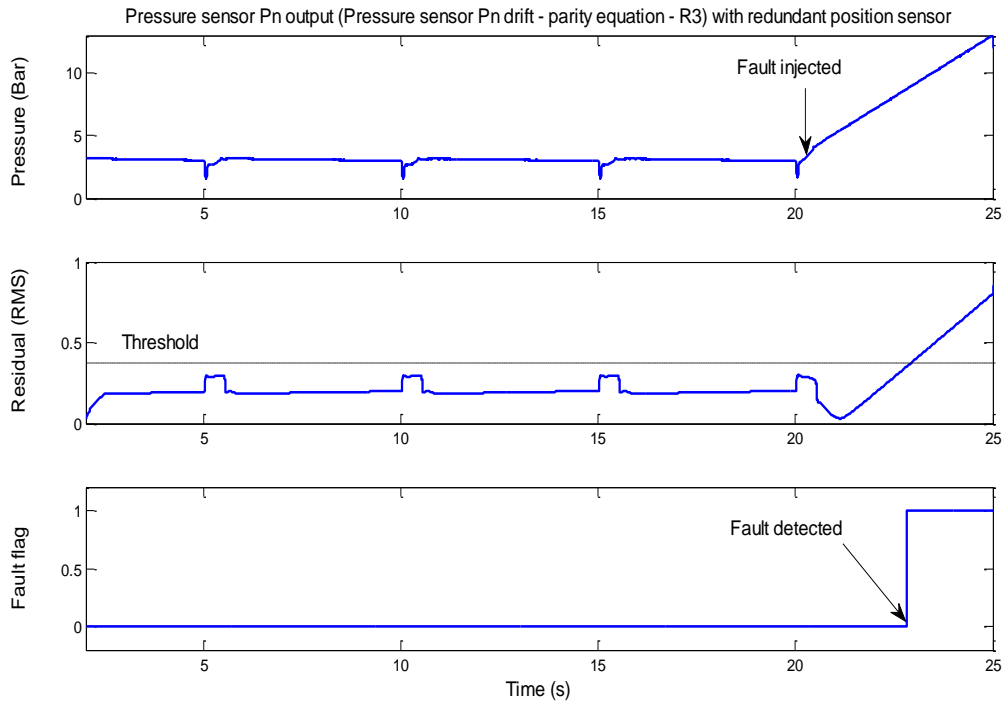
Figure 8.34: Pressure (Primary) sensor drift FPn(s), parity equation results - Pressure sensor Pn output (*R₃*)
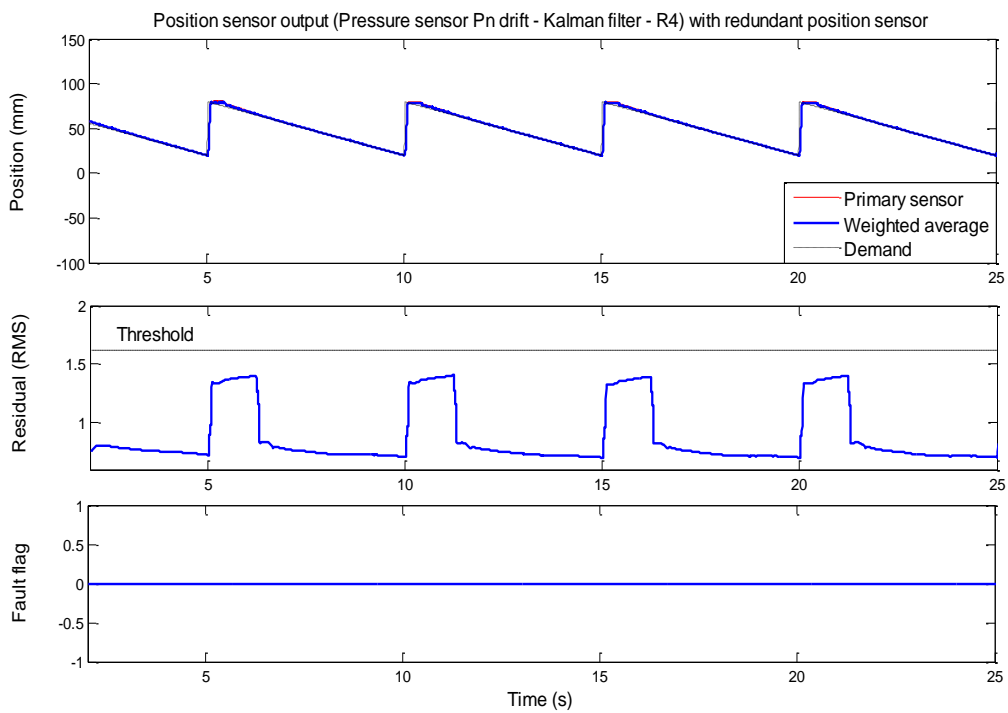
Figure 8.35: Pressure (Primary) sensor drift FPn(s), Kalman filter results - Position sensor output (*R₄*)
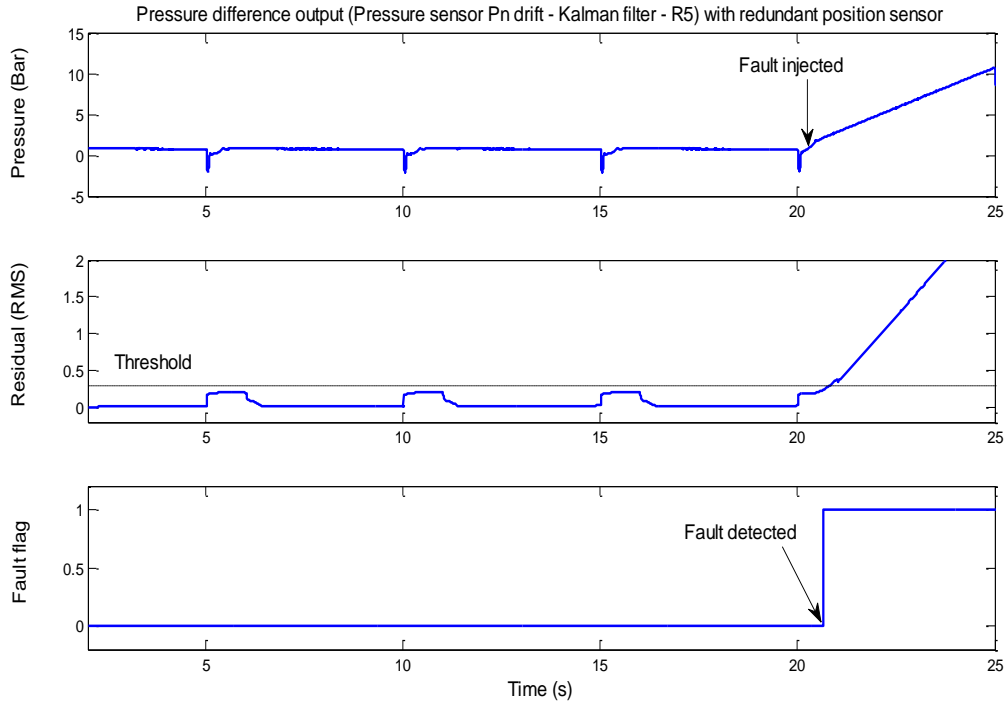
Figure 8.36: Pressure (Primary) sensor drift FPn(s), Kalman filter results – Pressure difference output (R_5)
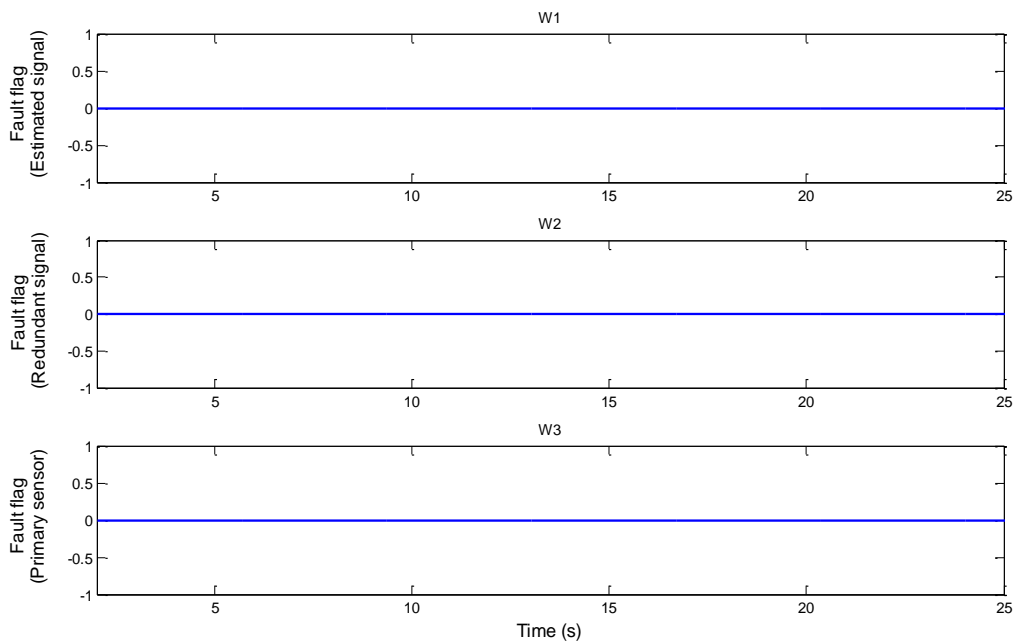
Figure 8.37: Position weighted average outputs for a pressure (Pn) sensor drift fault FPn(s)

8.2.6.2   Kalman filter – Pressure sensor drift fault

For the same drift fault applied. Using the Kalman filter scheme, Residual R_4 does not activate/cross its respective threshold (Figure 8.35) and the fault flag remains false. The RMS residual R_5 exceeds (Figure 8.36) its threshold at 20.66s and the fault is raised.

8.2.7.3   Weighted average outputs – Pressure sensor fault (sensor signal drift)

The weighted average outputs shown in Figure 8.37 indicate that w_1, w_2 and w_3 are not affected by the pressure sensor drift fault.

8.2.7.4   Discussion - Pressure sensor drift fault

Applying the drift bias to the pressure sensor Pn has no effect on the parity RMS residual R_1. The fault has no affect on the parity RMS residuals R_2. The RMS residual R_3 is affected. There is no affect on the RMS residual R_4. The pressure difference RMS residual R_5 is affected. The weighted average outputs w_1, w_2 and w_3 are not affected. The experimental results concur with the fault signatures detailed in Table 7.2. Comparing parity equations and Kalman filter schemes, the Kalman filter approach shows to have the faster response in detecting the fault.

8.3   Chapter conclusion

In this chapter the results of the experiments carried out on the single actuator test-rig were described and analysed. Various faults typical of pneumatic systems were induced. Using the designed integrated control and FDI scheme (chapter 7) fault detection was possible from the available measurements. However, certain faults were only detected and not isolated when using the residual generator methods. In particular, pneumatic faults, as these faults were clearly detected but not isolated. When these types of faults occur, pin-pointing the exact position where the fault has occurred was not possible from the available measurements. However, from the experimental results it is shown that system level knowledge has been developed and used to check plant and sensors for problems, to detect and identify certain faults as they develop, and in some cases (position sensor faults)

accommodation of the fault was possible using the redundant sensor and weighted average voting approach. The results for the experiments for the single actuator test rig are summarised in Table 8.1. The results show that the Kalman filter approach provides a faster detection time for a majority of the faults, when compared with the parity equations approach. These results concur with the theoretical fault signatures of Table 7.2. The next stage of this work is to apply the fault tolerant scheme to the Stewart-Gough platform, the results are described and analysed in chapter 9.

Table 8.1: Experimental results summary for single cylinder test rig

Type of fault	Time fault induced	Residual generation scheme	Fault flag raised	Time fault Detected/isolated	Time taken to detect fault
Position sensor loss	17.44s	Parity equation	R_1	17.46s	0.06s
		Kalman filter	R_4	17.45s	
		Weighted average	W_3	17.5s	
Control signal loss	13.3s	Parity equation	R_1 R_2 R_3	13.83s 15s 15s	1.7s
		Kalman filter	R_4 R_5	13.73s 13.9s	
Air leak	11.6s	Parity equation	R_1 R_2 R_3	15.1s 20s 12.5	8.4s
		Kalman filter	R_4 R_5	15s 15s	
Air blockage	17.2s	Parity equation	R_1 R_2 R_3	17.86s 20s 20s	2.8s
		Kalman filter	R_4 R_5	17.77s 18.02s	
Pressure sensor P_p loss	9.75s	Parity equation	R_2	10.05s	0.3s
		Kalman filter	R_5	9.87s	
Pressure sensor drift P_n	20.5s	Parity equation	R_3	22.88s	2.38s
		Kalman filter	R_5	20.66s	

Chapter 9

Experimental results – Stewart-Gough platform test-rig

9.1 Experimental results – Stewart-Gough platform

In chapter 7 a FDI scheme was designed and validated on the simulation model. In chapter 8, one part of that scheme was tested on the single cylinder test rig. This chapter will discuss application of FDI scheme applied to the Stewart-Gough platform. This will demonstrate that the designed FDI scheme which has been verified on the single (free moving) actuator will work effectively when integrated into the full Stewart-Gough platform. The designed FDI scheme will experience a number of unmeasured external loads and interactions (i.e. with other legs) which are not accounted for in the original design. In order to demonstrate the robustness of the integrated FDI scheme an assessment of robustness of the FDI scheme is conducted. The FDI scheme is only applied to one leg of the platform. However, the approach can be applied to all six pneumatic cylinder systems.

The experiments carried out are similar to the ones applied in chapter 8 for the single cylinder test-rig. The faults presented are actuator and position/pressure sensor faults (signal loss and signal drift), including air leaks and pipe blockages. The faults are applied physically by means of either disconnecting a signal or operating a switch or flow valve. The experiments are carried out using a redundant position sensor (as proposed in chapter 7). This allows reconfiguration after a sensor fault would otherwise cause serious damage to the test rig.

The demand input to the Stewart-Gough platform is a series of motions that represent the 6-degrees of movement, i.e. the longitudinal (surge), lateral (sway), and vertical (heave) motion, whereas angular motions are expressed as Eulerian angle rotations with respect to the x-axis (roll), y-axis (pitch), and z-axis (yaw). For these experiments the LQG control scheme (see chapter 5) has been employed.

9.1.1 Position sensor fault (sensor signal loss)

A fault FS(s) (see Figure 7.2) is applied to position primary sensor GS(s) at 42.69s. The fault injected is that the position signal has been disconnected. This is physically achieved

by means of a switch. Figures 9.1-9.3 show the time histories of this experiment (position sensor signal loss) for the parity equation scheme using the redundant sensor and voting scheme. Figures 9.4-9.5 show the time histories of this experiment (position sensor signal loss) for the Kalman filter scheme using the redundant sensor and voting scheme. Figure 9.6 depicts the time history of the weighted average outputs of the (position sensor) voting scheme.
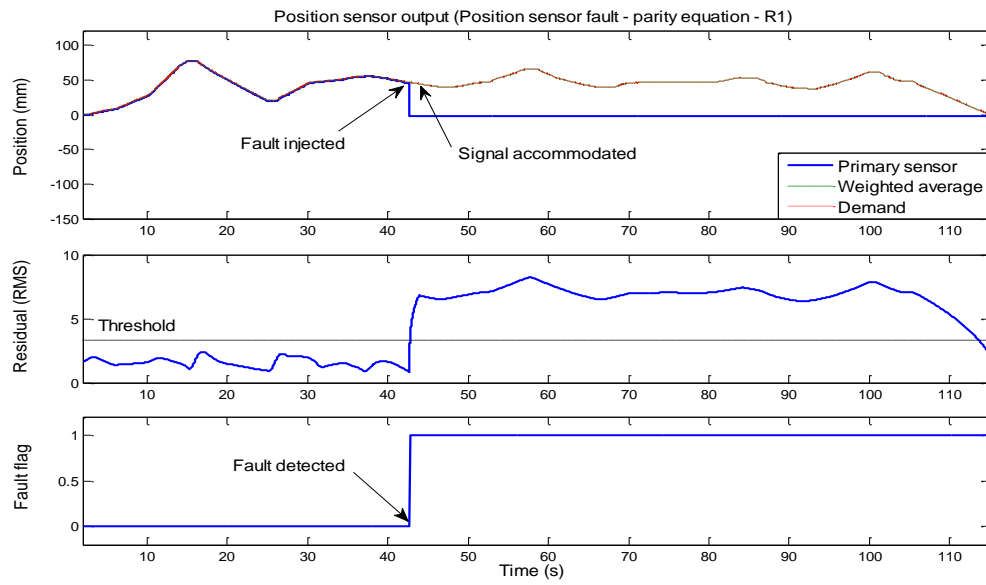
Figure 9.1: Position sensor fault (signal loss), parity equation results- position sensor output (*R₁*)
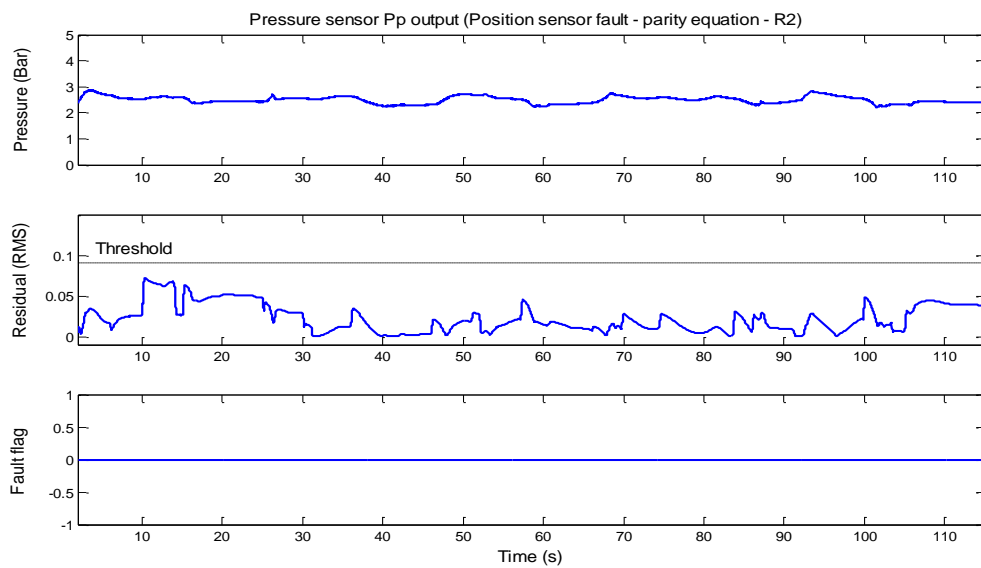
Figure 9.2: Position sensor fault (signal loss), parity equation results- Pressure sensor Pp output (*R₂*)

Figure 9.3: Position sensor fault (signal loss), parity equation results- Pressure sensor

Pn output (R_3)
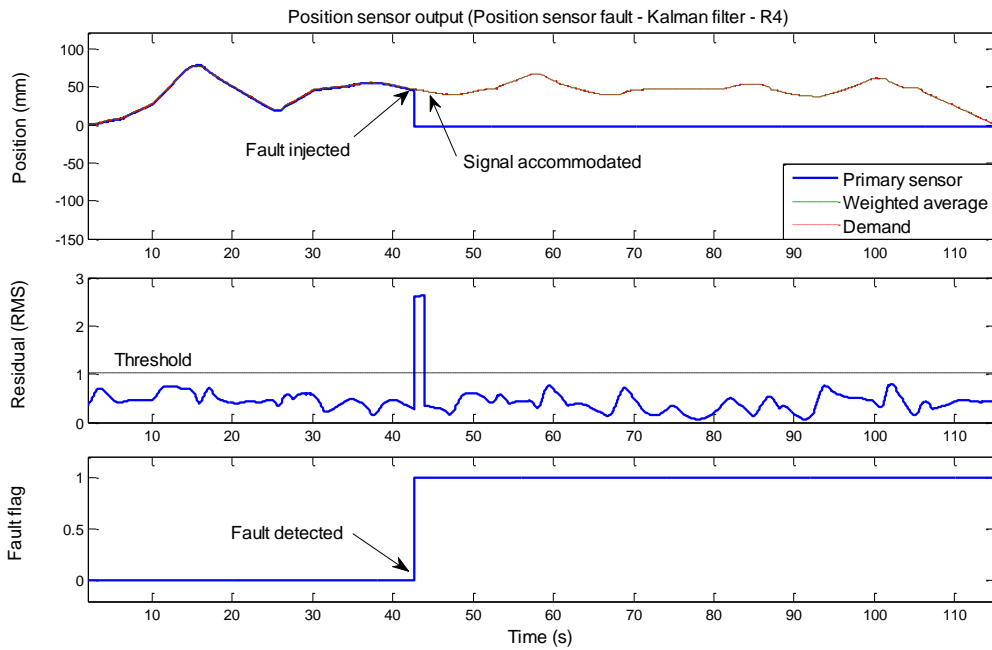
Figure 9.4: Position sensor fault (signal loss), Kalman filter results - position sensor

output (R_4)

167
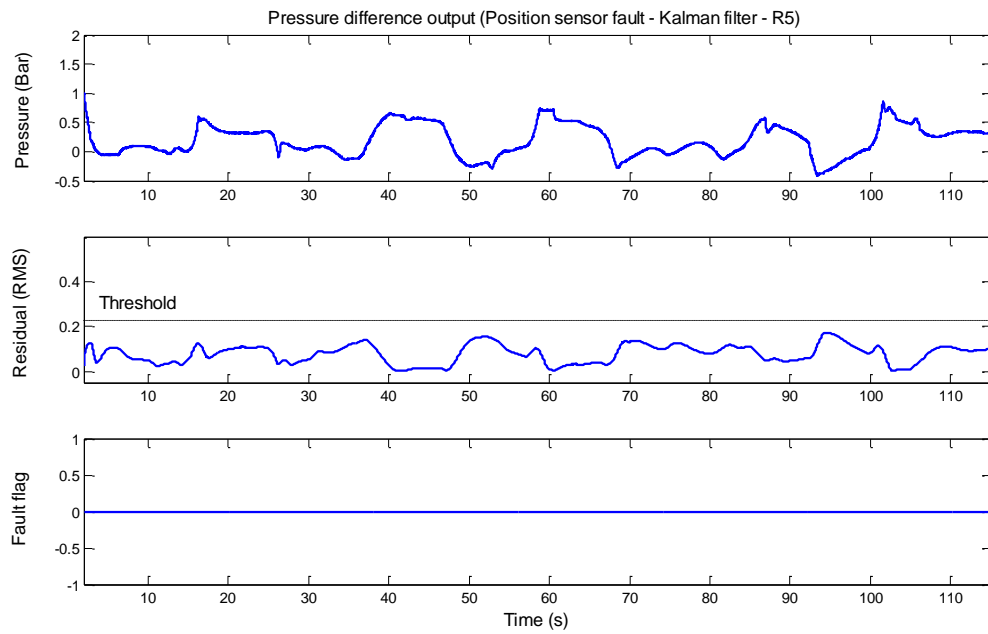
Figure 9.5: Position sensor fault (signal loss), Kalman filter results – Pressure

difference outputs (R_5)
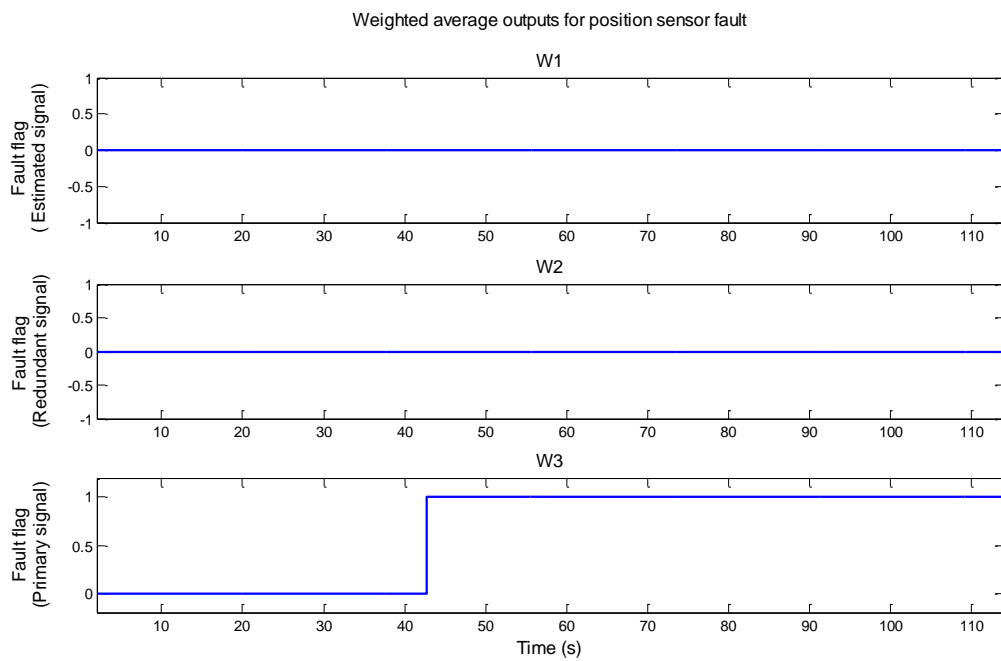
Figure 9.6: Weighted average outputs for a position (primary) sensor fault

9.1.1.1 Parity equations – Position sensor fault (sensor signal loss)

At 42.69s the fault is applied. From residual R_1 the fault is detected at 42.72s (Figure 9.1) and the fault flag is raised. The RMS residuals R_2 (Figure 9.2) and R_3 (Figure 9.3) do not activate/cross their respective thresholds.

9.1.1.2 Kalman filter - Position sensor fault (sensor signal loss)

Using the Kalman filter scheme the RMS residual R_4 exceeds its threshold at 42.7s and the fault is raised (Figure 9.4). This shows that the residual exceeds the threshold for 1.2s then falls back below the threshold. This is due to the gain of the Kalman filter (described in chapter 7) being set high. The gain is set high using Engineering judgment so that a "trade off" between signal tracking and fault detection is achieved. By increasing the Kalman gain further allows the Kalman to track the feedback position signal better, however, this makes the Kalman less sensitive to detect faults. Decreasing the Kalman gain decreases the Kalman filters ability to track the signal and increases the sensitivity of detecting faults, however, this allows increased false alarms to occur. By setting the Kalman gain to the current value allows a "trade off" between signal tracking and sensitivity of fault detection. In comparing the parity and Kalman approaches, the Kalman filter has a faster response to the fault; however, the parity approach tracks the fault better. The RMS residual R_5 (Figure 9.5) does not activate/cross its respective threshold and the fault flag remains false.

9.1.1.3 Weight average outputs – Position sensor fault (sensor signal loss)

The weighted average outputs shown in Figure 9.6 indicate that w_1 and w_2 are not affected by the primary position sensor fault. However, w_3 output shows that at 42.705s the fault flag is raised and a smooth switch from the faulty sensor to the remaining correct sensor is achieved and a smooth switch from the faulty sensor to the remaining correct sensor is achieved.

9.1.1.4   Discussion - Position sensor fault (sensor signal loss)

Applying a fault to the position sensor has an effect on the parity residual (R_1), this raises the fault flag. The fault has no affect on the pressure sensor parity residuals (R_2 and (R_3). The fault affects the position RMS residual R_4 and there is no affect on the pressure difference RMS residual R_5. The weighted average outputs w_1 and w_2 are not affected; w_3 is affected and raises the fault flag. These results concur with the fault signatures detailed in Table 7.2. Employing a redundant sensor scheme along with the triple input voting scheme shows that the fault does not affect the system performance and fault detection, isolation and accommodation is achieved. The results show that the parity equations and Kalman filter approaches detect the faults at the same time.

9.1.2   Pressure sensor Pn fault (sensor drift)

Harsh working conditions along with the gradual build up of dirt on the sensor and faulty circuitry can cause the effect of pressure sensor drift. A drift bias is added to pressure sensor Pn at 20s. Figures 9.7-9.9 shows the time histories for the parity equation scheme. Figures 9.10-9.11 shows the time histories of these experiments for the Kalman filter scheme. Figure 9.12 details the time history of the weighted average outputs of the voting scheme.

Figure 9.7: Pressure sensor drift fault, parity equation results - Position sensor output (R_1)

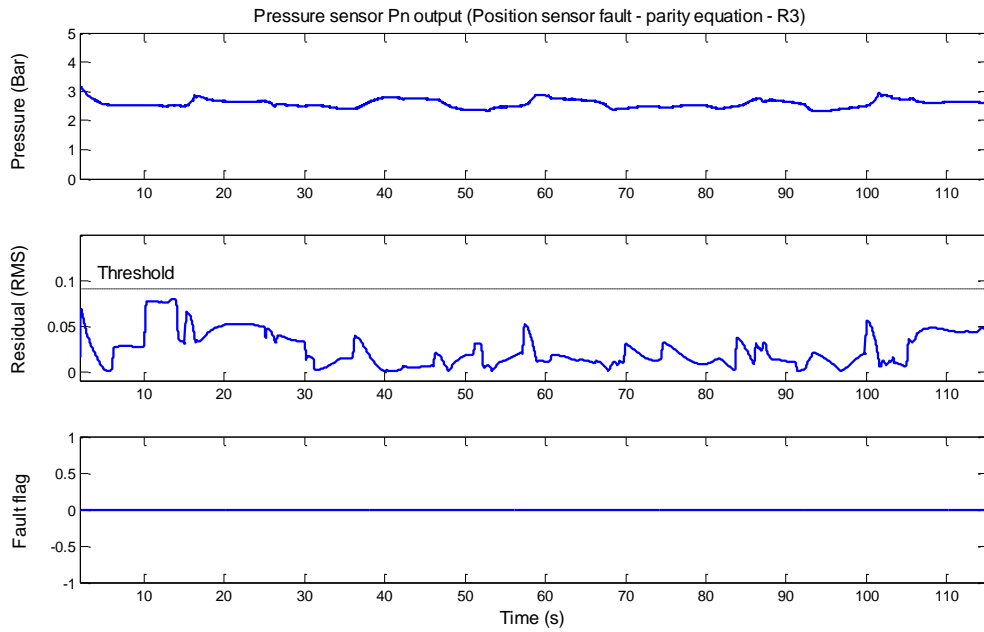Figure 9.8: Pressure sensor drift fault, parity equation results - Pressure sensor Pp

output (*R₂*)

Figure 9.9: Pressure sensor drift fault, parity equation results - Pressure sensor Pn

output (*R₃*)

Figure 9.10: Pressure sensor drift fault, Kalman filter results - Position sensor output (R_4)
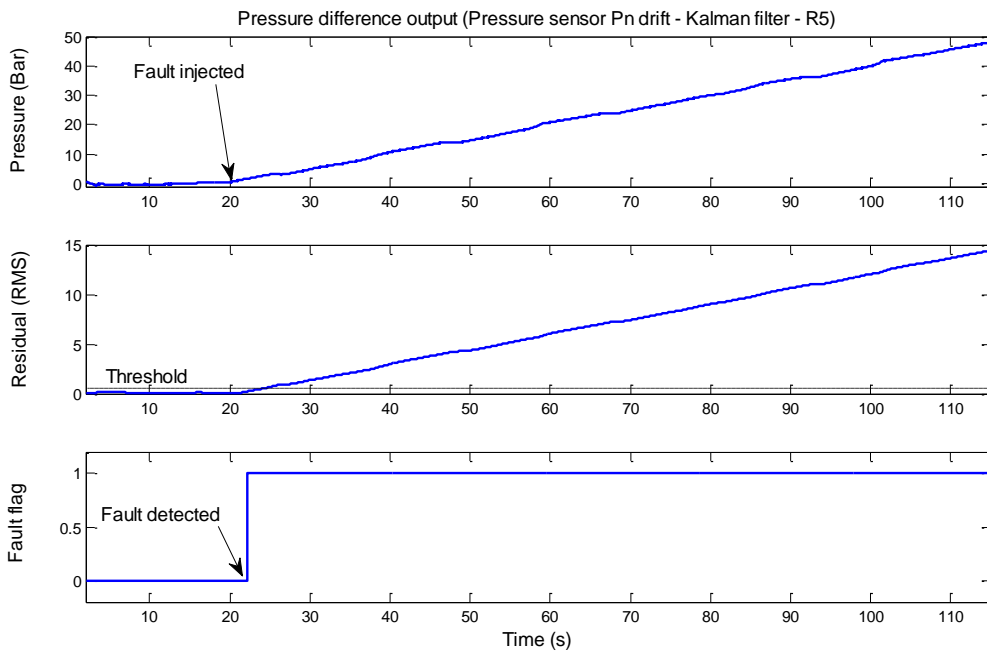
Figure 9.11: Pressure sensor drift fault, Kalman filter results - Pressure difference

output (R_5)

Weighted average for pressure sensor Pn drift
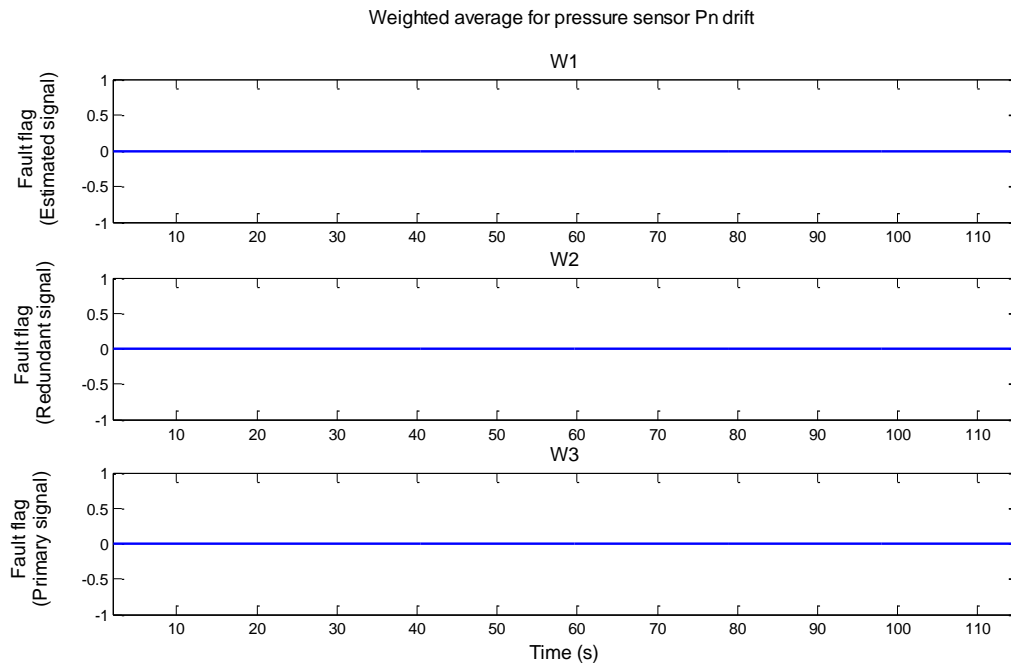
Figure 9.12: Weighted average outputs for a pressure sensor drift fault

9.1.2.1   *Parity equations – Pressure sensor drift fault*

At 20s a drift bias is added to the pressure signal. From the RMS residual R_1 (Figure 9.7) the pressure sensor drift fault has no effect. The RMS residual R_2 (Figure 9.8) is not affected by the pressure sensor fault. The RMS residual R_3 (Figure 9.9) exceeds its threshold at 22.47s, where the fault flag is raised and remains raised.

9.1.2.2   *Kalman filter - Pressure sensor drift fault*

For the same drift fault applied. Using the Kalman filter scheme, Residual R_4 does not activate/cross its respective threshold (Figure 9.10) and the fault flag remains false. The RMS residual R_5 exceeds (Figure 9.11) its threshold at 22.2s and the fault is raised.

9.1.2.3   *Weight average outputs – Pressure sensor fault (sensor signal drift)*

The weighted average outputs shown in Figure 9.12 indicate that w_1, w_2 and w_3 are not affected by the pressure sensor drift fault.

173

9.1.2.4   *Discussion - Pressure sensor drift fault*

Applying the drift bias to the pressure sensor Pn has no effect on the parity RMS residual R_1. The fault has no affect on the parity RMS residuals R_2. The RMS residual R_3 is affected. There is no affect on the RMS residual R_4. The pressure difference RMS residual R_5 is affected. The weighted average outputs w_1, w_2 and w_3 are not affected. The experimental results concur with the fault signatures detailed in Table 7.2. Comparing parity equations and Kalman filter schemes, the Kalman filter approach shows to have the faster response in detecting the fault.

9.1.3   *Actuator fault*

A fault Fa(s) (see Figure 7.2) is applied to the proportional valve at 20s. The fault injected is that the control signal has been disconnected. This is physically achieved by means of a switch. Figures 9.13-9.15 shows the time histories of this experiment (actuator fault) for the parity equation scheme. Figures 9.16-9.17 shows the time histories of this experiment (actuator fault) for the Kalman filter scheme. The time history of the weighted average outputs of the voting scheme is shown in Figure 9.18.
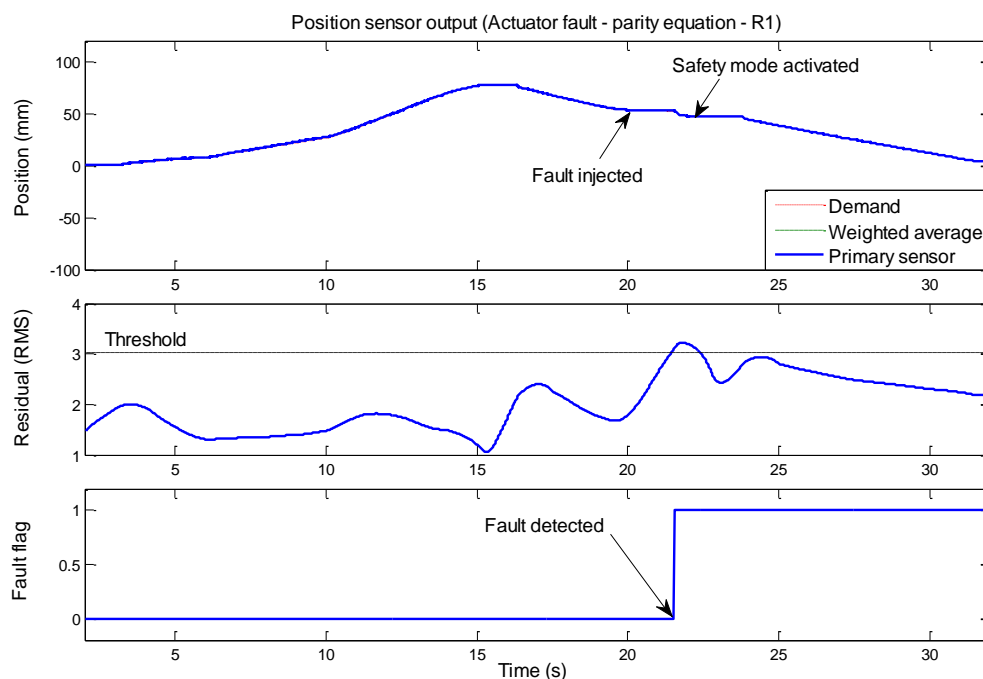
Figure 9.13: Actuator fault Fa(s) parity equation results- Position sensor output (R_1)
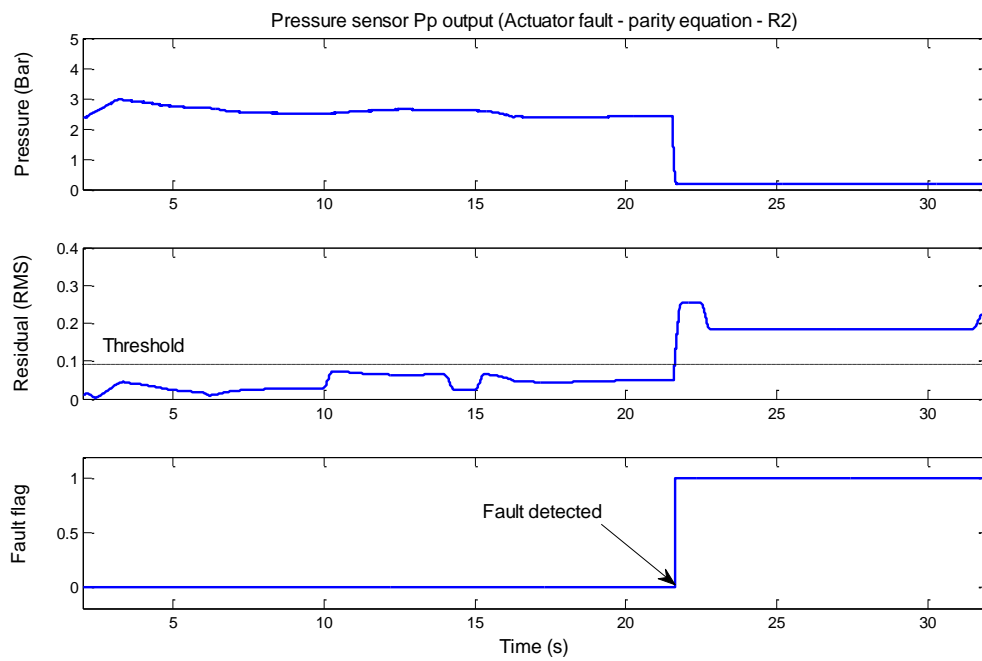
Figure 9.14: Actuator fault Fa(s) parity equation results- Pressure sensor Pp (R_2)
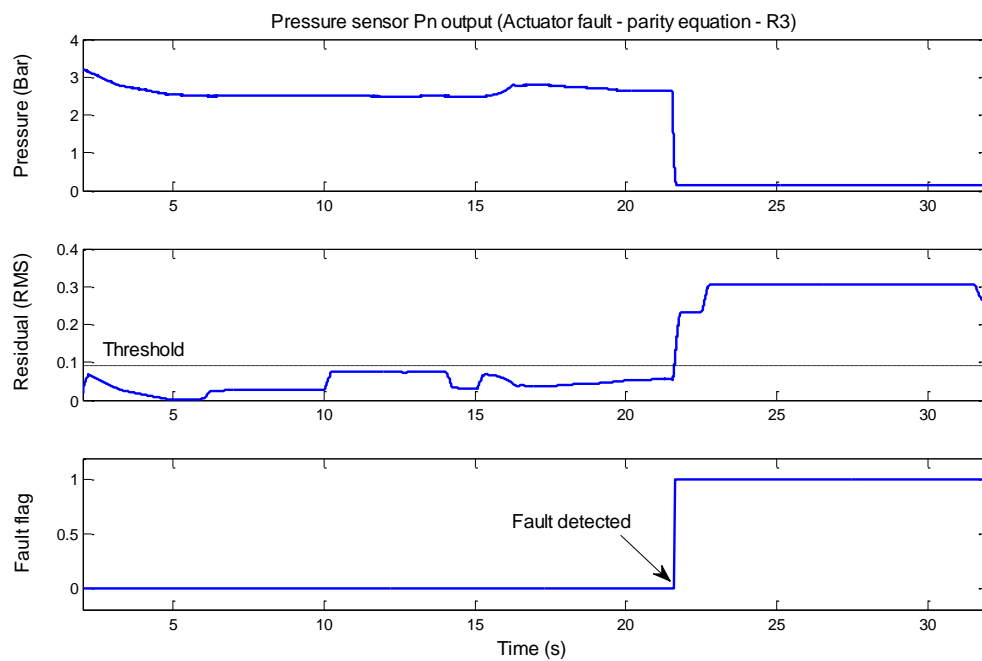
Figure 9.15: Actuator fault Fa(s) parity equation results- Pressure sensor Pn (R_3)
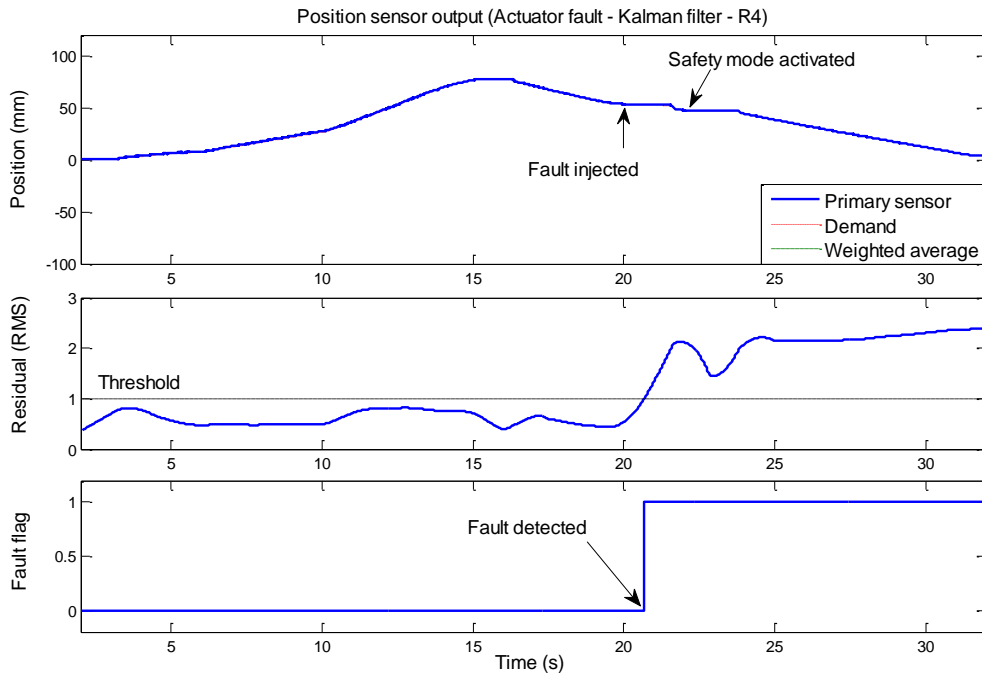
Figure 9.16: Actuator fault Fa(s), Kalman filter results - position sensor output (R_4)

Figure 9.17: Actuator fault Fa(s), Kalman filter results - Pressure difference output (R_5)
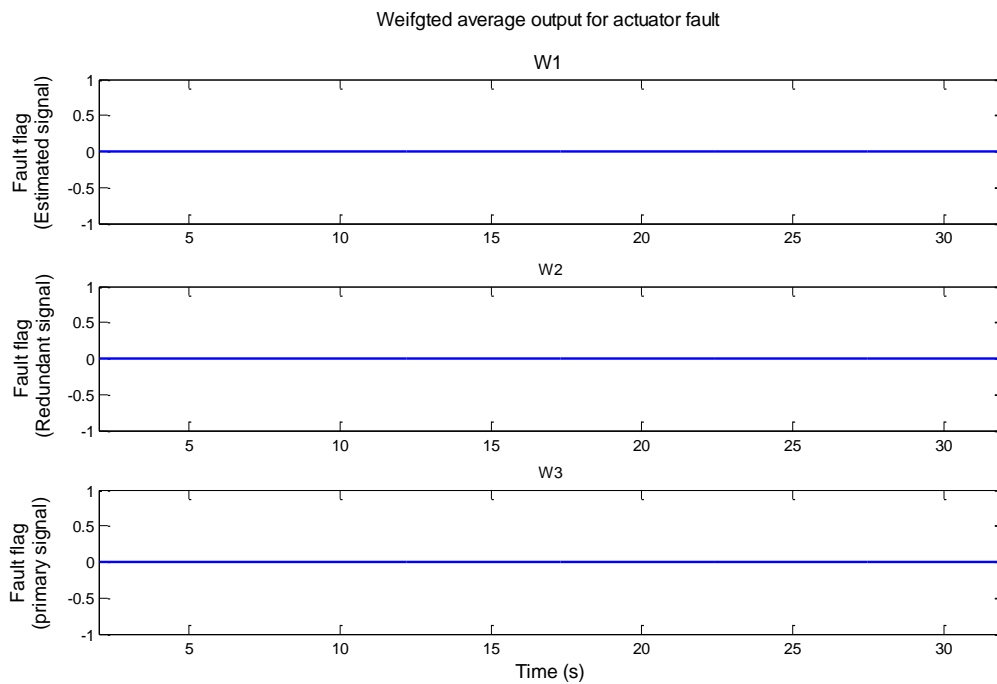
Figure 9.18: Weighted average outputs for an actuator fault

9.1.3.1   *Parity equations - Actuator fault (control signal loss)*

Figure 9.13 shows at 20s the fault is applied. From RMS residual R_1 the fault is detected at 21.55s and the fault flag is raised. RMS residual R_2 (Figure 9.14) exceeds its respective threshold at 21.61s and the fault flag is raised. RMS residual R_3 (Figure 9.15) exceeds its respective threshold at 21.62s and fault flag is raised. Once triggered all the fault flags remain raised.

9.1.3.2   *Kalman filter - Actuator fault (control signal loss)*

For the Kalman filter approach. From RMS residual R_4 (Figure 9.16) the fault is detected at 20.65s and the fault flag is raised and remains raised. The pressure difference RMS residual R_5 (Figure 9.17) exceeds its respective threshold at 20.96s and the fault flag is raised.

177

9.1.3.3   Weight average outputs – Actuator fault (control signal loss)

The weighted average outputs shown in Figure 9.18 indicate that residuals w_1, w_2 and w_3 are not affected and the respective fault flags remain low.

9.1.3.4   Discussion - Actuator fault (control signal loss)

Applying the disconnection fault to the control signal of the proportional valve has an effect on the parity residual (R_1), this raises the fault flag. The fault has an effect on the pressure sensor parity residuals (R_2 and R_3). Both position and pressure difference Kalman residuals (R_4 and R_5) are affected by the actuator fault and their fault flags are raised. Residuals w_1, w_2 and w_3 are not affected and the respective fault flags remain low. This agrees with the fault signatures detailed in Table 7.2. With this particular fault accommodation is not available as the control signal to the servo valve of pneumatic cylinder 2 is lost. This means that the desired positional movement of the rig is inadequate. From here (21.62s) the safety sequence is activated and the platform is made safe (i.e. brought back to its rest position).

From both methods (Kalman and parity) the Kalman approach tracks the fault better with a faster fault detection response time. Overall, it is clear that the parity equations and the Kalman filter approach can detect an actuator fault. However, neither method can isolate the fault in terms of discriminating between actuator and plant (cylinder) fault.

9.1.4   Air leak (between servo valve and pneumatic cylinder)

Air leaks may occur during normal operating conditions and can appear from any part of the pneumatic system. In this case the leak is injected between the servo valve and pneumatic cylinder at 18.6s. Figures 9.19-9.20 shows the time histories of this experiment (leak fault) for the parity equation scheme. Figures 9.21-9.22 shows the time histories of this experiment (leak fault) for the Kalman filter scheme. Figure 9.23 details the time history of the weighted average outputs of the voting scheme.
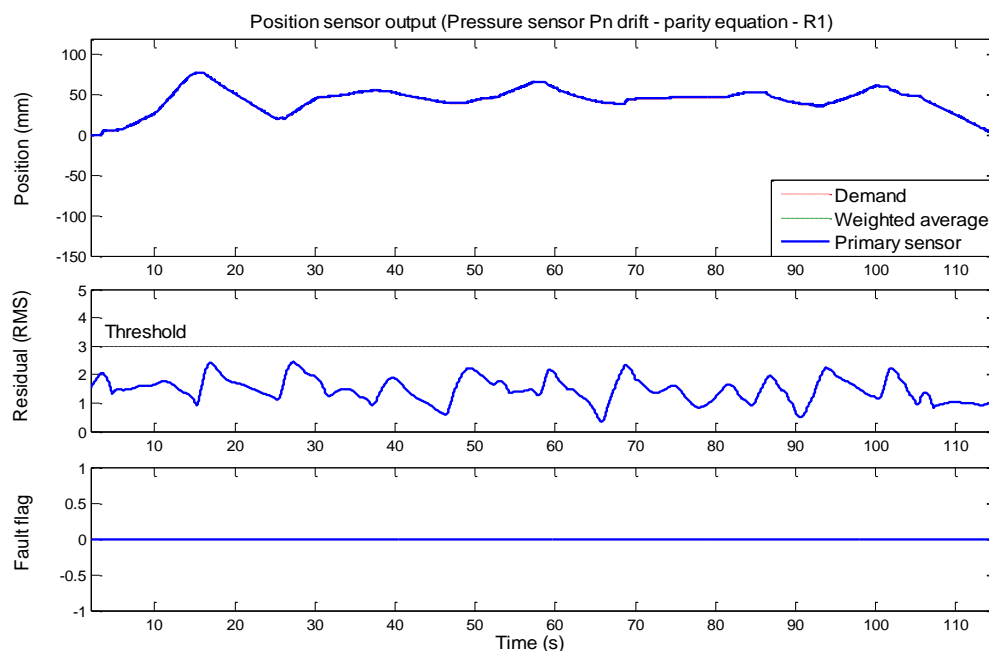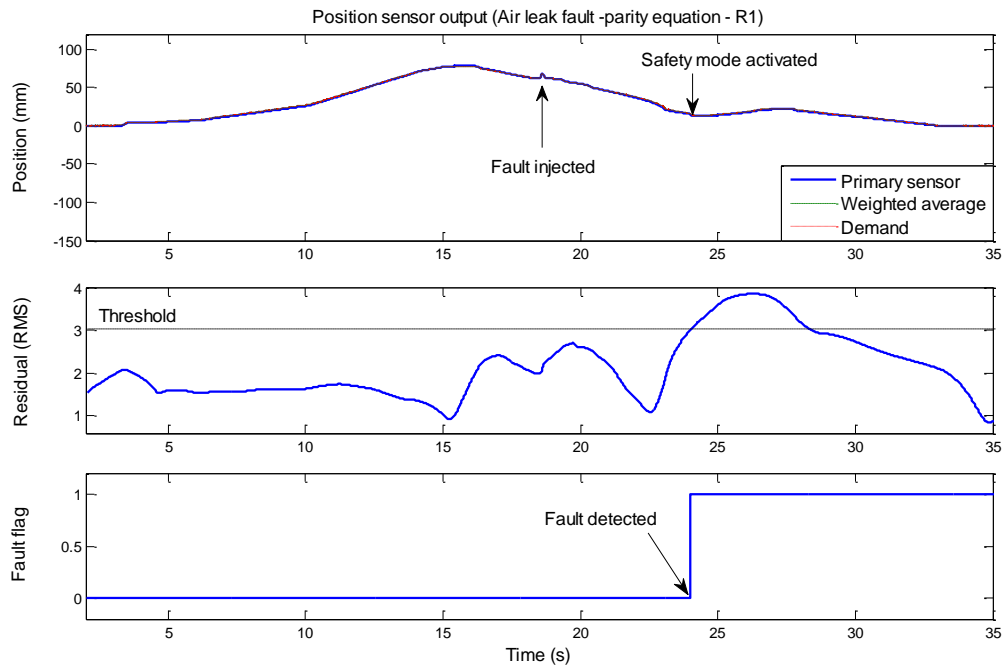
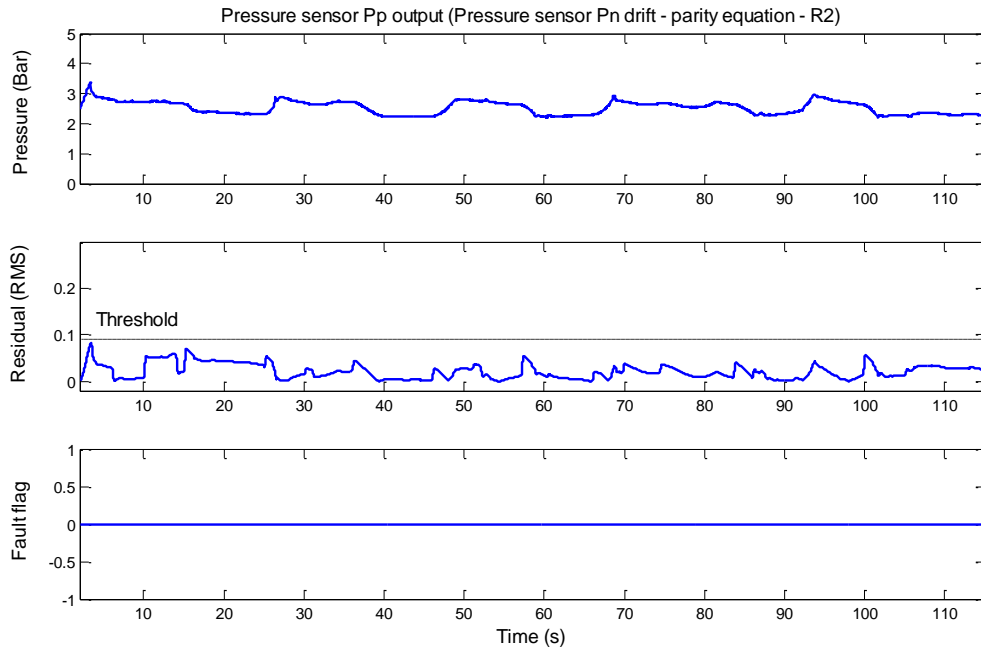Figure 9.19: Air leak, parity equation results - Position sensor output (R_1)
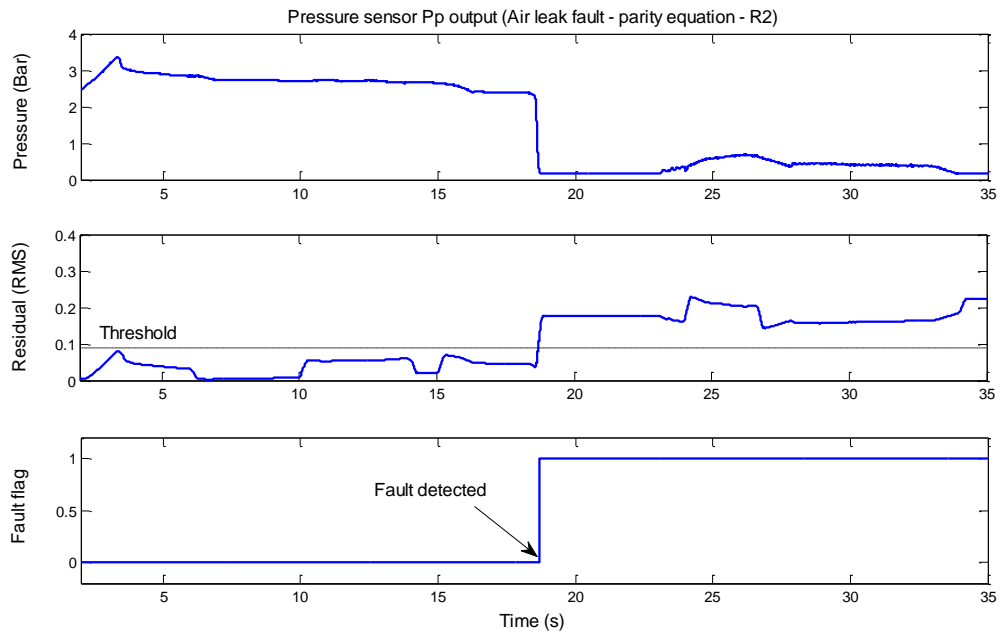
Figure 9.20: Air leak, parity equation results - Pressure sensor Pp output (R_2)

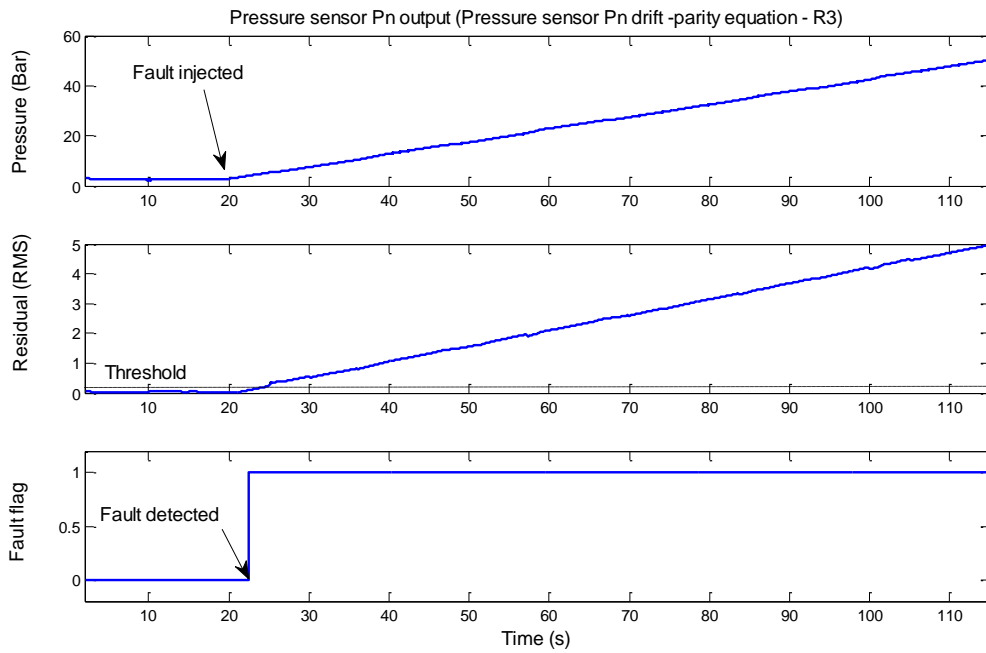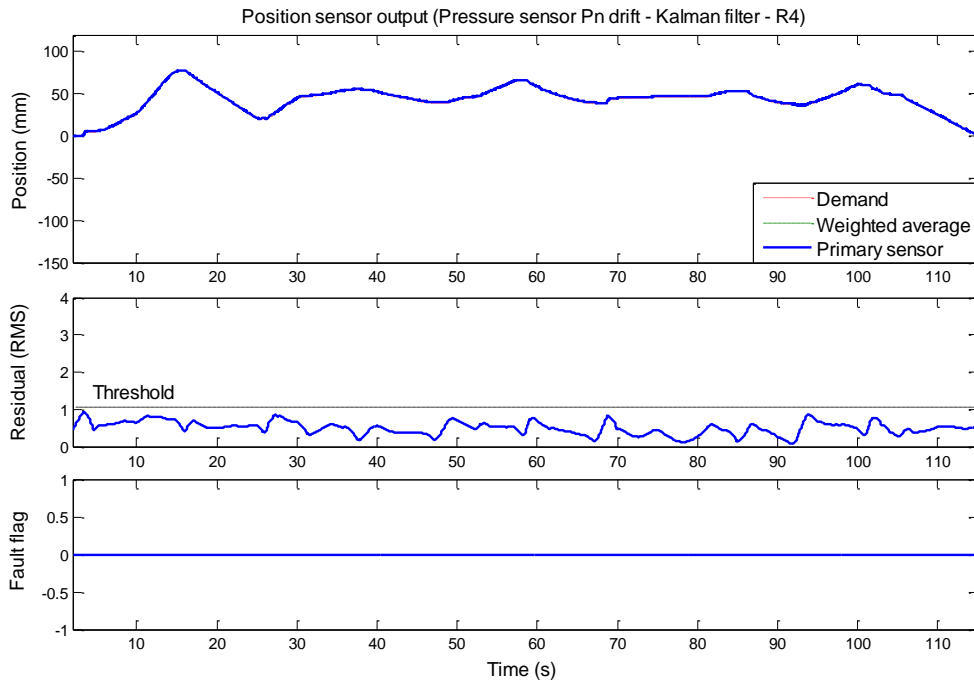Figure 9.21: Air leak, parity equation results - Pressure sensor Pn (R_3)

Figure 9.22: Air leak, Kalman filter results - Position sensor output (R_4)
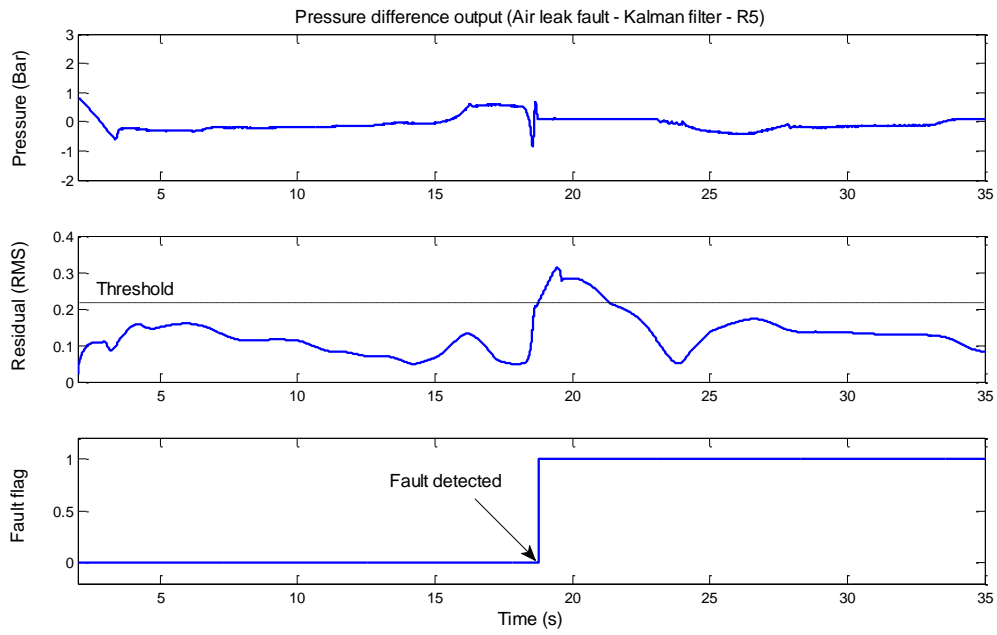
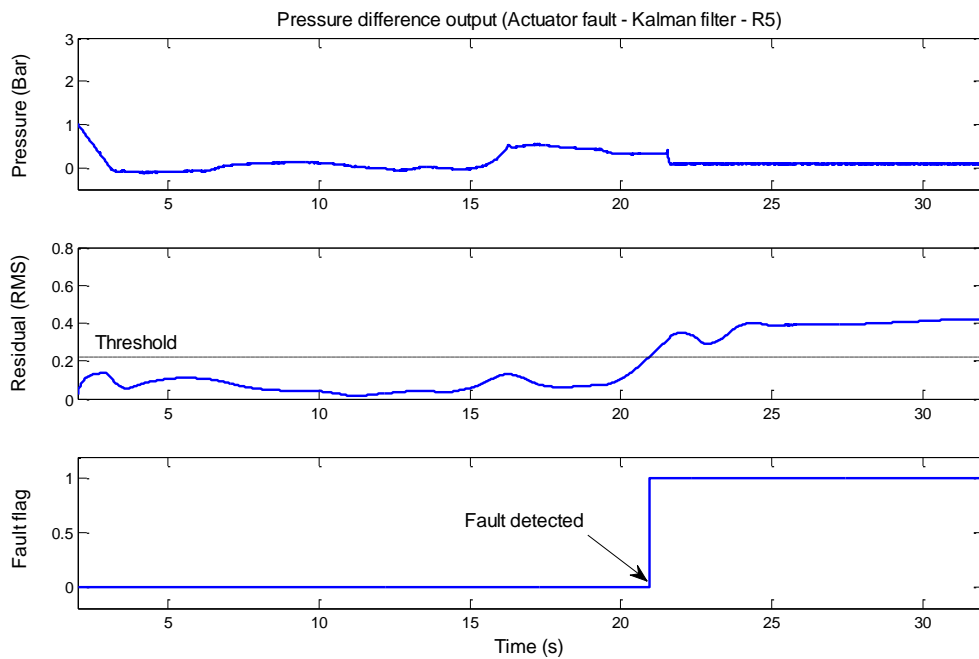Figure 9.23: Air leak, Kalman filter results - Pressure difference output (R_5)

Figure 9.24: Weighted average outputs for a leak fault

9.1.4.1   Parity equations – Air leak

An air leak fault is applied by means of operating a pressure relief valve, which is located between the proportional valve and the cylinder. The fault is applied at 18.6s. From the RMS residual R_1 (Figure 9.19) the fault is detected at 23.98s where the fault flag is raised and remains raised. The RMS residual R_2 (Figure 9.20) exceeds its respective threshold at 18.67s, where, the fault flag is raised. The RMS residual R_3 (Figure 9.21) exceeds its threshold at 18.5s and the fault flag is raised.

9.1.4.2   Kalman filter - Air leak

From the Kalman filter scheme, the RMS residual R_4 (Figure 9.22) exceeds its threshold at 18.92s and the fault flag is raised. The RMS residual R_5 (Figure 9.23) crosses its respective threshold at 18.78s and the fault flag is raised.

9.1.4.3.   Weight average outputs – Air leak

The weighted average outputs shown in Figure 9.24 indicate that residuals w_1, w_2 and w_3 are not affected by the pressure leak fault and the respective fault flags remain low.

9.1.4.4   Discussion - Air leak

Applying the leak fault to the pneumatic cylinder has an effect on the parity residual R_1, this raises the fault flag. The fault also has an affect on the pressure sensor parity residuals (R_2 and R_3). The fault affects the position residual R_4 and the pressure difference residual R_5. Residuals w_1, w_2 and w_3 are not affected and the respective fault flags remain low. This agrees with the fault signatures detailed in Table 7.2. With this type of fault, accommodation is not available as pressure is lost between the servo valve and pneumatic cylinder. This means that the desired positional movement of the rig is not achievable.

However, from the point where the fault is induced (18.6s) and the final residual (R_1) is raised (23.98s) a certain amount of fault tolerance is available (Figure 9.19). Once the final

residual fault flag is raised the safety sequence is activated and the platform is made safe (i.e. brought back to its rest position). Comparing RMS residuals R_1 and R_4 (position outputs), the Kalman filter approach when compared with the parity equation scheme has a faster fault detection response time.

9.1.5   *Pressure sensor fault (chamber Pp)*

A fault FPp(s) (see Figure 7.2) is applied to pressure sensor (Pp). The fault injected is at the pressure signal from Chamber Pp has been disconnected at 32.95s. This is physically achieved by means of a switch. Figures 9.25-9.27 shows the time histories of this experiment (pressure sensor fault) for the parity equation scheme. Figures 9.28-9.29 shows the time histories of this experiment (pressure sensor fault) for the Kalman filter scheme. The time history of the weighted average outputs of the voting scheme is shown in Figure 9.30.
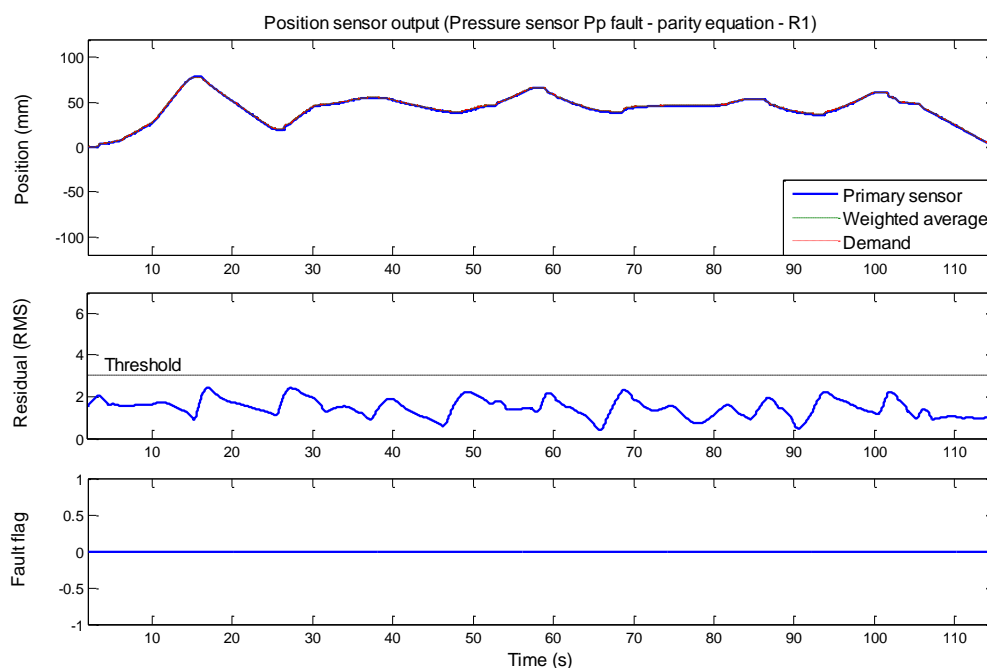
Figure 9.25: Pressure sensor Pp fault FPp(s), parity equation result - Position sensor output (R_1)
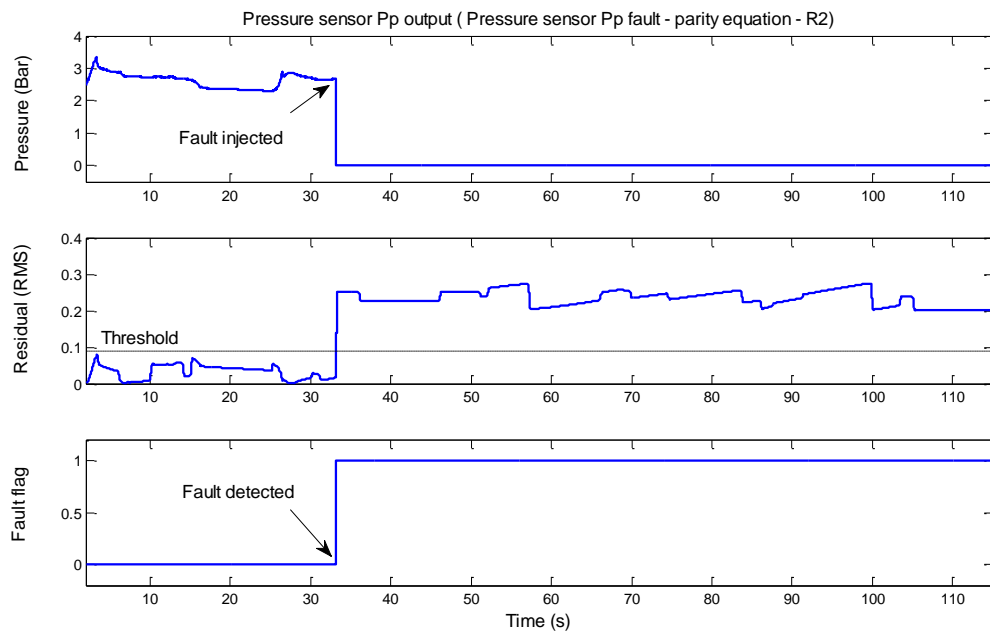
Figure 9.26: Pressure sensor Pp fault FPp(s), parity equation result - Pressure sensor Pp output (*R_2*)
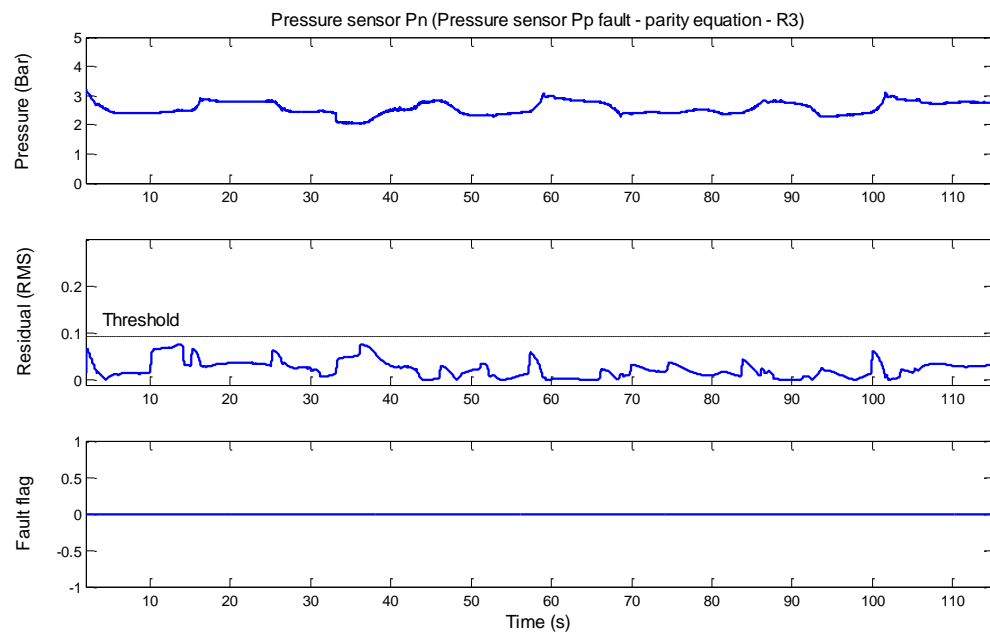
Figure 9.27: Pressure sensor Pp fault FPp(s), parity equation results - Pressure sensor Pn output (*R_3*)
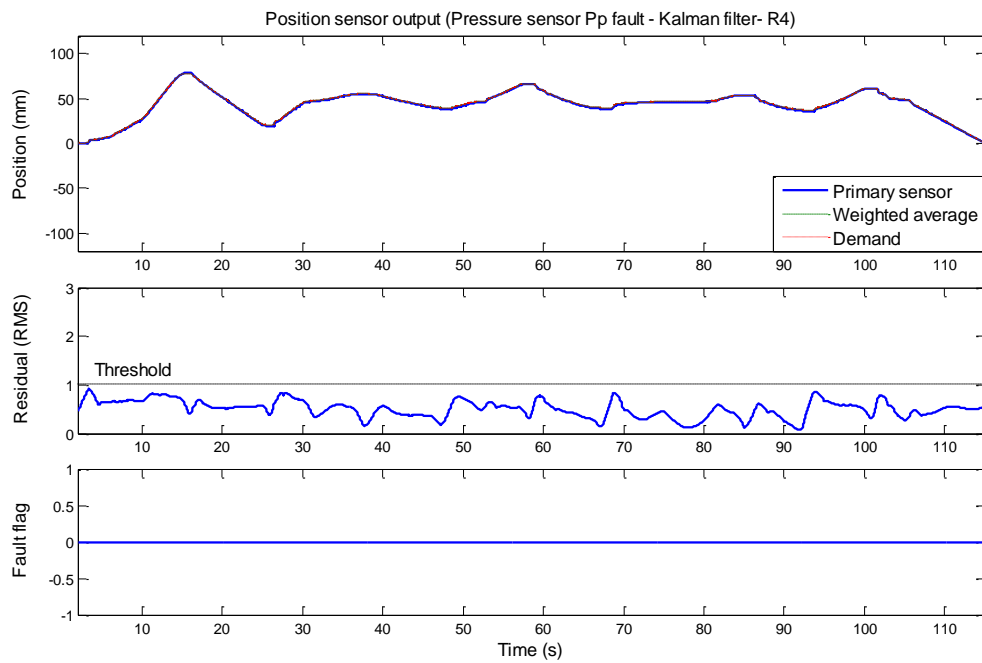
Figure 9.28: Pressure sensor Pp fault FPp(s), Kalman filter result - Position sensor output (R_4)
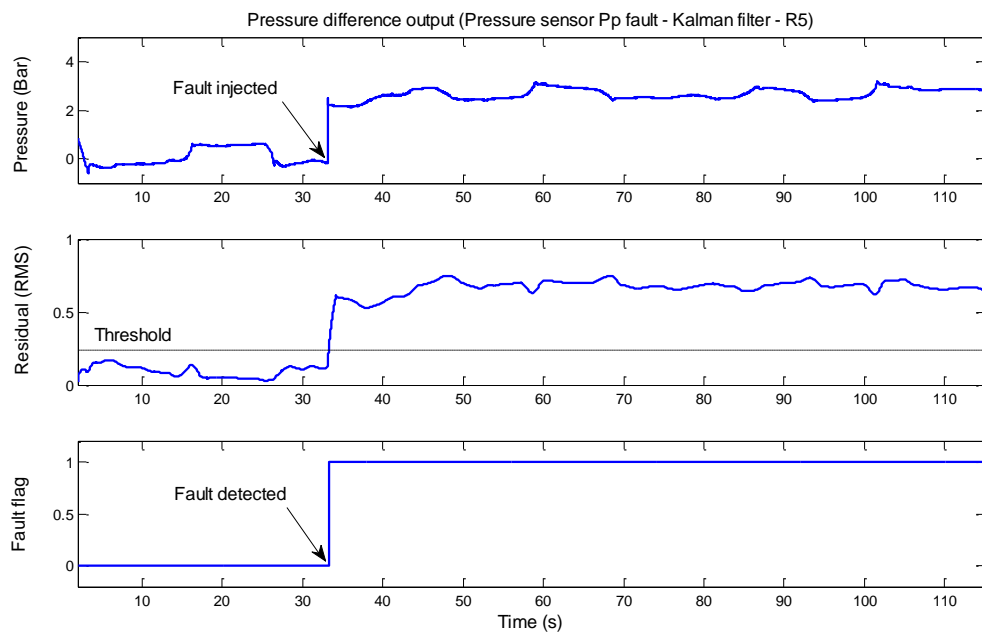
Figure 9.29: Pressure sensor Pp fault FPp(s), Kalman filter result- Pressure difference output (R_5)

Weighted average outputs for a pressure sensor Pp fault
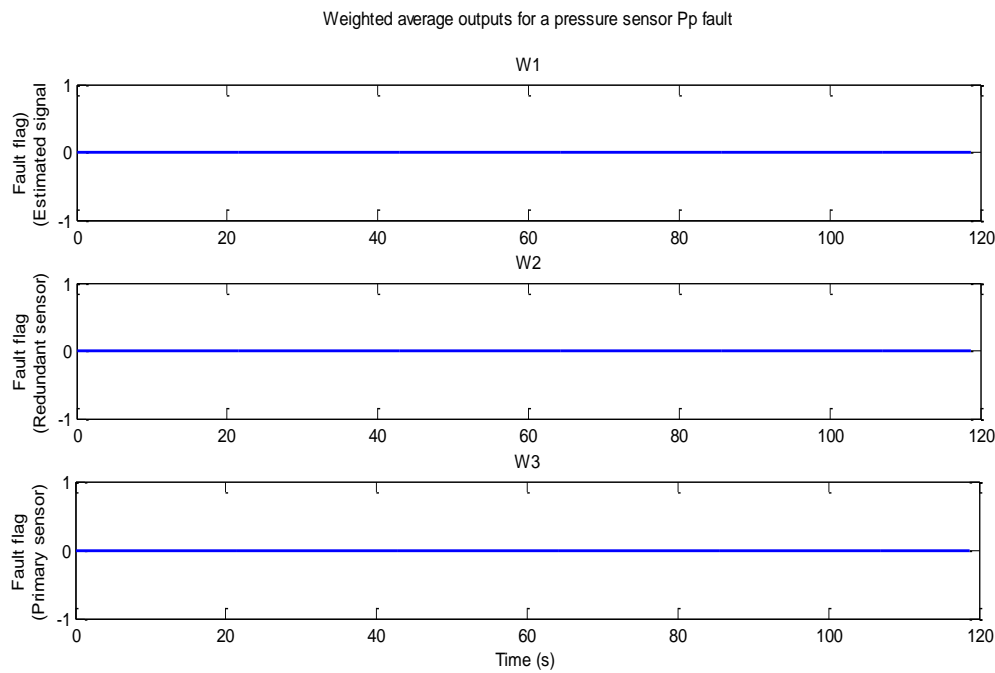
Figure 9.30: Weighted average outputs for a pressure sensor Pp fault FPp(s)

9.1.5.1 Parity equations – Pressure sensor fault (chamber Pp)

A fault is applied to the pressure sensor of chamber Pp at 32.95s. Using the parity equation scheme the RMS residual R_1 (Figure 9.25) is unaffected by this fault. However, the RMS residual R_2 (Figure 9.26) exceeds its threshold at 33.2s and the fault flag is raised. The RMS residual R_3 plot (Figure 9.27) shows that this residual is unaffected by this fault.

9.1.5.2 Kalman filter - Pressure sensor fault (chamber Pp)

The outputs from the Kalman filter scheme (Figure 9.28) show that the residual R_4 is not affected by a fault applied to the pressure sensor for chamber Pp and the R_4 fault flag remains false. For the same fault the RMS residual R_5 (Figure 9.29) exceeds its threshold at 33.2s and the fault flag is raised.

9.1.5.3 Weight average outputs – Pressure sensor fault (chamber Pp)

The weighted average outputs shown in Figure 9.30 indicate that residuals w_1, w_2 and w_3 are not affected by the pressure sensor fault and the respective fault flags remain low.

9.1.5.4 *Discussion – Pressure sensor fault (chamber Pp)*

Applying a fault to the pressure sensor (Pp) has no affect on the parity residual (R_1). The fault affects the pressure sensor residual (R_2). However, this fault does not have an effect on the residual R_3. The fault again showing to have no affect on the position RMS residual R_4. The RMS residual R_5 is affected by this fault. Residuals w_1, w_2 and w_3 are not affected and the respective fault flags remain low. These results concur with the fault signatures detailed in Table 7.2. Comparing the parity equations and Kalman filter approaches show that both approaches detect the fault at the same time.

9.1.6 *Air pipe blockage*

A blockage fault is applied to the pressure system at 35s. This is physically achieved by means of a cut-off valve located between the proportional valve and the pneumatic cylinder. Figures 9.31-9.33 shows the time histories of this experiment (blockage fault) for the parity equation scheme. Figures 9.34-9.35 show the time histories of this experiment (blockage fault) for the Kalman filter scheme. The time history of the weighted average outputs of the voting scheme is shown in Figure 9.36.
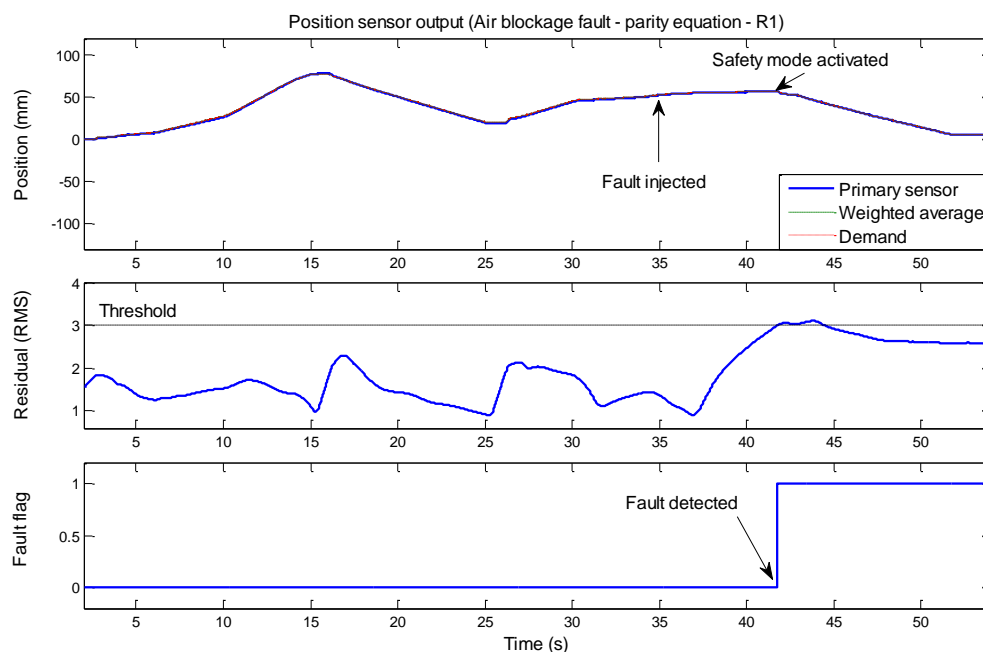
Figure 9.31: Air blockage fault, parity equation result- Position output sensor (R_1)
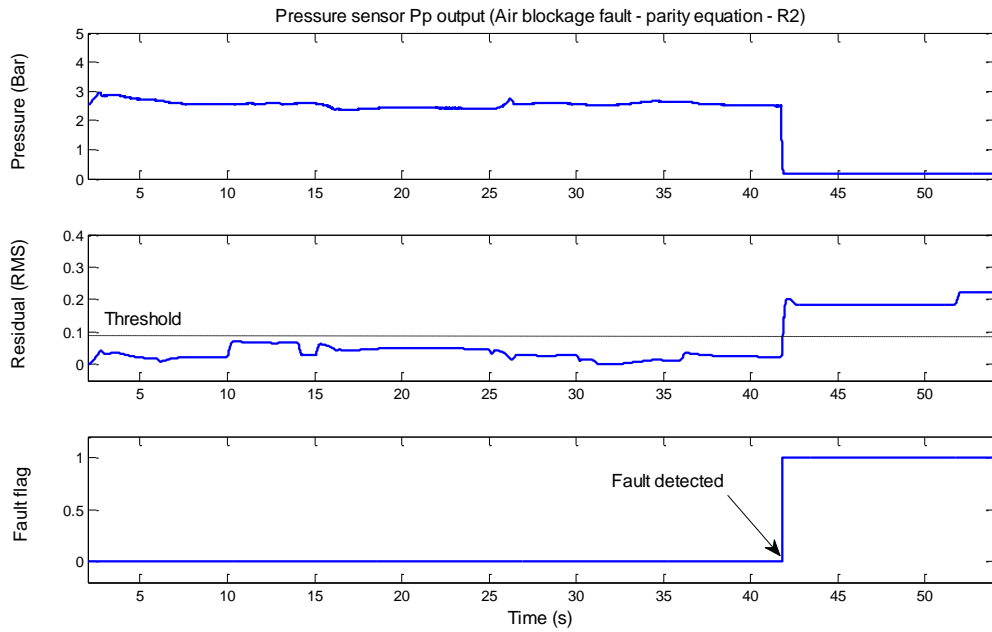
Figure 9.32: Air blockage fault, parity equation results- Pressure sensor Pp (*R₂*)
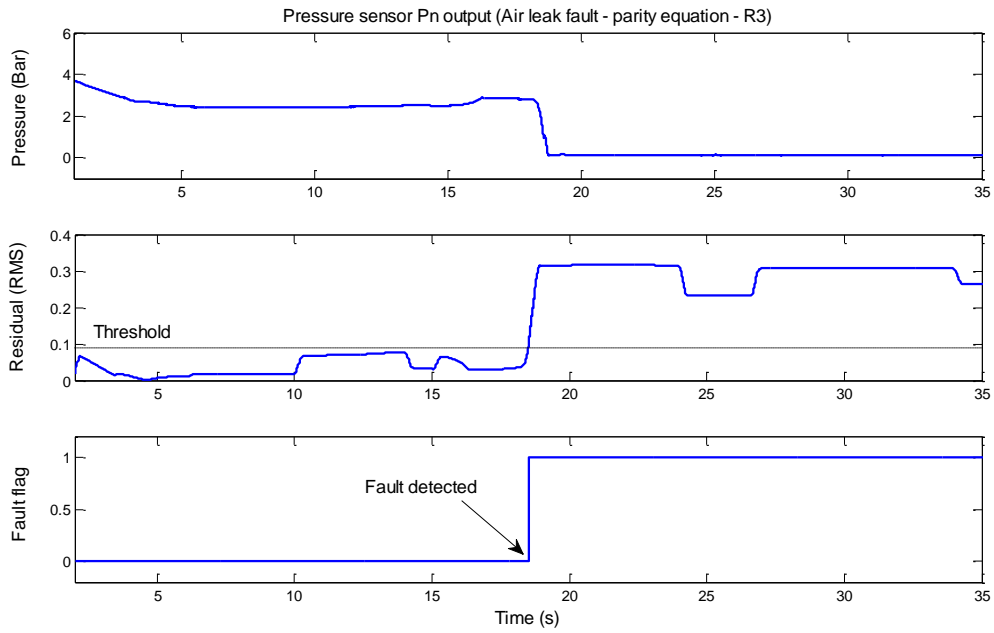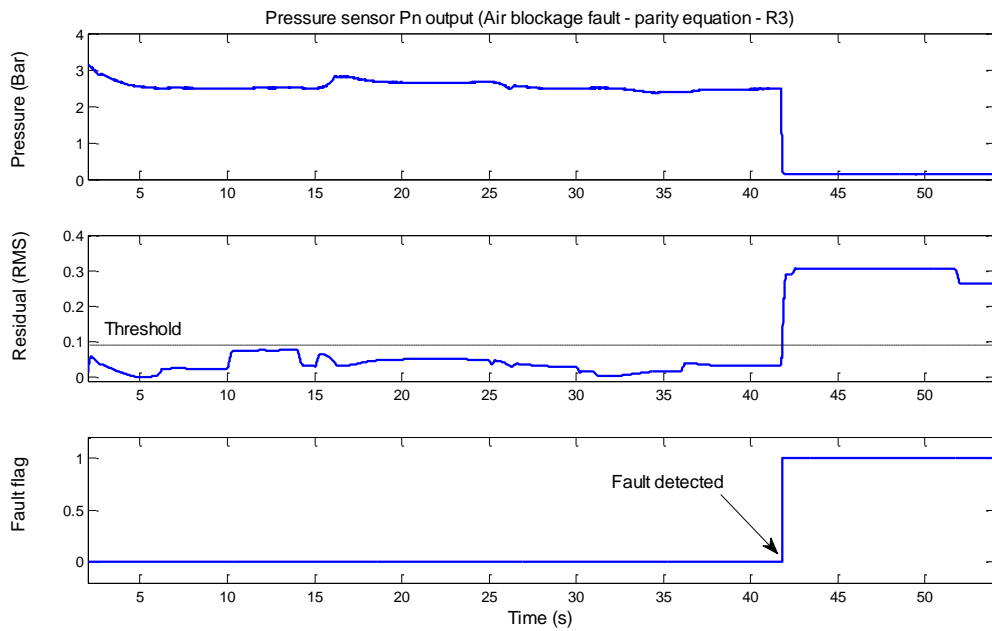

Figure 9.33: Air blockage fault, parity equation results- Pressure sensor Pn (*R₃*)
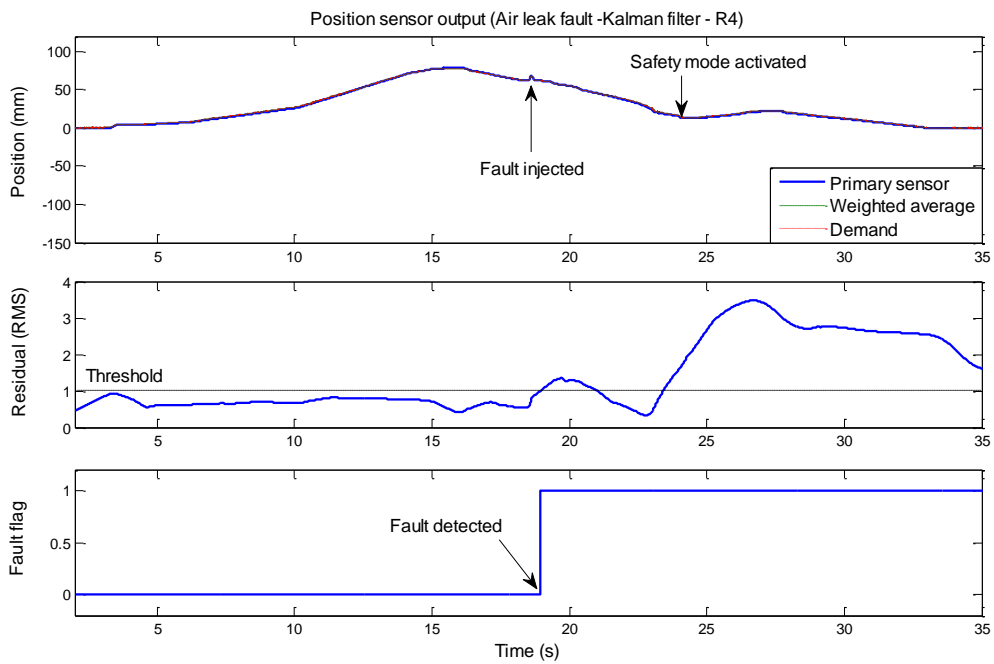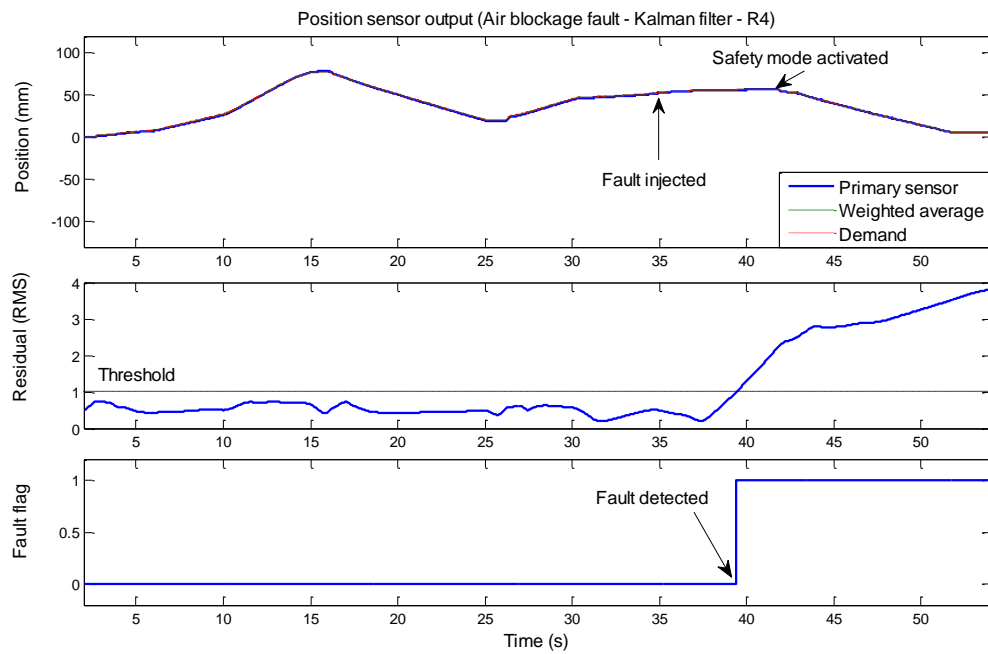
Figure 9.34 Air blockage fault, Kalman filter results - Position sensor output (R_4)
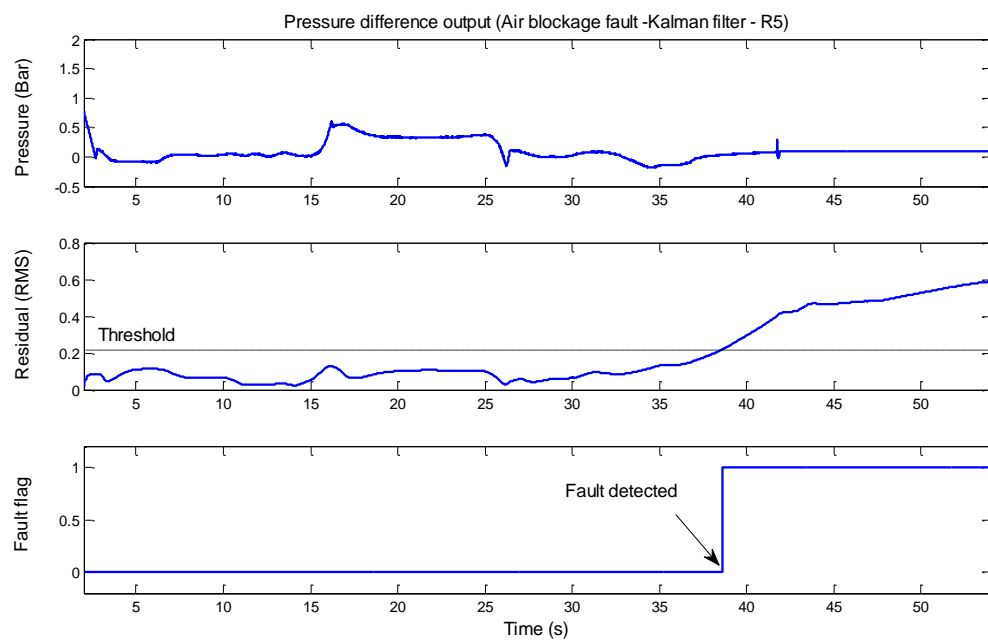
Figure 9.35: Air blockage fault, Kalman filter result - Pressure difference
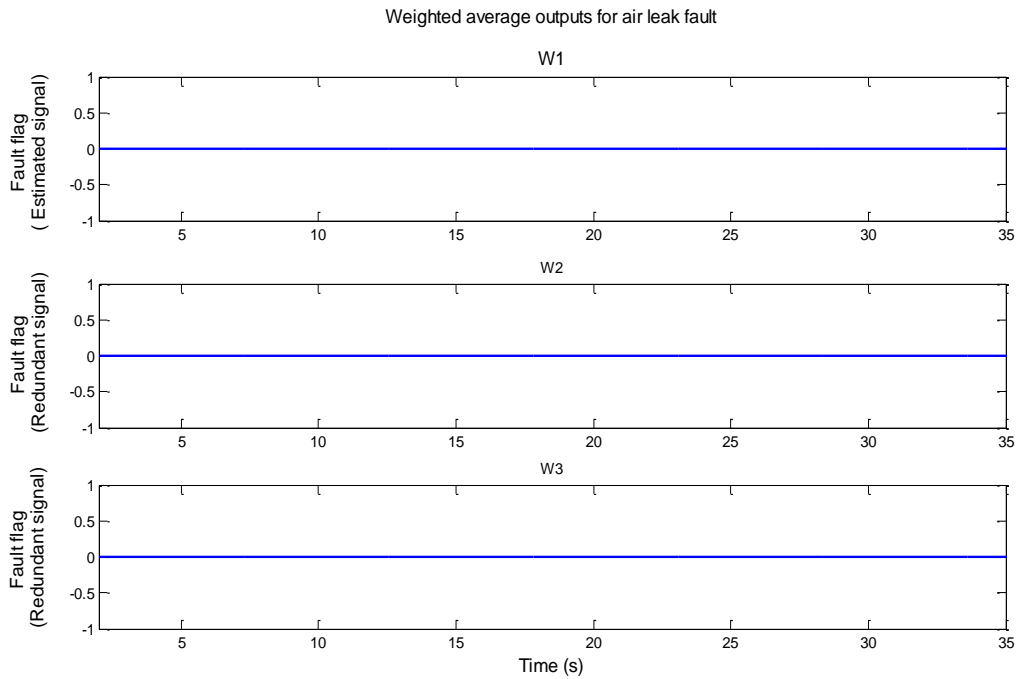
outputs (R_5)

Weighted average outputs for air blockage fault
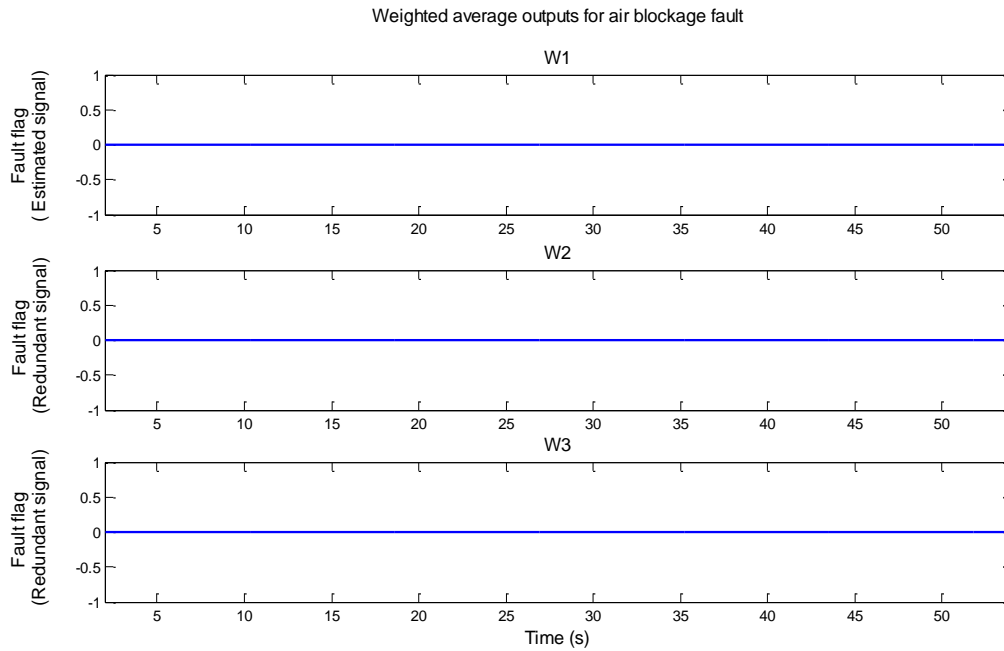
Figure 9.36: Weighted average outputs for an air blockage fault

9.1.6.1   Parity equations – Air pipe blockage

A blockage is applied to the pneumatic system. Using the parity equation scheme the RMS residual R_1 (Figure 9.31) exceeds its threshold at 41.84s and the fault flag is raised. RMS residual R_2 (Figure 9.32) and RMS residual R_3 (Figure 9.33), both exceed their respective thresholds at 41.8s, and raise their respective fault flags.

9.1.6.2   Kalman filter - Air pipe blockage

The outputs from the Kalman filter scheme show that the RMS residual R_4 is affected by a blockage applied to the system. The fault flag, shown in Figure 9.34 is raised at 39.39s. For the same fault, the RMS residual R_5 exceeds its threshold at 38.63s and the fault flag is raised shown in Figure 9.35.

9.1.6.3   Weight average outputs – Air pipe blockage

Figure 9.36 shows the weighted average outputs, it can be seen that residuals w_1, w_2 and w_3 are not affected by the pressure sensor fault and their respective fault flags remain low.

190

9.1.6.4   Discussion – Air pipe blockage

Applying a blockage fault to the air pipe has an effect on the parity residual R_1. The blockage also affects residuals R_2, R_3, R_4, and R$_5$. Residuals w_1, w_2 and w_3 are not affected and the respective fault flags remain low. These results correspond with the fault signatures detailed in Table 7.2. With this type of fault, accommodation is not available as pressure is blocked between the servo valve and pneumatic cylinder. This means that the desired positional movement of the pneumatic is not achievable. However, from the point where the fault is induced (35s) and the final residual (R_1) fault flag is raised (41.84s) a certain amount of fault tolerance is available (Figure 9.31). Once the final residual fault flag is raised the safety sequence is activated and the platform is made safe (i.e. brought back to its rest position). Table 9.1 summaries the results for the Stewart-Gough platform.

Table 9.1: Experimental results summary for Stewart-Gough platform test rig

Type of fault	Fault time	Residual generation scheme	Fault flag raised	Time fault Detected/isolated	Action taken	Time taken to detect fault
Position sensor loss	42.69s	Parity equation	R_1	42.72	Fault Accommodated	0.3s
		Kalman filter	R_4	42.7s		
		Weighted average	W_3	42.705s		
Pressure sensor (n) drift	20s	Parity equation	R_3	22.47s	No action	2.47s
		Kalman filter	R_4	22.2s		
Actuator fault (Control signal loss)	20s	Parity equation	R_1 R_2 R_3	21.55s 21.62s 21.61s	Safety mode activated	1.62s
		Kalman filter	R_4 R_5	20.65s 20.96s		
Air leak	18.6s	Parity equation	R_1 R_2 R_3	23.98s 18.67s 18.5s	Safety mode activated	5.38s
		Kalman filter	R_4 R_5	18.92s 18.78s		
Air blockage	35s	Parity equation	R_1 R_2 R_3	41.84s 41.8s 41.8s	Safety mode activated	6.84s
		Kalman filter	R_4 R_5	39.39s 38.64s		
Pressure sensor Signal loss (p)	32.95s	Parity equation	R_2	33.2s	No action	0.25s
		Kalman filter	R_5	33.2s		

9.2 Assessment of robustness of the FDI scheme

In order to assess the robustness of the designed FDI scheme a number of experiments are carried out on the Stewart-Gough platform. The experiments are conducted by varying the loads applied to the moving platform of the test-rig and without changing the FDI model. The initial assessment will show the FDI schemes performance with varying loads and at what load the performance starts to deteriorate (false alarms occurs) without injecting a fault. With a maximum loading capacity for the test-rig of 100N the results for the initial load tests are shown in Table 9.2, where zero (0) indicates that there are no false alarms and one (1) indicating that a false alarm has occurred.

Table 9.2: Loading test results

Load (Newtons)	Residuals							
	R_1	R_2	R_3	R_4	R_5	w_1	w_2	w_3
10	0	0	0	0	0	0	0	0
20	0	0	0	0	0	0	0	0
30	0	0	0	0	0	0	0	0
40	0	0	0	0	0	0	0	0
45	0	0	0	0	0	0	0	0
50	0	0	0	0	1	0	0	0
60	0	0	0	1	1	0	0	0
70	0	0	0	1	1	0	0	0
80	0	0	0	1	1	0	0	0
90	0	1	0	1	1	0	0	0
100	0	1	0	1	1	0	0	0

The results show that up to an applied load of 45N the FDI scheme performance has no loss in performance (i.e. no false alarms). At an applied load of 50N the Kalman residual R_5 raises a false alarm. Figure 9.37 shows the time history for Kalman RMS residual R_5 with 50N load applied, this shows that at 92s the residual exceeds the threshold limit. At this point the platform is engaged in an extreme manoeuvre (i.e. at maximum extension along the y-axis). If the movement along the y-axis is reduced to 85% travel then the Kalman RMS residual R_5 fault flag remains false.

At 60N both Kalman RMS residuals R_4 and R_5 raise the respective fault flags (false alarms) again at the maximum travel along the y-axis. This trend is apparent up to 80N load. Applying loads of 90-100N RMS residuals R_2, R_4 and R_5 raise false alarms.
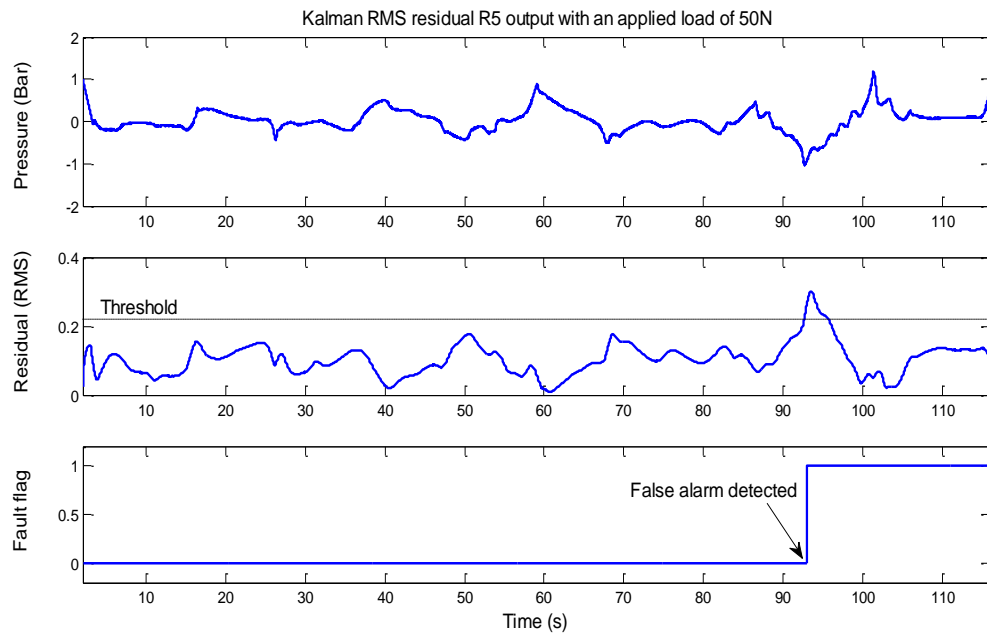
Figure 9.37: Kalman filter residual R_5 output with 50N load applied

Figures 9.38- 9.40 show the time histories for RMS residuals R_2, R_4 and R_5 with an applied load of 100N, these again showing that at the maximum travel along the y-axis the fault flags are raised.
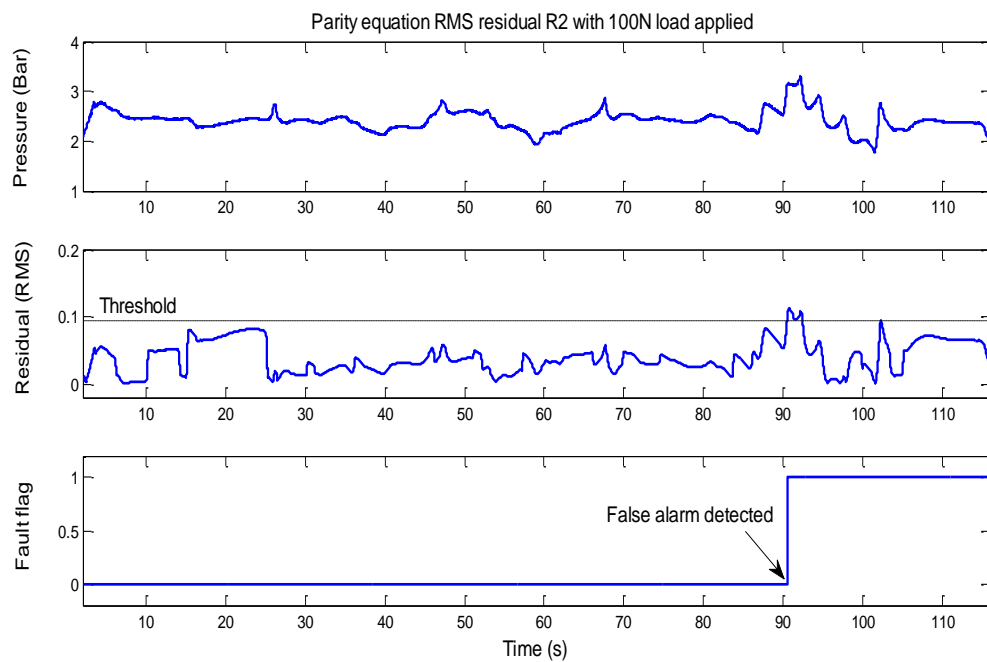
Figure 9.38: Parity equation RMS residual output with 100N load applied
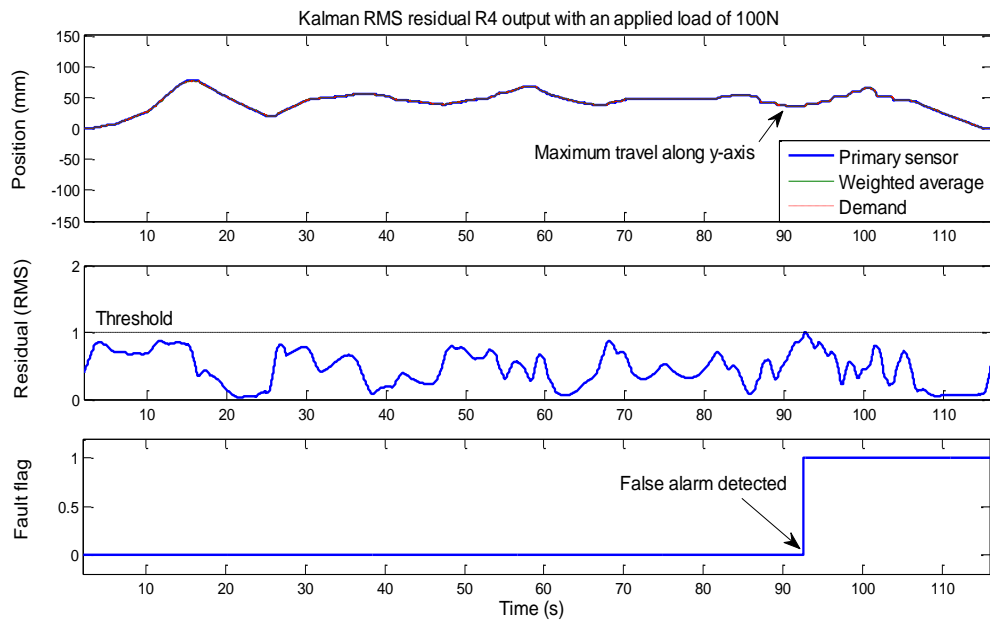
Figure 9.39: Kalman filter residual R_4 output with 100N load applied
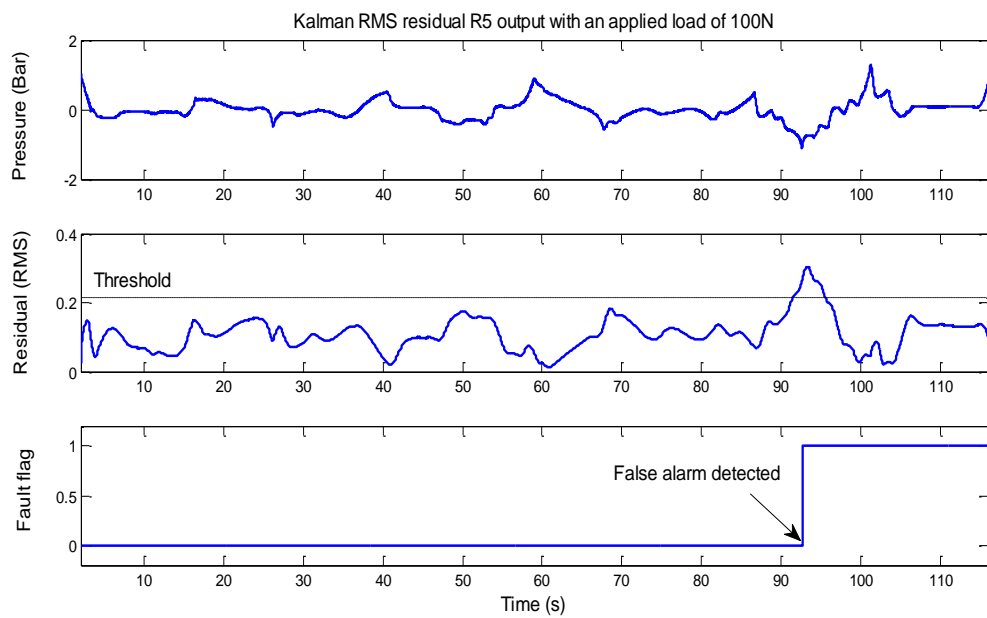
Figure 9.40: Kalman filter residual R_5 output with 100N load applied

194

9.2.1 *Assessment of robustness of FDI scheme with applied 45N load*

In this section an assessment of the robustness of the FDI scheme is described. Using an applied load of 45N the FDI scheme is assessed. The reason for this assessment is to determine what effect the applied load has on the FDI performance. A 45N load is used as this is the maximum load which can be applied before the FDI scheme fails (Table 9.2). Various experiments have been conducted where faults have been injected. The faults injected are similar to the faults applied in the experiments with no load applied (section 9.1). In order not to be repetitive only the air blockage fault is described.

A blockage fault is applied to the pressure system at 52s. This is physically achieved by means of a cut-off valve located between the proportional valve and the pneumatic cylinder. Figures 9.41-9.43 shows the time histories of this experiment (blockage fault) for the parity equation scheme. Figures 9.44-9.45 show the time histories of this experiment (blockage fault) for the Kalman filter scheme. The time history of the weighted average outputs of the voting scheme is shown in Figure 9.46.
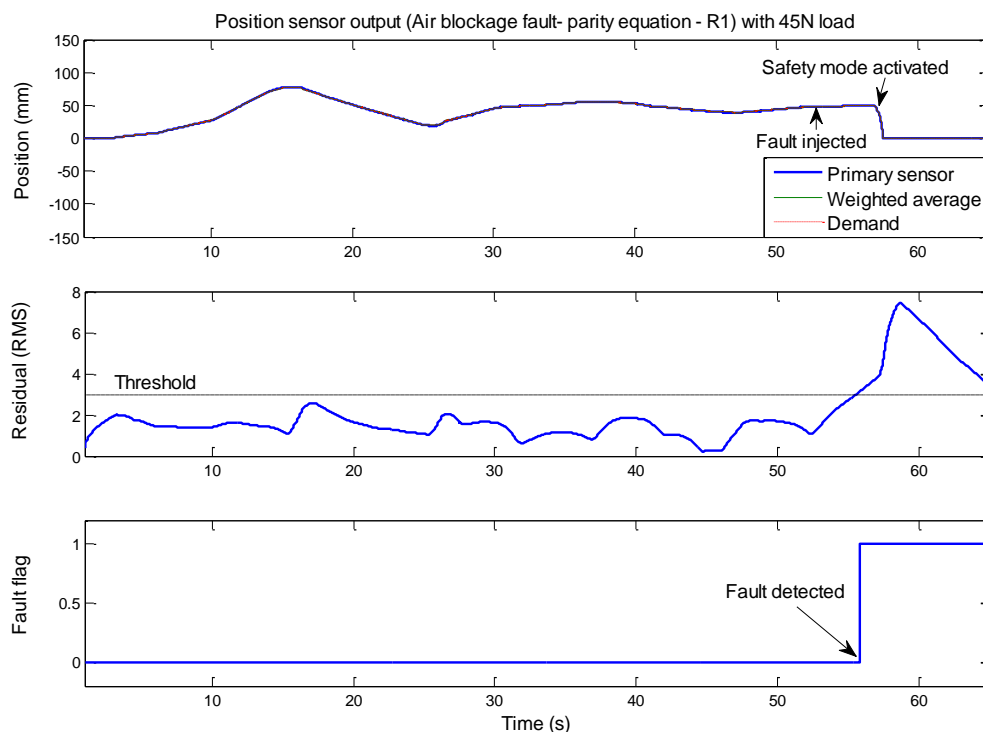
Figure 9.41: Air blockage fault, parity equation result- Position output sensor (R_1) with 45N load
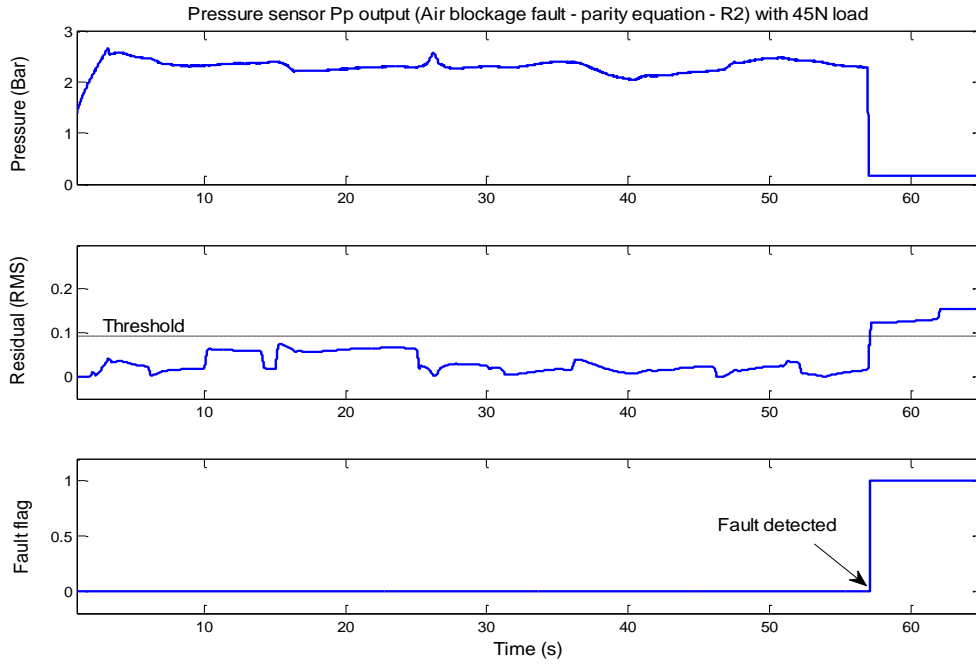
Figure 9.42: Air blockage fault, parity equation results- Pressure sensor Pp (R_2) with 45N load
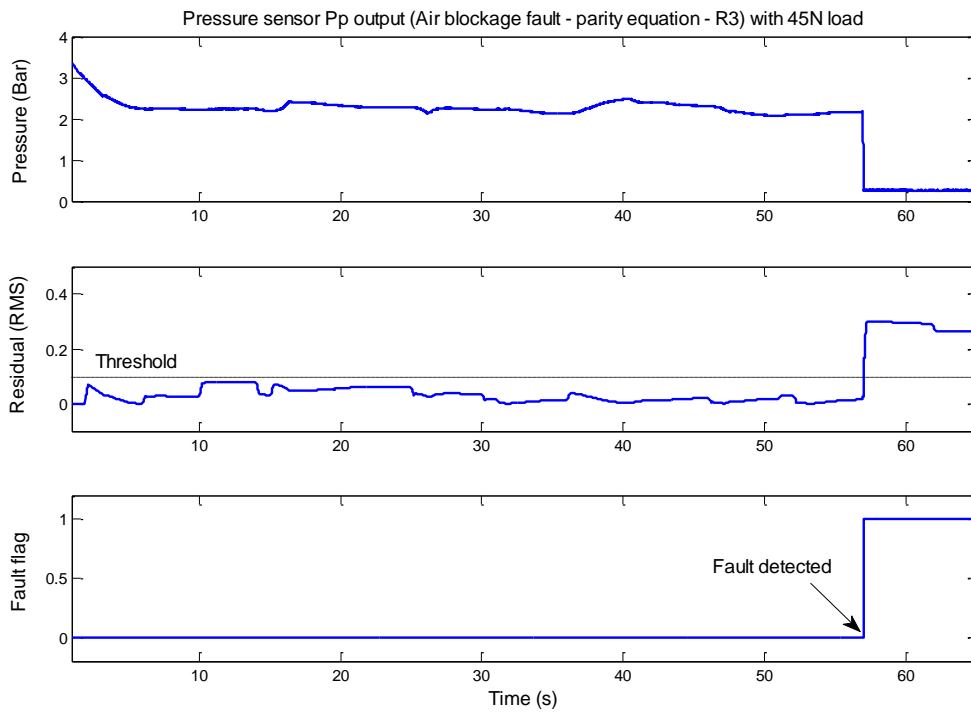
Figure 9.43: Air blockage fault, parity equation results- Pressure sensor Pn (R_3) with 45N load
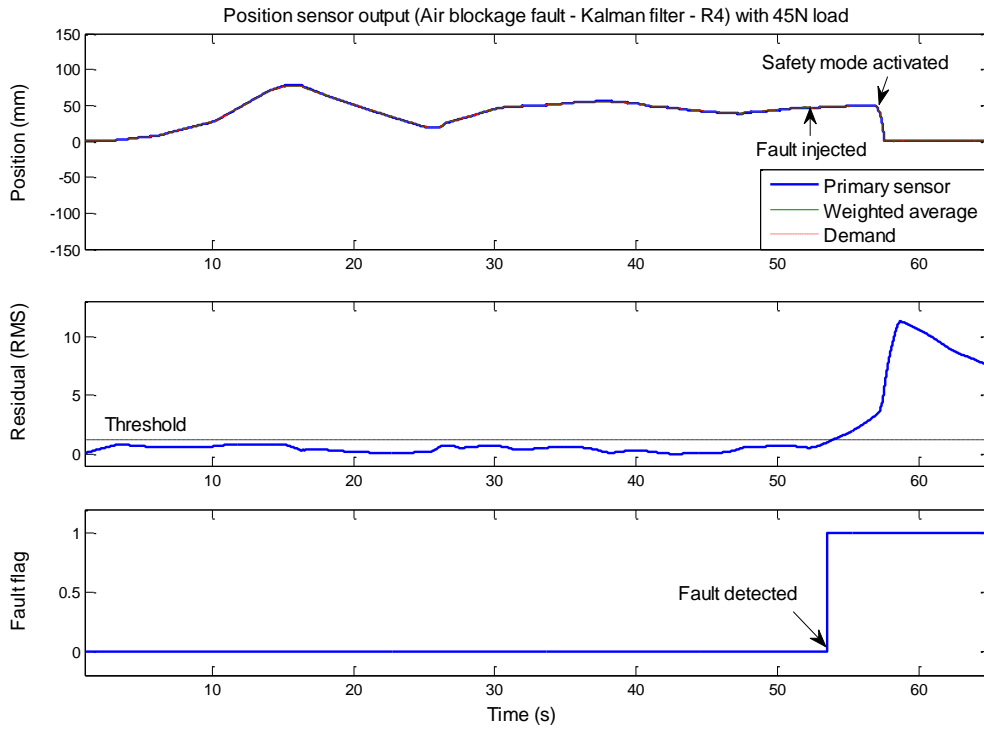
Figure 9.44 Air blockage fault, Kalman filter results - Position sensor output
(R_4) with 45N load
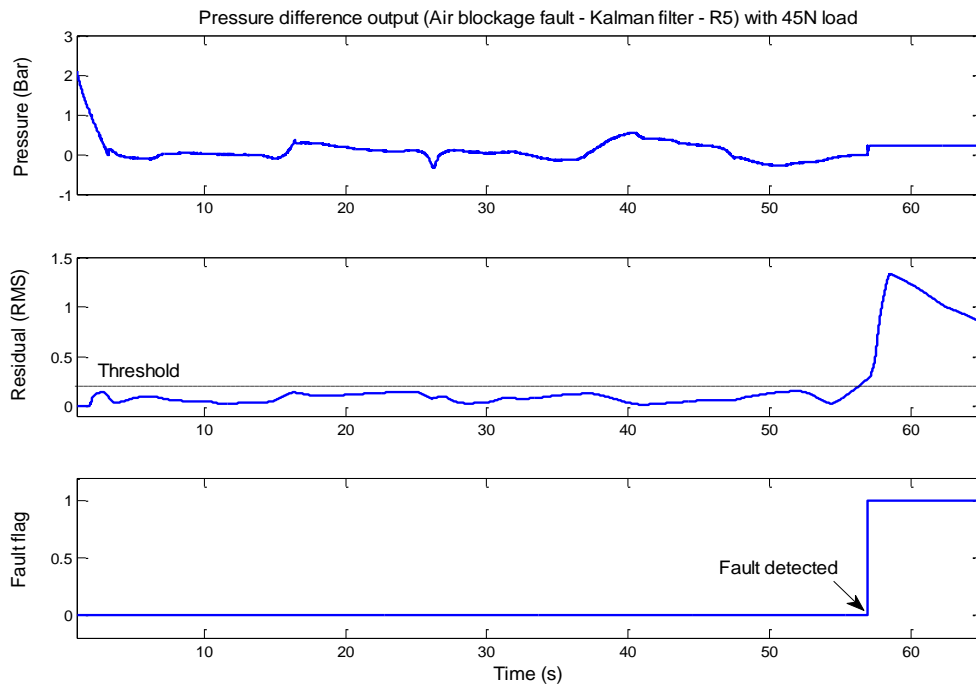
Figure 9.45: Air blockage fault, Kalman filter result - Pressure difference outputs (R_5) with
45N load

Weighted average outputs for air blockage fault with 45N load
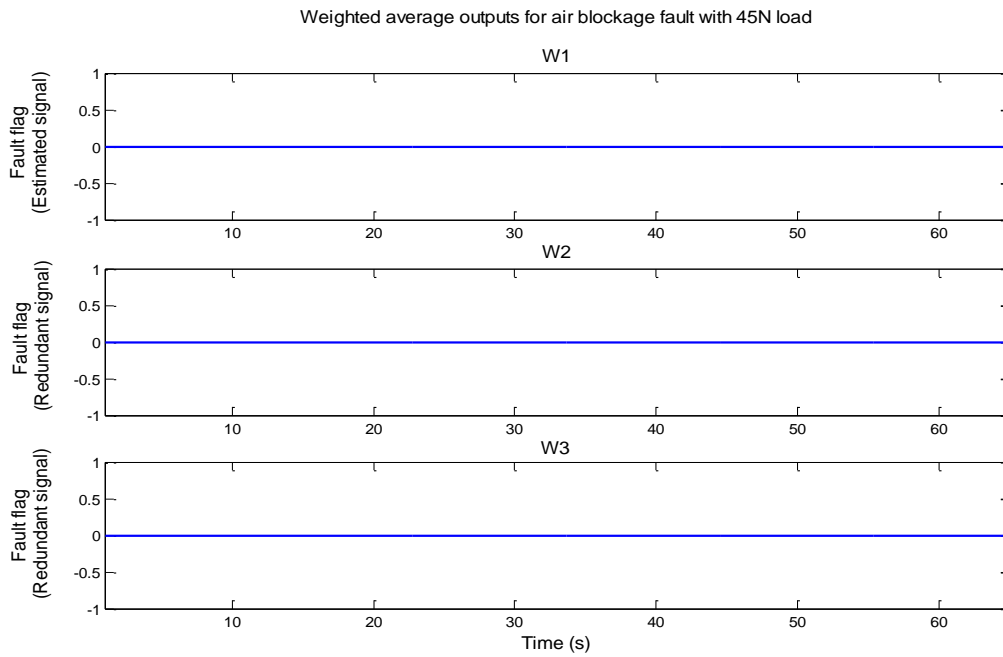
Figure 9.46: Weighted average outputs for an air blockage fault

9.2.1.1   *Parity equations – Air pipe blockage (45N load)*

A blockage is applied to the pneumatic system. Using the parity equation scheme the RMS residual R_1 (Figure 9.41) exceeds its threshold at 56.05s and the fault flag is raised. RMS residual R_2 (Figure 9.42) and RMS residual R_3 (Figure 9.43), both exceed their respective thresholds at 58.05s, and raise their respective fault flags.

9.2.1.2   *Kalman filter - Air pipe blockage (45N load)*

The outputs from the Kalman filter scheme show that the RMS residual R_4 is effected by a blockage applied to the system. The fault flag, shown in Figure 9.44 is raised at 53.3s. For the same fault, the RMS residual R_5 exceeds its threshold at 57.5s and the fault flag is raised shown in Figure 9.45.

9.2.1.3   *Weight average outputs – Air pipe blockage (45N load)*

Figure 9.46 shows the weighted average outputs, it can be seen that residuals w_1, w_2 and $w_3$are not affected by the pressure sensor fault and their respective fault flags remain low.

9.2.1.4   Discussion – Air pipe blockage (45N load)

Applying a blockage fault to the air pipe has an effect on the parity residual R_1. The blockage also effects residuals R_2, R_3, R_4, and R_5. Residuals w_1, w_2 and w_3 are not effected and the respective fault flags remain low, the fault is detected in 6.05s. These results correspond with the fault signatures detailed in Table 7.2. With this type of fault, accommodation is not available as air pressure is blocked between the servo valve and pneumatic cylinder. This means that the desired positional movement of the pneumatic is not achievable. Once the final residuals fault flags (R_2 and R_3) are raised the safety sequence is activated and the platform is made safe (i.e. brought back to its rest position). Comparing RMS residuals R_1 and R_4 (position outputs), the Kalman filter approach when compared with the parity equation scheme has a faster fault detection response time.

Assessing the FDI scheme under loaded conditions, the FDI scheme has shown to be robust up to a 45N load applied. The scheme has shown no decrease in performance and faults have been detected. However, exceeding a load of 50N shows the FDI scheme reduces in performance (i.e. raise false alarms). The false alarms are only raised for an extreme manoeuvre (i.e. at maximum extension along the y-axis).

One method to increase the performance of the FDI scheme would be to tune the thresholds of the RMS residuals. In this case increasing the thresholds until the false alarms are removed. If the loads applied to the Stewart-Gough platform are known then the threshold setting can be tuned for a particular load. However, tuning the threshold (increasing) can lead to missed faults at lower loads. Depending on the application of the Stewart-Gough platform a trade off can be made by tuning the threshold so that faults can be detected within the working range of the platform.

9.3   Conclusion

In this chapter the results of the experiments carried out on the Stewart-Gough platform test-rig were presented, described and analysed. Various faults typical of pneumatic systems were induced. Using the designed integrated control and FDI scheme (chapter 7) and applying the modular design from the single actuator set-up, fault detection was possible from the available measurements. The output results showed that using the described parity equation and Kalman filter methods; fault detection and isolation was

possible. An important reason for selecting the parity equation approach is that it is a relatively simple design approach. Basic equations of the system were used directly and compared to the system. The Kalman filter approach is more complex as the scheme takes into account noise variances. Use of the parity equations and Kalman filters schemes individually is not as effective for certain types of faults. For example, the Kalman filter approach cannot detect individual cylinder chamber pressure loss (this is due to system observability as discussed in chapter 7). Whereas, the parity equations are compared directly with the cylinder chamber pressures. For certain faults the Kalman filter approach when compared with the parity equation scheme was found to have a faster fault detection response time.

For position sensor faults, it was found that fault detection, isolation and accommodation could be achieved by employing a redundant sensor set-up coupled with a triple input weighted average voting scheme (chapter 7). Using the redundant sensor set-up and voting scheme can especially be important in a system such as this where safety is critical. Depending on the type of fault (pneumatic), where accommodation is not available the designed safety scheme is activated to bring the platform to a safe position.

An assessment of the FDI scheme performance was conducted by applying various loads to the top moving plate of the Stewart-Gough platform. The results showed that the FDI scheme performed adequately up to a 45N load. Increasing the load to 50N decreased the FDI schemes performance (i.e. false alarms). Methods were described to increase the FDI schemes performance.

From the experimental results it is shown that system level knowledge has been developed and used to check plant/actuator and sensors for problems, to detect and identify faults and where required take the appropriate action(s) as these problems develop.

Chapter 10

Conclusion

This chapter will draw together conclusions from the work. It will also summarise the basic design process that has been followed so that it could be applied by others (section 10.1). In section 10.2 conclusions are drawn based on the work described in the thesis. Finally (section 10.3), recommendations are made for future work that would extend that herein.

10.1   Fault tolerant control design procedure

This section describes the overall design procedure for a model-based fault tolerant control system that has been developed and followed in this thesis. A design procedure is shown in Figure 10.1 in the form of a flow chart. The flow chart describes the method applied in this thesis in order to design a model-based fault tolerant control (FDI) scheme. The flow charts starts with initially identifying the process/system (1) to which the FDI scheme is to be applied. In the case of this work a pneumatically actuated Stewart-Gough platform was the target (chapter 3). The next step involves modelling (2) the process, i.e. formulating the mathematical description of the identified process (chapter 4). This also includes identifying the process variables (i.e. position, pressure etc...). Next, the formulated model is validated (3). This is achieved by comparing the model to the actual system. Following successful model validation, the next step is to design a control system (4) for the process. The control system is designed (chapter 5) initially for the model, to meet the desired control objectives in terms of overshoot, gain and phase margins etc. The next step is to validate the designed control system (5) on the actual process. Once successful control of the process is achieved (i.e. to the required specifications) the next stage is to identify potential faults (6) that may typical for the identified system. The next step (7) is to formulate the residual generation equations (chapter 7). This can be achieved by using Kalman filters or parity equations, or a combination of both. Once this is achieved, a residual evaluation scheme can be applied. The residual evaluation scheme is essentially to check if the residual is responding to a fault. The next stage is to apply the FDI scheme (8) to the simulation model. Following this the next step is to test the FDI

scheme (9) on the simulation model. This involves applying simulated faults to the model and testing whether the FDI scheme is detecting faults. Following successful application of the FDI scheme to the simulation model the next stage is to combine the FDI scheme with the control scheme (10). By combining the FDI scheme to the control scheme (fault tolerant control), this allows for the appropriate actions to be taken. These include, controlling inputs to system components, whereby certain actions such as safety modes can be activated. An example of this in the current work is when a pneumatic fault was detected; the pressure in the cylinder chambers is released by activating the pressure release valves located between the proportional servo valve and the pneumatic cylinder. Following this the desired inputs to the system are then overridden in order to bring the system to a safe position (i.e. rest position). The next stage is to implement the designed FTC scheme (11) to the actual system. Following this, the FDI scheme can be tested (12) by applying various faults to the system, and finally the FDI scheme can be commissioned (13).

10.2   Thesis conclusion

Working to the guidelines set by the project sponsors BAE Systems, the research carried out in this thesis was to find a way to physically represent methods of providing an actual experimental test rig to simulate the fluid dynamics within a fuel tank under motion, including an approach to designing Fault Detection and accommodation schemes that could be demonstrated and later applied to other systems.

A pneumatically actuated Stewart-Gough platform was constructed as a means of providing an experimental test rig to simulate the fluid dynamics. As the Stewart-Gough platform was described as a safety critical application it was imperative that fault tolerant schemes were applied in order to provide a safe working environment.

In this thesis a model-based fault tolerant control scheme was designed and implemented on to the pneumatically actuated Stewart-Gough platform.

The thesis is divided into ten chapters. Namely, an introduction (chapter 1) which outlined the project aim and objectives. Chapter 2 detailed a literature review, which described various methods of fault detection and isolation currently available in literature. The review identified using parity equations and Kalman filter approaches as a way forward for detecting and isolating faults. Chapter 3 detailed the experimental set-ups used

System (1) → Identify system or subsystem requiring FDI scheme

Model system (2) → Identify system state variables / outputs

Validate model (3) → Validate model against system

Model validated? — No → Modify model

Yes

Design control Scheme (4) → Ascertain control specification requirements (i.e. overshoot, phase margin, gain margin) → Compare different control strategies

Control specifications satisfied? — No → Modify control scheme

Choose optimal control strategy

Yes

Validate control Scheme (5) → Validate control scheme on system

Control scheme validated ? — No → Modify control scheme

Yes

Figure 10.1: Fault tolerant control design procedure

to carry out the experiments, for both single cylinder test-rig and the Stewart-Gough platform test-rig. The experimental set ups were designed, built and commissioned by the author as test vehicles for this study. The chapter defined the components used for both

test-rigs and described their various layouts in detail. The main reasons for using a single cylinder set-up was so a modular designed scheme can be applied using the single cylinder set-up, then apply this modular design to each cylinder set-up of the Stewart-Gough platform arrangement. In chapter 4, a mathematical model of the pneumatic system was formulated. Various parameters were identified using experimental data. The model was validated by directly comparing it to the actual pneumatic system and found to represent the system adequately. In chapter 5 a review of various control techniques applied to pneumatic systems was described. For this work two control strategies were designed in order to successfully meet the desired control specifications. The control schemes include a PI control strategy and a LQG control scheme. By having evaluated the performance of the designed control schemes it was clear that either control scheme can be successfully applied to both test rig experiments. Chapter 6 discussed the kinematics and control (algorithms) used to provide motion for the Stewart-Gough platform. Two types of kinematic solutions were discussed, namely, inverse kinematics and forward kinematics. Due to the relative simplicity and with its low computational requirements the inverse kinematic approach was selected for use within the control strategy. In chapter 7, a fault detection and isolation scheme was designed for the pneumatic system. The FDI scheme is based on combining parity equation and Kalman filter based techniques. The parity and Kalman filter equations were formulated and used to generate residuals that in turn, were analysed to determine whether faults were present in the pneumatic system. The FDI scheme was initially designed on the single cylinder test-rig, and then modularly applied to one leg of the Stewart-Gough platform. Initially, simulation experiments were performed on the test-rig models using the designed model-based fault tolerant control scheme. The simulation results showed that using the designed scheme provided fault detection for the pneumatic system when various faults typical for a pneumatic system were applied. In chapter 8, various faults typical of pneumatic systems were induced. The results of the experiments carried out on the single actuator test-rig were described and analysed. The results found that the designed fault tolerant control scheme was successful in detecting and isolating faults for the single cylinder pneumatic system. In Chapter 9, the results of the experiments carried out on the Stewart-Gough platform test-rig are described and analysed. Using the designed integrated control and FDI scheme (chapter 7) and applying the modular design from the single actuator set-up. The output results showed that using the described parity equation and Kalman filter methods; fault detection and isolation was possible from the available measurements. The results showed that the use of the parity

equations and Kalman filters schemes individually is not as effective for certain types of faults. For example, the Kalman filter approach cannot detect individual cylinder chamber pressure loss. Whereas, the parity equations are compared directly with the cylinder chamber pressures. Overall, the author concludes that applying both schemes allows for better fault detection and fault isolation.

An assessment of the FDI scheme performance was conducted by applying various loads to the top moving plate of the Stewart-Gough platform. The results showed that the FDI scheme performed adequately up to a 45N load. Increasing the load to 50N decreased the FDI schemes performance (i.e. false alarms). Methods were described to increase the FDI schemes performance.

The claimed contributions are as follows

- A pneumatically actuated Stewart-Gough platform has been designed, built, and commissioned.
- A mathematical model has been developed and has been validated against experimental results.
- Two control approaches have been designed and compared and implemented (PI and LQG).
- A fundamental comparative study of parity equations and Kalman filter observer banks for fault detection in pneumatic actuators has been conducted.
- Extension of the parity equations and Kalman filter approach to provide a combined Fault detection scheme.
- Combination of the FDI and control in a modular Fault Tolerant Control scheme for a pneumatic actuator – validation by experiment.
- Extension of application of Fault Tolerant Control to all 6 actuators (and including fault management at top level) of Stewart-Gough platform.- validation by experiment.
- Accommodation and safety modes have been integrated within the FDI and control scheme.

Overall, this thesis has shown that system level knowledge has been developed and used to check plant/actuator and sensors for problems, to detect and isolate faults as they develop. For certain faults (i.e. position sensor faults) employing a redundant sensor set-up

coupled with a triple input weighted average voting scheme showed that fault detection, isolation, identification and accommodation was achieved. For a complex kinematic system (Stewart-Gough platform), using the redundant sensor set-up and voting scheme can especially be important in a positional system where safety is critical.

10.3   Future work

Future work will be focussed on extending the designed FTC scheme approach to the remaining pneumatic cylinders of the Stewart-Gough platform. In doing so, the all pneumatic Stewart-Gough platform legs can become fault tolerant to typical pneumatic faults. One suggestion for extending this research would be to further validate the design approach highlighted in Figure 10.1.

Another suggestion for extending this research is the fault identification problem within pneumatic systems. Fault identification is the most important of all the fault diagnosis tasks. When a fault is estimated, detection and isolation can be achieved since the fault nature can improve the diagnosis process. However, the fault identification problem itself has not gained enough research attention (Simani *et al*, 2002).

Most fault diagnosis techniques, such as, parity space, observer-based and parameter identification methods cannot be directly used to identify faults in sensors and actuators. Limited research has been done to overcome the fault identification problem. This is particularly apparent with the current work. One example is that for a pneumatic fault (i.e. leak, blockage, control signal loss), although the fault was successfully detected and isolated, identifying the fault was not possible from the generated information.

Patton *et al* (1989) proposed the Kalman filter for statistical testing and fault identification. However, the statistical testing methods imposed high computational demands and were not ideal for online identification (Simani *et al*, 2002). It is important to research methods which can tackle the fault identification problem online. One approach that may lead to identifying the fault(s), in particular for the work carried out in this thesis, is utilising an improved model for the cylinder pressures. As the faults that could not be identified were pneumatic faults (i.e. leaks, blockages, and actuator), so using an improved model that represents the cylinder chamber pressures may possibly lead to some way to solve this problem.

While the work in this thesis has provided some insight into model-based FDI system design for a pneumatic Stewart-Gough platform it has also raised a number of important questions. The answer to these questions is left for future research. For now, some of these questions are briefly itemised as follows:

- Although fault accommodation has been considered in this study and utilised in position sensor faults, accommodation for other subsystems of the pneumatic system, such as, cylinder faults and servo valve faults have not been considered. The only means of accommodation has been to bring the platform back to a safe position (rest position) if a pneumatic fault was detected. Due to the complex kinematic layout of the Stewart-Gough platform arrangement, each leg's (cylinder) position is crucial to the required platform orientation. Having an inactive leg (cylinder) will certainly jeopardise the required platform orientation. More work needs to be done in utilising the remaining legs as a means of redundancy (accommodation). This may be possible with or without increasing further hardware implementation to the Stewart-Gough platform arrangement. Other kinematic arrangements of the Stewart-Gough platform should be explored, which may assist in better fault accommodation. One approach is using the High Redundancy Actuation (HRA) approach. The idea of the HRA is to use a high number of small actuation elements both in parallel and in series. This increases the available travel and force over the capability of an individual element, and it makes the actuator resilient to faults where an element becomes loose or locks up (see for example Steffen *et al*, 2008).

- Accommodation of faults in servo valves is another dilemma. If as in the current case a servo valve fault is detected, again the only means of action (accommodation) is to bring the platform back to a safe position. In a practical sense if the servo-valve is faulty then having a redundant servo valve is really the only solution as a means of accommodation. Research can be focussed to find a solution to accommodate this fault with or without redundant servo valves.

References

Albertos, P., and Goodwin, G. C. (2002). Virtual sensors for control applications, *Annul reviews in Control*, **26**, pp. 101-112.

Al-Najjar, B. (1996). Total quality maintenance: An approach for continuous reduction in costs of quality products. *Journal of Quality in Maintenance Engineering*, **2**, pp. 2-20.

Andrighetto, P. L., Valdiero, A. C., and Carlotto, L. (2006). Study of friction behaviour in industrial pneumatic actuators, *ABCM Symposium series in Mechatronics*, **2**, pp. 369-378.

Astrom, K.J., and Rundqwist, L. (1989). Integrator windup and how to avoid it. In *proceedings of the American control conference,* **2**, pp. 1693-1698.

Baron, L. and Angles, J. (2000). The direct kinematics of parallel manipulators under joint-sensor redundancy, *IEEE Trans. Robotics and Automation*, **16** (1), pp. 12-19.

Belforthe, G., Raparelli, T., and Velardocchia, M. (1992). Pneumatic positioner with Fuzzy Control. *IFAC- Motion Control for Intelligent Automation,* Italy, pp. 229-234.

Blanke, M., Bogh, R. B., Jorgensen., and Patton, R. N. (1995). Fault detection for a diesel engine actuator- A benchmark for FDI. *Control Engineering Practice*, **3**, (12), pp. 1727-1730.

Blanke, M., Kinnaert, M., Lunze, J., and Starowiecki, M. (2003). Diagnosis and fault-tolerant control, *Springer*, Gremany.

Blanke, M., Izadi-Zamanabadi, R., Bogh, S. A., and Lunau, Z. P. (1997). Fault tolerant control systems- A holistic view, *Journal of Control, Engineering Practice*, **5**, (5), pp. 693-702.

Boian, R. F., Bouzit, M., Burdea, J., Lewis, J and Deutsch. (2005). Dual Stewart platform mobility simulator, *Proceedings of the 2005 IEEE 9th International Conference on Rehabilitation Robotics*, pp. 550-555.

Broen, R.B. (1975). New voters for redundant systems, *Journal of Dynamic Systems, Measurement and Control*, pp. 41-45.

Burrows, C. R. (1969). Non-linear pneumatic servomechanism. PhD Thesis, University of London, UK.

Chen, J. Patton, R. (1999). *Robust model-based fault diagnosis for dynamic systems.* Kluwer, Boston.

Chillari, S., Guccione, S., and Muscato, G. (2001). An experimental comparison between several pneumatic position control methods. *Proceedings of the 40th IEEE conference on Decision and Control.* Florida, USA, pp. 1168- 1173.

Cheung, J. T., and Stephanopoulos, G. (1990). Representation of process trends part 1. A formal representation framework. *Computers and Chemical Engineering*. **14**, (4-5), pp. 495-510.

Choi, G, S., Lee, H, K., and Choi, G, H. (1998). A study on tracking position control of pneumatic actuators using Neural Network. *IEEE,* pp. 1749-1753.

Chow , E. Y. and Willsky, A. S. (1984). Analytical redundancy and the design of robust failure detection systems, *IEEE Trans. on Automatic control*, **29**, (7), pp. 603-614.

Clark, R.N., Fosth, D.C., and Walton, V.M. (1975). Detection instrument malfunction in control systems. *IEEE Trans Aerospace Electronic Systems*, **AES-11**, PP. 465-473.

Clark, R. N. (1978). A simplified instrument detection scheme. *IEEE Transactions on Aerospace and Electronic Systems,* **14** (456-465), pp. 558-563.

Craig, J. J. (1989). *Introduction to Robotics, Mechanics and Control*. 2nd edition: Addison-Wesley publishing company, Reading, UK.

Dahl, P. R. (1968). A solid friction model, The Aerospace Corporation, El Segundo, CA, Tech. Rep, TOR-158 (3107-18).

Dasgupta, B., and Mruthyunjaya, T.S. (2000) The Stewart Platform Manipulator: A Review, *Mechanism and Machine Theory*, **35** (1), pp. 15-40.

Derkert, J.C., Desai, M.N., Deyst, J.J., and Willsky, V.M. (1977). DFBW Sensor Failure identification using analytic redundancy*, IEEE Trans, Automatic control*, **AC-22**, pp. 795-809.

Desai, M., and Ray, A. (1981). A fault detection and isolation methodology. *Proc. 20th Conference on Decision and Control*, pp. 1363-1369.

Dixon, R. (2003). Observer-based FDIA: Application to an electromechanical positioning system. *Control Engineering Practice.*

Edwards, C. and Postlethwaite, I. (1999). Anti-windup and bumpless transfer schemes. *Automatica* **34** 2, pp. 199–210.

Faugere, J., and Lazard, D. (1995). The Combinatorial Classes of Parallel Manipulators, Mechanism and Machine Theory, **30**, pp. 765–776.

Fichter, E. F. (1986). A Stewart platform-based manipulator: General theory and practical construction, *int. Journal of Robotics Research*, pp. 157-182.

Frank, P.M., and Ding, X. (1997). Survey of robust residual generation and evaluation methods in observer-based fault detection systems. *J. Proc. Cont.* **7**, (6), pp. 403-424.

Frank, P.M., and Keller, L. (1980). Sensitivity discriminating observer design for instrument failure detection. IEEE Trans. *Aerospace Electronic Systems*, **AES-16**, pp. 460-467.

Frank, P. M. (1987a). Fault diagnosis in dynamic systems via state estimation- A survey. In Tzafestas, S., Singh, M., and Schmidt, *System Fault Diagnostics, Reliability and Related Knowledge-Based Approaches,* **1**, pp. 35-98.

Frank, P. M. (1987b). Advanced fault detection and isolation schemes using non-linear and robust observers. 10th *IFAC World Congress*, Munich, pp. 27-31.

Frank, P. M. (1990). Fault diagnosis in dynamic systems using analytical and knowledge-based redundancy: A survey and some new results. *Automatica*, **26,** pp. 459-474.

Frank, P. M. (1996). Analytical and qualitative model-based fault diagnosis- A survey and some new results. *European journal of control*. **2**, pp. 6-28.

Frank, P. M., Alcorta-Garcia, E., and Koppen- Seliger, B. (2000). Modelling for fault detection and isolation verses modelling for control. *Mathematics and Computers in Simulation*, **53**, (4-6), pp. 259-271.

Franklin, G. F., Powell, J. D. and Emami-Naeini, A. (2002). *Feedback control of dynamic systems: 4th edition*, Prenntice-Hall, London.

Geladi, P., and Kowalski, B, R. (1986). *PLS tutorial. Anal. Chim. Acta*. **185**, pp 1-17.

Gerler, J. J. (1998). *Fault detection and Diagnosis in Engineering systems*, Marcel Dekker, Inc., USA.

Gertler, J., and Singer, D (1990). A new structural framework for parity equation based failure detection and isolation. *Automatica*, **26**, pp. 381-388.

Girone, M., Burdea, M., Bouzit, M and Popescu, V. (2001). A Stewart platform-based system for ankle telerehabilitation, *Autonomous Robots*, 10, pp. 203-212.

Gough, V. E., and Whitehall, S. G. (1962). Universal tyre test machine, *Proceeds of the 9ᵗʰ International Technical Congress F.I.S.I.T.A*, pp. 117-137.

Grewal, K.S., Dixon, R. and Pearson, J. (2008). Development of a fault tolerant actuation system- modelling and validation. *Actuator 08, 11ᵗʰ international conference on new actuators,* pp, 469-472.

Grimm, G., Hatfield, J., Postlethwaite., Teel, A., Turner, M., and Zaccarian, L. (2003). Anti-windup for stable linear systems with input saturation: an LMI-based synthesis. *IEEE Trans. Aut. Cont. (A),* **48,** (9), pp. 1509-1525.

Gross, D.C., and Rattan, K.S. (1998). An adaptive multiplayer neural network for trajectory tracking control of a pneumatic cylinder. *IEEE International Conference on Systems, Man, and Cybernetics,* **2,** pp. 1662-1667.

Hamiti, K., Voda- Besancon, A., and Roux- Buisson, H. (1996). Position control of a pneumatic actuator under the influence of stiction. *Control Engineering Practice,* **4**, (8), pp. 1079-1088.

Henley, E. J. (1984). Application of expert systems to fault diagnosis. *In AIChE annual meeting*. San Francisco, CA.

Hesselroth, T., Sarker, K., Van der Smagt, P, P., and Schulten, K. (1994). Neural network control of a pneumatic robot arm. *IEEE International Conference on Systems, Man, and Cybernetics,* **24,** (1) pp. 28-38.

Isermann, R. (1984). Process fault detection based on modelling and estimation methods- A survey. *Automatica*, **20**, pp. 387-404.

Isermann, R. (1984). Fault diagnosis of machines via parameter estimation and knowledge processing- tutorial paper. Automatica, **29**, (4), pp. 815-835.

Isermann, R. (1997). Supervision, Fault-Detection and Fault Diagnosis methods- An Introduction, *Control Engineering Practice*, **5**, (5), pp. 639-652.

Isermann, R. (2006). *Fault-Diagnosis Systems, An introduction from fault detection to fault tolerance*. Springer-Verlag Berlin Heidelberg.

Kaitwanidvilai, S., and Parnichkun, M. (2005). Force control in a pneumatic system using hybrid adaptive neuro-fuzzy model reference control. *Mechatronics.* **15,** pp. 23-41.

Kalman, R. E. (1960). A new approach to linear filtering and prediction problems. *ASME Transactions on Journal of Basic Engineering.* 82-D, 35-45.

Kiencke, U and Nielsen, L. (2005). *Automotive control systems: For Engine, Driveline and Vehicle*, Springer. USA.

Kothare, M., Campo, P., Morari, M., and Nett, N. (1994). A unified framework for the study of anti-windup designs. *Automatica,* **30,** (12), pp. 1869-1883.

Kraus, T. W., and Myron, T. J. (1984). Self-tuning PID Controller uses pattern recognition approach. *Control Engineering*, **31**, (6), pp. 106-111.

Krivits, I. L and Krejnin, G. V. (2006). *Pneumatic actuating systems for automatic equipment.* Taylor and Francis, London.

Lee, K. H., Choi, G. S and Choi, G. H. (2001). A study on tracking position control of pneumatic actuators, *Mechatronics*, 12, pp. 813-831.

Lipnickas, A., Sa da Costa, J., and Bocaniala, C. (2004). FDI based on two stage classifiers for fault diagnosis of valve actuators. Application to DAMADICS benchmark. *11th International conference EPE-PEMC'2004, Riga*. pp. 147-153.

Liu, S., and Bobrow, J.E. (1988). An analysis of a pneumatic servo system and its application to a computer controlled robot. *ASME, Journal of Dynamic Systems, Measurement and Control.* **110,** (3), pp. 228-235.

Muscato, G., and Travato, G. (1998). Motion control of a pneumatic climbing robot by means of a fuzzy processor. *First International Symposium CLAWAR '98 Climbing and Walking Robots.* Brussels.

Nanua, P., Waldron, K. J. and Murthy, V. (1990). Direct kinematic solution of a Stewart platform, *IEEE Trans. Robot Automation*, **6**, (4), pp. 438-444.

Nichkawde, C., Harish, P., and Ananthkrishnan, N. (2004). Stability analysis of a Multibody system model for coupled sloth-vehicle dynamics, *Journal of Sound and Vibration*, 275, pp. 1069-1083.

Nguyen, C.C., and Pooran, F.J. (1988). Adaptive control of robot manipulators with closed-kinematic chain mechanisms , *Robotics and Manufacturing recent trends in research education, and application, chapter 4, AMSE Press*, New York, pp. 177-186.

Nouri, B., AL-Bender, F., Swevers, J., Vanherck, P. and Van Brussel, H. (2000). Modelling a pneumatic servo positioning system with friction. *Proceedings of the ACC 2000*, pp. 1067-1071.

Olsson, H., Astrom, K. J., Candas de Wit, C., Gafvert, M. and Lischinsky, P. (1998). Friction models and friction compensation, *European Journal of Control*, **4** (3), pp. 176-195.

Onken, R., and Stuckenburg, N. (1979). Failure detection in signal processing and sensing in flight control systems. *Proceedings of IEEE Conference on Decision and Control*, San Diego, pp. 449-454.

Patton, R.J., Chen, J., and Nielsen, S. B. (1995). Model-based methods for fault diagnosis: some guidelines. *Trans, Inst, Machine Control*, **17**, (2), pp. 73-83.

Patton, R.J., Frank, P.M., and Clark, R.N. (2000). *Issues in fault diagnosis of dynamic systems.* Springer Verlag. London

Patton, R.J (1997). Fault-tolerant control: The 1997 situation. *Proceedings of the third symposium on fault detection, supervision and safety for technical processes (SAFEPROCESS'97).* **3,** pp, 1029-1052.

Patton, R.J., Frank, P.M., and Clark, R.N. (1989). *Fault Diagnosis in Dynamic Systems, Theory and Applications*. Prentice-Hall, Englewood Cliffs, New Jersey.

Perondi, E. A. (2002). Cascade non-linear control with friction compensation of a pneumatic servo positioning, Ph.D Thesis Mechanical Engineering Department, Federal University of Santa Catarina, Brazil, pp. 178.

Potter, I.E., and Suman, M.C. (1977). Thresholdless redundancy management with arrays of skewed instruments. Integrity in Electronic Flight Control Systems, *AGARDDOGGRAPH*-**224**, pp. 11-15 to 15-25.

Scavarda, S., Kellal, A., and Richard, E. (1987). Linearized models for electropneumatic cylinder servovalve system. *Proceedings of the 3rd International conference on Advanced Robotics.* France. pp. 149-160.

Shearer, J. L. (1956). Study of pneumatic processes in he continuous control of motion with compressed air I and II, *Tran. AMSE,* pp. 233-249.

Shieh, L. S., Dib, H. M., Ganesan, S., and Yates, R.E. (1988). Optimal pole-placement for state-feedback systems possessing integrity, *International Journal of Systems Science,* **19** (8), pp. 1419-1435.

Shunmugham, R. P., and Hayakawa, Y. (1997). Practical design of adaptive model- based sliding mode control of pneumatic actuators. *Proceedings of Advanced Intelligent Mechatronics AIM'97,* Japan.

Simani, S., Fantuzzi, C., and Patton, R. (2002). *Model-based fault diagnosis in dynamic systems using identification techniques*. London: Spring-Verlag.

Song, S. K., and Kwon, D. S. (2001). New closed-loop direct kinematic solution of the 3-6 Stewart-Gough platform using the tetrahedron approach, *Proceedings of the International Conference on Control, Automation and Systems*, pp. 484-487.

Steffen, T., Pearson, J., Dixon, R., Goodall, R.M., Zolotas, A., and Davies J. 2008. Failure modes and probabilities of a high redundancy actuator. *17th IFAC World Congress*, July 6-11, Seoul, Korea

Stewart, D. (1965). A Platform with six degrees of freedom, *Proceedings of the Institution of Mechanical Engineers*, **180**, (15), pp. 371-386.

Theilliol, D., Noura, H., and Sauter, D. (1998). Fault-tolerant control method for actuator and component faults. In Proceeds of IEEE Conference on Decision and Control, **13**, pp. 604-608.

Uppal, F., Patton, R., and Witczak, M. (2006). A neuro-fuzzy multiple-model observer approach to robust fault diagnosis based on the DAMADICS benchmark problem. *Control Engineering Practice*, **14**, pp. 699-717.

Valdiero, A. C., Andrighetto, P. L., Carlotto, L. (2005). Dynamic modelling and friction parameters estimation to pneumatic actuators, *Proceedings of MUSME 2005, the International Symposium of Mulibody Systems and Mechatronics*, Brazil.

Van Varseveld, R.B., and Bone, G.M. (1997). Accurate position control of a pneumatic actuator using on/off solenoid valves. *IEEE/ASME Transactions on Mechatronics,* **2,** (3).

Verrelst, B., Daerden, F., Lefeber, D., Van Ham D, and Fabri, T. (2000). Introducing Pleated Pneumatic Artificial Muscles for the actuation of legged robots: a one-dimensional set-up, *Proceedings of the 3rd International Conference on Climbing and Walking Robots*, pp. 583–590.

Venkatasubramanian, V., Rengaswamy, R., Yin, K., and Kavuri, S.N. (2003a). A review of process fault detection and diagnosis. Part I: Quantitative model-based methods. *Computers and Chemical Engineering*, **27**, pp. 293-311.

Venkatasubramanian, V., Rengaswamy, R., and Kavuri, S.N. (2003b).). A review of process fault detection and diagnosis. Part II: Qualitative models and search strategies. *Computers and Chemical Engineering*, **27**, pp. 313-326.

Venkatasubramanian, V., Rengaswamy, R., Kavuri, S.N., and Yin, K. (2003c). A review of process fault detection and diagnosis. Part III: Process history based methods. *Computers and Chemical Engineering*, **27**, pp. 327-346.

Wang, J., and Gosselin, C. M. (1998). A new approach for the dynamic analysis of parallel manipulators, *Multibody System Dynamics*, 2, pp. 317-334.

Wang, J., Pu, J., and Moore, P. (1999). A practical strategy for servo-pneumatic actuator systems. *Control Engineering Practice,* **7**, pp. 1483-1488.

Waldron, K. J., Raghavan, M. and Roth, B. (1989). Kinematics of a hybrid series-parallel manipulation system. *Journal of Dynamic Systems, Measurement and Control,* **111**, (2), pp. 211–221.

Wang, J., Pu, J., Moore, P. R., and Zhang, Z. M. (1998). A practical control strategy for servo-pneumatic actuators systems, *Control Engineering Practice*, **7**, pp. 1483-1488.

Willsky, A.S. (1976). A survey of design methods for failure detection in dynamic systems. *Automatica*, **12**, pp. 601-611.

Yang, D. C. H., and Lee, T.W. (1984) Feasibility study of a platform type of robotic manipulators from a kinematic viewpoint. *Transactions of the ASME, Journal of mechanisms, transmissions, and automation in design,* **106,** pp. 191-198.

Zanganek, K.E., Sinatra, R., and Angeles, J. (1997). Kinematics and dynamics of a six-degrees-of-freedom parallel manipulator with revolute legs, Robot, **15**, pp. 385-394.

Zhao, Q., and Xu, Z. (2004). Design of a knowledge-based fault detection and isolation scheme. *IEEE Transactions on Systems, Man, and Cybernetics,* **34,** (2). pp. 1089-1095.

Zheng, A., Kothane, M., and Morari, M. (1994). Anti-windup design for internal model control. *Int. J. of Control,* **60,** (5), pp. 1015-1024.

Zhuang, Z., and Frank P.M. (1997). Qualitative observer and its application to fault detection and isolation systems. *Proc. Instn Mech Engrs,* **211**, (1), pp. 253-262.

Bibliography

Ackermann, J. (1993). *Robust Control, Systems with Uncertain Physical Parameters*, Springer-Vela, USA.

Ailon, A. (1996). Output controllers based on iterative schemes for set-point regulations of uncertain flexible- joint robot models. *Automatica*, **32**, pp. 1455-1461.

Albertos, P., Strietzel, R., and Morts, N. (1997). *Control Engineering Solutions, A Practical Approach*, The IEEE Press, London.

Altintas, Y., and Yellowley, I. (1989). In process detection of tool failure in milling using cutting force models. *ASME, Journal of Engineering for Industry*, **111**, pp. 149-157.

Andry, A.N., Shapiro, E.Y., and Chung, J.C. (1983). Eigenstructure assignment for linear systems. *IEEE Transactions on Aerospace Electronic Systems*, **19**, pp.717-729.

Armstrong-Helouvy, S., Dupont, P., and Canudas De Wit, C. (1994). A survey of models, analysis tools and compensation methods for the control of machines and friction. *Automatica,* **30**, pp.1483-1488.

Astrom, K.J. (1996). Adaptive Control around 1960, *IEEE Control Systems*, **16**, (3), pp. 44-49.

Beard, R. V. (1971). Failure Accommodation in Linear Systems through Self-Reorganisation. Dept MVT-71-1, Man Vehicle Laboratory, Cambridge, MA.

Bodson, M. and Groszkiewicz, J. (1997). Multivariable adaptive algorithms for reconfigurable flight control. *39th IEEE Transactions on control systems technology*. 5, pp. 217-229.

Boskovic, J. D. and Mehra, R. K. (1998). A multiple model-based reconfigurable flight control system design. *In Proceedings of 37th Conference on Decision and Control*, **9**.

Chandrasekharan, P. C. (1996). *Robust Control of Linear Dynamical Systems*, Academic Press, USA.

Chen, J. and Jhang, H. (1991). Robust detection of faulty actuators via unknown input observers. *Int. J. Sys. Sci.,* **22** (10), pp. 1829-1839.

Close, C., M. and Frederick, D. K. (1978). *Modelling and Analysis of Dynamic Systems*, Houghton Mifflin Company, USA.

Davey, A., Grosvenor, R., Morgan, P., and Prickett, P. (1996). Petri-net based machine tool failure diagnostics. *Condition Monitoring and Diagnostic Engineering Management*. **96**, pp. 723-732.

Desoer, J.C., and Vidyasagar, M. (1975). *Feedback Systems: Input- Output Properties*, Academic, New York.

Desovski, D., Liu, Y., and Cukic, B. (2006). Linear randomised voting algorithm for fault tolerant sensor fusion and corresponding reliability model, *IEEE, Proceedings of the 9th IEEE International Symposium on High-Assurance Systems Engineering*, pp. 153-162.

Ding, X; Frank, P.M; and Guo, L. (1990). Fault detection via adaptive observers based on orthogonal functions. *Proceedings IFAC Symposium on advanced information processing in automatic control*, Nancy, Pergamon, pp.95-100.

Doebelin, E. (2004) *Measurement systems, Application and design,* 5th edition: London: McGraw-Hill.

Dorf, C. and Bishop, R. (2001). *Modern control system*, 9th edition: Prentice-Hall, USA.

Doyle, J.C., Francis, B.A., and Tannenbaum, A.R. (1992). *Feedback control theory*, Macmillan Publishing, New York.

Eterno, J. S., Looze, D. P., Weiss, J. L., and Willsky, A. S. (1985). Design issues for fault-tolerant restructurable aircraft control. *Proc. 24th IEEE. Conf. On Decision and Control*, Fort Lauderdale, pp. 900-905.

Frank, P.M. and Wünnenberg, J. (1987). Sensor fault detection via robust observers. In Tzafestas, S., Singh, M., and Schmidt, G., editors, *System fault detection diagnostics, reliability and related knowledge-based approaches*, volume 1, pages 147-160. D. Reidel Press, Dordrecht.

Fujita, M. and Shimemura, E. (1988). Integrity against arbitrary feed-back failure in linear multivariable control systems, *Automatica*, **24** (6), pp. 765-772.

Fussell, J.B. (1977). Fault tree analysis-state of the art. *IEEE Transactions on Reliability,* **23**, (1), pp. 51-53.

Gao, Z., and Antsaklis, P. (1991). Stability of the pseudo-inverse method for reconfigurable control. *International Journal of Control*, 53, pp. 717-729.

Isidori, A., and Kang, W. (1995). H_∞ Control via measurement feedback for general non-linear systems. *IEEE Transactions on Automatic Control,* **AC-40,** pp. 466-472.

Jamshidi, M., Krohling, R.A., Coelho, L., and Fleming, P. (2003). *Robust Control Systems with Genetic Algorithms*, CRC Press, London.

Jantunen, E. (1999). A solution for tool wear diagnosis, *Proceedings of COMADEM 99*. England, pp. 95-105.

Johns, C., and Prickett, P. (1997). Machine tool axis signals for tool breakage monitoring. *Condition Monitoring and Diagnostic Engineering Management*. **97**, pp. 450-459.

Jones, H.L. (1973). *Failure detection in linear systems*. Ph.D Thesis, MIT, Cambridge, MA.

Kelly, R., Ortega, R., Ailon, A., and Loria, A. (1994). Global regulation of flexible joints robots using approximate differentiation. *IEEE Transactions on Automatic Control,* **AC-39,** pp. 1222-1224.

Landau, I.D. (1974). A survey of model reference adaptive techniques: Theory and applications. *Automatica,* **10**, pp. 353-379.

Latif-Shabgahi, G. (2004). A novel algorithm for weighted average voting used in fault tolerant computing systems, *Microprocessors and Microsystems*, **28**, pp. 357-361.

Lewis, F.L. (1986). *Optimal Estimation with an Introduction to Stochastic Control Theory*, John Wiley & Sons. London.

Liu, K., Fitzgerald, M., Dawson, D., and Lewis, F. (1991). Modelling and control of a Stewart platform manipulator. *ASME, Control of systems with inexact dynamic models,* **33**, pp. 83-89.

Looze, D. P., Krolowski, S. M., Weiss, J. I., Eterno, J. S., and Gully, S. W. (1984). An approach to restructurable control system design. *Proc. 23rd IEEE. Conf. On Decision and Control*, Las Vegas, pp. 1392-1397.

Maciejowski, J. M. (1999). Modelling and predictive control: enabling technologies for reconfiguration. *Annual reviews in control*, **23**, pp. 12-23.

Mariton, M. (1989). Detection delays, false alarm rates and reconfiguration of control systems. *International Journal of Control*. **49**, (3), pp. 981-992.

Marquez, H. J. and Diduch, C. P. (1990). Sensitivity robustness in failure detection: Afrequency domain approach. *Proceedings at 10ᵗʰ IFAC World congress*, Munich.

Maybeck, P. S. (1999). Multiple model adaptive algorithms for detecting and compensating sensor and actuator/ surface failures in aircraft flight control systems. *International Journal of Robust and Non-linear Control.* **9**, pp. 1051-1070.

Maybeck, P. S. (1999). *Stochastic models, estimation, and control.* Academic press, INC, London.

Maybeck, P. S., and Stevens, R. D. (1991). Reconfigurable flight control via multiple adaptive control method. *IEEE Trans. Aerospace Electronic Systems.* **27**, pp. 470-479.

Meressi, T., Chen, D., and Paden, B. (1993). Application of Kharitonov's theorem to mechanical systems. *IEEE Transactions on Automatic Control,* **AC-38,** pp. 488-491.

Merkle, R. C. (1997) A new family of six degrees of freedom positional devices, *Nanotechnology*, **8**, pp. 47-52.

Messina, A., Giannoccaaro, N., and Gentile, A. (2005). Experimenting and modelling the dynamics of pneumatic actuators controlled by the pulse width modulation (PWM) technique. *Mechatronics,* **15**, pp. 859-881.

Musgrave, J. L., Guo, T. H., Wong, E., and Duyar, A. (1997). Real-time accommodation of actuator faults on a reusable rocket engine. *IEEE Trans, Control System Technology.* **5**, pp. 100-109.

Napolitano, M. R., and Swaim, R. L. (1990). New technique for aircraft flight control reconfiguration, *J. Guid. Con and Dyn*, **14**, (1), pp. 184-190.

Paul, A.K., Mishra, J.K., and Radke, M.G. (1994). Reduced order sliding mode control for pneumatic actuator. *IEEE, Transactions on Control Systems Technology,* **2,** (3), pp. 271-276.

Rauch, H. E. (1995). Autonomous Control Reconfiguration, *IEEE Control Systems Magazine*, **15**, (6), pp. 37-48.

Sage, G.H., DE Mathelin, F. M., and Ostertag, E. (1999). Robust Control of Robot manipulators: A Survey. *International Journal of Control,* **72,** (16), pp. 1498-1522.
Seliger, R. and Frank, P. M. (1991). Robust component fault detection and isolation in non-linear dynamic systems using non-linear unknown input observers. *IFAC/IMACS Symposium SAFEPROCESS '91*, Baden-Baden, pp. 313-318.

Siljak, D. D. (1980). Reliable control using multiple control systems, *International Journal of Control*, **31** (2), pp. 303-329.

Skogestad,S., and Postlethwaite, I. (2007). *Multivariable Feedback Control: Analysis and Design*, John Wiley and Sons Ltd, UK.

Tsui, C. (1993). A general failure detection, isolation and accommodation system with model uncertainty and measurement noise. 12th IFAC World Congress, Sydney, Austrailia. **6**, pp.231-238.

Venkatasubramanian, V., & Rich, S. H. (1988). An object-oriented two-tier architecture for integrating compiled and deep-level knowledge for process diagnosis. Computers and Chemical Engineering 12 (9_ 10), 903_ 921.

Vingerhoeds, R. A., Janssens, P., Netten, B. D., and Aznar Fernandez-Montesinos. (1995). Enhancing off-line and on-line condition monitoring and fault diagnosis. *Control Engineering Practice*. **3**, (11), pp. 1515-1528.

Wang, J., Wang, J.D., Moore, P., Pu, J. (2001). Modelling study, analysis and robust servocontrol of pneumatic cylinder actuator systems. *IEE, Proc.-Control Theory. Applications.* **148**, pp. 35-41.

Wilbers, D.N., and Speyer J.L. (1989). Detection filters for aircraft sensors and actuator faults. *Proc. ICCON '89 Int. Conf. On Control and Applications*, Jerusalem,

Zhao, Q. and Jiang, J. (1998). Reliable state feedback control system design against actuator failure. *Automatica*. **34**, pp.1267-1272.

Appendix A

CAD drawings

22 | 22

10

R16.75

28

M10 Thread

7/8-14 UNF Thread

50
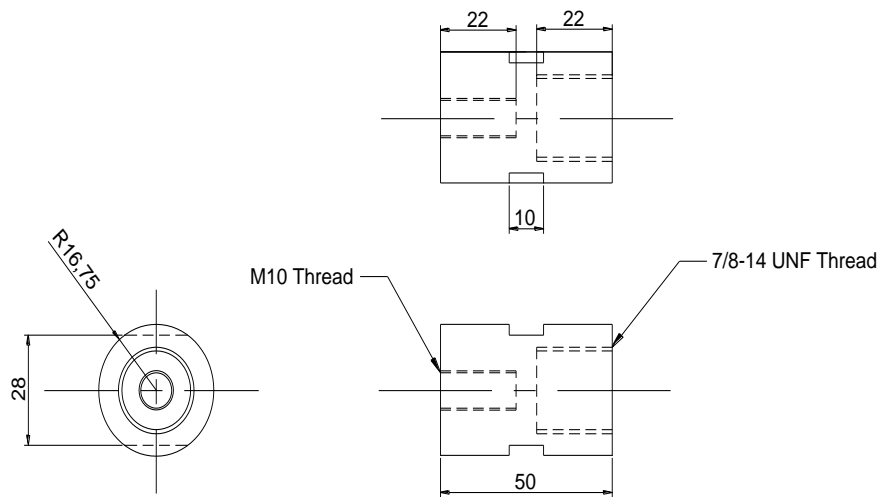
Bottom axial joint to cylinder connector
Material - Aluminum
Dimensions in mm
Jan 09
K.S.Grewal

R5

R50

R225

90° 120°

90°

120°

20
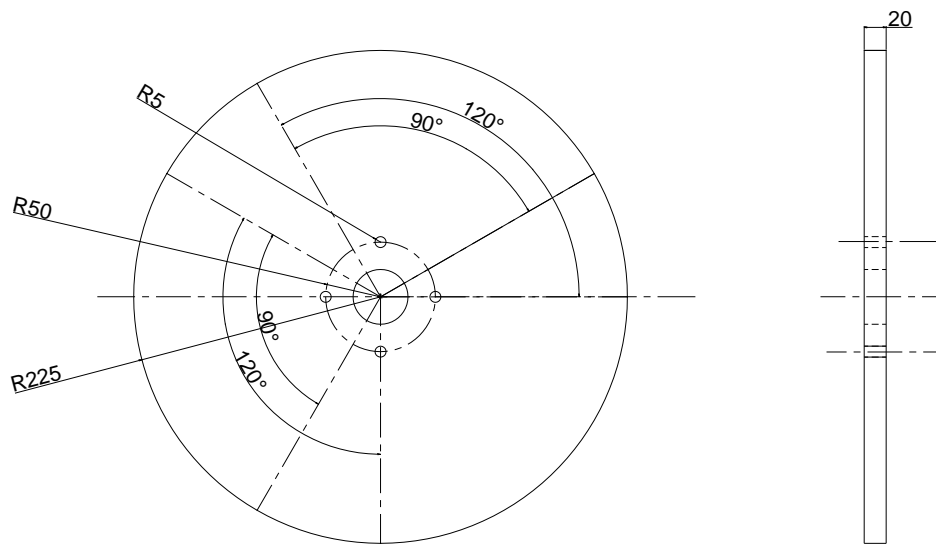
Bottom plate
(Fixed)
Material - Mild steel
Dimensions in mm
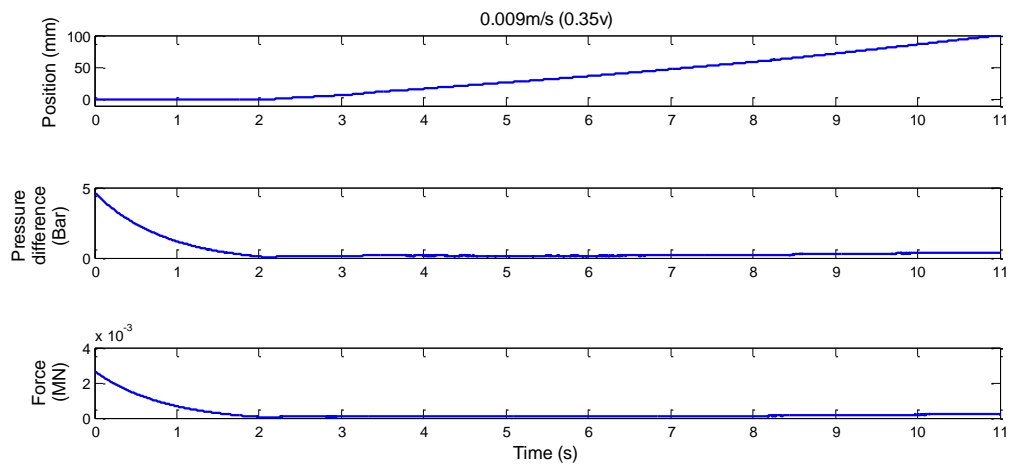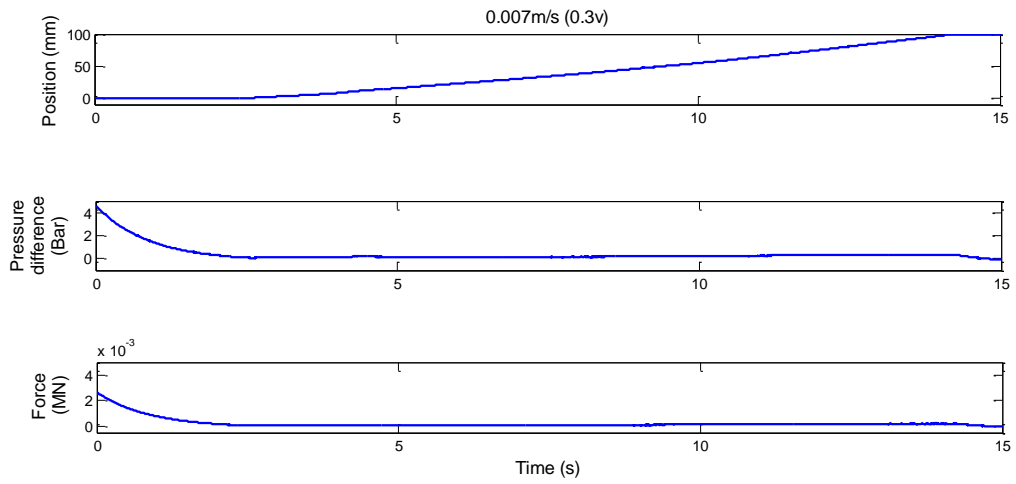Jan 09
K.S.Grewal

15

90° 120°

175

90°

120°
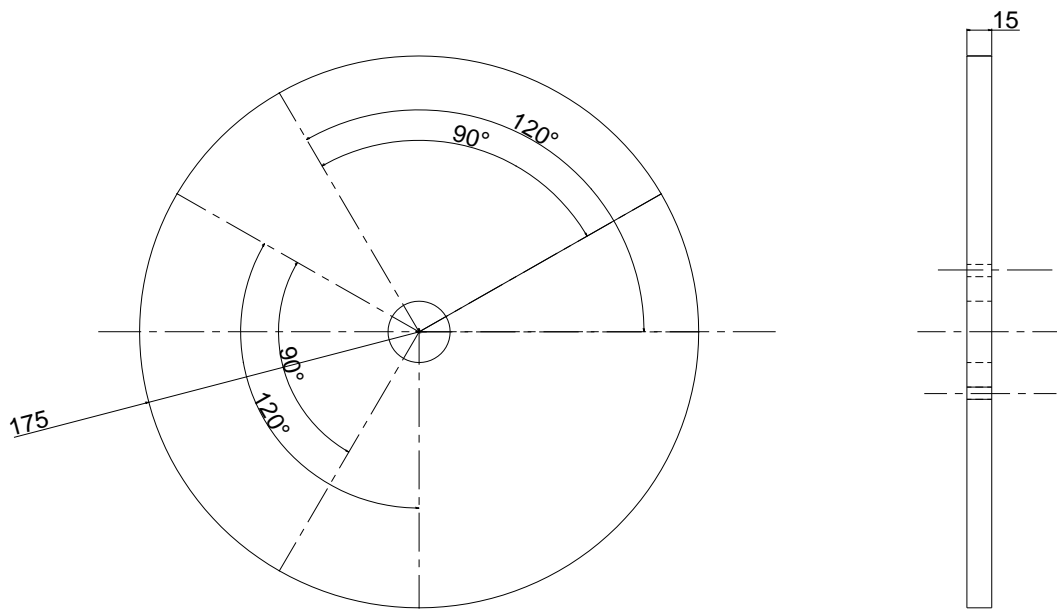
Top plate (Moveable)
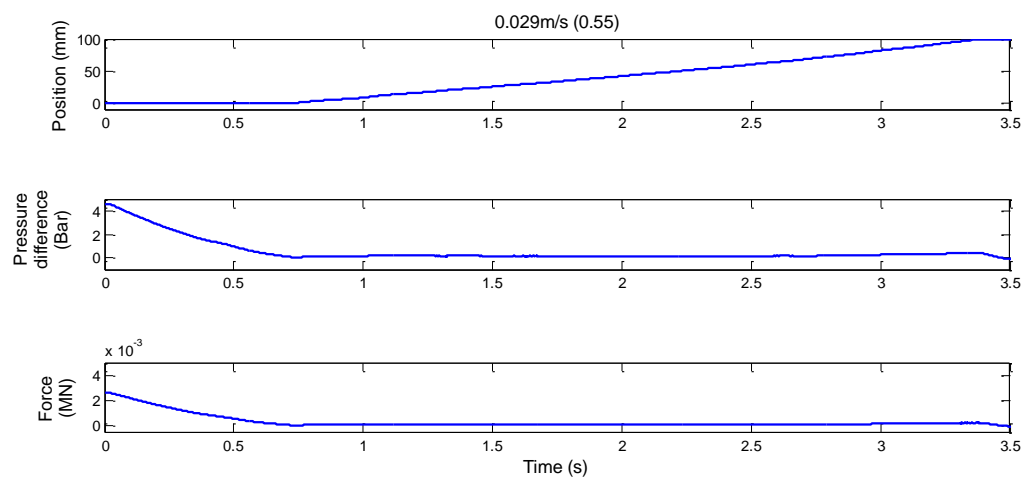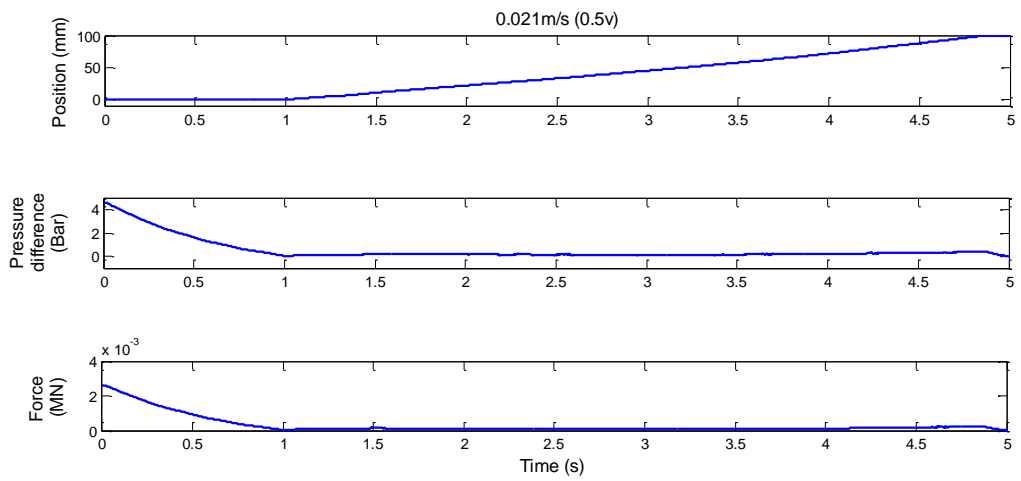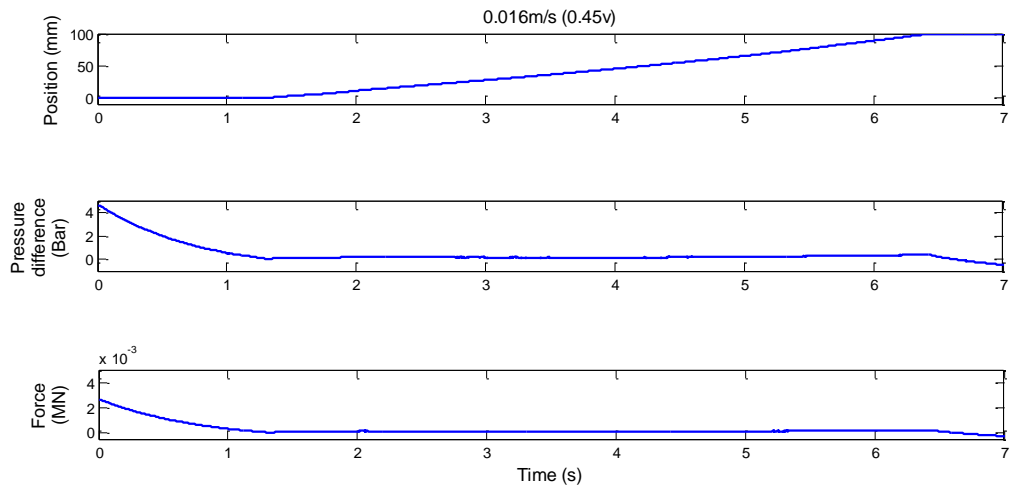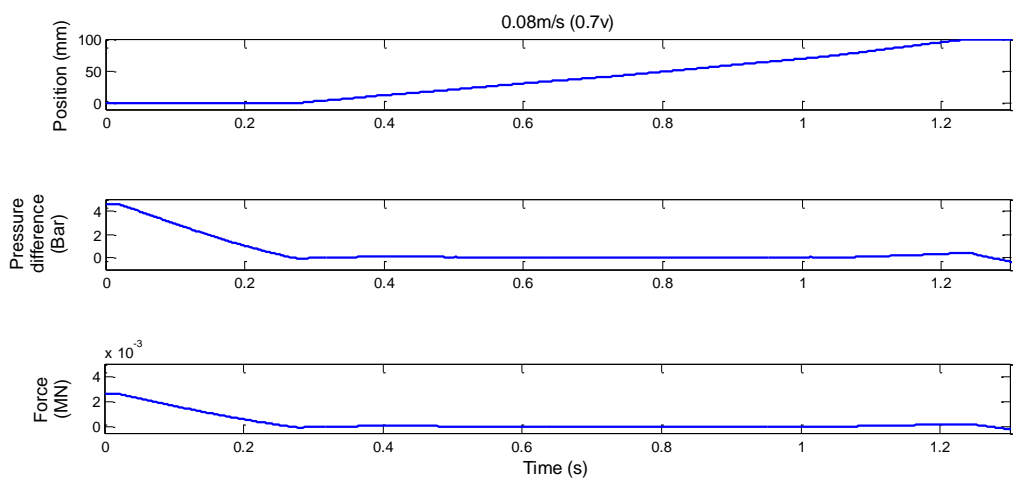Material - Aluminum
Dimensions in mm
Jan 09
K.S.Grewal

Appendix B

Friction identification plots

This section details all the friction identification plots in terms of velocity, position, pressure difference and force (chapter 4). The plots are summarised in Table B1.
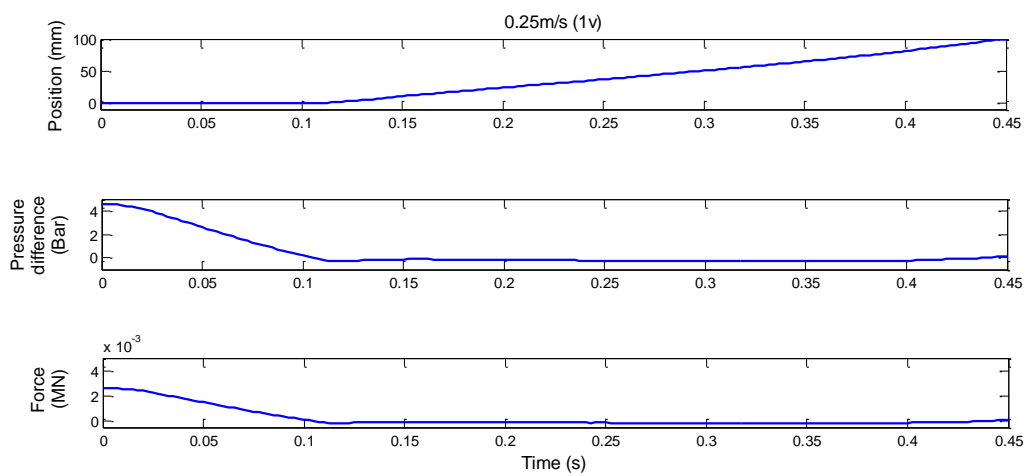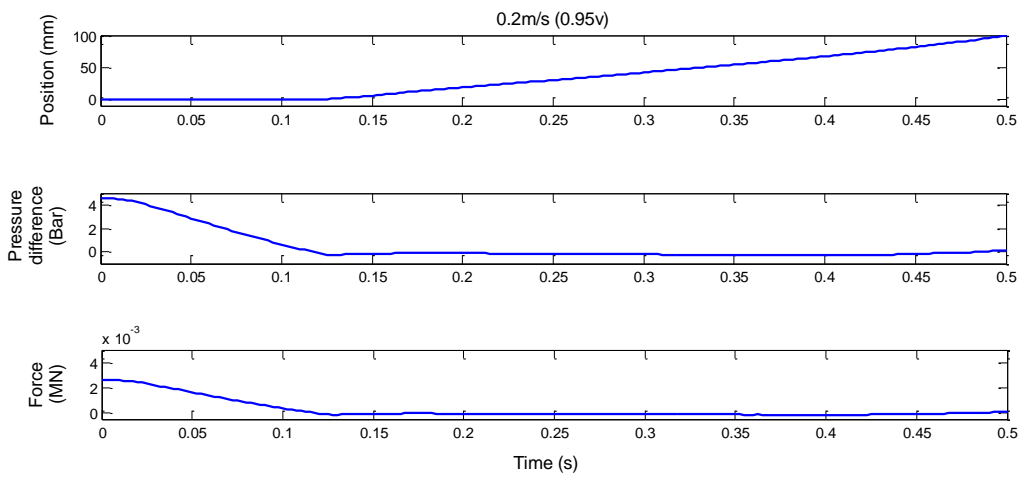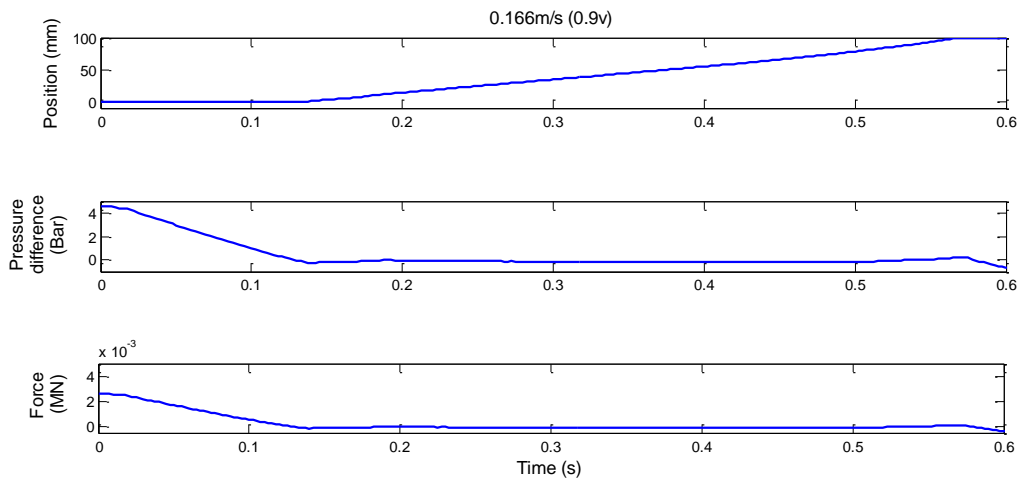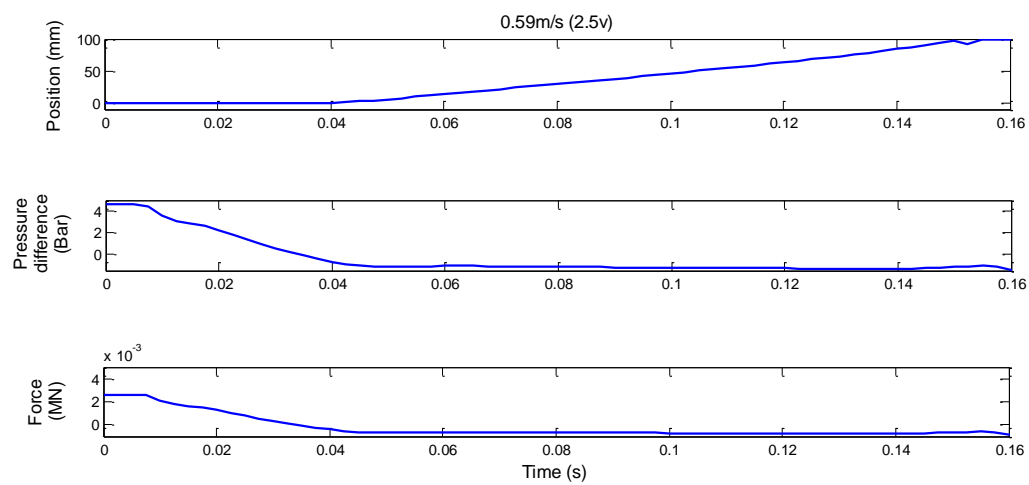
0.016m/s (0.45v)

0.021m/s (0.5v)

0.029m/s (0.55)

0.043m/s (0.6v)

0.057m/s (0.65v)

0.08m/s (0.7v)

0.11m/s (0.75v)

0.125m/s (0.8v)

0.143m/s (0.85v)

0.166m/s (0.9v)

0.2m/s (0.95v)

0.25m/s (1v)

0.71m/s (3v)

0.77m/s (3.5v)

0.85m/s (4v)

0.9m/s (4.5v)

1.1m/s (5v)
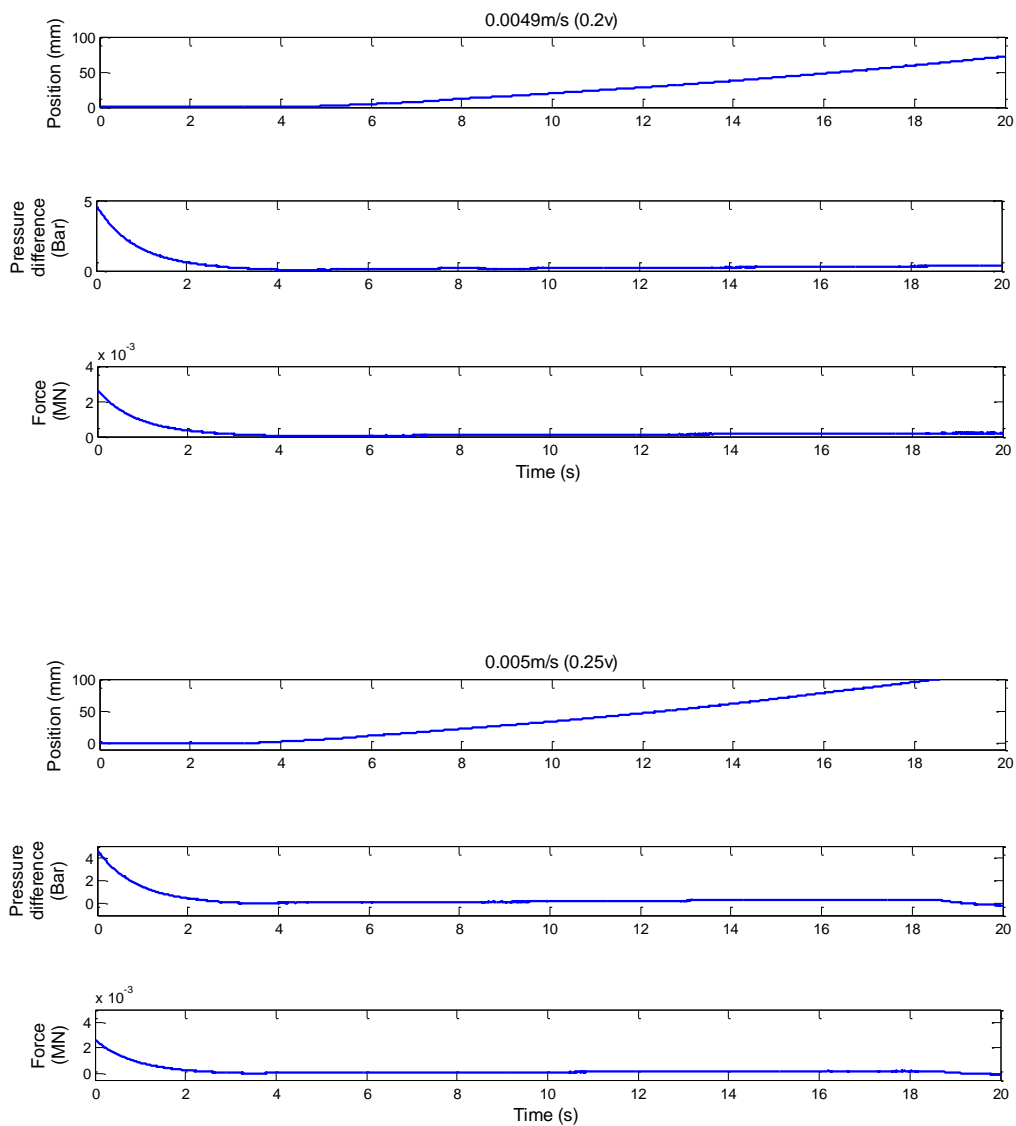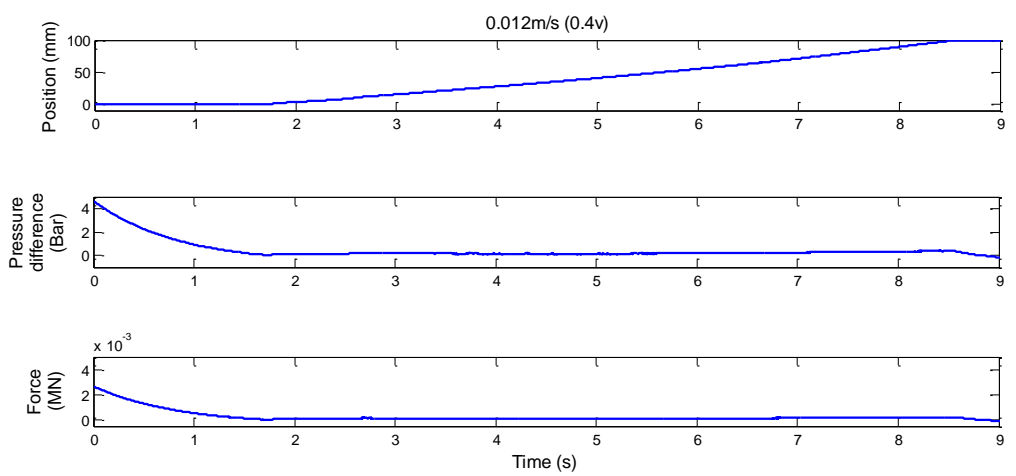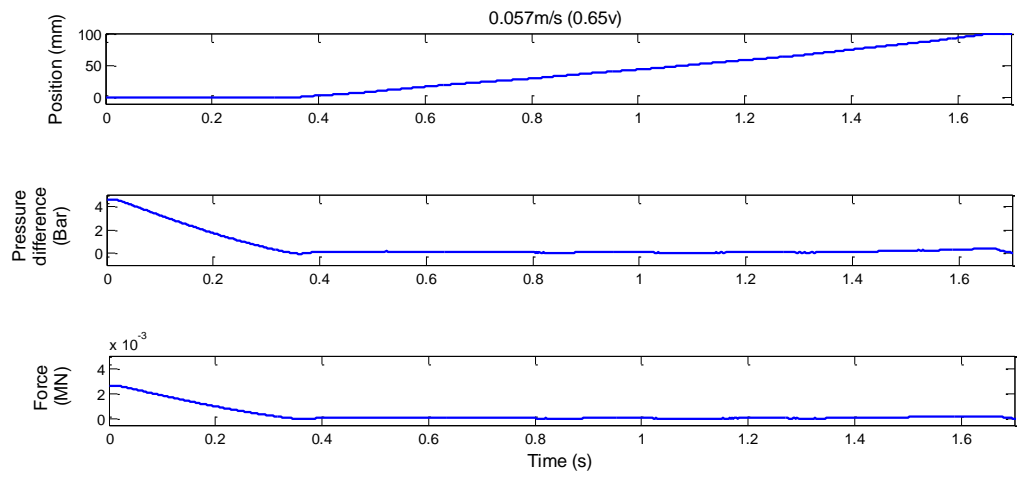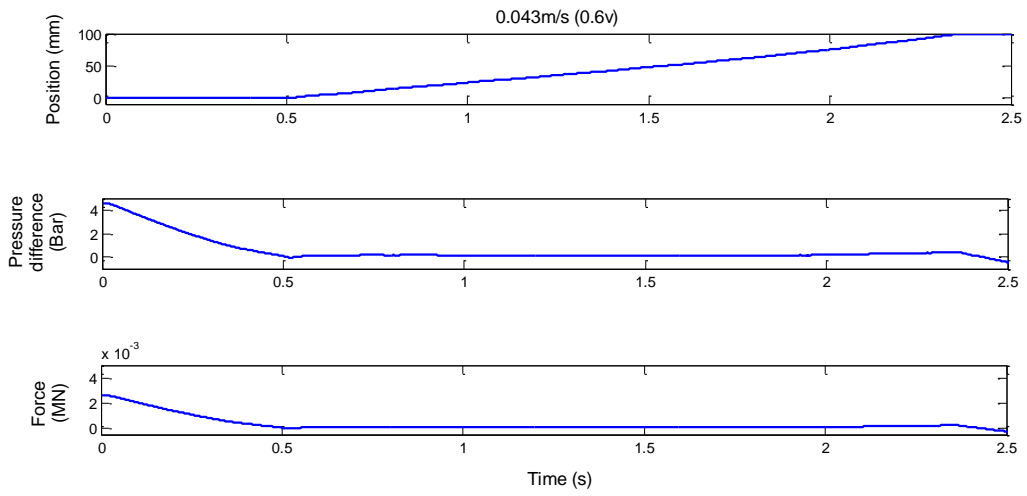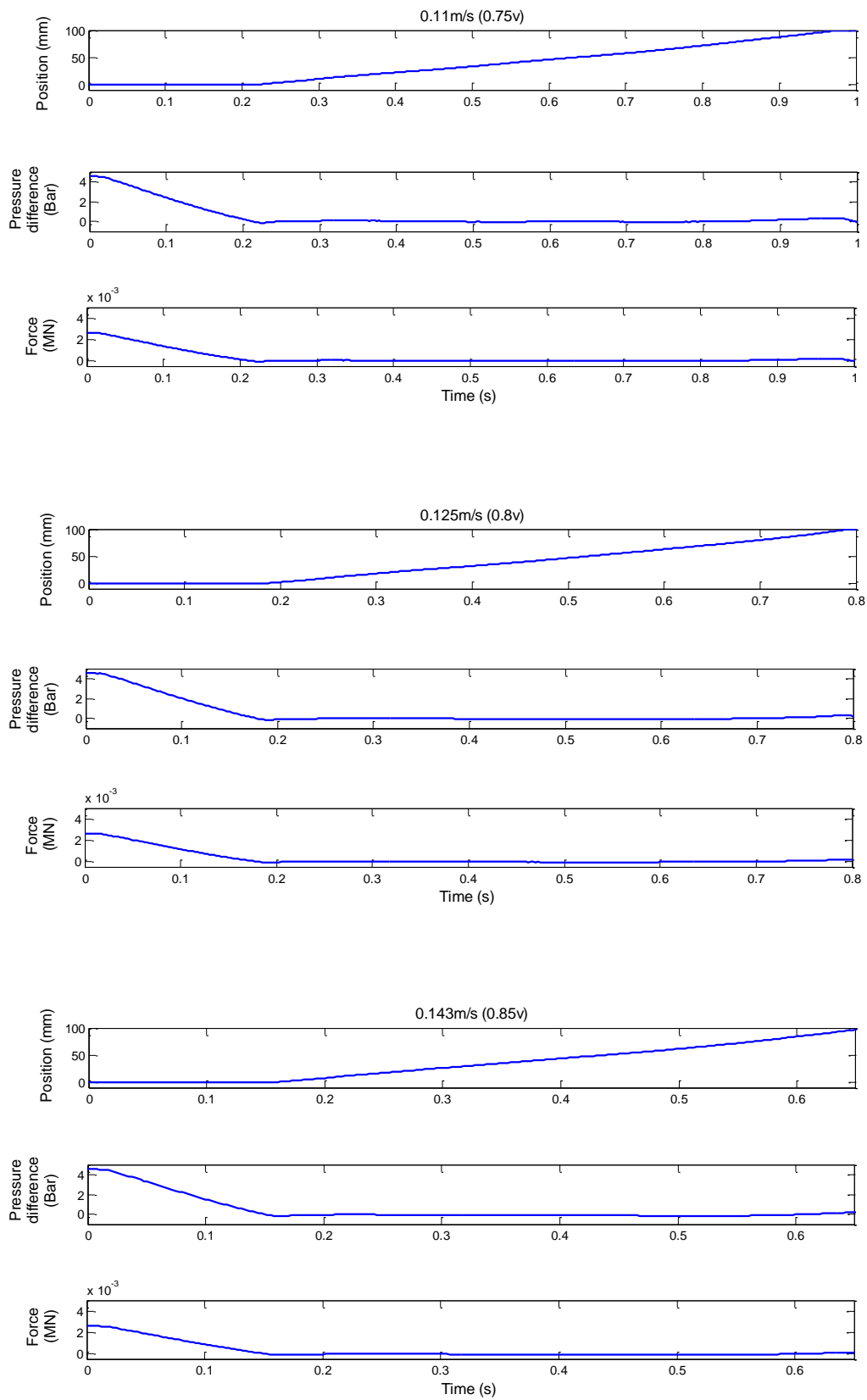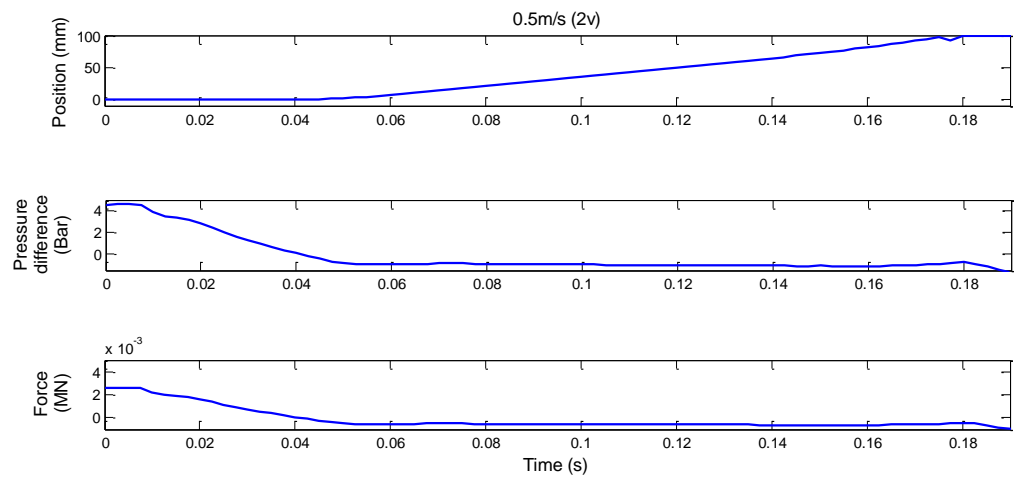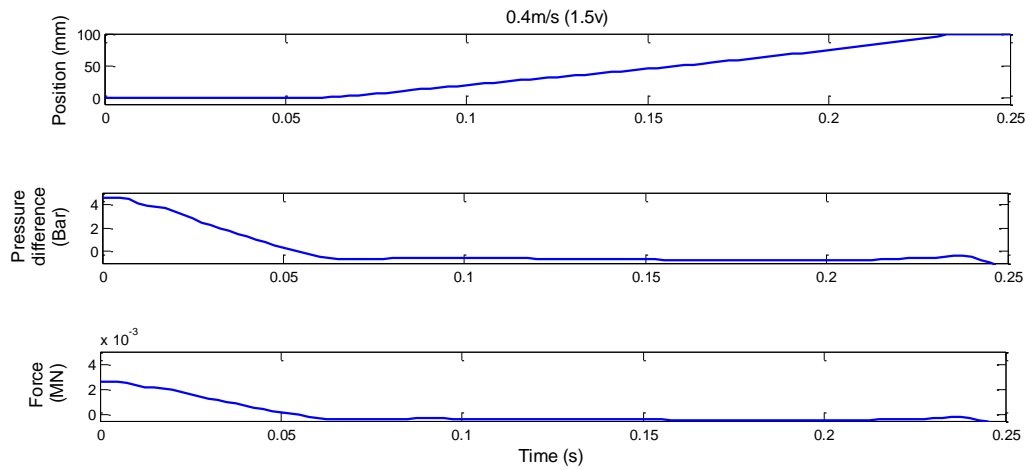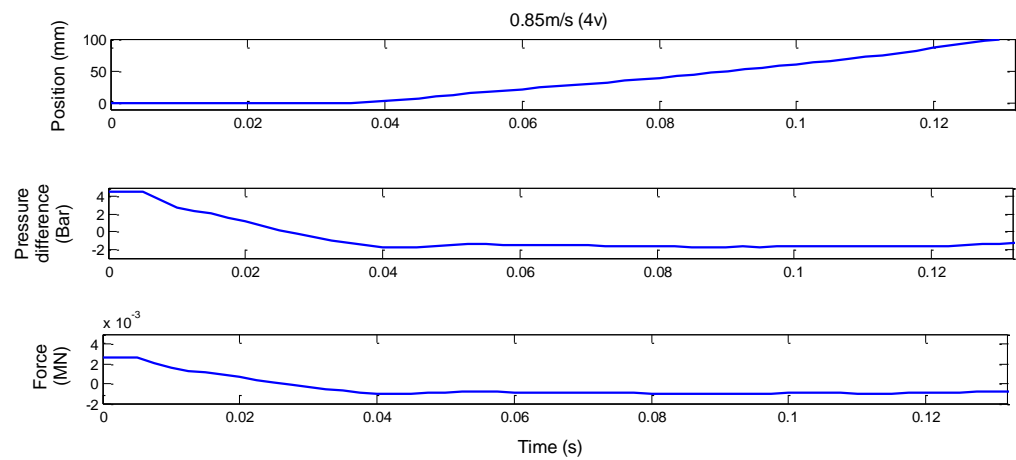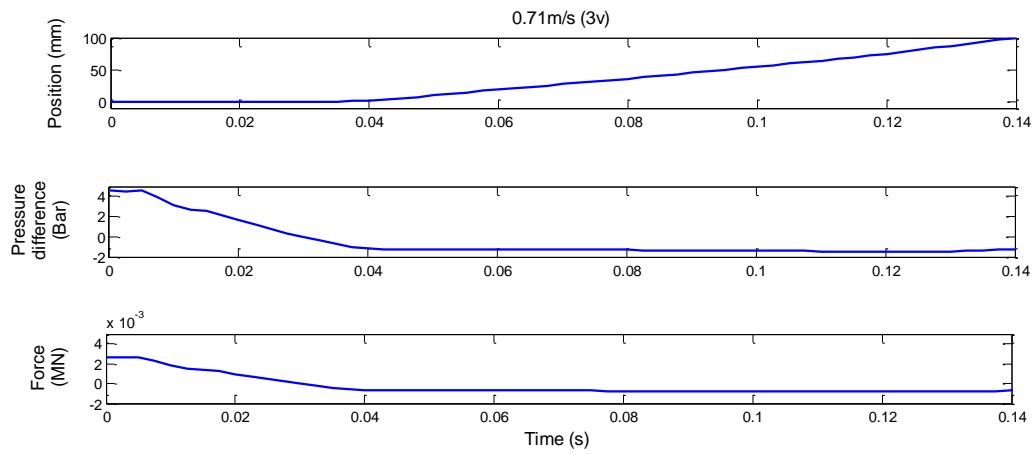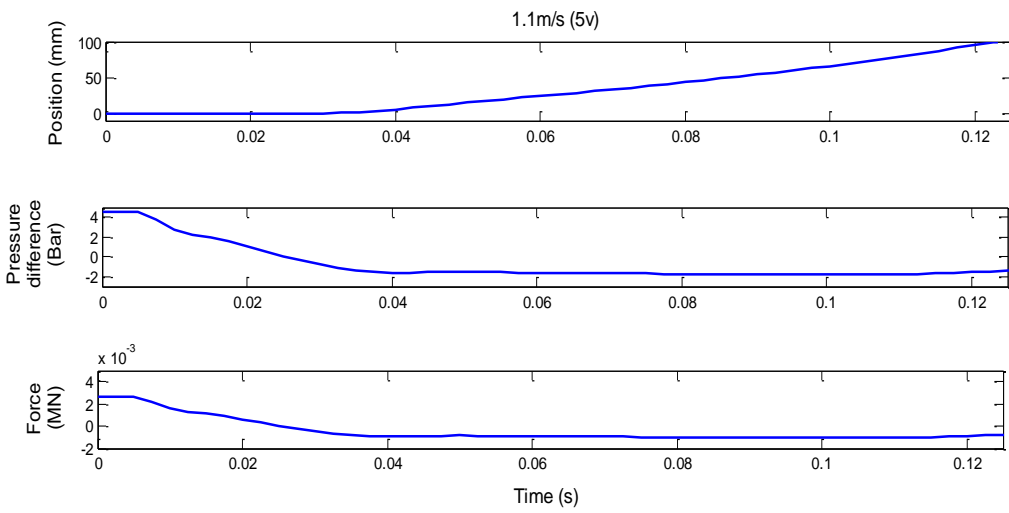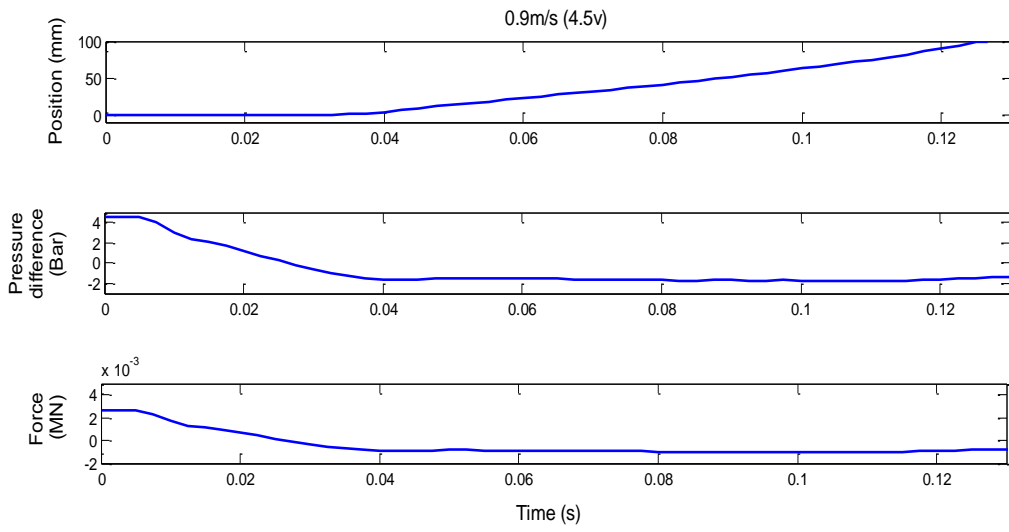
Table B1: Friction identification parameters

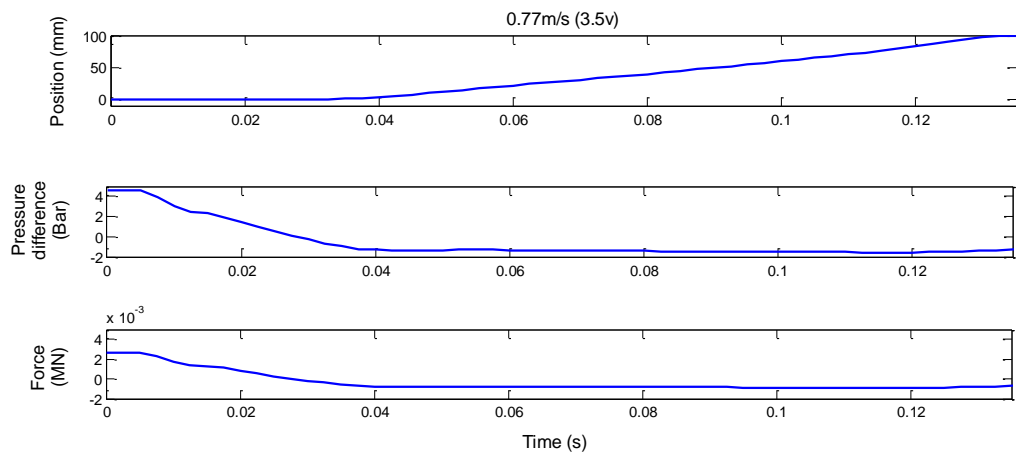| Input (v)	Velocity (m/s)	Pressure difference (bar)	Force (N)
0.1	0.0028	0.2	48
0.2	0.0049	0.193	14
0.25	0.005	0.19	13
0.3	0.007	0.174	12
0.35	0.009	0.17	10
0.4	0.012	0.165	9.5
0.45	0.016	0.16	9
0.5	0.021	0.154	8.5
0.55	0.029	0.118	6.5
0.6	0.043	0.114	6
0.65	0.057	0.085	5
0.7	0.08	0.043	2.5
0.75	0.11	0.046	1
0.8	0.125	0.073	5
0.85	0.143	0.122	7
0.9	0.166	0.155	8
0.95	0.2	0.225	10
1	0.25	0.27	14
1.5	0.4	0.7	42
2	0.5	1.04	60
2.5	0.59	1.24	70
3	0.71	1.385	73
3.5	0.77	1.47	80
4	0.85	1.71	96
4.5	0.9	1.723	100
5	1.1	1.73	108

Appendix C

Electrical component specification

This section details the electrical components used in chapter 3.

Host PC

The host PC is usually a desktop computer which has installed MATLAB®, Simulink®, Real-Time Workshop®, and xPC Target; a notebook computer may also be used.

Software Requirements for the Host PC -Table C1 lists the minimum software xPC Target requirements for the host PC.

Table C1: Minimum software requirements of xPC Target for host PC

Software	Description
Operating system MATLAB Simulink Real-Time Workshop	A Microsoft Windows platform supported by The MathWorks Version 6.5 Version 5.0 Version 5.0
C language compiler	Microsoft Visual C/C++ versions 5.0, 6.0, or 7.0 Watcom C/C++ versions 10.6 or 11.0
xPC Target	Version 2.0

Hardware Requirements for the Host PC- Table C2 lists the minimum resources xPC Target requires on the host PC.

Table C2: Minimum resources requirements of xPC Target for the host PC

Hardware	Description
Communication	One free serial port (COM1 or COM2) with a 9-pin or 25-pin D-sub connector, or an Ethernet card connected to a network
CPU	Pentium, Athlon or later
Peripherals	Hard disk drive with 60 Mbytes of free space One 3.5-inch floppy disk drive CD-ROM drive
RAM	128 Mbytes or more

Target PC

The target PC has to be a PC compatible system. For this work a second desktop computer is used as the target PC.

Software Requirements for the Target PC- Table C3 lists the minimum software xPC Target requires on the target PC system.

Table C3*: Minimum software requirements of xPC Target of the target PC system

Software	Description
Operating system	None. If you have an operating system installed on the target PC, the xPC Target kernel does not affect it.
BIOS	PC compatible

Hardware Requirements for the Target PC- Table C4 lists the minimum resources xPC Target requires on the target PC system.

Table C4: Minimum resources requirements of xPC Target of the target PC system

Hardware	Description
Chip set	PC compatible with UART, programmable interrupt controller, keyboard controller, and counter
Communication	One free serial port (COM1 or COM2) with a 9-pin or 25-pin D-sub connector or an Ethernet card connected to a network. The xPC Target software includes a serial null modem cable and an Ethernet card for the target PC
CPU	Intel 386/486/ Pentium or AMD K5/K6/Athlon with or without a floating point processor or unit. We recommend a Pentium, Athlon or later CPU
Keyboard and mouse	Needed to control the target PC when you create stand-alone applications **Note** If a keyboard is not connected, the BIOS may display an error message (keyboard failure). With a newer BIOS, you can use the BIOS set-up to skip the keyboard test.
Monitor	The recommendation is to use a monitor, but it is not necessary. You can get all of the target information using xPC Target functions on the host PC.
Peripheral	One 3.5 inch floppy disk drive. A hard disk drive is not required.
RAM	8 Mbytes or more

Table C5: Pneumatic cylinder engineering specifications

The Bimba® Position Feedback Cylinder Engineering specifications	
Repeatability	±0.0254mm (0.001") Cylinder Only
Non-linearity	± 1 percent of full stroke
Resolution	Infinite
Signal Input	10 VDC typical
Rated Life of LRT Wiper	1609344m (1000 miles) of travel
Input Impedance Required	1 MOhm
Signal Output	> 0 to slightly less than FS signal input (The internal electrical stroke is slightly larger than the mechanical stroke of cylinder)
Maximum speed:	0.635m/s
Rated Life of Probe	10 million cycles
Air Requirements	Filtered to 5 micron with 0 degree dew-point recommended. Moisture inside cylinder will cause output signal fluctuation
Pressure Rating	150 psi (10.34 bar)
Temperature Rating	0° to 200°F (-17.8° to 93.3°C)
Interface	153mm (6″) standard leads
Cylinder Body	304 stainless steel
Piston Rod	Hard chrome plated carbon steel with blackened threads and wrench flats
Rod Bushing	Sintered bronze
End Caps	Anodised Aluminium alloy
Piston Seal	Internally lubricated urethane
Rod Wiper	Internally lubricated Buna N (Nitrile) Excellent resistance to petroleum-based oils and fuels, water and alcohols
Rod Seal	Internally lubricated Buna N (Nitrile)

Table C6: 5/3-way directional proportional control valve

5/3-way directional proportional control valve technical data	
Valve function	5/3-way, normally closed
Constructional design	Piston spool, directly actuated, controlled piston spool position
Sealing principle	Hard
Actuation type	Electrical
Type of reset	Mechanical spring
Type of pilot control	Direct
Direction of flow	Non-reversible
Operating medium	Compressed air, filtered (to 5 μm), unlubricated
Standard nominal flow rate	700 l/min
Product weight	330 g
Power supply	17 … 30 VDC
Maximum current consumption: In mid-position At full stroke	 100 mA 1100 mA
Setpoint value Voltage type	10 V DC
Maximum hysteresis	0.4 %
Critical frequency	100 Hz

Table C7: Safety release valve technical specifications

General technical specifications	
Valve function	3/2-way valve with external pilot air supply
Normal operation	Closed
Pneumatic spring reset method	Yes
Mechanical spring reset method	No
Design	Piston spool
Sealing principle	Soft
Actuation type	Electric
Control type	Piloted
Pilot air supply	Internal or external
Direction of flow	Reversible for external pilot air supply
Exhaust function	Flow control
Standard nominal flow rate	400 [l/min]
Switching time on/off	14/14 [ms]
Operating medium	Filtered compressed air, lubricated or unlubricated, grade of filtration 40 μm
Operating pressure	2.5 … 8 [bar]
Pilot pressure	2.5 … 8 [bar]
Operating voltage	24 [V DC]+10/−15%
Power consumption	1.28 [W]
Cover material	Polyamide
Housing material	Die-cast aluminium

Appendix D

Matlab code

```
%-----------------------------------------------------%
%   Pneumatic System Model
%   06.06.08
%-----------------------------------------------------%

%Variables
 Area1=5.72e-4;%---------------%Bore area (m^2),
 y1=1.4;%---------------------%Ratio of specific heat,
 R1=287;%---------------------%Universal gas constant,
 Ts1=300;%--------------------%Temperature (Kelvin),
 K1=0.0023;%------------------%Pressure regulator constant (kg/s),
 m1=0.3;%---------------------%Piston mass (kg),
 Ppo1=3.1e5;%-----------------%Nominal pressure in chamber p (Pa),
 Pno1=3.1e5;%-----------------%Nominal pressure in chamber n (Pa),
 Vpo1=2.863e-5;%--------------%Nominal volume in chamber p (m^3),
 Vno1=2.075e-5;%--------------%Nominal volume in chamber n (m^3),
 Ff1=47;%--------------------%Friction forces (N/m^2),(Viscous
friction, coulomb friction)
 a1=(-y1*Area1*Ppo1)/Vpo1;
 b1=(y1*Area1*Pno1)/Vno1;
 c1=(K1*y1*R1*Ts1)/Vpo1;
 d1=(-K1*y1*R1*Ts1)/Vno1;

 A1=[0 0 (a1-b1)
    0 0 1
    Area1/m1 0 -Ff1/m1];

 B1=[(c1-d1)
     0
     0];

 C_vel1=[0 0 1];

 C_pos1=[0 1 0];

 C_presdiff1=[1 0 0];

 D=0;
 ------------------------------------------------------------------
 %PI Controller gains
 Kp=0.12;
 Ki=0.1;
 ------------------------------------------------------------------
 %Kalman variables

 Area=5.72e-4;%---------------%Bore area (m^2),
 y=1.4;%---------------------%Ratio of specific heat,
 R=287;%---------------------%Universal gas constant,
 Ts=300;%--------------------%Temperature (Kelvin),
 K=0.0023;%------------------%Pressure regulator constant (kg/s),
 m=0.3;%--------------------%Piston mass (kg),
```

```
 Ppo=3.1e5;%-----------------%Nominal pressure in chamber p (Pa),
 Pno=3.1e5;%-----------------%Nominal pressure in chamber n (Pa),
 Vpo=2.863e-5;%--------------%Nominal volume in chamber p (m^3),
 Vno=2.075e-5;%--------------%Nominal volume in chamber n (m^3),
 Ff=47;%--------------------%Friction forces (N/m^2),(Viscous friction,
coulomb friction)
 a=(-y*Area*Ppo)/Vpo;
 b=(y*Area*Pno)/Vno;
 c=(K*y*R*Ts)/Vpo;
 d=(-K*y*R*Ts)/Vno;

 A=[0 0 (a-b)
    0 0 1
    Area/m 0 -Ff/m];

 B=[(c-d)
     0
     0];

 C_vel=[0 0 1];

 C_pos=[0 1 0];

 C_presdiff=[1 0 0];

 D=0;

 G=[B1];
 ts=1e-4;
 process_var=2e-7;
 meas_var=1e-6;
 process_var_pr=1e-6;
 meas_var_pr=1;



[L,q,Ee]=lqe(A,G,C_pos,process_var*eye(1),meas_var)

Am=[0 (a-b)
    Area/m -Ff/m];
Bm=[(c-d)
      0];
Gm=Bm;
C_vel_m=[0 1];
C_presdiff_m=[1 0];

[Li,q,Ee]=lqe(Am,Gm,C_vel_m,process_var*eye(1),meas_var)

Gm=[1 0;0 1]
[Lii,q,Ee]=lqe(Am,Gm,C_presdiff_m,diag([10 1e-5]),meas_var_pr)

 ------------------------------------------------------------------
%lqg controller

Q2=12;

R=1e-5;
Q1=C_pos1'*C_pos1;
```

```
Q=Q2*Q1;
%check for controllability;
rank_of_M=rank(ctrb(A,B))
system_order=length(A)
[K,S,e]=lqr(A,B,Q,R)
K2=20;
```

```
%----------------------------------------------------%
%   Calculate leg lengths using alpha,beta,gamma,X,Y,Z
%   06.02.09
%----------------------------------------------------%
```

```
function [Length,L,B,Pf,R] = Calc_length(i,alpha,beta,gamma,X,Y,Z)
% This block supports the Embedded MATLAB subset.
% See the help menu for details.

rp=155;
rb=185;

lam = [0 0 0 0 0 0];
Del = [0 0 0 0 0 0];

%Lambda matrix
lam(1) = ((pi/3)-(pi/4));
lam(2) = lam(1) + (pi/2);
lam(3) = (((3*pi)/3)-(pi/4));
lam(4) = lam(3) + (pi/2);
lam(5) = (((5*pi)/3)-(pi/4));
lam(6) = lam(5) + (pi/2);

Del(1) = (pi/3) - (pi/12);
Del(2) = Del(1) + (pi/6);
Del(3) = ((3*pi)/3) - (pi/12);
Del(4) = Del(3) + (pi/6);
Del(5) = ((5*pi)/3) - (pi/12);
Del(6) = Del(5) + (pi/6);

% R matrix values
r11 =  cos(alpha)*cos(beta);
r12 = (cos(alpha)*sin(beta)*sin(gamma))-(sin(alpha)*cos(gamma));
r13 = (cos(alpha)*sin(beta)*cos(gamma))+(sin(alpha)*sin(gamma));
r21 = (sin(alpha)*cos(beta));
r22 = (sin(alpha)*sin(beta)*sin(gamma))+(cos(alpha)*cos(gamma));
r23 = (sin(alpha)*sin(beta)*cos(gamma))-(cos(alpha)*sin(gamma));
r31 =  -sin(beta);
r32 =  cos(beta)*sin(gamma);
r33 =  cos(beta)*cos(gamma);

R = [r11 r12 r13;r21 r22 r23;r31 r32 r33];

% P Matrix Values
P = [rp*cos(lam(i)) rp*sin(lam(i)) 0];
```

241

```
% B Matrix Values
B = [rb*cos(Del(i)) rb*sin(Del(i)) 0];


L = (R*P')+([X Y Z]'-B');
Pf = B' + L;
Length = sqrt((L(1)^2)+(L(2)^2)+(L(3)^2));
%Lengthsqrd = X^2 + Y^2 + Z^2 + rp^2 +
rb^2+(P(3)^2)+(2*((r11*P(1))+(r12*P(2))+(r13*P(3)))*(X-B(1)))+
(2*((r21*P(1))+(r22*P(2))+(r23*P(3)))*(Y-B(2)))+
(2*((r31*P(1))+(r32*P(2))+(r32*P(3)))*(Z-B(3)))- (2*((X*B(1))) +
(Y*B(2))+ (Z*B(3)));
%Length = sqrt(Lengthsqrd);
```

```
%-----------------------------------------------------------%
%   Plot leg lengths using alpha,beta,gamma,X,Y,Z as inputs
%   06.02.09
%-----------------------------------------------------------%



alpha = 0;
beta = 0;
gamma = 0;
X = 30;
Y = 0;
Z = 400;
Length = [0 0 0 0 0 0];
L = zeros(6,3);
B = zeros(6,3);
P = zeros(6,3);

for i=1:6
    [Length(i),L(i,:),B(i,:),P(i,:),R] =
Calc_length(i,alpha,beta,gamma,X,Y,Z);
end

figure;
plot3([B(1,1) P(1,1)],[B(1,2) P(1,2)],[B(1,3) P(1,3)],'b',...
    [B(2,1) P(2,1)],[B(2,2) P(2,2)],[B(2,3) P(2,3)],'k',...
    [B(3,1) P(3,1)],[B(3,2) P(3,2)],[B(3,3) P(3,3)],'r',...
    [B(4,1) P(4,1)],[B(4,2) P(4,2)],[B(4,3) P(4,3)],'y',...
    [B(5,1) P(5,1)],[B(5,2) P(5,2)],[B(5,3) P(5,3)],'g',...
    [B(6,1) P(6,1)],[B(6,2) P(6,2)],[B(6,3) P(6,3)],'m',...
    [0 0],[0 0],[0 450],'--k',...
    [P(1,1) P(2,1)],[P(1,2) P(2,2)],[P(1,3) P(2,3)],'b',...
    [P(2,1) P(3,1)],[P(2,2) P(3,2)],[P(2,3) P(3,3)],'b',...
    [P(3,1) P(4,1)],[P(3,2) P(4,2)],[P(3,3) P(4,3)],'b',...
    [P(4,1) P(5,1)],[P(4,2) P(5,2)],[P(4,3) P(5,3)],'b',...
    [P(5,1) P(6,1)],[P(5,2) P(6,2)],[P(5,3) P(6,3)],'b',...
    [P(6,1) P(1,1)],[P(6,2) P(1,2)],[P(6,3) P(1,3)],'b');
```

Appendix E

Simulation results

E.1 Single actuator simulation results

Detailed below are the results for the designed FDI and fault management scheme for the single actuator simulation model.

E1.1 Actuator fault – control signal loss

A fault Fa(s) (see Figure 7.2) is applied to the proportional valve. The fault injected is that the control signal has been disconnected at time 15.5s. Figures E.1- E.3 shows the time histories of this experiment (actuator fault) for the parity equation scheme. Figures E.4 - E.5 shows the time histories of this experiment (actuator fault) for the Kalman filter scheme. The time history of the weighted average outputs of the voting scheme is shown in Figure E.6.
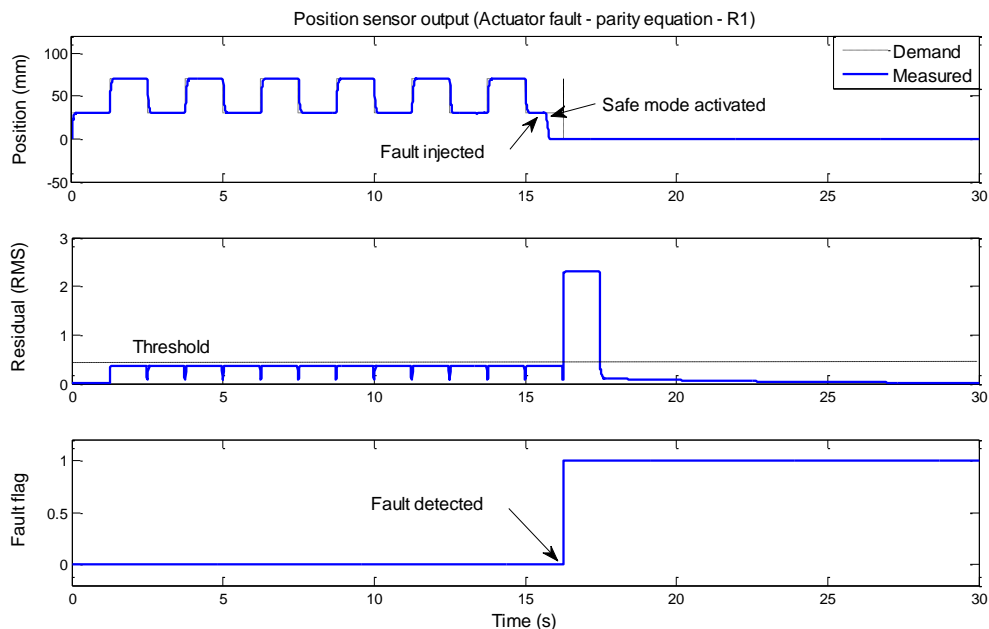
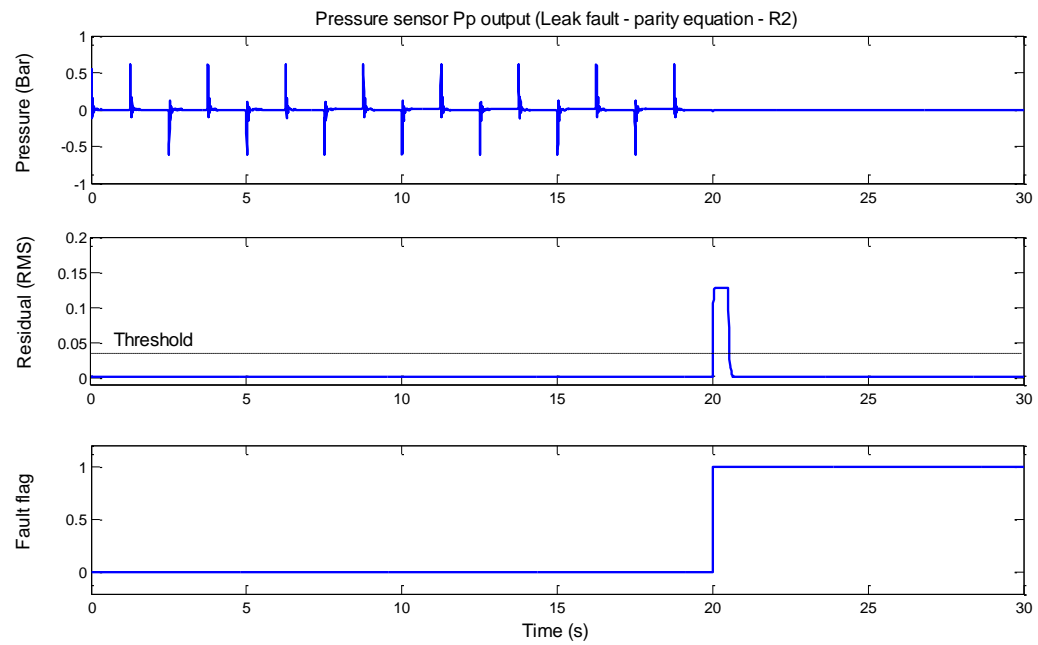Figure E.1: Actuator fault, parity equation - position sensor output (R_1)
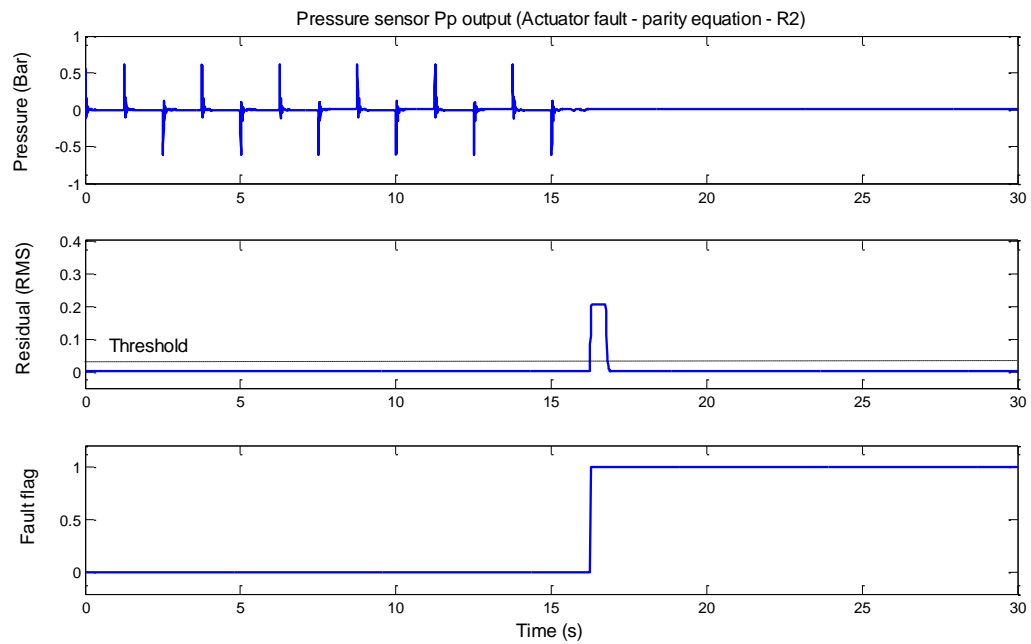
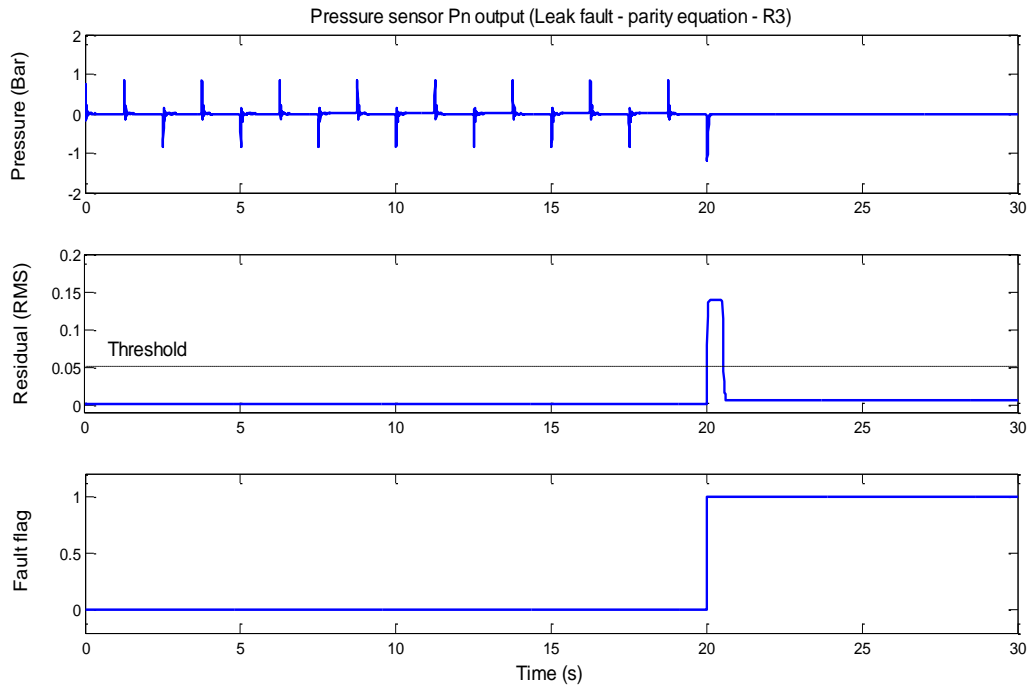Figure E.2: Actuator fault, parity equation – Pressure sensor (Pp) output (R_2)
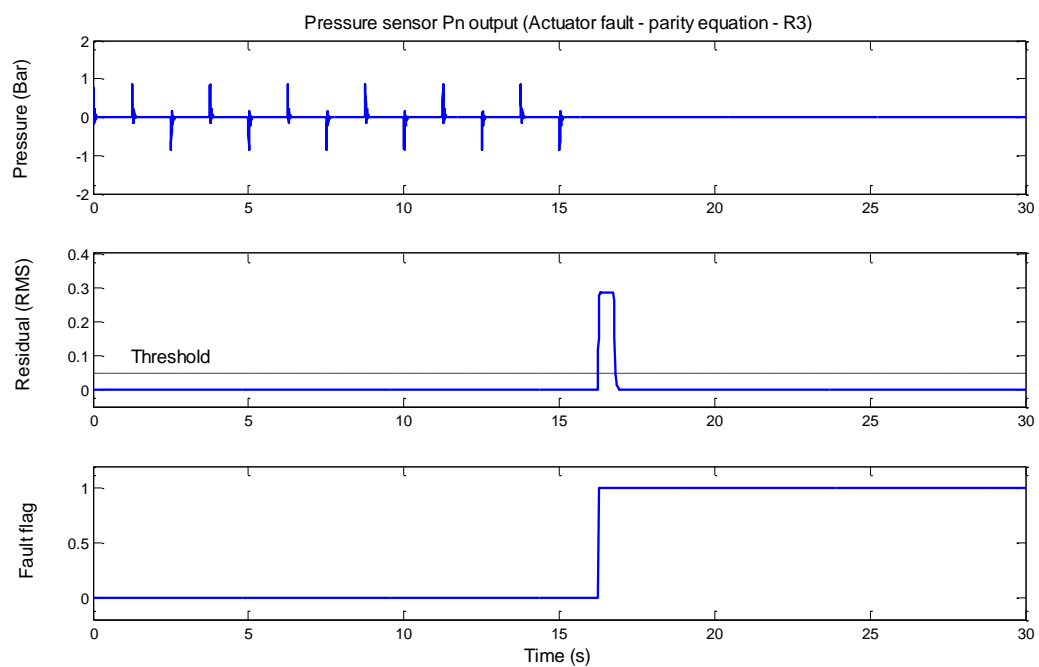
Figure E.3: Actuator fault, parity equation – Pressure sensor (Pn) output (R_3)
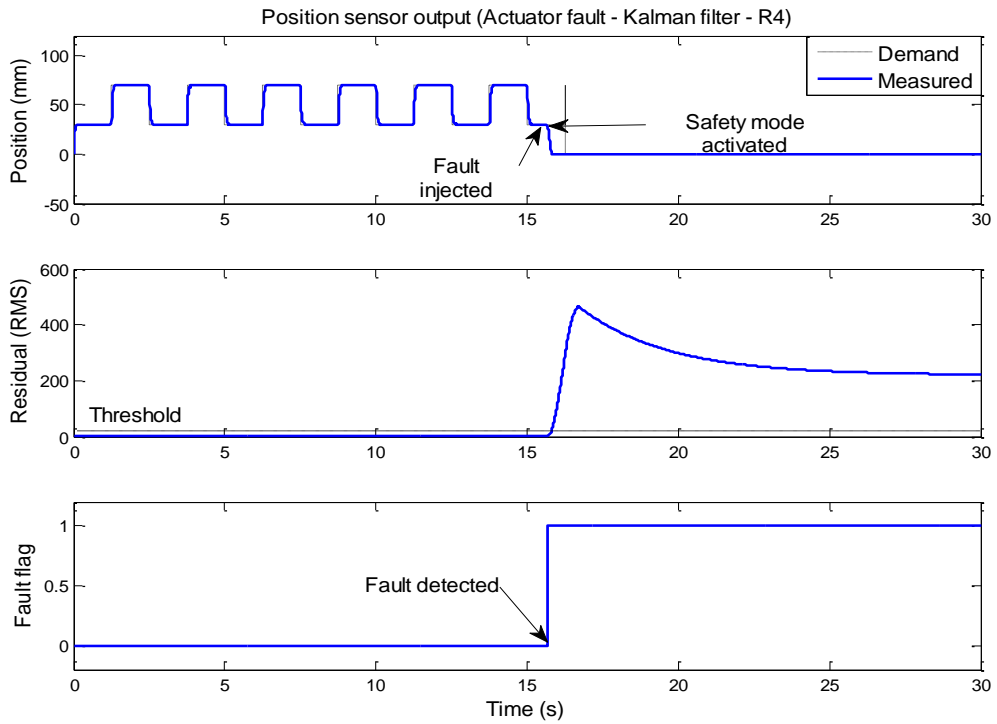
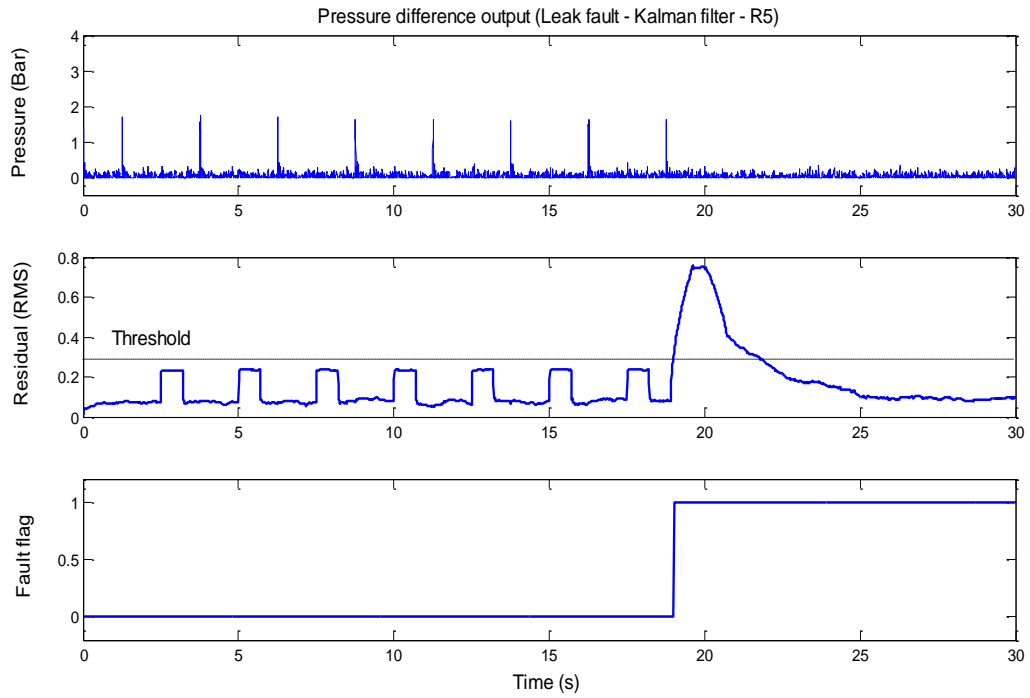Figure E.4: Actuator fault, Kalman filter – Position sensor output (R_4)
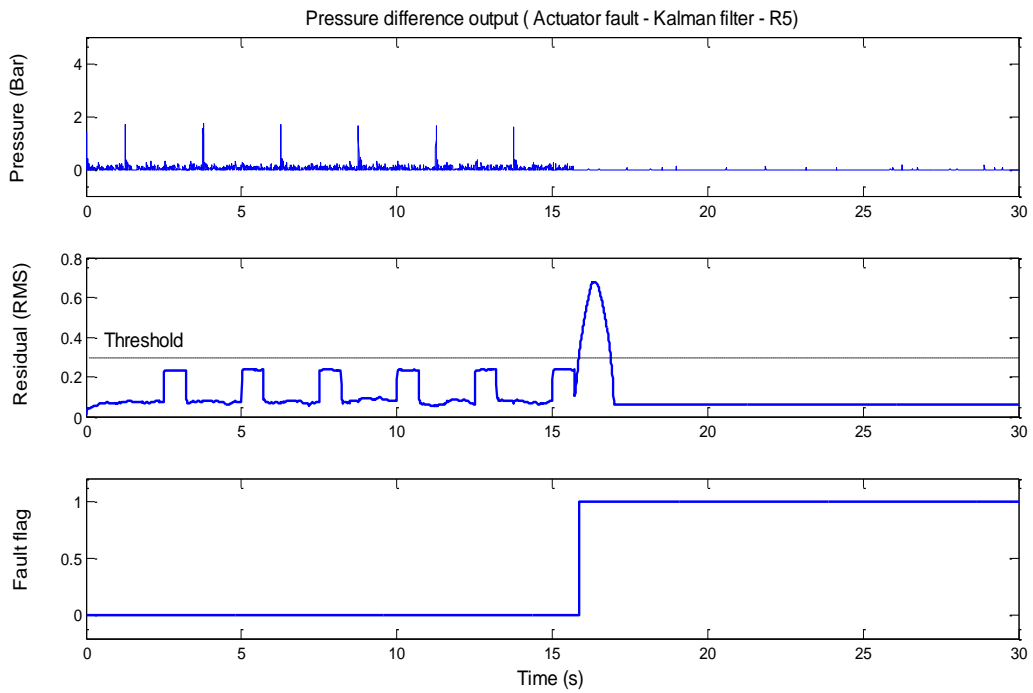
Figure E.5: Actuator fault, Kalman filter – Pressure difference output (R_5)
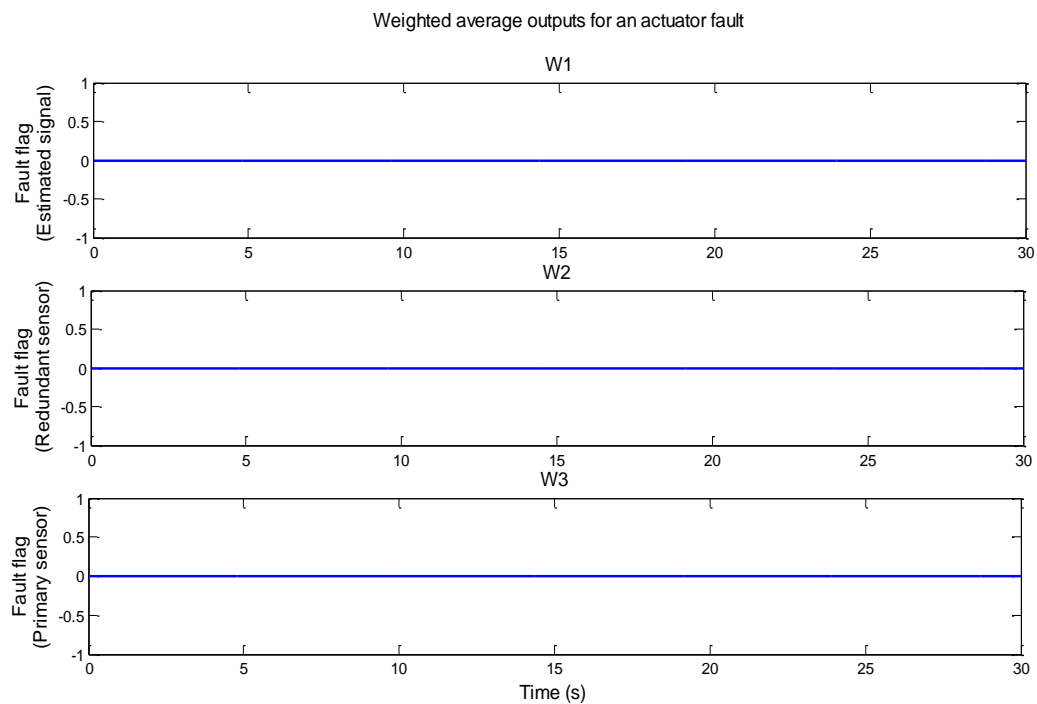
Figure E.6: Weighted average outputs for an actuator fault

E.1.1.1   *Discussion - Actuator fault (control signal loss)*

Applying the disconnection fault to the control signal of the proportional valve has an effect on the parity residual (R_1), this raises the fault flag. The fault has an effect on the pressure sensor parity residuals (R_2 and (R_3). Both position and pressure difference Kalman residuals (R_4 and R_5) are affected by the actuator fault and their fault flags are raised. Residuals w_1, w_2 and w_3 are not affected and the respective fault flags remain low. This agrees with the fault signatures detailed in Table 7.2.

E.1.2   *Air leak*

A leak fault is applied at 18s. Figures E.7-E.9 shows the time histories of the leak fault for the parity equation scheme. Figure E.10-E.11 shows the time histories of the leak fault for the Kalman filter scheme. Figure E.12 details the time history of the weighted average outputs of the voting scheme.
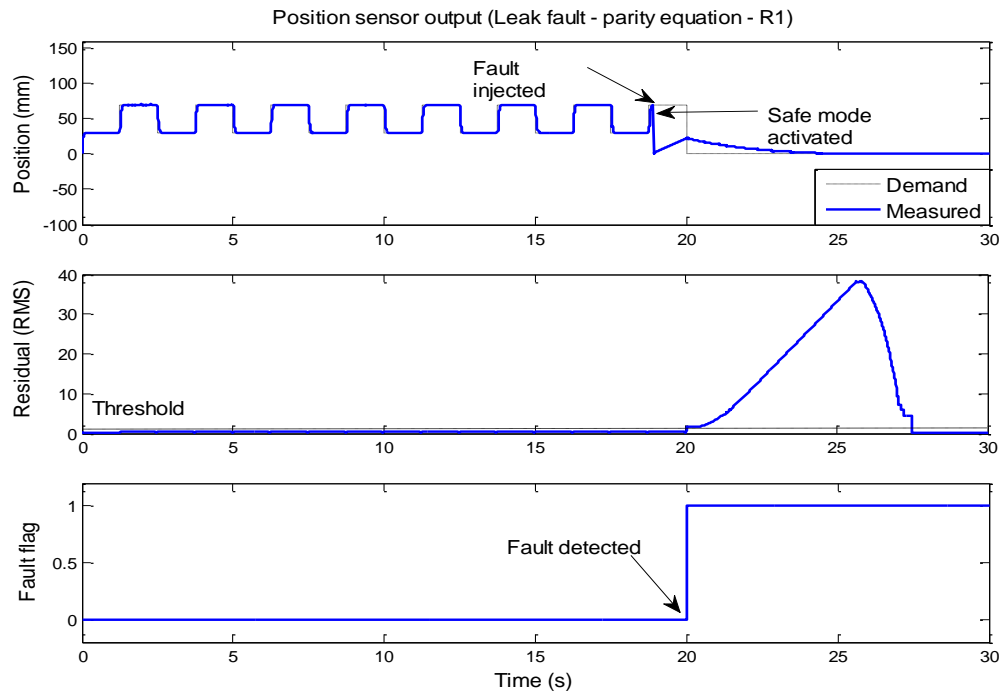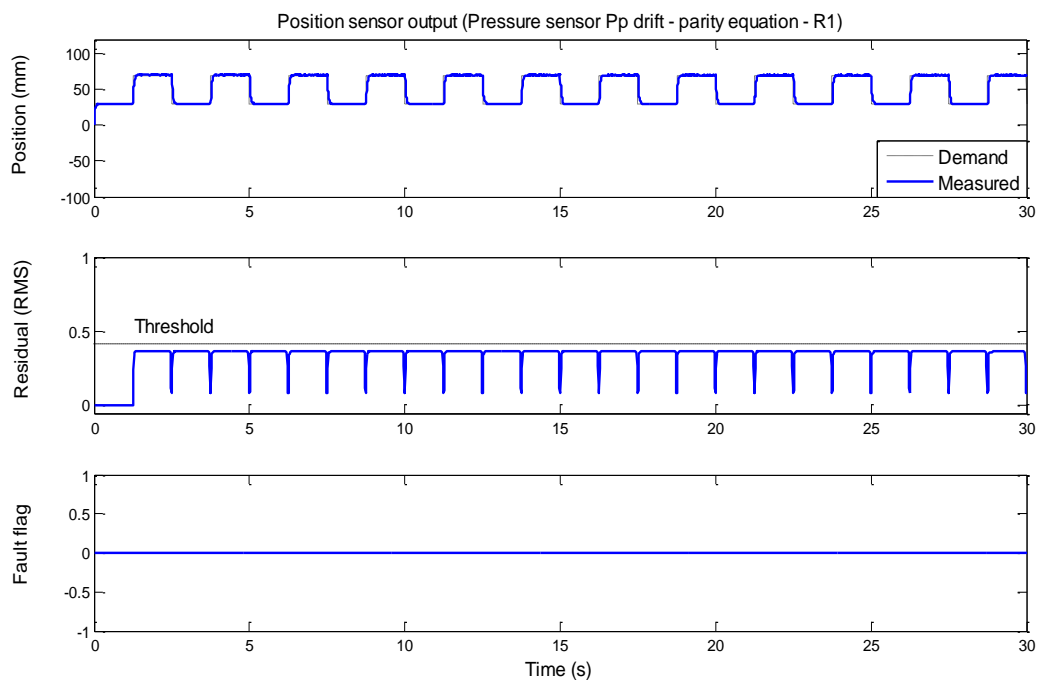
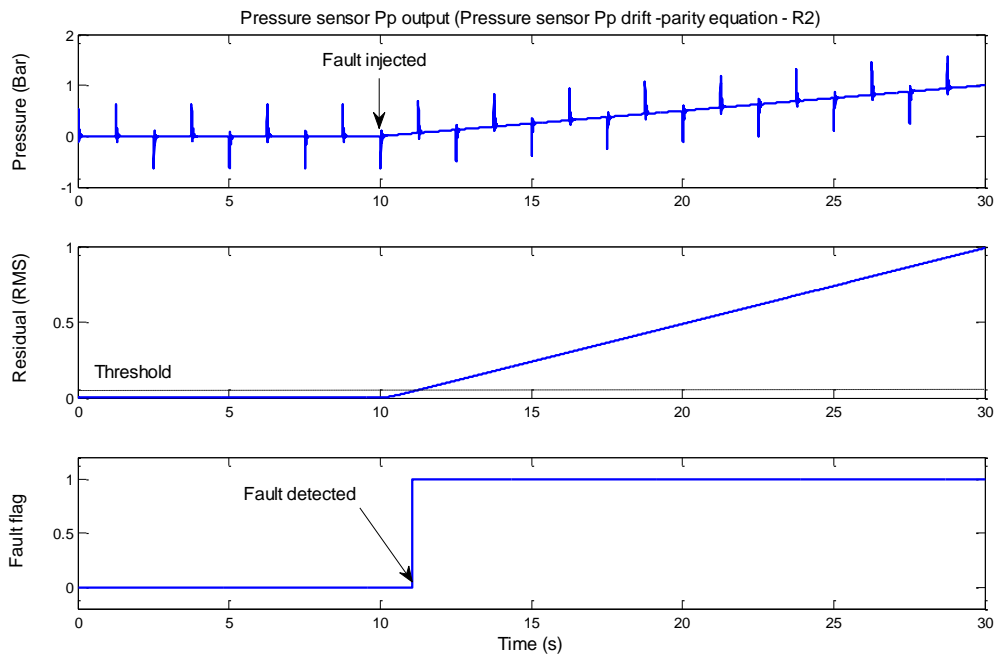Figure E.7: Leak fault, parity equation - Position sensor output (R_1)

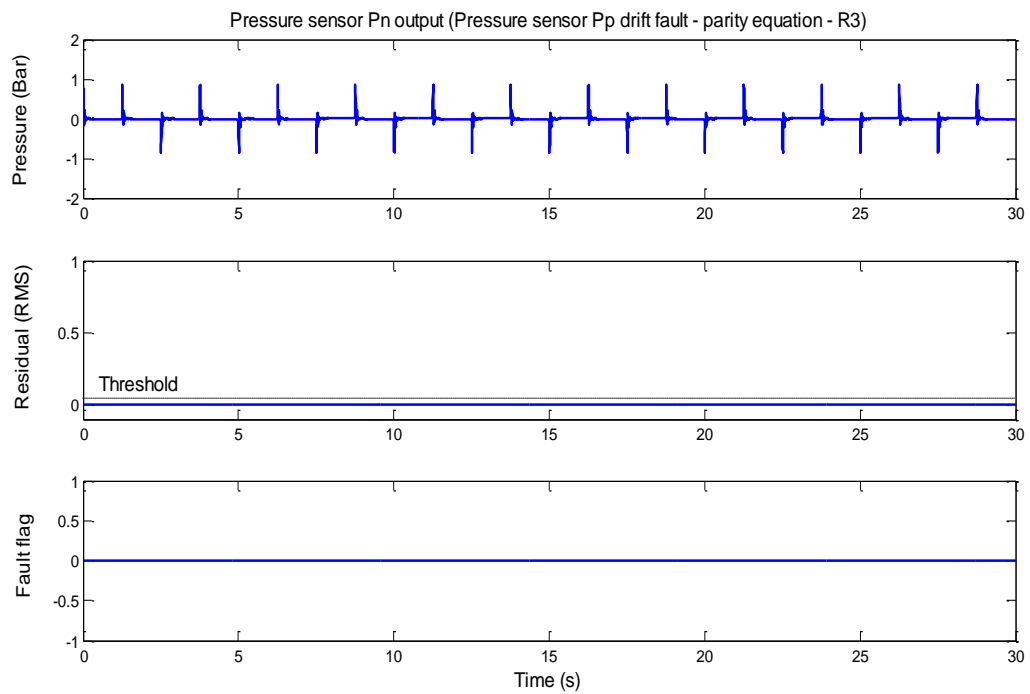Figure E.8: Leak fault, parity equation - Pressure sensor (Pp) output (R_2)

Figure E.9: Leak fault, parity equation - Pressure sensor (Pn) output (R_3)
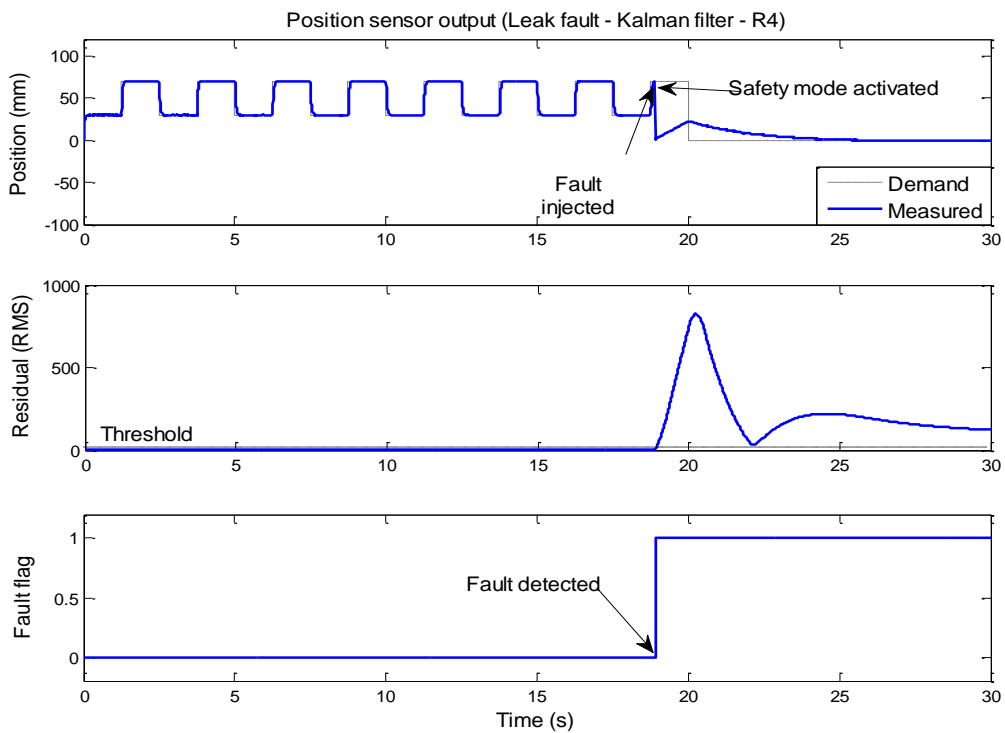
Figure E.10: Leak fault, Kalman filter- Position sensor output (R_4)

Figure E.11: Leak fault, Kalman filter- Pressure difference output (R_5)
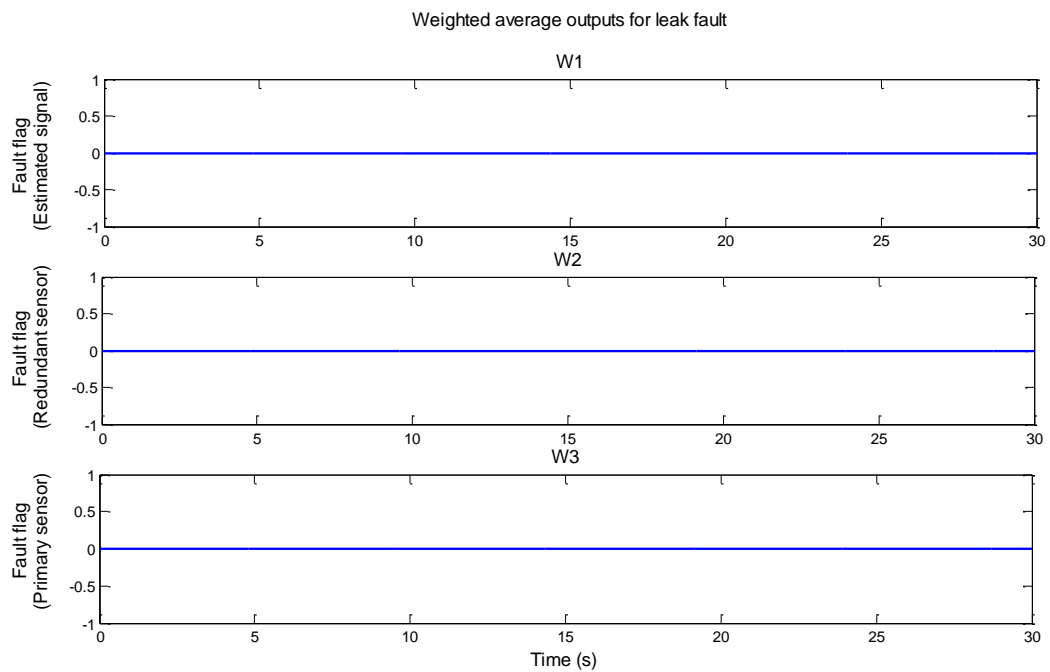
Figure E.12: Weighted average outputs for a leak fault

E.1.2.1 Discussion - Pressure leak

Applying the leak fault at time 18s to the pneumatic single cylinder model has an effect on the parity residual (R_1), this raises the fault flag. The fault also has an effect on the pressure sensor parity residuals (R_2 and R_3). The fault affects the position residual R_4 and the pressure difference residual R_5. Residuals w_1, w_2 and w_3 are not affected and the respective fault flags remain low. This agrees with the fault signatures detailed in Table 7.2.

E.1.3 Pressure sensor (Pp) drift fault

With the gradual build up of dirt on the sensor and faulty circuitry this can cause the effect of sensor drift. A drift fault FPp(s) (see Figure 7.2) is applied to pressure sensor (Pp) at 10s. Figures E.13-E.15 shows the time histories for the parity equation scheme. Figure E.16-E.17 shows the time histories of these experiments for the Kalman filter scheme. Figure E.18 details the time history of the weighted average outputs of the voting scheme.

Figure E.13: Pressure sensor (Pp) drift fault, parity equation - Position sensor output (R_1)

Figure E.14: Pressure sensor (Pp) drift fault, parity equation - Pressure sensor Pp output
(R_2)

Figure E.15: Pressure sensor (Pp) drift fault, parity equation - Pressure sensor Pn output
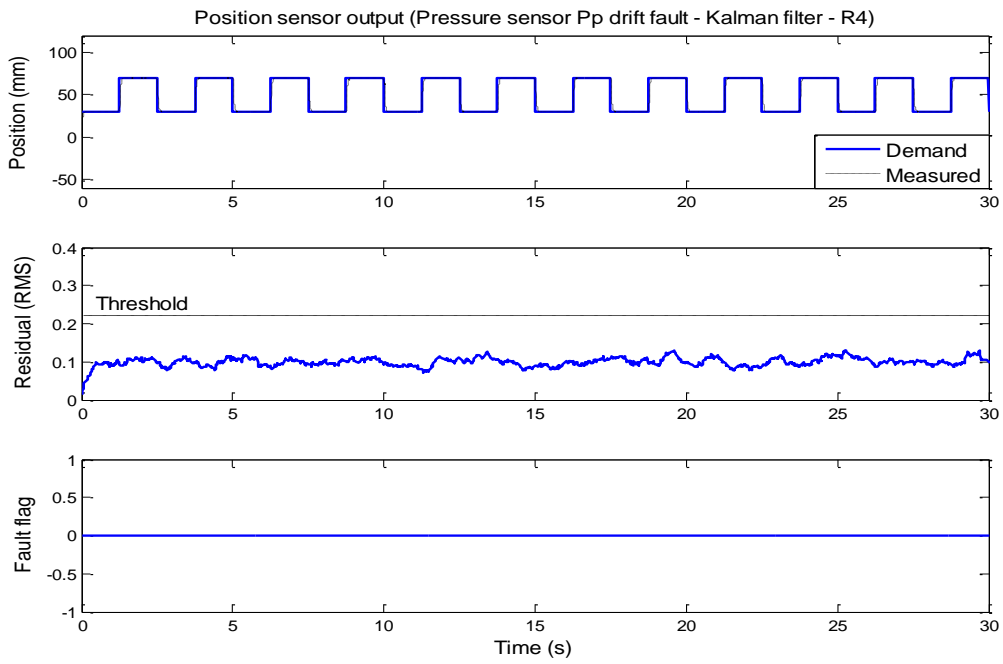(R_3)

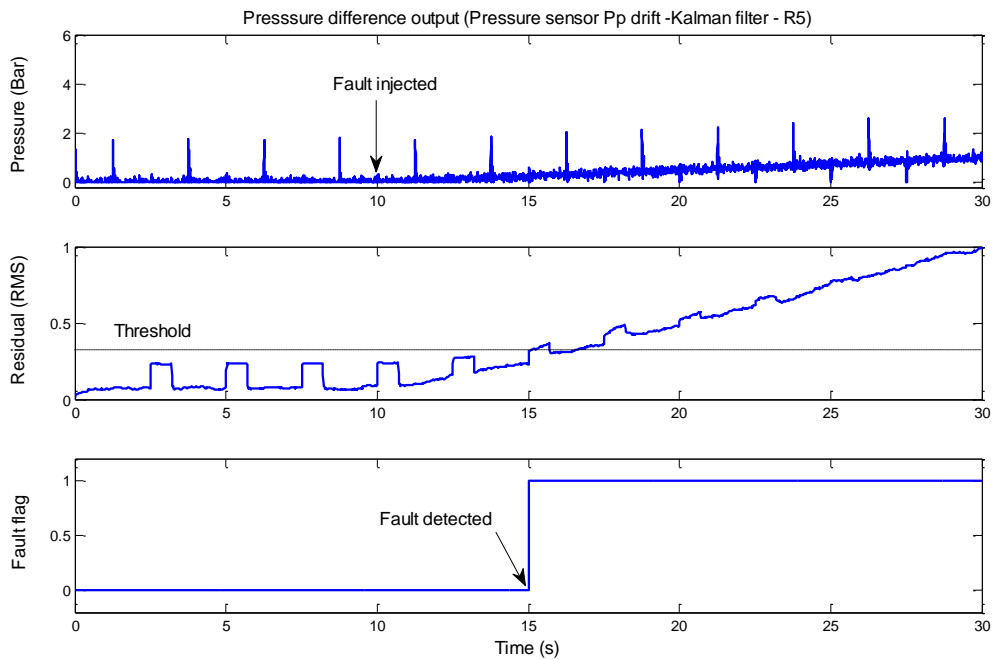Figure E.16: Pressure sensor (Pp) drift fault, parity equation - Position sensor output (R_4)

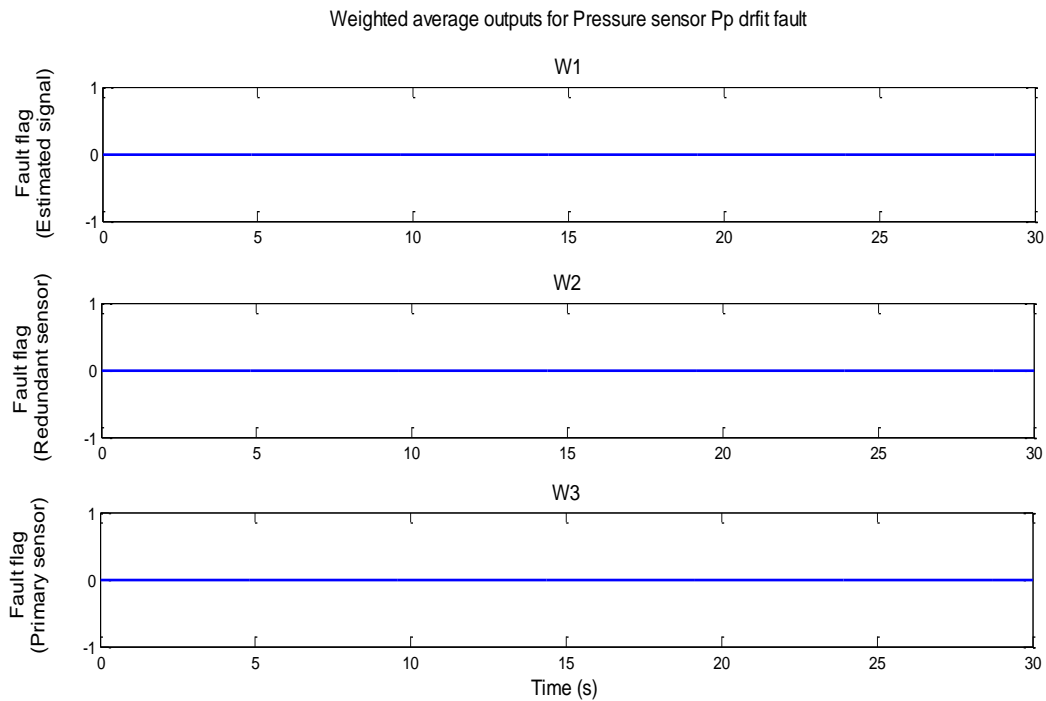Figure E.17: Pressure sensor (Pp) drift fault, parity equation – Pressure difference   output

(R_5)

Figure E.18: Weighted average outputs for a pressure sensor Pp drift fault

E.1.3.1 Discussion - Pressure sensor Pp drift fault

Applying a drift fault at time 10s to the pressure sensor (Pp) has no affect on the parity RMS residual (R_1). The fault affects the pressure sensor RMS residual (R_2). However, this fault does not have an effect on RMS residual R_3. The fault again showing to have no affect on the position RMS residual R_4. The RMS residual R_5 is affected by this fault. Residuals w_1, w_2 and w_3 are not affected and the respective fault flags remain low. These results concur with the fault signatures detailed in Table 7.2.

E.2 Stewart-Gough platform simulation results

A number of experiments were carried out on the pneumatic Stewart platform simulation model (see chapter 7). Detailed below are the results for the designed FDI and fault management scheme for certain faults applied to the platform. It should be noted that

all the experiments have been conducted with the redundant sensor/weighted average voting scheme.

E.2.1 Position sensor fault (signal loss)

A fault FS(s) (see Figure 7.2) is applied to position sensor GS(s) at approximately 20s. The fault injected is that the position signal has been disconnected. Figures E.19-E.21 shows the time histories for the parity equation scheme. Figures E.22-E.23 shows the time histories of these experiments for the Kalman filter scheme. Figure E.24 details the time history of the weighted average outputs of the voting scheme.
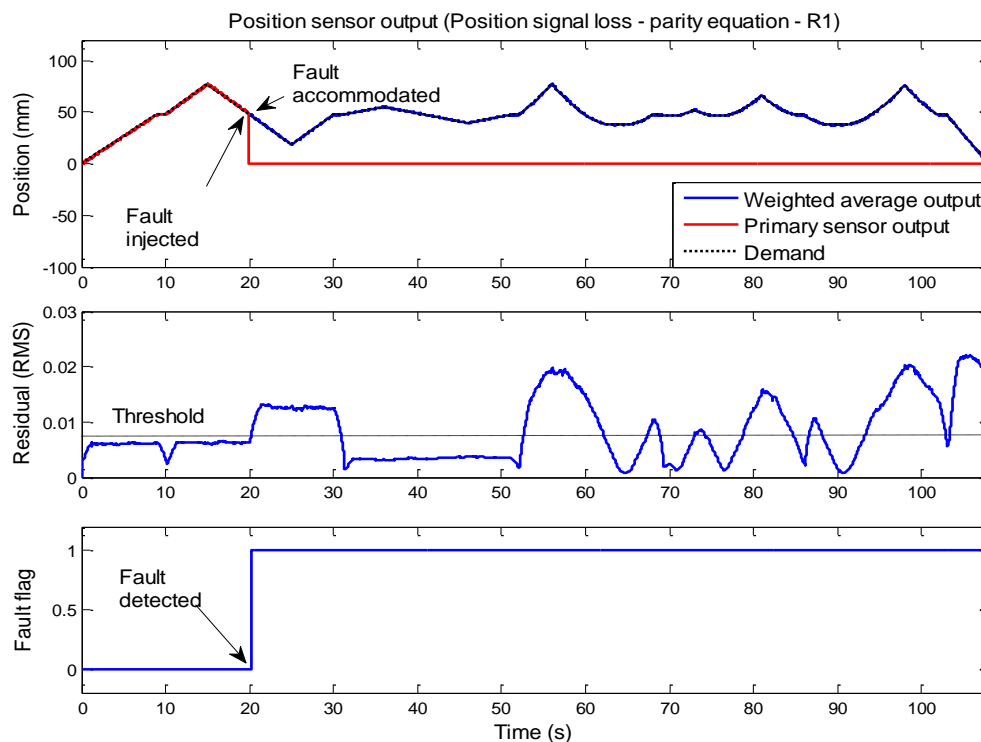
Figure E.19: Position signal loss, parity equation - Position sensor output (R_1)
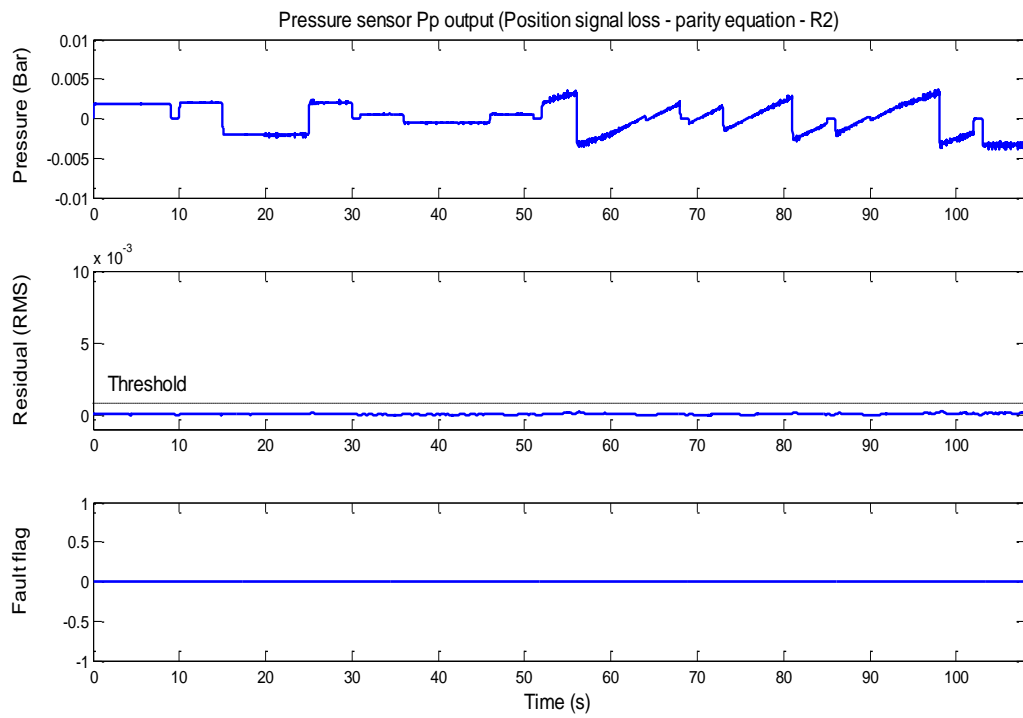
Figure E.20: Position signal loss, parity equation - Pressure sensor Pp output (R_2)
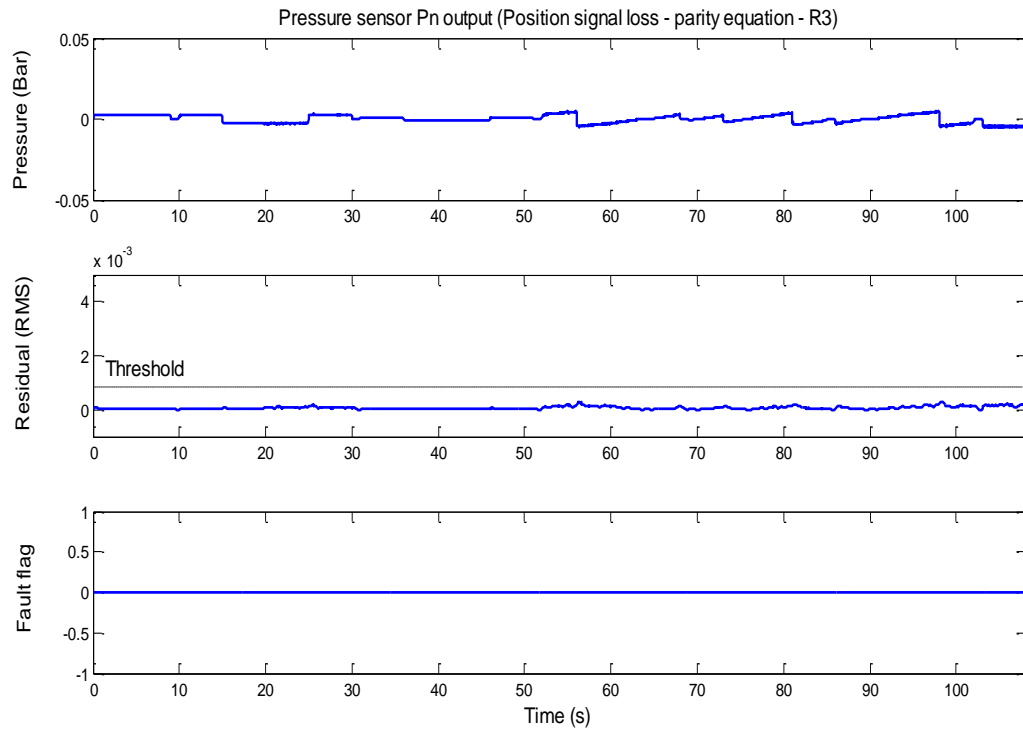
Figure E.21: Position signal loss, parity equation - Pressure sensor Pn output (R_3)
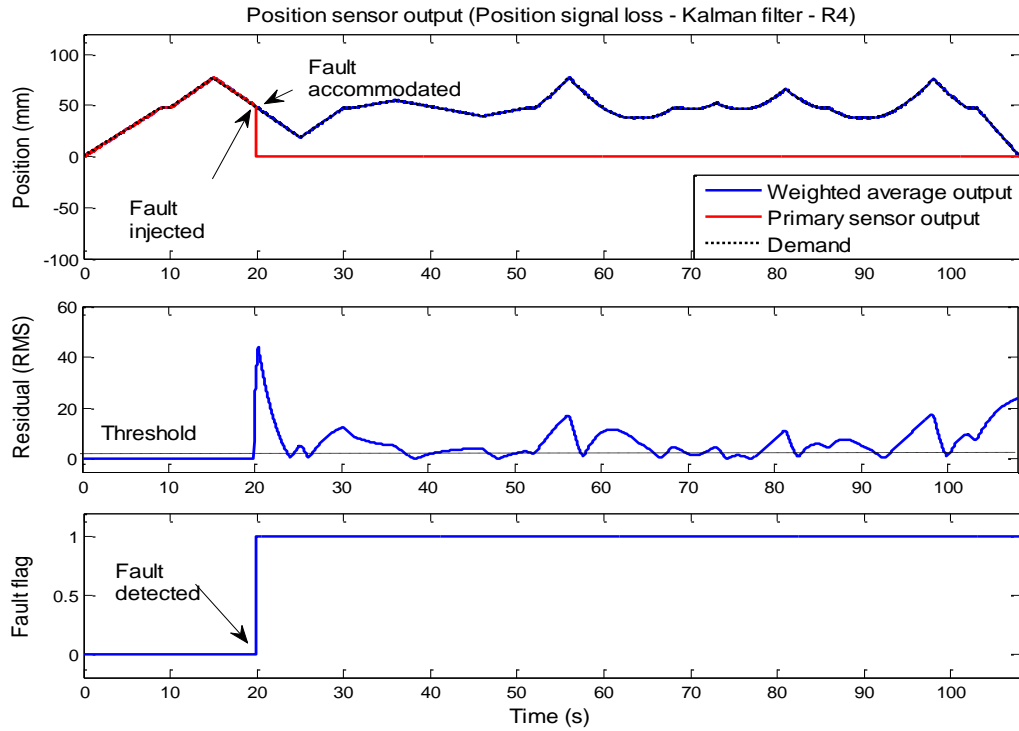
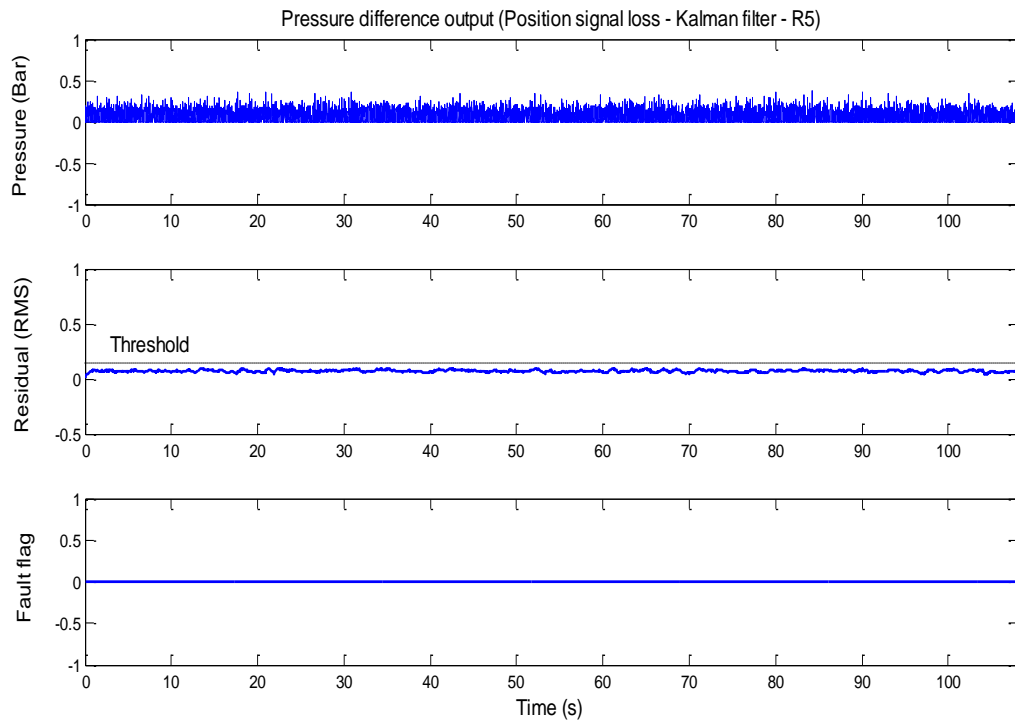Figure E.22: Position signal loss, Kalman filter – Position sensor output (*R₄*)

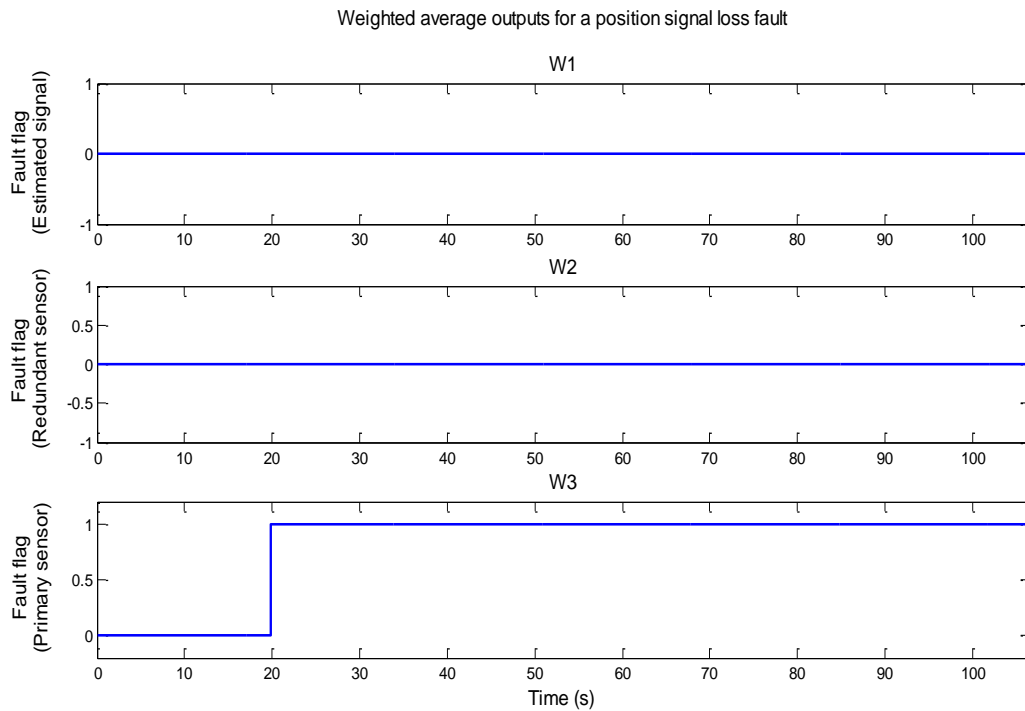Figure E.23: Position signal loss, Kalman filter – Pressure difference output (*R₄*)

Weighted average outputs for a position signal loss fault

Figure E.24: Weighted average outputs for a position signal loss fault

E.2.1.1   *Discussion - Position sensor fault (sensor signal loss)*

Applying a fault to the position sensor has an effect on the parity RMS residual (R_1), this raises the fault flag. The fault has no affect on the pressure sensor parity RMS residuals (R_2 and (R_3). The fault affects the position RMS residual R_4 and there is no affect on the pressure difference RMS residual R_5. The weighted average outputs w_1 and w_2 are not affected; w_3 is affected and raises the fault flag. These results concur with the fault signatures detailed in Table 7.2. Employing a redundant sensor scheme along with the triple input voting scheme shows that the fault does not affect the system performance and fault detection, isolation and accommodation is achieved.

E.2.2   *Actuator fault – control signal loss*

A fault Fa(s) (see Figure 7.2) is applied to the proportional valve. The fault injected is that the control signal has been disconnected at time 45s. Figures E.25- E.27 shows the

time histories of this experiment (actuator fault) for the parity equation scheme. Figures E.28 - E.29 shows the time histories of this experiment (actuator fault) for the Kalman filter scheme. The time history of the weighted average outputs of the voting scheme is shown in Figure E.30.
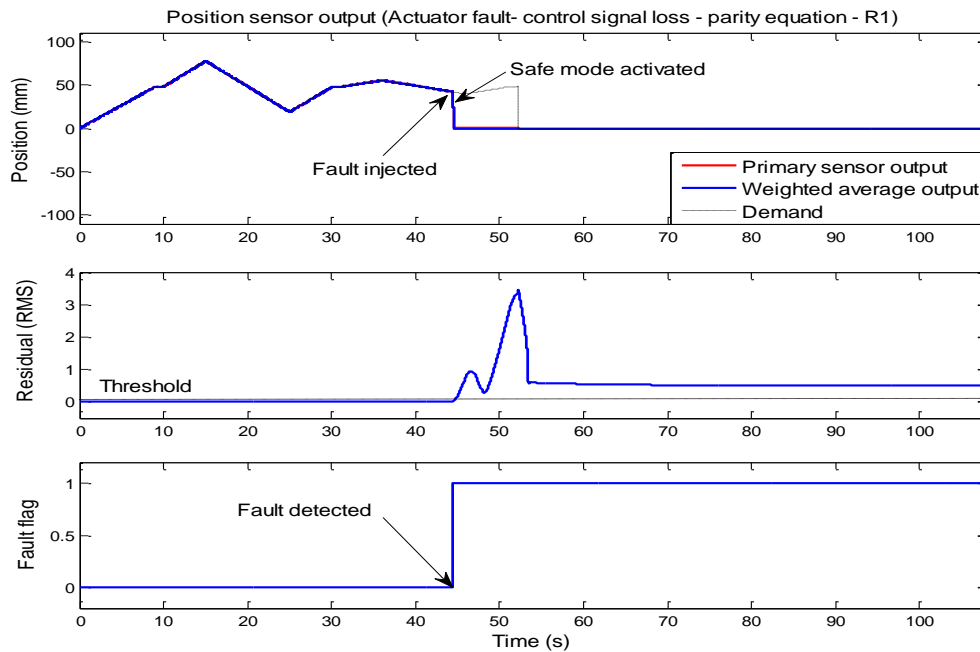

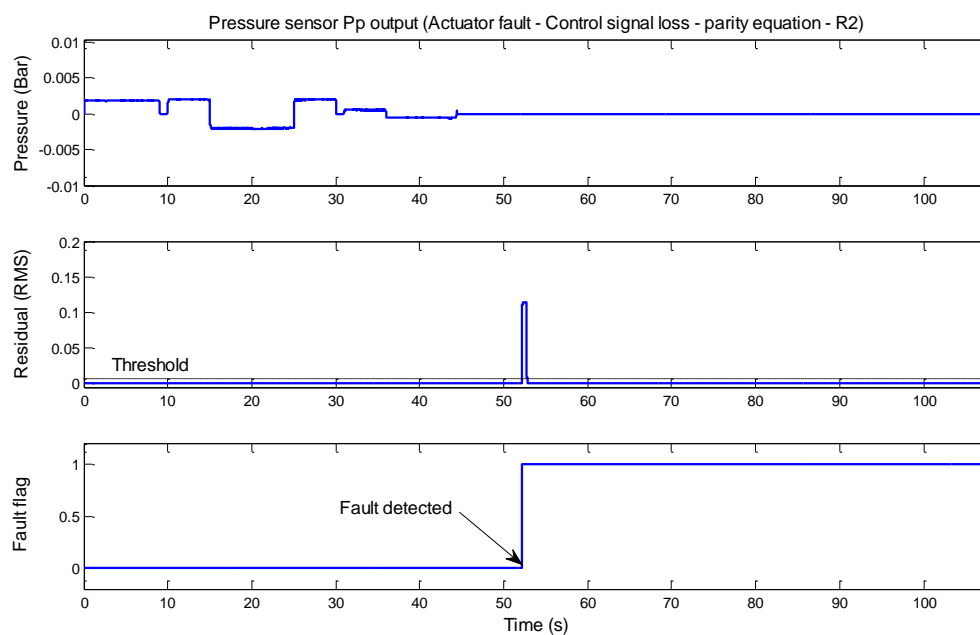Figure E.25: Actuator fault, parity equation - position sensor output (R_1)

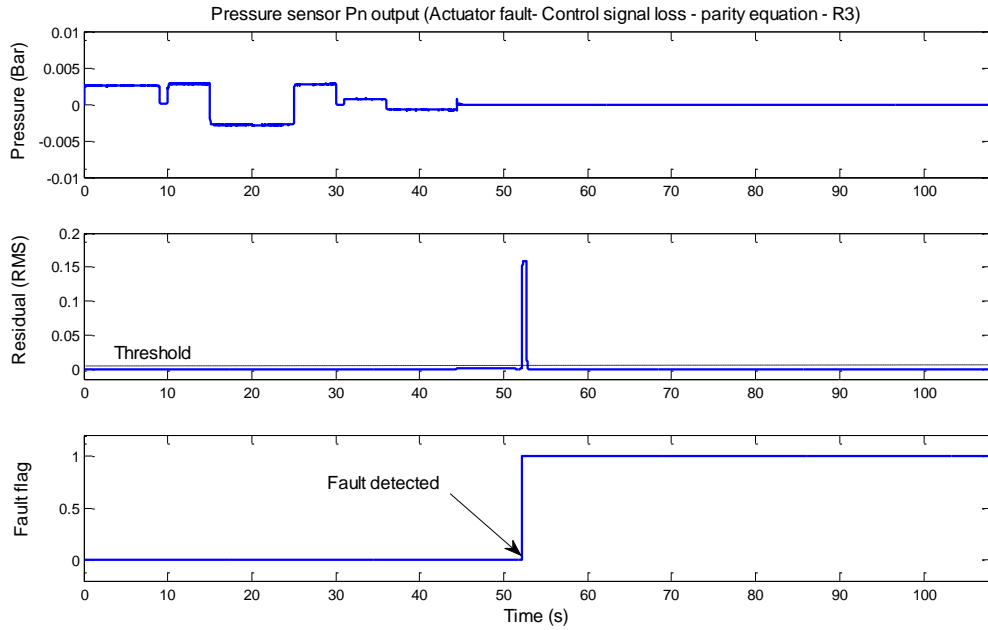Figure E.26: Actuator fault, parity equation – Pressure sensor (Pp) output (R_2)

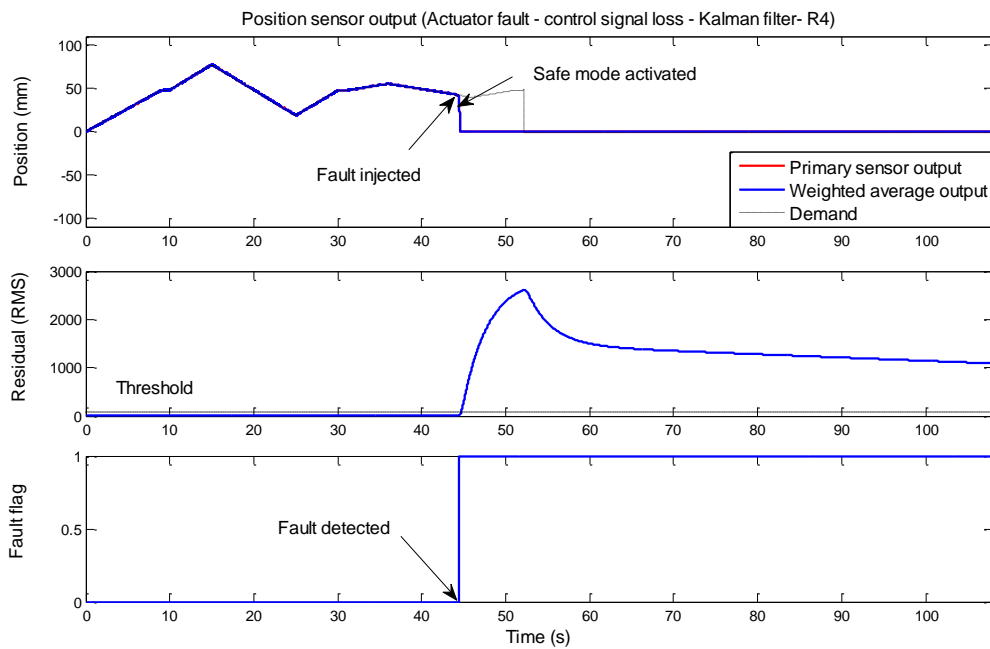Figure E.27: Actuator fault, parity equation – Pressure sensor (Pn) output (R_3)

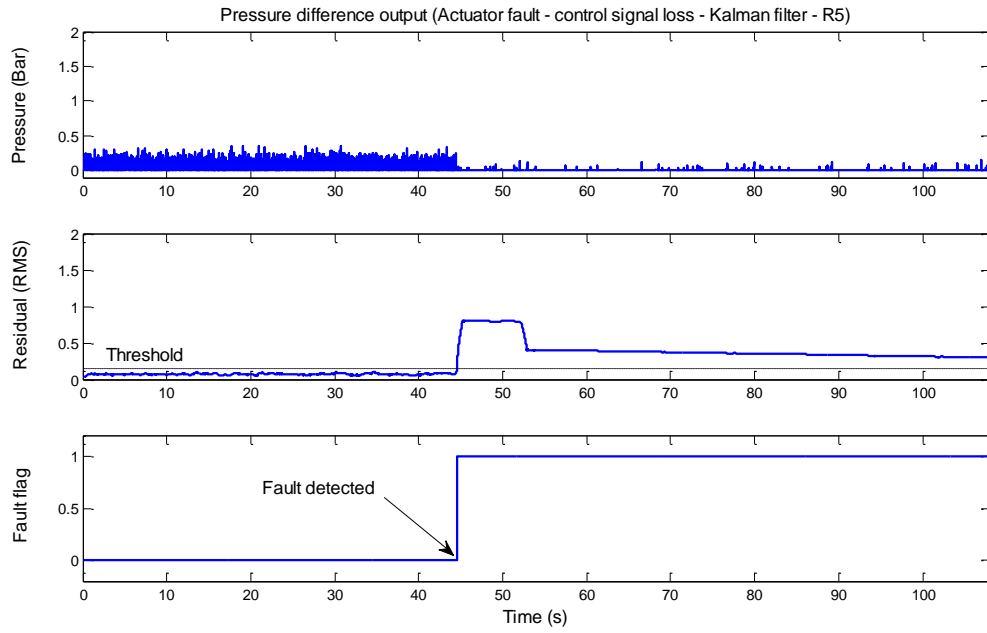Figure E.28: Actuator fault, Kalman filter – Position sensor output (R_4)

Figure E.29: Actuator fault, Kalman filter – Pressure difference output (R_5)
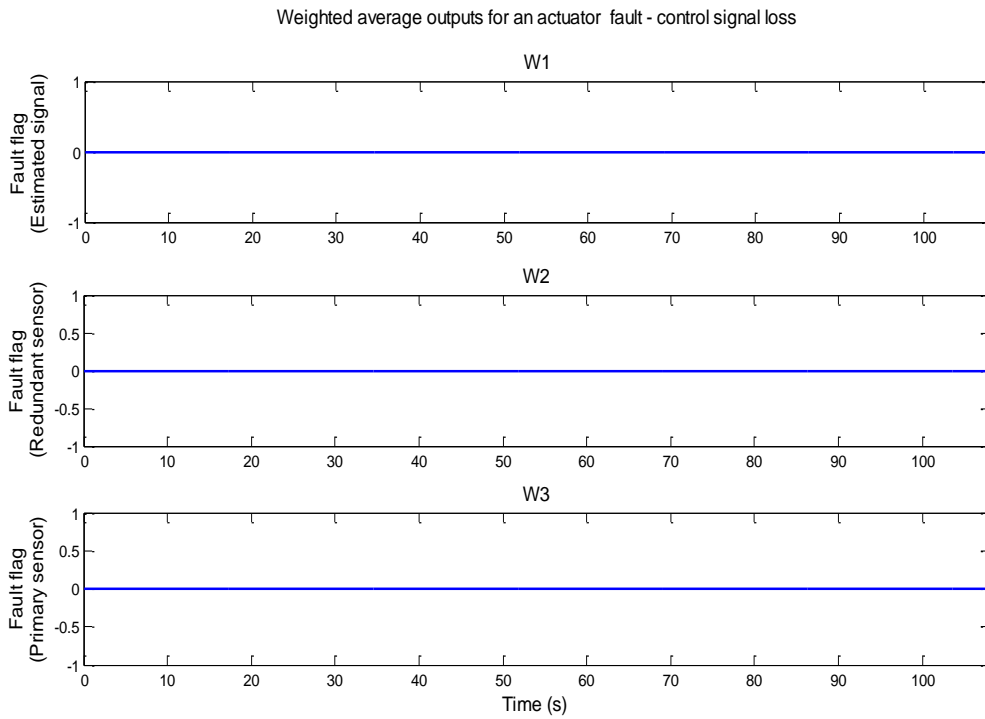

Figure E.30: Weighted average outputs for an actuator fault

E.2.2.1 Discussion - Actuator fault (control signal loss)

Applying the disconnection fault to the control signal of the proportional valve has an effect on the parity residual (R_1), this raises the fault flag. The fault has an effect on the pressure sensor parity residuals (R_2 and (R_3). Both position and pressure difference Kalman residuals (R_4 and R_5) are affected by the actuator fault and their fault flags are raised. Residuals w_1, w_2 and w_3 are not affected and the respective fault flags remain low. This agrees with the fault signatures detailed in Table 7.2. With this particular fault accommodation is not available as the control signal to the servo valve of pneumatic cylinder is lost. This means that the desired positional movement of the rig is inadequate. From here (51.5s) the safety sequence is activated and the platform is made safe (i.e. brought back to its rest position).